Nanoparticle Sensors for the Detection of DNA Related to Disease

by

Lee Barrett

2012

University of Strathclyde

Department of Pure and Applied Chemistry

Nanoparticle Sensors for the Detection of DNA

Related to Disease

By

Lee Barrett

A thesis presented to the Department of Pure and Applied Chemistry, University of Strathclyde, in fulfilment of the requirements for the degree of Doctor of Philosophy.

2012

Acknowledgements

I would like to begin by thanking Prof. Duncan Graham and Dr. Karen Faulds for their continued advice, support and encouragement throughout my PhD.

A big thank you to the members of the Centre for Molecular Nanometrology, both past and present, for all the great times we had over the past few years. Special mention to Eleanore Jane Irvine, Kirsty Gibson, Sara Rooney, Danny van Lierop, Iain Larmour and Luca Guerrini for all the great nights out, the undeniably hilarious chat and, on occasion, insightful scientific discussions!

Thanks to Luca again for all his help with discussions on oligonucleotide-nanoparticle conjugates, SERRS and for showing me how to implement the difference spectra for my results.

To my family and friends, thank you for supporting me during my PhD. Thanks, especially, to my mum and dad for believing in me and for their limitless encouragement and advice. Thanks to my brother, Kyle, for your friendship and encouragement over the last few years. To Dominic and Adam, for putting up with some particularly unpleasant bad moods from time to time, thank you for being there and being great friends.

Finally, my biggest thank you to Dr Jennifer A. Dougan for her continued support ("Can I borrow some buffer?"), advice ("The synthesiser's broken again.") and encouragement ("Write your thesis!"). I couldn't have done it without you so thank you for believing in me, being there to listen to me rant and helping me through the last few years (and beyond).

Abstract

The aim of this research was to develop stable dye-labelled oligonucleotide-nanoparticle conjugates for the detection of DNA related to disease using surface enhanced resonance Raman scattering (SERRS) spectroscopy.

In order to achieve this, both gold and silver nanoparticle conjugates were successfully functionalised with thiol- and thioctic acid-modified oligonucleotides. To investigate their viability as biosensors, the stability of the conjugates and their hybridisation efficacy was investigated. It was discovered that the thioctic acid-modified oligonucleotide-nanoparticle conjugates remain stable under these conditions for a substantial period of time compared to thiol-modified oligonucleotide nanoparticle conjugates. The nanoparticle conjugates were functionalised for use in surface enhanced resonance Raman scattering (SERRS) spectroscopy by the incorporation of an isothiocyanate dye molecule. Not only were the conjugates SERRS active, they were also proven to exhibit enhanced stability for both thiol- and thioctic acid-modified oligonucleotide nanoparticle conjugates.

The thioctic acid-modified oligonucleotide nanoparticle conjugates were investigated for their use as sensors to detect specific DNA sequences. Both gold and silver nanoparticle conjugates were shown to retain their biological activity by hybridising with complementary DNA sequences. This was monitored colorimetrically, due to the characteristic colour changes associated with aggregation of gold and silver nanoparticles, and by monitoring the hybridisation-induced red-shift of the surface plasmon band by UV-Vis spectroscopy. The hybridisation-induced aggregation methodology was also extended to dye-labelled nanoparticle conjugates that were investigated by SERRS.

A method for characterising oligonucleotide-nanoparticle conjugates using a fluorescent DNA intercalator, SYBR green I, was developed. This study showed that SYBR green I can be used as a rapid method for determining the melting profiles of individual nanoparticle conjugates and the hybridisation efficiency of the immobilized oligonucleotides.

Abbreviations

A	Adenine
Abs	Absorbance
Ac	Acetyl
AFM	Atomic Force Microscopy
AU	Absorbance Units
BODIPY-650	6-(((4,4-difluoro-5-(2-pyrrolyl)-4-bora-3a,4a-diaza-*s*-indacene-3-yl)styryloxy)acetyl)aminohexanoic acid
bp	Base pairs
BRCA-1	Breast cancer 1
BTT	5-Benzylthio-1*H*-tetrazole
C	Cytosine
CCD	Charge Coupled Device
Comp	Complementary
Conc.	Concentration
CPG	Controlled Pore Glass
CML	Chronic myeloid leukemia
d	Doublet (NMR)
d	Deoxy (DNA)
DAPI	4',6-diamidino-2-phenylindole
dATP	Deoxyadenosinetriphosphate
dNTP	Deoxynucleotidetriphosphate
D	Dextrorotatory
Dbpr	Dye-base pair ratio
dd	Doublet of doublets
ddNTP	Dideoxynucleotidetriphosphate
DCC	Dicyclohexyl Carbodiimide
DCM	Dichloromethane
DEAE	Diethylaminoethyl
DIPEA	Di-*iso*-propylethylamine

DLS	Dynamic Light Scattering
DMF	*N,N*-Dimethylformamide
DMSO	Dimethylsulfoxide
DMTr	Dimethoxytrityl
4-DMAP	4-*N,N*-Dimethylaminopyridine
DNA	2'-Deoxyribose Nucleic Acid
DPN	Dip-pen nanolithography
Ds	Disulfide
dsDNA	Double-stranded DNA
DTT	Dithiothreitol
E	Electronic excited state
EDC	*N*-(3-Dimethylaminopropyl)-*N'*-ethylcarbodiimide
EDITH	3-Ethoxy-1,2,4-dithiazoline-5-one
EDTA	Ethylenediaminetetraacetic acid
EI	Electron Impact
eq	Equivalents
Et	Ethyl
ETT	5-Ethylthio-1*H*-tetrazole
F	Fluorophore
FAM	Carboxyl Fluorescein
FAMITC	FAM isothiocyanate
Fmoc	9-Fluorenylmethoxycarbonyl
FRET	Förster Resonance Energy Transfer
G	Guanine
h	Hour(s)
HDA	Helicase-dependent amplification
HEG	Hexaethylene glycol
HEX	Hexachlorofluorescein
HGP	Human genome project
HIV	Human Immunodeficiency Virus
HMD	Hexamethylene diamine
HOBT	Hydroxybenzotriazole

HPA	Hydroxypiccolinic acid
HPLC	High Performance Liquid Chromatography
HPV	Human papillomavirus
IE	Ion-exchange
IPA	*iso*-propyl alcohol
IR	Infrared
l	Litre
LAMP	Loop mediated isothermal amplification
LCAA	Long Chain Alkyl Amine
LFM	Lateral Force Microscopy
LNA	Locked Nucleic Acid
LSPR	Localised surface plasmon resonance
LWD	Long Working Distance
M	Molar
MALDI-TOF	Matrix-Assisted Laser Desportion Ionisation – Time of Flight
Mass spec.	Mass Spectrometry
Max.	Maximum
MBA	Mercaptobenzoic acid
Me	Methyl
MEF	Metal enhanced fluorescence
MGITC	Malachite green isothiocyanate
MHA	Mercaptohexadecanoic acid
min	Minute(s)
MMTr	Monomethoxy trityl
mod	Modified
mRNA	Messenger RNA
MRSA	methicillin-resistant *Staphylococcus aureus*
MS	Mass Spectrometry
m/z	Mass/charge ratio
NA	Numerical Aperture
NASBA	Nucleic acid sequence based amplification
NHS	*N*-Hydroxysuccinimide

NMR	Nuclear Magnetic Resonance
PAGE	Polyacrylamide gel electrophoresis
PBS	Phosphate buffered saline
PCR	Polymerase Chain Reaction
PDDA	Poly(diallyldimethylammonium chloride)
PEG	Polyethylene glycol
PNA	Peptide nucleic acid
p.p.m.	Parts per million
Q	Quencher
RCA	Rolling circle amplification
RNA	Ribonucleic acid
ROX	Carboxy-X-rhodamine
ROXITC	ROX isothiocyanate
RP	Reversed phase
RPA	Recombinase polymerase amplification
r.p.m.	Revolutions per minute
RSD	Relative Standard Deviation
RT	Real time
s	Singlet
SAM	Self Assembled Monolayer
SAMSA	5-((2-(and-3))-S-(acetylmercapto)-succinoyl) amino)
SDS	Sodium dodecyl sulfate
SEC	Size Exclusion Chromatography
SEM	Scanning Electron Microscopy
SERS	Surface Enhanced Raman Scattering
SERRS	Surface Enhanced Resonance Raman Scattering
SG	SYBR green I
SNP	Single Nucleotide Polymorphism
SPR	Surface Plasmon Resonance
ssDNA	Single-stranded DNA
SDA	Strand displacement amplification
t	Triplet

T	Thymine
TA	Thioctic acid
TAMRA	Carboxytetramethylrhodamine
TRITC	TAMRA isothiocyanate
TEAA	Triethylammonium acetate
TEM	Transmission Electron Microscopy
THF	Tetrahydrofuran
T$_m$	Melting Temperature
TMA	Transcription mediated amplification
TMAMC	Tetramethylammonium chloride
Tris	Tris(hydroxymethyl)aminomethane
tRNA	Transfer RNA
U	Uracil
UV	Ultra Violet
Vis	Visible

Contents

1 Introduction

1.1 Deoxyribonucleic Acid (DNA)

Deoxyribonucleic acid, DNA, is the source of all genetic information necessary for life. Present in every living cell, DNA is responsible for the transcription of ribonucleic acid, RNA, which, in turn, is responsible for the translation of the genome into proteins to produce functioning cells. Research concerning DNA has a long and illustrious history, dating back to 1869 when the physician, Friedrich Miescher, inadvertently discovered a crude isolate of DNA, which he called 'nuclein', from cells found in pus contained within wound dressings he collected from surgical hospitals. [1] Later, in the early 1900's, the nucleotide components of DNA were isolated from yeast nucleic acid by Phoebus Levene, [2] who later reported the base, sugar and phosphate components. [3] William Astbury, in 1937, made the first steps in elucidating the structure of DNA by reporting the first X-ray diffraction patterns, which concluded DNA had a regular structure. [4] This famously led to James Watson and Francis Crick's journey to the discovery of the definitive structure for DNA. [5]
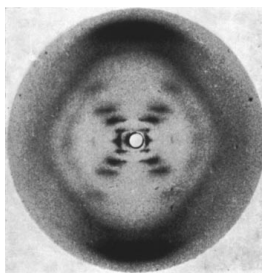
Figure 1.1. X-ray diffraction image of DNA, reported by Rosalind Franklin in 1953. [6]

Together with X-ray diffraction data (Figure 1.1) provided by Rosalind Franklin, Raymond Gosling and Maurice Wilkins *et al.*, [6] [7] [8] Watson and Crick were able to determine the double helical structure of DNA and show the complementary nature of the individual nucleotides. [9] [10] The DNA double helix is one of the most

instantly recognizable structures known and its discovery gave birth to a new era of biological research. [11] [12] Of the more recent and significant output from DNA research has undoubtedly been the completion of the Human Genome Project (HGP), which endeavoured to determine the entire nucleotide sequence of the human genome and provide an insight into genetic disease and heredity. [13]
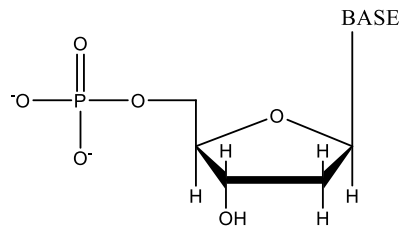
Figure 1.2. A single nucleotide unit comprising three sub-units: the sugar, the phosphate and the base.

1.1.1 Primary Structure of DNA

DNA is essentially a long, polymeric molecule constructed from many repeating monomeric structures known as nucleotides. Each nucleotide contains three sub-units – two of these, the *deoxyribose sugar* and the *phosphate*, do not change from nucleotide to nucleotide. The third sub-unit, the *nitrogen-containing base*, can be one of four molecules, the order of which determines the genetic code responsible for life (Figure 1.2). The four possible bases are adenine (A), thymine (T), guanine (G) and cytosine (C). The bases can be categorized as either purines or pyrimidines. The bicyclic purines are adenine and guanine and the monocyclic pyrimidines are thymine and cytosine (Figure 1.3). However, in ribonucleic acid, RNA, another base, uracil (U), takes the place of thymine, which differs, structurally, by the absence of the 5'-methyl group.
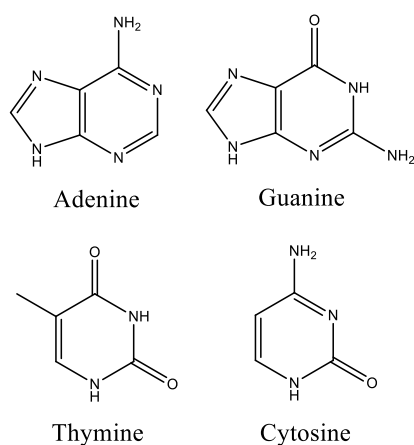
Figure 1.3. The DNA bases. Purines (top): adenine and guanine; pyrimidines (bottom): thymine and cytosine.

The sugar component of the nucleotide is 2'-deoxy-β-D-ribose. The bases form *N*-glycosidic bonds *via* the N-9 of the purines or the N-1 of the pyrimidines with the 1'-carbon atom of the 2'-deoxyribose sugar. If the phosphate is removed from the structure of a nucleotide leaving only the sugar and base, this is referred to as a nucleoside (Figure 1.4). In RNA there is a hydroxyl group located at C-2' making a D-ribose sugar.
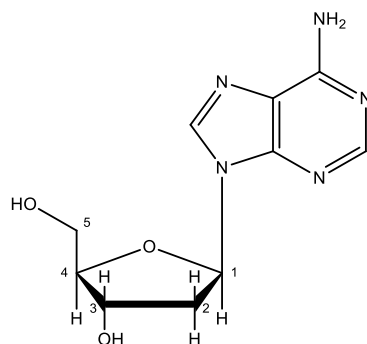
Figure 1.4. Example of a nucleoside, deoxyadenosine, showing the N-glycosidic bond between C-1' of the sugar and N-9 of the adenine base.

Nucleotides form a polymeric network through the phosphodiester backbone. The 5'-hydroxyl group on the 2'-deoxyribose sugar forms a bond with the 3'-hydroxyl group on the 2'-deoxyribose sugar of an adjacent nucleotide, thereby forming a polynucleotide. A dimer comprised of guanine and cytosine is shown in figure 1.5.
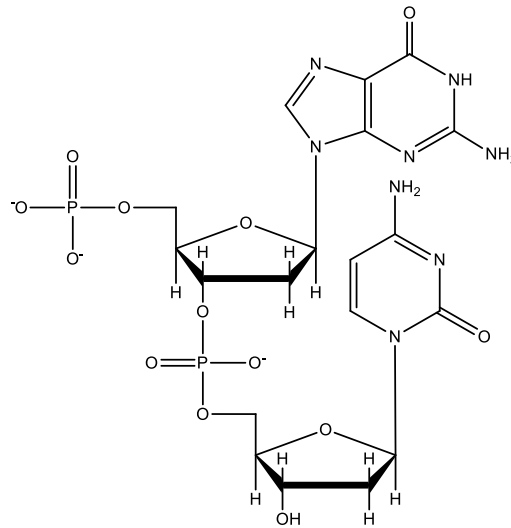
Figure 1.5. A DNA dimer of G and C showing the 5'-3' phosphodiester bonds linking the sugar units together.

1.1.2 Secondary Structure of DNA

The discovery of the secondary structure of DNA dates back to 1950, where Edwin Chargaff undertook enzymatic degradation studies of DNA that revealed nucleotides exist in a universal 1: 1 ratio, *i.e.* the number of adenosine nucleotides is equal to the number of thymine nucleotides present and, similarly, the number of guanine nucleotides is equal to the number of cytosine nucleotides present, regardless of the source of the DNA. [14] This discovery led to what is known as the Chargaff Rule of Base Pairing which states that, in any source of DNA, the proportion of purines to pyrimidines is always the same.

Later, in 1953, James Watson and Francis Crick published, in *Nature*, the secondary structure of DNA. [9] [10] They deduced that DNA exists as two right-handed helical strands coiled around a common axis, interconnected *via* the purine and pyrimidine bases, which run anti-parallel to one another. Each strand is constructed from phosphate diester groups linking 2'-deoxyribose sugar units through the 3'- and 5'-hydroxyl groups and, at the 1'-carbon, each sugar unit has a nitrogenous base linked *via* an *N*-glycosidic bond. Complementarity of the two strands is achieved through hydrogen bonding of the nitrogenous bases, intermolecularly holding the two strands together in a double helix conformation. The nitrogenous bases form a hydrophobic core at the centre of the helix, while the charged phosphate groups of the

phosphodiester backbone form a polyanionic network and comprise the hydrophilic outer surface of the double helix (Figure 1.6).
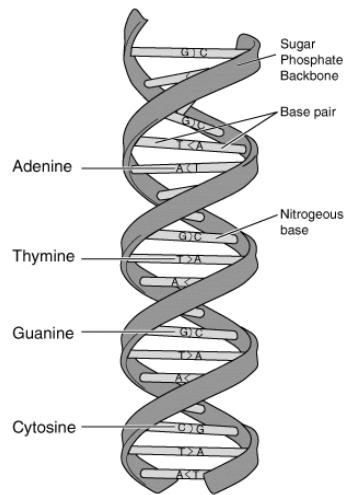
Figure 1.6. Schematic representation of the DNA double-helix. [15]

Watson and Crick revealed that the two polynucleotide strands are held together in the helix by hydrogen bonds between the purine and pyrimidine bases. This observation led Watson and Crick to deduce that a purine base is always bonded to a pyrimidine base: adenine bonds only with thymine and guanine bonds only with cytosine. This specificity arises from the availability of hydrogen bonds between the bases: adenine pairs with thymine *via* two hydrogen bonds and guanine pairs with cytosine *via* three hydrogen bonds (Figure 1.7). This specific base-pairing, or "Watson-Crick" base-pairing, is supported by Chargaff's rule. [14]
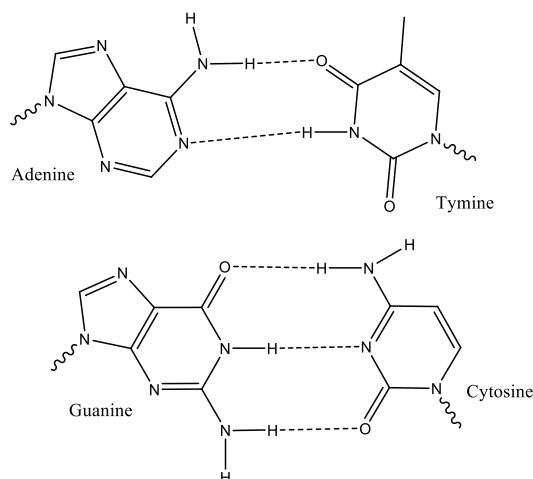
Figure 1.7. Hydrogen bonding between the four bases: A-T and G-C as proposed by Watson and Crick. [9]

The double helical structure of DNA gives rise to two distinguishable grooves, which run the length of DNA, called the major and minor grooves. The major groove has a width of approximately 22 Å and the minor groove has a width of approximately 12 Å. [16] The nucleotide bases are more accessible in the major groove - allowing proteins that are necessary for DNA to function to bind, such as those required for replication of DNA or transcription of DNA to RNA. [17]

Maurice Wilkins and Rosalind Franklin observed differences in DNA conformation when exposed to variations in humidity. Wilkins reported that keeping the DNA fibres moist while conducting X-ray diffraction experiments resulted in X-ray patterns that were consistent with those obtained from intact biological samples. [8] Franklin, on the other hand, reported two forms of DNA – the A- and B-forms. A-DNA occurs at low humidity, the major and minor grooves are similar in width and there are about 11 bases per turn in A-DNA. In comparison, B-DNA occurs at high humidity, the bases are stacked one above the other, perpendicular to the long axis of DNA and there are 10.4 bases per turn in B-DNA. Franklin's investigation led to the conclusion that the charged phosphate groups would need to be on the outside and the bases on the inside of the structure of DNA in order for water to influence its conformation. [7]

The discovery of the secondary structure of DNA led Watson and Crick to consider the biological implications of base-paring and the role it plays on passing on genetic information.

1.1.3 DNA in Biology

DNA holds the genetic code that is responsible for passing on our inheritable traits. The genetic information encoded in DNA is passed on from cell to cell during cell division - the key process necessary for life. In cells, DNA is housed in structures called chromosomes. The chromosomes are organised into distinct regions containing genes, regulatory sequences and "junk" DNA. The cumulative term for these regions is the genome. Genes are the important functional part of DNA and code for inheritable traits. DNA itself is not strictly a functional molecule; it simply contains the information necessary for translation into RNA and proteins. It is the products of DNA that determine the physical characteristics and development of an individual.

In a cell DNA is transcribed to RNA, which is translated into proteins. This flow of genetic information is known as the "central dogma" and was originally conceived by Francis Crick in the 1950's (Figure 1.8). [18] [19] Protein synthesis begins in the cell nucleus by a process called transcription. During transcription, a segment of DNA corresponding to a particular gene is read by an RNA polymerase, producing complementary, antiparallel RNA. If the gene encodes a protein, the resulting RNA is known as messenger RNA (mRNA). The mRNA undergoes several chemical changes before being ejected from the nucleus into the cell cytoplasm. Next, the mRNA is used as a template to begin production of a protein, by a process called translation. Occurring in the ribosome, translation involves mRNA, containing codons, hybridising to transfer RNA (tRNA), containing anticodons. tRNA comprises a triplet of nucleotides at one end and a corresponding amino acid at the other end. Amino acids, like nucleotides to DNA, are the basic building blocks of proteins. The mRNA enters the ribosome where it base-pairs with the complementary tRNA molecule, thereby introducing a new amino acid to a growing polypeptide chain. Once base-pairing has ceased the polypeptide is transformed into a functioning protein by spontaneously folding and coiling, eventually forming a

specific three-dimensional structure. The primary structure of a protein is directly related to the nucleotide sequence while secondary, tertiary and quaternary structures of proteins determine functionality. It is of great importance, therefore, that determining the specific nucleotide sequence of an organism's genome can reveal information about how cells function which is important for our understanding of genetic inheritance, disease and mutation.
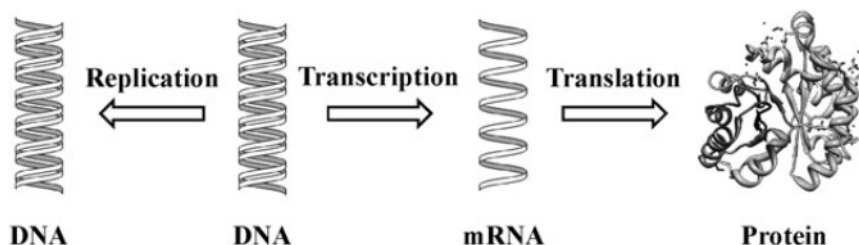
Figure 1.8. The flow of genetic information from DNA to RNA to protein, known as the "central dogma" as proposed by Francis Crick. [20]

1.1.4 Chemical Synthesis of DNA – A History

The elucidation of the chemical structure of DNA naturally led to advances in nucleotide chemistry, with researchers focused on chemically synthesising nucleotides in the lab. Researchers later managed to chemically synthesise single-stranded nucleic acids consisting of two or more deoxyribonucleotides linked together by phosphodiester bonds. These synthetic nucleic acids are called oligodeoxyribonucleotides or, simply, oligonucleotides. Oligonucleotides have become an indispensable tool in many research disciplines, most notably as probes for DNA sequencing, as primers in the polymerase chain reaction (PCR), as therapeutics for manipulating gene expression and in DNA microarray technology. [21] [22] [23] [24] [25] Today, oligonucleotide synthesis is fully automated using bench-top synthesisers and all nucleotide building blocks and reagents necessary for chemical synthesis are commercially available for analysts, biologists and chemists alike. Oligonucleotide synthesis methodology has a long history and many of the concepts that were established over 60 years ago remain unchanged and are still employed in commercial oligonucleotide synthesis to this day.

1.1.4.1   Evolution of Oligonucleotide Synthesis

The first attempted synthesis of an oligonucleotide was conceived by Michelson and Todd in 1955, who published a method for the preparation of a dithymidinyl nucleotide. [26] Their report described the formation of a phosphate link between two thymidine nucleosides by using phenylphosphoryl chloride to prepare a 5'-benzoyl protected thymidine with a 3'-phosphoryl chloride group which was then reacted to the 5'-hydroxyl group of a 3'-protected thymidine. They found, however, that the reaction was slow and the phosphoryl chloride intermediate was not stable so another suitable method had to be employed. Within the next few years, another researcher, H. Gobind Khorana, introduced key concepts to oligonucleotide synthesis that are still used by chemists today. One of these concepts was the phosphodiester approach to forming a dinucleotide. Khorana reported the use of a stable phosphorylated nucleoside that, once activated, coupled to the desired nucleoside. [27] [28] He accomplished this by using a condensation reagent, dicyclohexyl carbodiimide (DCC), to facilitate the coupling between a 5'-protected nucleoside 3'-phosphate and a 3'-protected nucleoside *via* the 5'-hydroxyl group. In addition to the phosphodiester approach, Khorana also introduced the concept of nucleoside protecting groups that would later become a mainstay in oligonucleotide synthetic chemistry. [29] [30] [31] In the early 1960's, Khorana reported a protection strategy for the exocyclic amine groups located on adenine, guanine and cytosine (thymine has no exocyclic amine groups, therefore requires no protection scheme) and the 5'-hydroxyl group on the sugar. The amine groups are protected *via* a benzoyl group for adenine, an isobutyryl group for guanine and an acetyl group for cytosine (Figure 1.9). [31]

N-benzoyl adenine   *N*-isobutyryl guanine   *N*-acetyl cytosine
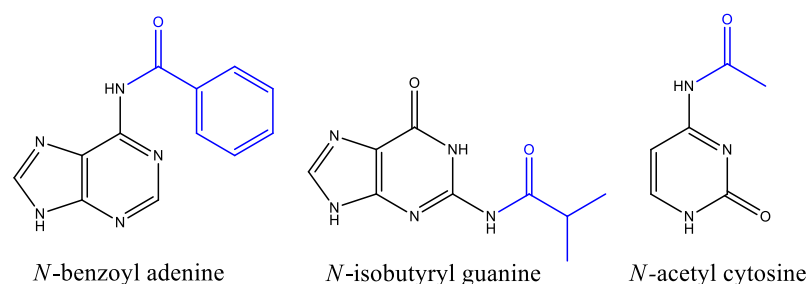
Figure 1.9.   Protection of exocyclic amines on the bases.   Protecting groups are highlighted in blue for clarification.

The 5'-hydroxyl group on the sugar is protected by the inclusion of an acid-labile dimethoxytrityl (DMT) group (Figure 1.10). [29] [30] The removal of the DMT group during oligonucleotide synthesis is important as the cation of DMT, once removed from the nucleotide in the growing oligonucleotide chain, is orange in colour, with a high extinction coefficient, allowing the absorbance to be measured optically, thereby providing a convenient means of determining the coupling efficiency of nucleotides during synthesis. Khorana's phosphodiester method of oligonucleotide synthesis dominated for many years and, in 1970, he published the total synthesis of a tRNA molecule consisting of 72 nucleotides. [32] However, in 1969, Robert Letsinger, reported the phosphotriester approach to oligonucleotide synthesis. [33] This method built upon Khorana's research and introduced a scheme for protecting the phosphate group in the internucleotide linkage, thereby preventing branching during synthesis – an unwanted side-reaction that plagued Khorana's method. The protecting group employed for the protection of the phosphate group, which is still in use today, was a β-cyanoethyl group that can be readily removed *via* treatment with ammonium hydroxide (Figure 1.11).
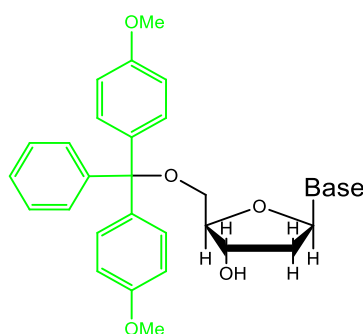
Figure 1.10. Protection of the 5'-hydroxyl group on the sugar. The DMT protecting group is highlighted in green for clarity.
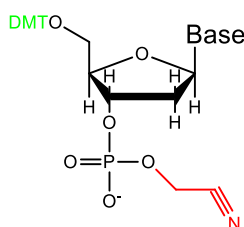
Figure 1.11. Protection of the phosphate using a β-cyanoethyl group, highlighted in red, as proposed by Robert Letsinger. [33]

Researchers were moving closer and closer to a definitive chemistry for oligonucleotide synthesis and in the mid-1970's, Robert Letsinger, again, introduced another innovation that would become another mainstay in oligonucleotide synthesis. Letsinger and Lunsford described the phosphite-triester method of synthesis that utilizes phosphorus in the more reactive P $^{(III)}$ state, which is later, oxidized to the natural P $^{(V)}$ state. [34] This method afforded shorter coupling times due the highly reactive phosphomonochloridite intermediates. However, like the methods before it, the phosphite-triester method of oligonucleotide synthesis was not without its drawbacks – the phosphomonochloridite intermediates were highly susceptible to hydrolysis.

A solution was presented, in the 1980's, by Marvin Caruthers, who proposed the phosphoramidite method of oligonucleotide synthesis. To overcome the shortcomings of the phosphite-triester method, Beaucage and Caruthers reported the inclusion of an *N*, *N*-diisopropyl amine on the phosphate group, which produced a stable nucleoside that could be made and stored as a powder until needed (Figure 1.12). All that was required was activation by a weak acid, tetrazole, to allow the phosphoramidites to form internucleotide phosphite linkages. [35] [36] The inclusion of Caruthers's protection group in the nucleotide marked the pivotal innovation that revolutionised oligonucleotide synthesis and the phosphoramidite method is now the most widely accepted method for automated, solid-phase synthesis of oligonucleotides.
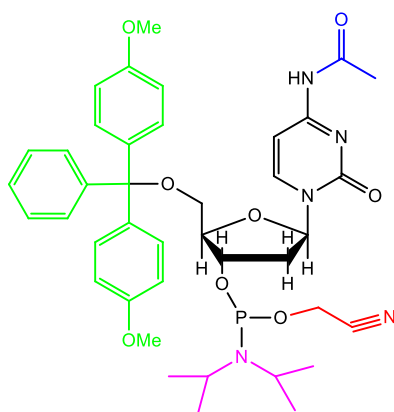
Figure 1.12.   A 5'-(4, 4'-Dimethoxytrityl)-N-acetyl-2'-deoxycytidine, 3'-[(2-cyanoethyl)-(N, N-diisopropyl)]-phosphoramidite. Protecting groups: DMT (green), cyanoethyl (red), acetyl (blue) and N, N-diisopropyl (pink).

1.1.5 Oligonucleotide Synthesis

1.1.5.1   Solid-Phase Oligonucleotide Synthesis

In most laboratories today, solid-phase oligonucleotide synthesis is performed on automated bench-top synthesisers. Solid–phase synthesis of oligonucleotides dates back to the 1960's where Robert Letsinger, inspired by on-support synthesis of peptides, reported synthesis of dimer and trimer oligonucleotides attached to a polymer support through N-4 of a 2'-deoxycytidine nucleoside. [37] [38] This result was the innovation required for the first steps towards automated oligonucleotide synthesis. The advantage to automating the process was clear – with the growing oligonucleotide chain immobilized on a support it was easier to remove excess reagents without a loss of product. In 1967, Letsinger *et al.* concluded that the most efficient approach to solid-phase oligonucleotide synthesis was functionalising the nucleoside at the 3' hydroxyl group, a process still carried out today. [39] The major disadvantage of Letsinger's approach was that the support was prone to swelling – a problem that was overcome in the early 1980's by Caruthers. Caruthers and Matteucci published the use of inorganic material, such as silica, as the solid support, which was found to eliminate swelling and improve coupling efficiency. [40]
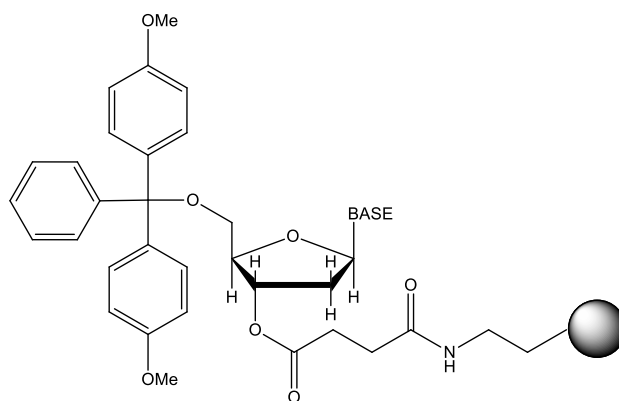
Figure 1.13. A solid-support for oligonucleotide synthesis fully protected at the 5'-hydroxyl group and base.

Oligonucleotide synthesis is normally performed on automated synthesisers using controlled pore glass (CPG) as the solid-support. [41] Typically, the first nucleoside required for synthesis of the oligonucleotide chain is attached to the CPG support *via* a long chain alkyl amine at the 3'-hydroxyl group (Figure 1.13). On the support, the nucleoside can be a fully protected adenine, cytosine, guanine or thymine and the 5'-hydroxyl moiety is protected with a DMT group. The CPG is housed in a column that is placed directly into the synthesiser. The phosphoramidites and reagents are injected into the column, flow over the CPG and finally washed away after each step of the synthesis cycle.
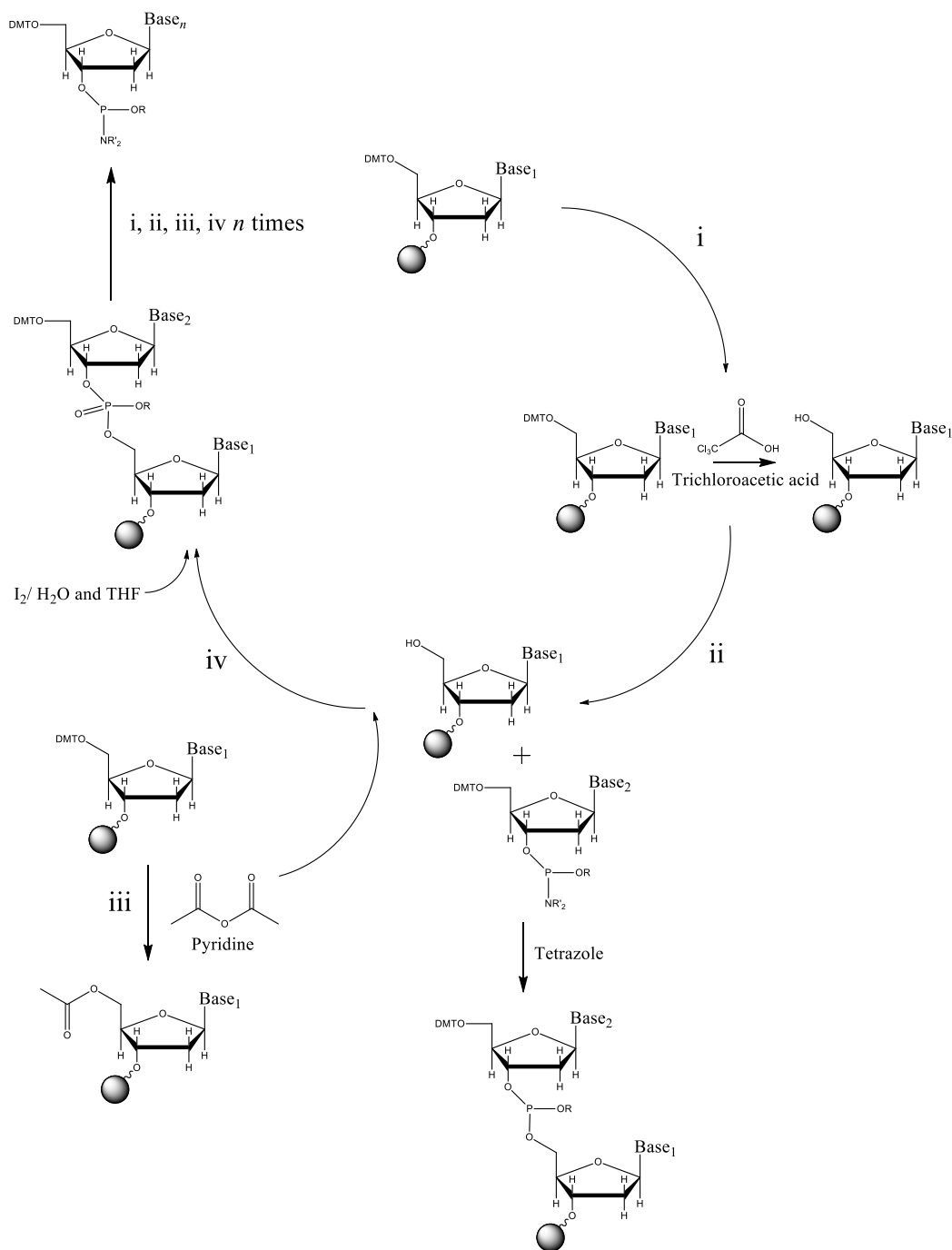
Figure 1.14. Overview of the solid-phase oligonucleotide synthesis cycle using the phophoramidite method. i. Deprotection ii. Coupling iii. Capping iv. Oxidation. Where R is a cyanethyl group and R'₂ is an N, N-diisopropyl group.

1.1.5.2   Oligonucleotide Synthesis Cycle

Oligonucleotide synthesis proceeds in a 3'- to 5'-direction, with each nucleotide delivered to the column one-by-one over four steps (Figure 1.14):

(i) Deprotection

Nucleosides immobilized on the solid support, and in phosphoramidites, are equipped with a 5'-hydroxyl-protecting DMT group that must be removed in order to grow the oligonucleotide chain. This is achieved in mild acidic conditions, such as addition of trichloroacetic acid, which liberates the DMT cation. The cation has a distinctly bright orange colour and a high extinction coefficient that allows the real-time monitoring of reaction progress during synthesis. By comparing the values of liberated DMT groups, an indication of the coupling efficiency of the phosphoramidites can be achieved. The free 5'-hydroxyl group is available to react with another phosphoramidite.

(ii) Coupling

The coupling step involves the formation of a phophite link between the deprotected 5'-hydroxyl group of the immobilized nucleoside and the 3'-hydroxyl group of a secondary nucleoside phosphoramidite. This is achieved under weakly acidic conditions, typically using a tetrazole derivative such as 5-ethylthiotetrazole (ETT). When the incoming phosphoramidite and the tetrazole are mixed in the column, the N, N-diisopropyl group leaves the 3'-phosphate, allowing the formation of the phosphite linkage between the 3'-hydroxyl group of the phosphoramidite and the 5'-hydroxyl group of the immobilized nucleoside.

(iii) Capping

The coupling step proceeds to ~ 99 % efficiency leaving a small number of molecules with unprotected 5'-hydroxyl groups. [42] These exposed groups can react with other phosphoramidites in subsequent coupling steps forming failure sequences that can become problematic during later purification stages. To prevent this from occurring, the 5'-hydroxyl groups are acetylated using acetic anhydride in THF/ pyridine solution and catalysed using N-methylimidazole. [43]

(iv) Oxidation

The final step in oligonucleotide synthesis is oxidation, where the reactive P $^{(III)}$ phosphite triester is converted to a stable phosphotriester P $^{(V)}$. Oxidation is achieved

by the addition of iodine, mixed with water and THF, and pyridine, which is added to neutralize the formation of HI.

Oxidation marks the end of one cycle and the addition of one nucleoside to the oligonucleotide chain. The steps are repeated for each subsequent phosphoramidite until the desired length of oligonucleotide has been synthesised.

1.1.5.3   Oligonucleotide Synthesis – Cleavage and Deprotection

Once the desired oligonucleotide has been synthesised it is necessary to cleave the oligonucleotide from the solid support and remove the protecting groups on the bases and the phosphate group (Figure 1.15). Cleavage can be achieved in one hour at room temperature by employing concentrated ammonium hydroxide to hydrolyse the ester linkage between the 3'-hydroxyl group of the nucleoside and the long-chain alkyl amine of the solid support. To remove the protecting groups from the exocyclic amine bases and the β-cyanoethyl group from the phosphate concentrated ammonium hydroxide is applied for a greater length of time and, typically, at an elevated temperature; 55 °C for 16 hours or room temperature for 48 hours. Other exocyclic amine groups are available, for example phenoxyacetyl dA and dimethylformamidine dG, that provide milder deprotection conditions and, in addition, alternative agents to ammonium hydroxide are available which can reduce the time and temperature required for removal of protection groups. [44] [45] [46] [47] [48]

When deprotection is complete the resulting mixture contains failure sequences, protecting groups and the desired oligonucleotide, which must be separated before the oligonucleotide can be used.
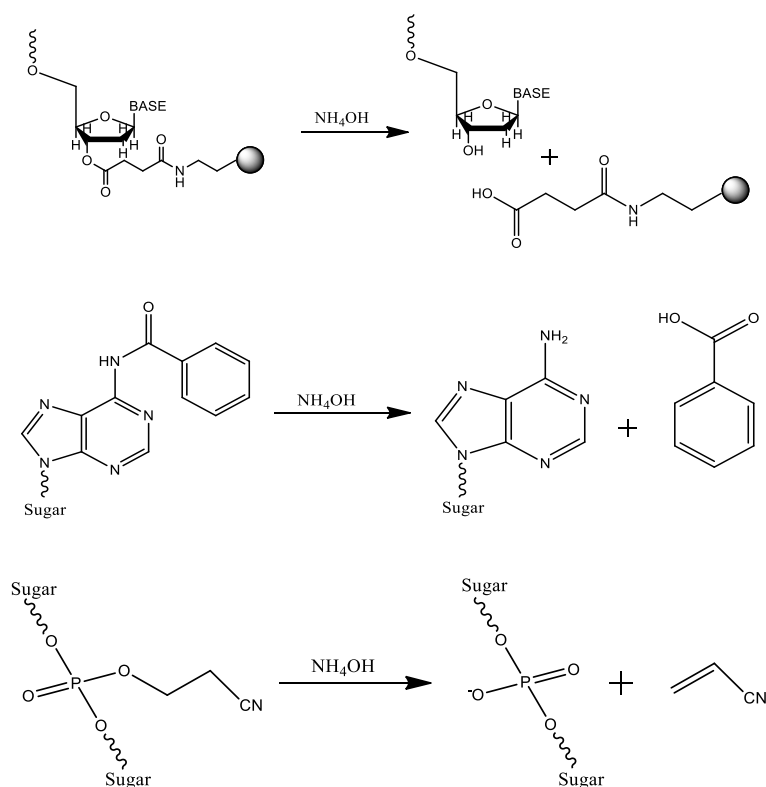
Figure 1.15. Deprotection of oligonucleotides, from top to bottom: cleavage of ester linkage between solid support and oligonucleotide, removal of exocyclic amine protecting groups and removal of β-cyanoethyl group from phosphate by concentrated ammonium hydroxide.

1.1.5.4   Purification of Oligonucleotides

The deprotected oligonucleotide solution contains a number of impurities, the most abundant of which are shorter failure sequences that arise due to inefficient capping of the 5'-alcohol of the phosphoramidite. It is necessary, then, that these failure sequences, as well as other impurities, are isolated from the mixture before the desired oligonucleotide can be used. The most common methods employed for oligonucleotide purification are:

- Polyacrylamide gel electrophoresis (PAGE), and
- High performance liquid chromatography (HPLC)

The choice of method is largely dependent on the type of oligonucleotide and the application.

1.1.5.4 (a) Polyacrylamide gel electrophoresis (PAGE) purification

PAGE is a technique used to purify oligonucleotides by separating the components according to variations in length. [49] The oligonucleotide mixture is suspended in a container of polyacrylamide gel, which is attached to a power source. As an electric field is applied across the gel, the oligonucleotides separate, according to length, due to the affinity of the negatively charged phosphate backbone to the positive electrode. The mobility of a fragment in the gel is determined by the net negative charge of the phosphate backbone, *i.e.* longer fragments with a larger net negative charge move towards the anode more slowly due to increased resistance within the gel, while shorter fragments with a smaller net negative charge can migrate towards the anode faster, experiencing less resistance from the gel. In respect to oligonucleotide purification, this is due to smaller failure sequences that terminate closer to the anode due to their reduced net negative charge from the sugar-phosphate backbone compared to the full-length product oligonucleotide which will terminate closer to the cathode due to having more negatively-charged sugar-phosphate linkages. Secondary structures can interfere with the mobility of the oligonucleotide through the gel so incorporation of additives such as formamide or urea (which interrupt hydrogen bonding in DNA) are commonly used in a method known as denaturing PAGE purification. [50] The oligonucleotides can be visualized on the gel by incorporating a dye stain into the gel, such as ethidium bromide, which fluoresces under UV light when intercalated into DNA.

1.1.5.4. (b) High-performance liquid chromatography (HPLC) purification

Liquid chromatography is a separation technique where the analyte, mixed in a mobile phase, is pumped through a column containing a stationary phase for which the components of the mobile phase have different affinities. Separation is achieved according to the strength of interactions between the analyte and the stationary phase. In respect to oligonucleotide purification, and other biomolecule analysis, high performance liquid chromatography (HPLC) is commonly coupled to UV-Vis spectroscopy to separate the desired sequence from the failure sequences. There are a number of HPLC methods employed for oligonucleotide purification, including reversed-phase, ion-exchange and size-exclusion HPLC.

(i)   Reversed-phase   high   performance   liquid   chromatography (RP-HPLC)

Reversed-phase high performance chromatography (RP-HPLC) separates oligonucleotides, and other biomolecules, according to differences in hydrophobicity. [51] In RP-HPLC, the stationary phase is non-polar, usually constructed from silica functionalised with long chain alkyl groups, commonly C_8 (octyl silane) or C_{18} (n-octadecyl silane). In order to aid elution of the analyte, the mobile phase is a combination of an aqueous buffer and an organic solvent. The organic solvent is water-miscible, usually acetonitrile or methanol, while the buffer is selected to maintain pH. Since oligonucleotides are negatively charged biomolecules, the aqueous buffer is usually an ion-pairing agent, for example triethylammonium acetate (TEAA), which aids binding of the oligonucleotide to the stationary phase.

In RP-HPLC, elution of the analyte is achieved by differences in hydrophobicity, with the more hydrophobic species retained longest on the column due to increased affinity for the stationary phase. The organic solvent component of the mobile phase is usually raised incrementally, *i.e.* gradient elution, during the run-time of the purification, in order to resolve the analytes in a minimum of time.

Automated oligonucleotide synthesis allows the user to keep the final DMT group "on" the final base in the oligonucleotide sequence. This method greatly aids purification as the DMT group provides a hydrophobic "handle" that greatly increases the affinity of the desired oligonucleotide for the stationary phase; thereby ensuring the desired oligonucleotide is completely separated from the non-DMT incorporated failure sequences. While this method is useful, it does require another post-purification step in order to remove the DMT group from the oligonucleotide. However, the resolution achieved by DMT-on RP-HPLC remains an attractive method for oligonucleotide purification.

(ii)   Ion-exchange chromatography (IE-HPLC)

Ion, or anion, exchange high performance liquid chromatography (IE-HPLC) separates oligonucleotides, and other biomolecules, according to differences in charge. [52] Oligonucleotides are polyanionic, containing many charged phosphate

groups, which are separated according to the length of the sequence. The stationary phase is commonly composed of agarose or cellulose beads functionalised with, for negative analytes, an anion exchanger like diethyl aminoethyl (DEAE). The mobile phase consists of an aqueous buffer to maintain a constant pH and a salt solution that acts to compete with the adsorbed analyte components for binding to the charged functional groups on the surface of the stationary phase. Like RP-HPLC, the mobile phase is introduced *via* an incremental gradient that increases the salt concentration to desorb the stationary phase-bound oligonucleotides. The longer, therefore more charged sequences, i.e. the desired oligonucleotide, are retained longer on the column due to being more charged than the shorter failure sequences. IE-HPLC is usually accompanied by a size-exclusion chromatography step to remove the excess salts from the oligonucleotide sequence.

(iii)   *Size-exclusion high performance liquid chromatography (SE-HPLC)*

Size-exclusion high performance liquid chromatography (SE-HPLC) separates biomolecules, oligonucleotides or proteins, according to differences in size. [53] The stationary phase is constructed from small, porous polymeric beads that are designed in such a way as to allow only small molecules to pass through the pores, while larger molecules flow straight through the column. In oligonucleotide purification, after IE-HPLC, the salt molecules are removed by size-exclusion, called "desalting", because the salt molecules are small enough to fit in to the pores, while the larger oligonucleotide molecule cannot fit in to the pores and elute unretained from the column. The mobile phase in this process is strictly employed as a solvent carrier for the analyte and does not participate in the separation. Size-exclusion chromatography can be used to separate other small molecules by selecting a column with appropriate pore sizes.

1.1.6 Modification of Oligonucleotides

Solid-phase oligonucleotide synthesis provides a robust chemistry to incorporate functional moieties (dye labels, surface seeking groups, other biomolecules, *etc*) into a desired oligonucleotide sequence, tailoring the structure for specific applications, such as those mentioned previously, *i.e.* PCR, microarrays, DNA sequencing and gene therapy. [21] [22] [23] [24] [25] An oligonucleotide provides many avenues for

attachment of such modifications, for example at the 5'-terminus *via* a modified phosphoramidite, or at the 3'-terminus *via* a modified solid support, or mid-sequence by incorporating functionality at the C-5 position of a pyrimidine base or the C-8 position of adenine. In addition, modification can be made to the sugar and phosphate backbones of oligonucleotides in order to, for example, increase the stability of the oligonucleotide in a duplex.

5'-modification of an oligonucleotide is commonly achieved *via* a phosphoramidite with the desired modification "built" in. In this manner, the modified phosphoramidite is incorporated into the oligonucleotide as the final base in the sequence during automated synthesis. Coupling of the modified phosphoramidite to the oligonucleotide is achieved by standard deprotection of the 5'-alcohol of the final base and activation/ coupling of the phosphoramidite to the free alcohol. Using a 5'-modified phosphoramidite is common practice in automated oligonucleotide synthesis for incorporating, for example thiol, [54] amino [55] or fluorescent labels. [56] 5'-modifiers are commercially available for a range of applications and some examples are shown in figure 1.16 and figure 1.17.
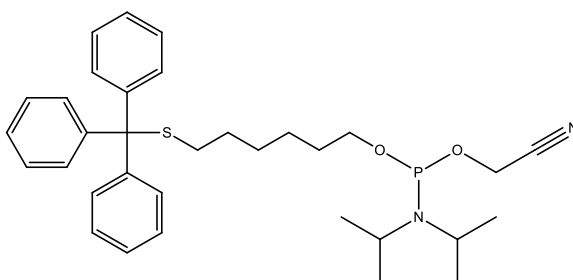
Figure 1.16. Commercially available 5'-thiol phosphoramidite. The thiol (-SH) is protected by a DMT group that is removed post-purification.
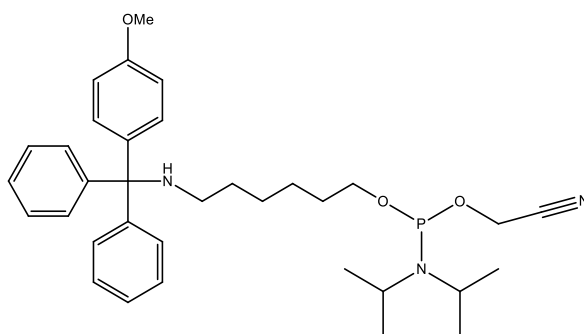
Figure 1.17. Commercially available 5'-amino phosphoramidite. The amino (-NH₂) *group is protected by a monomethoxytrityl (MMT) group that requires extended* *deprotection protocols to be subsequently removed post-purification.*

The 5'-terminus of oligonucleotides is probably the most common location for modification due to ease of access. However, 3'-modification is possible by using specialised solid-supports with the required modification attached directly to the CPG. Since oligonucleotide synthesis progresses in a 3'- to 5'-direction, the modified support includes a branched, protected alcohol adjacent to the modification that is readily deprotected using standard synthesis protocols to facilitate the step-wise addition of the base phosphoramidites. [57] [58] When using 3'-modified supports, the first base in the sequence, usually attached to the CPG, must now be added to the synthesis cycle. There are many commercially available 3'-modified CPG columns (figure 1.18), including, 3'-amino, -thiol, fluorescent labels, *etc*.
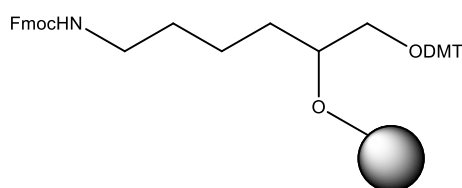
Figure 1.18. Commercially available 3'-amino modified CPG column. The -NH₂ *group is protected by Fmoc and the hydroxyl group is protected with DMT which* *must be removed to grow the oligonucleotide chain.*

Modification of the sugar component of an oligonucleotide is a convenient method for conferring extra stability and resistance to enzymes. One of the more widely

known sugar modifications is locked nucleic acid (LNA). [59] LNAs are ribonucleotide analogues containing a methylene bridge between the 2'-oxygen and 4'-carbon of the ribose sugar (Figure 1.19). LNA is known to have high binding efficiencies for both DNA and RNA, improving thermal stability and general selectivity, thereby making their incorporation into oligonucleotides an attractive prospect for use as diagnostic or therapeutic probes. In respect to oligonucleotide synthesis, LNAs are commercially available as phosphoramidites and simply replace the standard DNA phosphoramidites during synthesis.
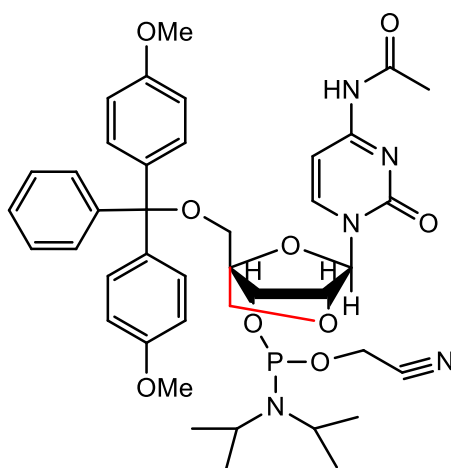
Figure 1.19. A commercially available locked nucleic acid (LNA) phosphoramidite. The methylene bridge between the 2'-oxygen and the 4'-carbon is highlighted in red.

Backbone modification involves alterations to the phosphodiester linkages between bases, which can offer enhanced stability, and resistance to enzymatic attack. One example of backbone modification is phosphorothioate oligonucleotides. [60] Phosphorothioate oligonucleotides contain a sulfur atom on the phosphate group, replacing the charged oxygen group during the oxidation step of oligonucleotide synthesis (Figure 1.20). This is routinely achieved by replacing the oxidising agent with a sulfurising agent, 3-ethoxy-1, 2, 4-dithiazoline-5-one (EDITH), during synthesis. Other backbone modifications exist, for example, peptide nucleic acid (PNA), which is another analogue of DNA capable of forming Watson-Crick base pairing with complementary DNA and shows promising antisense capabilities. [61] [62] PNA oligonucleotides contain a N-(2-aminoethyl)-glycine unit linked by amide bonds serving as the oligonucleotide backbone, while the pyrimidine and purine

bases are attached *via* methylenecarbonyl groups (Figure 1.21). PNA provides increased resistance to nucleases and are stable across a wide range of pH's making PNA-incorporated oligonucleotides ideal candidates for antisense therapeutics.
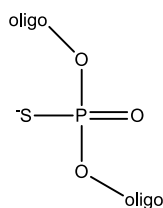
Figure 1.10. A phosphorothioate linkage incorporated into an oligonucleotide. The charged oxygen is replaced by sulfur in the phosphodiester linkage.
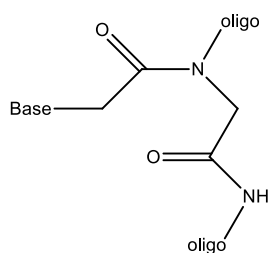
Figure 1.21. A peptide nucleic acid (PNA) linkage incorporated into an oligonucleotide. The phosphodiester backbone is replaced by aminoethyl-glycine linkages with the bases attached via methylenecarbonyl groups.

1.1.7 Determination of DNA Duplex Stability

The duplex, or double stranded (ds), form of DNA is constructed from two individual strands of polynucleotides linked and bound together *via* hydrogen bonds in a manner known as Watson-Crick base-pairing. The number of hydrogen bonds taking place between the two polynucleotides governs the stability of the DNA duplex. The stability of a duplex, either DNA isolated from cells or DNA hybridisation between complementary oligonucleotides, can be measured by spectrophotometry using UV-Vis. DNA absorbs light in the ultraviolet region of the electromagnetic spectrum, between ~ 260 and 280 nm, caused by electronic transitions taking place within the purine and pyrimidine bases. A DNA duplex will absorb more UV light than single-stranded DNA in a process known as hypochromicity – a reduction in absorption due to base-base stacking interactions between nucleotides. To measure this effect, DNA is monitored at, typically, 260 nm while increasing the temperature to produce a

"melting curve", in a process called DNA melting (Figure 1.22). The point at which half of the DNA is in the double-stranded duplex state and half is in the single-stranded state is known as the melting temperature, or T_m. The determination of T_m is useful for tools such as PCR, sequencing or microarrays, where oligonucleotide primers must be designed to specifically hybridise at a particular temperature to the target DNA. There are a number of factors that can influence the stability (and, hence, the T_m) of a DNA duplex, including: [64]
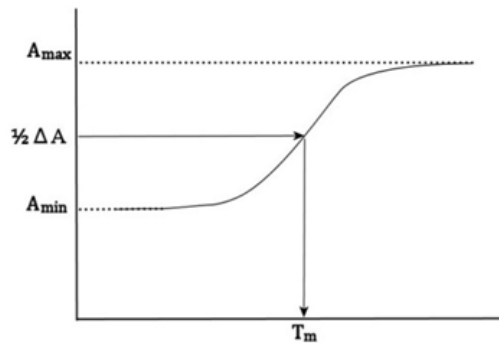
Figure 1.22. A typical melting curve obtained from the denaturation of a DNA duplex. Duplex, or double stranded (ds) DNA, absorbs less light than single-stranded (ss) DNA resulting in a transition. The point at which half the DNA is in the ds- and half is in the ss-state is known as the melting temperature, or T_m.

(i) Base Composition

Duplexes containing a higher ratio of G-C base-pairs have higher melting temperatures due to G-C base-pairs having three hydrogen bonds compared to A-T base-pairs which only have two hydrogen bonds.

(ii) Temperature

The rate of duplex re-association after melting is governed by temperature – at lower temperatures the re-association rate increase, then plateaus and, finally, decreases. At high temperatures, however, the re-association rate of DNA reduces to zero – resulting in instability within the duplex and the subsequent melting of the two polynucleotide strands.

(iii)   ***Counterion Concentration***

DNA duplexes are long, polyanionic molecules and, as such, require monovalent cations, such as salt, usually in the form of Na $^+$, to shield the negative phosphodiester backbone in order for the two polynucleotide strands to come together. The concentration of the salt ions present, therefore, has an effect on the stability of the duplex, and, therefore the T_m of the duplex.   At high salt concentrations the melting temperature is higher than at lower salt concentrations. In addition, divalent cations, such as Mg $^{2+}$, can also raise the melting temperature of DNA duplexes. However, conventionally, Na $^+$ is used as a counterion species.

(iv)   ***Sequence Length***

Short duplexes, such as those comprised of chemically synthesised oligonucleotides, tend to have significantly different melting temperatures compared to longer duplexes obtained from natural sources. This arises from the energy required to form an initial base-pair, which in longer duplexes, is insubstantial.   This results in concentration dependence for shorter duplexes – the higher the concentration, the higher the melting temperature.

(v)   ***Modifications***

Modifications to the DNA bases or the phosphodiester backbone can have a significant effect on the melting temperature of duplexes. Commonly, modifications are built into chemically synthesised oligonucleotides, such as LNA or PNA, which can improve duplex stability, thereby increasing the melting temperature.

(vi)   ***Solvents***

Duplex stability can be affected by the addition of solvents, either increasing or decreasing the melting temperature depending on which solvent is employed. Additives such as urea or formamide are known to lower the melting temperature of duplexes, while others such as polyethylene glycol (PEG) or dextran sulphate are known to improve hybridisation kinetics and increase the melting temperature.

1.2 DNA Detection and Analysis

The elucidation of the chemical structure of DNA has allowed research to blossom across various disciplines, including breakthroughs in fields such as molecular biology, biochemistry, genetics and biotechnology. This has allowed researchers to discover the fundamental role of DNA in all of life's processes – the importance of heredity and the diagnosis of infectious disease have had considerable input in medicine, medical diagnostics and forensics. Discussing all of these developments in detail is beyond the scope of this thesis; however, the techniques associated with the detection of DNA for diagnostic applications are reviewed.

1.2.1 DNA Sequencing

The order in which the four DNA bases are read in an organism has a long and diverse history. DNA sequencing was first reported by Walter Gilbert and Allan Maxam at Harvard and Fredrick Sanger at the University of Cambridge. [65] [66] The Maxam-Gilbert method of DNA sequencing, known as the cleavage method, involves using chemical agents to break the individual nucleotide bases (adenine, cytosine, guanine, and thymine) of a terminally labelled DNA sequence. The cleavage at each base produces a set of radioactive (^{32}P) fragments extending from the labelled end of the DNA sequence to the position of the cleaved base. These fragments can then be separated by polyacrylamide gel electrophoresis, resolving the fragments according to size. The Sanger method, which is the preferred method of DNA sequencing used today and which all next-generation DNA sequencing technology has been built upon, uses a chain-termination process to determine the nucleotide sequence (Figure 1.23). [67] This process requires the DNA template, a DNA primer and deoxynucleotidetriphosphates (dNTPs). The reaction mixture is divided into four samples, each sample corresponding to one of the nucleotides (adenine, thymine, guanine and cytosine). As the DNA polymerase reads the DNA primer, it incorporates one of the dNTPs into the growing chain. However, into each of the reaction mixtures, in addition to the dNTPS is one of four dideoxynucleotidetriphosphates (ddNTPs) corresponding to each nucleotide. The ddNTPs block chain elongation, which is achieved because the 3'-hydroxyl group is missing from the ddNTP thereby preventing the formation of a phosphodiester bond

between the nucleotides. The result is a mixture of fragments that can be visualised, by incorporation of ^{32}P label, on a polyacrylamide gel. Each band in the gel corresponds to a DNA fragment that has been terminated by one of the ddNTPs. Breakthroughs in fluorescent labelling led to the development of fluorescently labelled ddNTPs and primers that can be incorporated into the chain-termination method leading to automated, high-throughput sequencing. [68]

In the post-Human Genome Project era research has progressed in the development of next-generation DNA sequencing platforms, such as micro-electrophoretic methods, [69] sequencing by hybridisation, [70] real-time observation of single molecules using nanopores [71] and cyclic-array sequencing. [74] Recently, DNA sequencing has been successfully used to diagnose difficult-to-identify diseases in humans – the first time the technology has been successfully used in the clinic. [75]
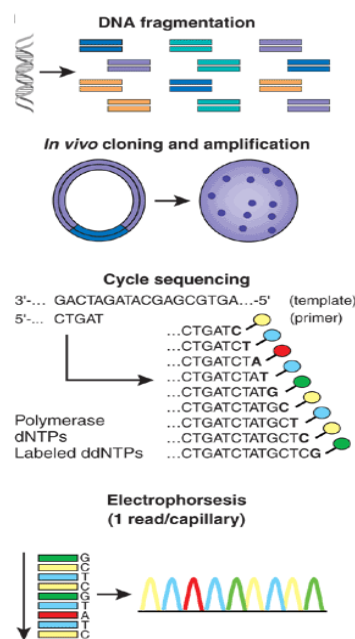
Figure 1.23. Representation of high-throughput shotgun Sanger sequencing. Genomic DNA is fragmented, cloned to a plasmid vector and used to transform E. coli. Each sequencing cycle occurs within a microliter-scale volume, generating a ladder of ddNTP-terminated, dye-labelled products, which are subjected to high-resolution electrophoretic separation. The fluorescently labelled DNA fragments pass a detector to generate a four-channel emission spectrum containing the sequencing trace. [76]
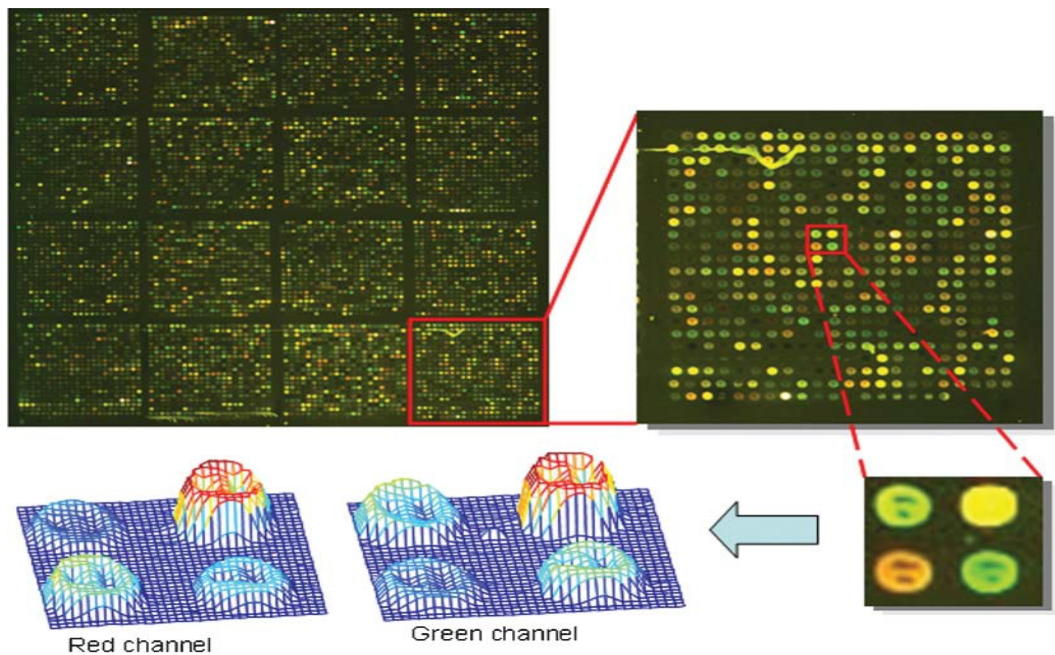
Figure 1.24. A typical spotted microarray image, showing enlargements of a sub-array and four spots. The mesh plots show the intensity maps of the red and green channels individually for the four spots. [77]

1.2.2 Microarrays

Modern microarray technology evolved from Southern blotting and dot blotting, where target DNA is attached to a substrate and probed with complementary DNA to determine the identity of the sequence. [78] [79] Early DNA microarrays were performed on filter paper, [80] however modern microarrays typically use glass slides. [81] [25] In a basic DNA microarray experiment, the support (usually a glass microscope slide) is arranged into discrete "spots" each containing millions of immobilized probe DNA sequences that are complementary to the target DNA sequence. The target DNA is fluorescently labelled and hybridised on the surface of the microarray. Successful hybridisation results in an increase in fluorescence due to the complementarity between the immobilized probe DNA and target DNA sequence. An example of a spotted microarray image is shown in figure 1.24. The basic operating principle is the same in most microarray technologies; however, the method for depositing DNA on the substrate varies from *in situ*-hybridised high-density oligonucleotide arrays, [82] [83] photolithography-activated arrays, [84] [85] "printing" with ink-jet technology, [86] high-density bead arrays [87] [88] and electronic

microarrays. [89] DNA microarrays are commonly used for gene expression and whole-genome analysis. [90] However, microarrays have been utilized as platforms in diagnostics of infectious diseases. Microarrays have been used for the detection of bacteria in blood cultures, [91] for parasitic and viral pathogen detection, [92] [93] identification of HIV-1 and hepatitis B and C viruses, [94] [95] [96] rapid detection of high-risk HPV, [97] identification of MRSA, [98] and probing drug-resistance in *M. Tuberculosis.* [99]

1.2.3 DNA Amplification

1.2.3.1 Polymerase Chain Reaction

Samples isolated for detection of specific DNA sequences usually lack a key component – a detectable level of DNA. The low concentrations in a sample can be overcome by enzymatic amplification of the DNA present to a more readily detectable level. This method is known as the polymerase chain reaction (PCR). Introduced by Kary Mullis in 1983, PCR has become one of the most valuable and indispensable techniques in the molecular biology tool kit, finding uses in medicine, diagnostics and forensics. [100] [101] PCR allows for minute quantities of DNA to be amplified into a billion identical copies in a matter of hours, thereby aiding further analysis of the DNA. [102] [103] [104] To accomplish this a reaction mixture containing two oligonucleotide primers, dNTPs (A, C, G and T), magnesium chloride, buffer solution, the DNA to be amplified and a heat-stable DNA polymerase undergoes repeated stages of heating and cooling to produce identical copies of the target DNA sequence. A schematic representation of the PCR process is shown in Figure 1.25. The procedure involves heating the double-stranded target DNA to denature the double helix thereby producing two single-stranded DNA sequences. The reaction is then cooled to allow the two oligonucleotide primers, which are complementary to the region to be amplified, to anneal. Finally, the reaction is heated to an optimum temperature to allow the DNA polymerase to read along the primers, producing two identical copies of the dsDNA target. This process is repeated over several cycles to produce more and more of the required target. Typically, a PCR consists of three steps continuously repeated over a number of defined cycles. The steps are:

1. **Denaturation**   The double stranded DNA is heated to around 95°C in order to separate the strands. This process lasts around 1 minute.

2. **Annealing**   The temperature is dropped to around 55°C to let the primers bind to their specific sites along the now single-stranded DNA. This process takes 1 minute.

3. **Extension**   The DNA polymerase extends the primers by adding new nucleotides to the sequence at a temperature of around 70°C. This process takes around 1 minute.
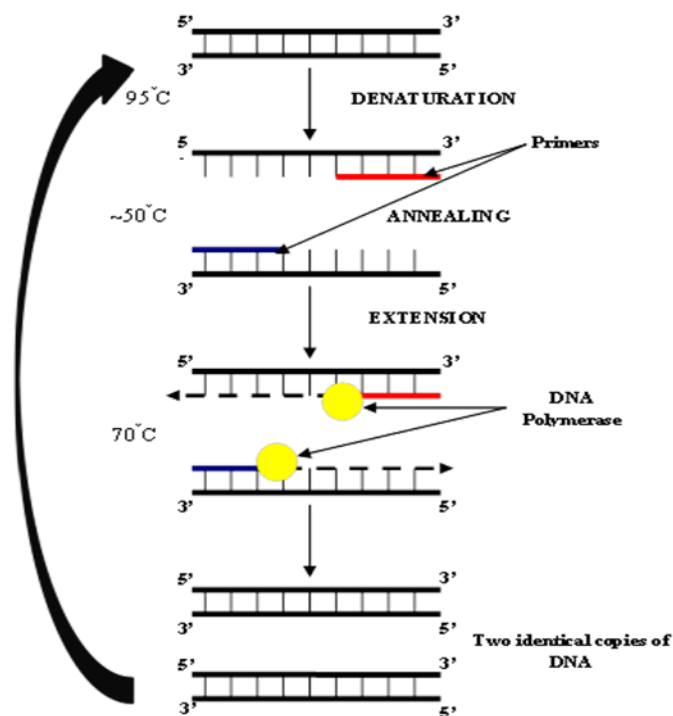
*Figure 1.25. Schematic representation of the polymerase chain reaction. First, the target DNA is heated to 95 °C to separate the two strands (**DENATURATION**); second, the temperature is lowered to ~50 °C to allow the primers to hybridise to their complementary regions on the target (**ANNEALING**); third, the DNA polymerase reads along the primer, sequentially adding the complementary nucleotide to form a new target duplex (**EXTENSION**) and finally, the cycle is repeated several times to generate more target DNA.*

The heat-stable DNA polymerase, isolated from *thermus aquaticus* in 1976, has an optimum temperature at around 70°C and can withstand the high temperatures required during the reaction to denature the DNA duplex. [105] The amplification process is an exponential reaction, with potentially 2^n, where *n* is the number of cycles in the reaction, of copies of target DNA produced. Considerable care must be taken when using PCR to reduce contamination, as the presence of foreign DNA not belonging to the target of interest has the potential to be amplified producing false results. After PCR is complete, the product is isolated by gel electrophoresis. The presence of the correct product is confirmed by comparing the bands in a gel with a molecular weight marker (known as a DNA ladder) of known DNA lengths.

Since PCR's inception, a number of variations on the basic protocol have emerged. For example; hot-start PCR, where the activity of the polymerase is only activated once the denaturation temperature is reached, cleaving inhibiting groups from the enzyme thereby reducing non-specific amplification; [106] asymmetric PCR, where one of the strands is amplified preferentially by an excess of one of the primers, generating ssDNA; [107] multiplex PCR, where a number of different primers are added to the one reaction mixture, resulting in the simultaneous amplification of multiple, different DNA sequences; [108] nested PCR, where two sets of primers are used to amplify the region of interest, thereby reducing non-specific DNA amplification [109] and reverse transcription PCR (RT-PCR), where DNA is amplified from RNA by using reverse transcriptase – an enzyme that transcribes RNA into DNA which is then amplified by PCR. [110]

1.2.3.2   Isothermal Amplification

While PCR requires repeated heating cycles to initiate amplification, other techniques exist where isothermal amplification of the target DNA is achieved. Some of these techniques include transcription mediated amplification (TMA) and nucleic acid sequence based amplification (NASBA), [111] rolling circle amplification (RCA), [112] strand displacement amplification (SDA), [113] loop mediated isothermal amplification (LAMP), [114] recombinase polymerase amplification (RPA) [115] [116] and helicase-dependent amplification (HDA). [117]

1.2.4 Fluorescence Detection of Nucleic Acids

To confirm the desired product was amplified, earlier incarnations of PCR required that the products be compared on gels with molecular weight markers post-amplification. This, however, is time consuming and requires opening of the PCR tubes, thereby exposing the products to possible contamination. To overcome this, modern PCR techniques adopt a "closed tube" format, where PCR is coupled with fluorescence detection to allow real-time monitoring of target amplification during the reaction.

1.2.4.1   Real-Time Polymerase Chain Reaction

1.2.4.1 (a)   Non Sequence-Specific DNA Detection

The simplest method of achieving real-time fluorescence detection during amplification is using DNA intercalating dyes. [118] The most common dye, SYBR green I, is a small molecule DNA binder that is weakly bound to ssDNA but has a high quantum yield when bound to dsDNA. [119] [120] [121] The major advantage of SYBR green I is high sensitivity due to the fact that multiple SYBR green molecules can bind to one duplex. [122] However, SYBR green I binds indiscriminately to dsDNA, meaning it can bind to non-specifically amplified DNA, generating false positive results.

1.2.4.1 (b)   Sequence-Specific DNA Detection

(i)   Förster Resonance Energy Transfer (FRET)

The most common methodology to detect specific DNA sequences during PCR is the process whereby fluorescence is induced by a probe only if hybridised to the complementary target DNA. This process is known as Förster resonance energy transfer (FRET). FRET relies on the distance dependence of a fluorophore and quencher pair. When in close proximity to one another fluorescence is quenched, however, increasing the distance between the pair activates fluorescence. The fluorophore acts as a donor and the quencher an acceptor so when in close proximity excitation energy is transferred from donor to acceptor using non-radiative energy transfer, returning the fluorophore to the ground state without emitting a photon. When the donor and acceptor are separated the fluorophore is able to achieve the

required emission spectrum. The FRET process is explained in Figure 1.26. The FRET concept has been utilized in detection techniques such as molecular beacons and TaqMan.
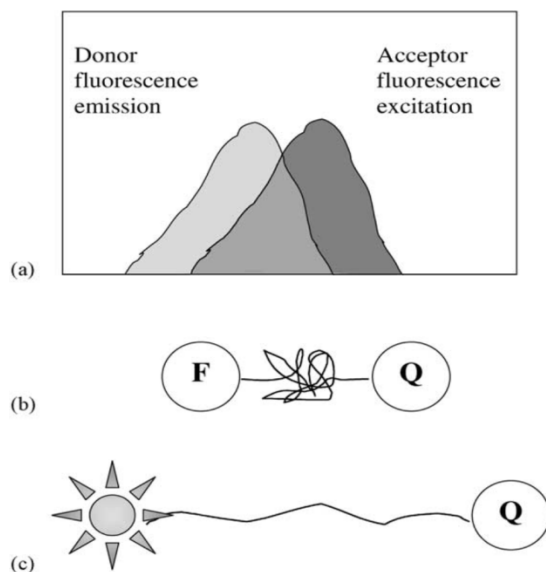
Figure 1.26. Diagram explaining the FRET process. (a) The overlapping spectra of the donor emission and the acceptor excitation, (b) with donor (F) and quencher (Q) in proximity, no fluorescent signal is generated, but (c) when separated, the donor is able to emit fluorescence uninhibited. [123]

(ii)   Molecular Beacons

Molecular beacons are oligonucleotide probes that can be used in PCR to generate real-time detection of the required target. [124] A typical molecular beacon consists of two major components: the stem and the loop. The stem constitutes two short oligonucleotides that are complementary to one another, a fluorophore attached at the 5'-end and a quencher attached at the 3'-end. The loop contains the region complementary to the target of interest. In the looped state, due to the close proximity of the donor-quencher pair, FRET is induced and no fluorescence is emitted. In the presence of the complementary target, a conformational change occurs, opening the loop to allow hybridisation and with the donor-quencher pair no longer in close proximity, fluorescence is induced. The formation of the hybridised loop-target duplex is more thermodynamically favourable than the stem section of the molecular beacon due to the presence of more bonded base-pairs. The mode of action of the molecular beacon is outlined in figure 1.27. Molecular beacon assays

have been utilized both free in solution [125] and in an array format. [126] Multiplex detection of DNA using molecular beacons can be achieved by incorporation of multiple fluorophores. [127]
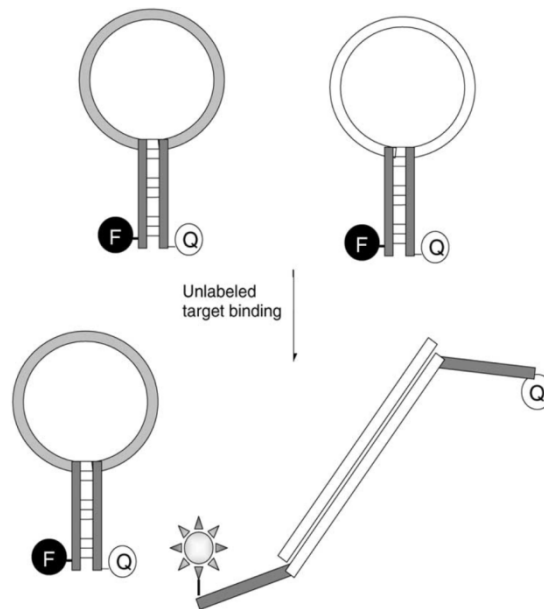
Figure 1.27. Mode of action of molecular beacons. Different oligonucleotide probe sequences are represented as coloured solid bars. In the hairpin configuration, the fluorophore and quencher are in proximity and no signal is formed. Upon specific target binding, the reporter group is able to fluoresce uninhibited and a signal is measured. [123]

(iii)   TaqMan

TaqMan probes exploit the 5'-exonuclease activity of *Taq* DNA polymerase to cleave an oligonucleotide from the target during the extension phase of PCR, inducing a fluorescence signal. [128] [129] The probe consists of an oligonucleotide modified with fluorescent dyes at both the 5'- and 3'-termini – one acting as the fluorophore and the other the quencher. [130] [131] The mode of action of a TaqMan probe is represented in figure 1.28. When unhybridised to the complementary target, FRET is induced and no fluorescence is observed. During the annealing phase of PCR, in addition to the primers hybridising, the TaqMan probe hybridises to the target down-stream of the primer. The *Taq* DNA polymerase has an inherent

5' to 3' exonuclease activity. Extension of the primers results in cleavage of the TaqMan probe from the target, releasing the fluorophore from the quencher, thereby eliminating FRET. Accumulation of the fluorescence signal can be monitored in real-time, eventually reaching a plateau as the TaqMan probes, like the primers are consumed, during the reaction. [132] Multiplex detection using TaqMan probes is possible by incorporation of different fluorescent dyes. [133] [134]
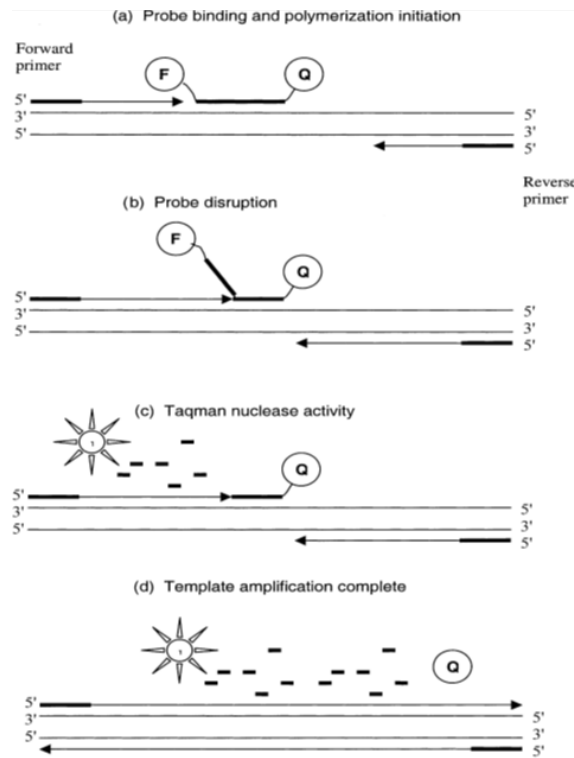
Figure 1.28. Mode of action of TaqMan probe. The probe has a quencher (Q) and a fluorophore (F). The F emission is quenched when bound to its target (a and b). The TaqMan enzyme initiates polymerization and separates F from Q, providing the fluorescence signal (c and d). [123]

The discovery of the structure of DNA has allowed research to blossom across the physical and life science disciplines, in addition to heralding the age of biotechnology. While it is outside the scope of this thesis to discuss all of these aspects, an interesting development in DNA-based research has been the merging of bio and nanotechnologies to create new methodologies for the sensitive detection of DNA.

1.3 Nanotechnology

Nanotechnology refers to the manipulation of matter on the molecular and atomic scale. More specifically, nanotechnology, or 'nanotech', is described as materials, devices or other structures with dimensions between 1 – 100 nanometres (nm). Norio Taniguchi, who was investigating semi-conductor processes, at the Tokyo University of Science, coined the term 'nanotechnology' in the mid-1970s. However, the basic concept of nanotechnology was inspired by Richard Feynman who, in the late-1950s, delivered his seminal speech entitled "There's Plenty of Room at the Bottom." [135] In his speech, Feynman postulated the "bottom up" approach to manipulating matter, stating that, in the future, it would be possible to write objects on the atomic scale; an idea he expressed by proposing the question *"why cannot we write the entire 24 volumes of the Encyclopaedia Britannica on the head of a pin?"* Feynman recognized that by improving the electron microscope much of the processes in biology that eluded scientists at the time could be answered, like the order of the bases in DNA and how they relate to amino acid and protein synthesis. He also looked to biology for inspiration, stating that cells are objects capable of so many amazing chemical feats – all on a small scale – so, he asks *"consider the possibility that we too can make a thing very small, which does what we want – that we can manufacture an object that maneuverers at that level"*. While only a vision to Feynman at the time, here he first describes the merging of biology and nanotechnology to probe biological processes, years before scientists would realise the technology to make it a reality, technology which today is almost synonymously linked to other scientific disciplines such as chemistry, biology and physics.

1.3.1 Nanomaterials: An Introduction

Nanoscale materials display unique chemical and physical properties compared to the bulk material due to quantum mechanical confinement of particles. This leads to favourable size-dependent optical, [136] electrical, [137] magnetic [138] and catalytic [139] properties, which can be tuned to suit any number of possible applications. Nanomaterials can be constructed from organic or inorganic materials by "top down" or "bottom up" process. Top down processes involve the physical manipulation of

the bulk material to assemble smaller materials using tools such as ball-milling, ion- and electron-beam lithography, photolithography, vapour deposition and etching. Bottom up processes rely on the assembly of nanoscale materials *via* chemical synthesis from building blocks composed of individual molecules, sometimes by self-assembly of the molecules or using techniques such as dip-pen nanolithography (DPN) to "write" molecules onto surfaces. Key examples of bottom up processes exist in biology, for example nucleic acids providing the information for the synthesis of proteins or chloroplasts harvesting light to produce chemical energy.

The tuneable optical and physical properties of nanomaterials such as metallic nanoparticles, [140] semiconductor nanocrystals (quantum dots), [141] carbon nanotubes, [142] nanowires, [143] nanoshells [144] and nanorods [145] make them attractive substrates for a variety of applications including biosensors, [146] drug delivery, [147] medical imaging [148] and cancer therapy. [149] In order to be utilized as biosensors, nanomaterials must be functionalised with biomolecules, such as DNA, [150] proteins, [151] aptamers [152] or antibodies, [153] to trigger a molecular recognition event between the nanomaterial and the target molecule in order to generate a detectable signal. To review all of these applications is beyond the scope of this work and the focus will primarily be on the synthesis and properties of metallic nanoparticles and their functionalisation with DNA for biosensing applications.

1.3.2 Metallic Nanoparticles

1.3.2.1   Nanoparticles: A Brief History

Nanoparticles can be produced from a number of different metals, such as gold, [154] silver, [155] copper [156] and platinum, [157] and their synthesis, characterisation and applications have been extensively reviewed in the literature. However, for the purposes of this work the focus will primarily be on nanoparticles constructed from gold (Au) and silver (Ag). From a historical perspective, nanoparticles were used in antiquity to colour glass and ceramics. Perhaps the most well known example of this is the Lycurgus cup – depicting King Lycurgus of Thrace as he is trapped by Ambrosia, who was transformed into a vine by Mother Earth, for his evil behaviour. [158] The Lycurgus cup is of particular interest because the glass appears

green in reflected light and red in transmitted light, an effect attributed to the gold nanoparticles dispersed throughout the glass (Figure 1.29). In addition to the unusual colorimetric properties of colloidal gold for use in glass and ceramics, there are documented examples throughout history where gold nanoparticles were employed for their supposed curative properties, where physicians would recommend patients to drink red solutions of dissolved gold nanoparticles. [154] However, it was Michael Faraday, in 1857 that reported the first scientific production of colloidal gold. [160] In his manuscript, Faraday outlines the formation of a deep-red solution of colloidal gold by the reduction of an aqueous solution of chloroaurate ($AuCl_4^-$). He also investigated the optical properties of dried colloidal gold thin films by exhibiting mechanical compression upon them, observing various reversible colour changes in what is regarded as the first scientific publication on colloidal gold.

Figure 1.29. The Lycurgus cup on display in the British Museum. Throughout the glass, colloidal gold nanoparticles are dispersed, resulting in a colour change from green in reflected light (left) to red in transmitted light (right). [159]

1.3.2.2   Synthesis of Gold and Silver Nanoparticles

The most common method for producing stable solutions of gold nanoparticles is the citrate reduction method. In this method, first reported by Turkevitch, an aqueous solution of $HAuCl_a$ is reduced using sodium citrate to produce nanoparticles ~ 20 nm in diameter. [161] However, in 1973, a method reported by Frens showed the production of gold nanoparticles with sizes ranging from 16 – 147 nm, which was accomplished by altering the ratio of reducing/stabilizing agents, *i.e.* citrate-to-gold ratio. [162] This method is still commonly used to produce stable gold nanoparticle solutions of different sizes.

While the Frens method allows the formation of gold nanoparticles with a loose ligand shell of controllable sizes, other methods, reported later, used alkanethiols to stabilize gold nanoparticles allowing gold nanoparticles to be produced with sizes in the range 1 – 5 nm. These methods were inspired by observations that thiol molecules form well-ordered monolayers on the surface of gold nanoparticles. [163] [164] [165] Mulvaney, in 1993, was the first to report the stabilization effect of alkanethiols on gold nanoparticles. [166] He used electrophoresis to deposit alkanethiol-capped gold nanoparticles onto a carbon-coated copper grid, observing that the interparticle distance depended on the length of the alkane chain used to stabilize the gold nanoparticles. A year later, the Brust-Schiffrin method for gold nanoparticle synthesis was published that utilized the stabilizing effect of alkanethiols on gold surfaces. This method, which was inspired by Faraday's two-phase system, uses tetraoctylammonium bromide to phase-transfer $AuCl_4^-$ to toluene and $NaBH_4$ as a reducing agent in the presence of dodecanethiol. [167] The nanoparticles produced were found to be in the range of 1 – 3 nm. However, by increasing the thiol/gold mole ratio it was found that smaller average core sizes could be obtained while fast reductant addition and cooler solutions produced more monodispersed particles. The Brust-Schiffrin method synthesis shifted to a single-phase system, published in 1995, using *p*-mercaptophenol to produce stabilized gold nanoparticles. [168] Other ligands have been investigated for their stabilizing effect on gold nanoparticles. However, to discuss all of these would be outside the scope of this thesis.

In a similar fashion to gold nanoparticles, silver nanoparticles are produced *via* reduction of a silver precursor, commonly $AgNO_3$. The chemical synthesis of silver nanoparticles was first reported in 1982 by Lee and Meisel who used citrate to reduce an aqueous solution of $AgNO_3$. [169] This method is attractive, as it does not require extensive laboratory skills to perform; a solution of sodium citrate is added to a boiling solution of $AgNO_3$ and stirred for approximately one hour before being allowed to cool. The citrate in the reaction not only acts as a reducing agent but also as a stabilizer for the silver nanoparticles. [170] Despite their synthesis being simple, citrate-reduced silver nanoparticles do have some drawbacks – there tends to be a large size distribution (20 – 600 nm) and a number of different shapes associated

with this method, which are not useful for bulk colloidal analysis. [171] In addition, citrate is not a particularly effective stabilizing agent and can be easily displaced from the surface. To this end, other synthesis methods for silver nanoparticles have been investigated over the years, including the borohydride reduction of $AgCl_4$, [172] ethylenediaminetetraacetic acid (EDTA) reduction of $AgNO_3$ [173] and hydroxylamine hydrochloride reduction of $AgNO_3$. [174] These methods have been the subject of many comparative studies in the literature. [175] [176] [177] [178]

Gold and silver nanoparticles are attractive substrates for biosensing applications due to their unique optical properties that are controlled by their size and shape. The most well known and most exploited property of gold and silver nanoparticles is the localized surface plasmon resonance band arsing when a particular wavelength of light interacts with the nanoparticles.

1.3.2.3 *Surface Plasmon Resonance (SPR)*

The strong ruby-red colour and strong absorbance in the visible region associated with gold nanoparticles arises from an interaction with light. When light – electromagnetic waves – interact with nanoparticles an oscillating cloud of electrons is induced at the nanoparticle surface, called surface plasmon resonance, which is responsible for producing the red colour in gold nanoparticles. The surface plasmon resonance phenomenon is produced due to the collective oscillation of conduction-band electrons at the surface of nanoparticles induced by an interaction with the incoming electromagnetic field (Figure 1.30). When the surface plasmon resonance is confined to nanometre sized particles, *i.e.* gold and silver nanoparticles, the plasmon is termed localized surface plasmon resonance (LSPR).

Gustav Mie, in 1908, published an influential manuscript entitled *"Contributions to the optics of turbid media, particularly of colloidal metal solutions"* in order to shed some light on the surface plasmon resonance phenomenon. [179] In his document, Mie applies Maxwell's equations to spherical particles with diameters comparable to the wavelength of light. Mie explained that the surface plasmon band in spherical particles is a result of dipole oscillations in the free conduction band electrons occupying the energy states directly above the Fermi energy level. [136] The surface plasmon band in gold (15 nm diameter) and silver (35 nm diameter) nanoparticles

results in absorbance at 520 nm and 400 nm, respectively, however, the absorbance is largely dependent on nanoparticle size, shape, temperature and the dielectric constant of the surrounding medium. [180]
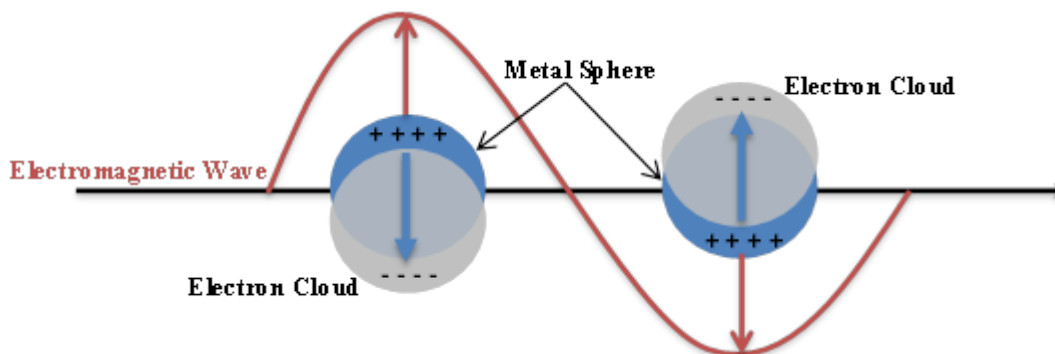
Figure 1.30. A schematic representation of surface plasmon resonance induced by an electromagnetic field in a metal sphere. Interaction with the electromagnetic field causes a net displacement of the negative charge at the positive metal core resulting in a charge difference across the metal sphere. A restorative force produces a dipolar oscillation.

The most useful feature of metallic nanoparticles for biosensing applications is the distance-dependent absorption characteristics of the surface plasmon band when two or more nanoparticles come into close proximity with one another. This proximity between nanoparticles results in a coupling of the surface plasmons, resulting in a red-shift of the absorbance of the nanoparticles to longer wavelengths. [181] The extent of the red-shift is largely distance-dependent; the shorter the distance between nanoparticles, the larger the red-shift in absorbance. [182] The plasmon coupling event is usually accompanied by a colour change, for example, gold nanoparticles change from a ruby-red colour to a blue-purple colour when the interparticle distance is decreased.

1.3.3 DNA-Linked Nanoparticles

The immobilization of alkanethiol moieties to the surface of gold nanoparticles was a much pursued avenue of research. However, in 1996 the thiol-gold relationship was taken to another level when two independent research groups published,

simultaneously, in the same issue of *Nature*, the functionalisation of gold nanoparticles with thiol-modified oligonucleotide sequences. [183] [184] Both publications outlined the discrete assembly of gold nanoparticles *via* a biomolecular recognition event, *i.e.* Watson-Crick DNA base pairing through hybridisation of complementary oligonucleotides. The assembly process was accompanied by a characteristic colour change, from red to blue, associated with gold nanoparticle aggregation. In addition, it was reported that the assembly process was reversible, since heating the bridging oligonucleotide duplex between the particles above the melting temperature resulted in the restoration of the red colour indicative of monodispersed gold nanoparticles. This research was a significant step towards interfacing nanotechnology and biology, inspiring further research into nanoparticle-based DNA biosensing approaches.

1.3.3.1 Oligonucleotide-Nanoparticle Assembly: An Introduction

In 1996, Chad Mirkin, of Northwestern University, published a manuscript in *Nature* entitled *"A DNA-based method for rationally assembling nanoparticles into macroscopic materials"*. [183] The manuscript outlined Mirkin's efforts to functionalise gold nanoparticles with thiol-modified oligonucleotides as well as their assembly into larger structures through DNA hybridisation. The method employed by Mirkin's group to accomplish this was to add an excess of 3'-alkane thiol-modified oligonucleotides to a colloidal suspension of gold nanoparticles so that each nanoparticle would have multiple oligonucleotides on its surface. Two batches of gold nanoparticles were prepared in this manner, each with differing oligonucleotide sequences that were non-complementary to one another. These two batches were then mixed and an oligonucleotide sequence added that was complementary to both oligonucleotides on the nanoparticles. Under hybridisation conditions, Watson-Crick base paring occurred between the oligonucleotides, resulting in duplex formation. This biomolecular recognition event led to aggregation of the gold nanoparticles, accompanied by a characteristic colour change from ruby-red to blue-purple associated with the coupling of the surface plasmons of the nanoparticles. As the assembly process continued it was observed that the nanoparticle solution turned colourless as a result of large aggregates forming and precipitating from solution. In a method analogous to non-surface bound oligonucleotides, Mirkin monitored the

assembly process by UV-Vis spectroscopy at 260 nm and 700 nm, plotting the absorbance as a function of time, which showed the reversibility of the aggregation process due to denaturation of the oligonucleotide duplex above the melting temperature.

In the same issue of *Nature*, Paul Alivisatos, of the University of California, published his findings on the organization of nanoparticles using DNA. [184] In contrast to Mirkin's research, Alivisatos *et al.* investigated the formation of dimer and trimers of DNA-linked nanoparticles rather than large clusters of aggregated DNA-linked nanoparticles. To accomplish this, Alivisatos's group controlled, stoichiometrically, the ratio of oligonucleotide to gold nanoparticles (1:1). Oligonucleotides were synthesised, modified both at the 3'- and 5'-termini with alkane thiol moieties, and coupled to 1.4 nm monomaleimido-gold nanoparticles. The oligonucleotides were modified at both termini so the arrangement of the nanoparticles when hybridised to a complementary target could be controlled. When introduced under hybridisation conditions, the complementary target oligonucleotide forms a duplex with the nanoparticle bound oligonucleotides in either a "head-to-head" or "tail-to-tail" arrangement producing dimer or trimer structures. These structures were characterised by transmission electron microscopy (TEM) and gel electrophoresis.

Both researchers demonstrated, for the first time, the applicability of a biomolecular recognition event inherent in DNA base-pairing for the 'bottom-up' assembly of nanoscale materials. This pioneering research naturally led to other advancements in oligonucleotide-nanoparticle assembly, for example, Alivisatos *et al.* refined their initial findings by expanding the assembly process using 5 and 10 nm gold nanoparticles, [185] quantum dots [186] and branching DNA. [187] Alivisatos *et al.* were responsible for introducing a number of methods using oligonucleotide-nanoparticle conjugates, including the isolation of nanoparticles bearing specific numbers of oligonucleotides by gel electrophoresis and plasmon rulers based on the distance between nanoparticles using varying lengths of DNA interconnects. [188] [189] Research based upon oligonucleotide-nanoparticle assembly is extensive and beyond the scope of this work, however, Chad Mirkin provided a comprehensive review of

DNA-template materials synthesis in 1999. [190] Mirkin's work is of particular interest as the visible colour change observed when the nanoparticles come into close proximity during DNA hybridisation provides an avenue for biosensors based on oligonucleotide-nanoparticle assembly.
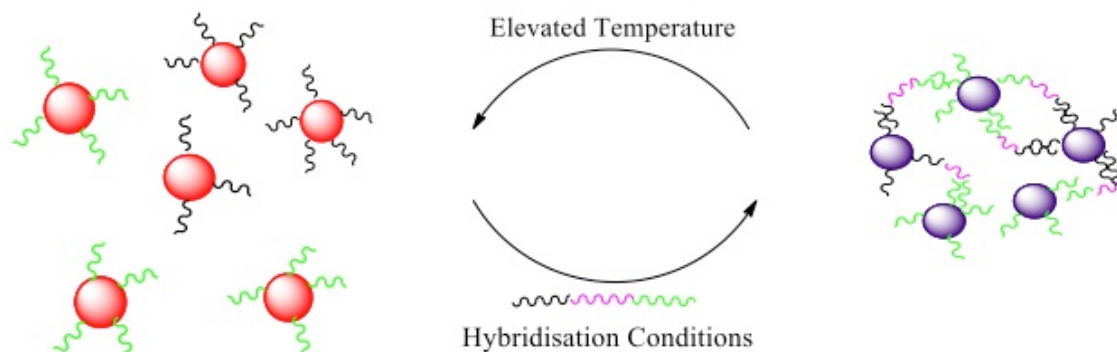
Figure 1.31. Illustration of the hybridisation-induced aggregation of oligonucleotide-nanoparticle conjugates. Aggregation, and a colour change, is only observed when a complementary target is introduced under hybridisation conditions. A red colour indicates monodispersed nanoparticles in the absence of target and a blue-purple colour indicates aggregation after addition of target DNA. By heating the DNA duplex above the T_m, re-dispersion of the nanoparticles and a colour change, from blue-purple to red, is observed.

1.3.3.2   Oligonucleotide-Nanoparticle Assembly: DNA Sensing

Mirkin *et al.* had established a framework for the detection of oligonucleotides by exploiting the unique optical changes that occur during aggregation of oligonucleotide-nanoparticle conjugates (figure 1.31). In 1997, Elghanian *et al.*, reported the use of thiol-modified oligonucleotide-gold nanoparticle conjugates for the detection of multiple base-pair mismatched oligonucleotides based on the characteristically sharp melting transition profiles of the conjugates. [191] Storhoff *et al.* utilized the characteristically sharp melting profiles of the conjugates to differentiate oligonucleotides containing various base-pair mismatches in a single pot. [192] The field of molecular diagnostics is dominated by fluorescence-based amplification methods for DNA detection; however, Mirkin's group has shown the oligonucleotide-gold nanoparticle conjugates can be spotted onto a C_{18} silica plate for easy discrimination between the complementary and non-complementary target

sequences. A red spot indicates that no hybridisation has occurred or that the spot was added at a temperature above the melting temperature of the duplex. A blue spot appears if the complementary sequence is added and hybridisation has occurs below the melting temperature of the duplex. Spotting the oligonucleotide-nanoparticle conjugates in this manner allows a permanent record of the assay to be kept.

Mirkin's group investigated the factors that influence melting characteristics of the oligonucleotide-gold nanoparticle conjugates. [193] [194] These studies revealed that oligonucleotide density, nanoparticle size, salt concentration and inter-particle distance play important roles in influencing the melting characteristics of the conjugates. It was reported that the sharp melting transition observed for oligonucleotide-gold nanoparticle conjugates was attributed to a cooperative melting effect due to multiple duplexes on the particle surface and a reduction in local salt concentration as the duplexes melt. [194] In addition, it was later reported that the oligonucleotide target concentration influences the aggregation process, with more target resulting in more aggregation. [195]

The studies so far had employed synthetic oligonucleotides; however, in 2000 Mirkin employed the spot test to detect the presence of a biological warfare agent, anthrax. [196] To do this, Mirkin used two oligonucleotide-gold nanoparticle conjugates as probes to hybridise to an internal position of a 141-bp PCR fragment of anthrax. Since the PCR product was double-stranded, the DNA was heated to denature the duplex and, upon cooling, the conjugates were added to hybridise to the complementary region. It was found that due to their small size, the conjugates were kinetically favourable to hybridise to the complementary region over the single-stranded PCR fragment. Upon spotting, a blue spot had indicated aggregation had occurred and therefore confirmed the presence of anthrax. This was compared to a control spot containing no anthrax target that appeared blue in colour showing that the presence of the anthrax was sequence specific.

Mirkin *et al.* have demonstrated PCR-like sensitivity in the detection of anthrax utilizing a so-called bio-bar-code assay format. [197] This format uses oligonucleotide-gold nanoparticle conjugates containing two different sequences, one complementary to the target of interest and the other complementary to oligonucleotide-

functionalised magnetic microparticles. After hybridisation of the target sequences to the gold conjugates, the conjugates were then hybridised to the magnetic microparticles, which were subsequently separated with the application of an external magnetic field. The hybridised target were removed from the particles by heating past the melting temperature of the duplex and the magnetic field applied again to remove the magnetic microparticles. The free target oligonucleotides were then captured onto a microarray chip using a second set of oligonucleotide-gold nanoparticle conjugates in which signal amplification was induced by the addition of silver to coat the gold conjugates by reduction of hydroquinone. The array was analysed by measuring the scattered light generated from the silver-enhanced oligonucleotide-gold nanoparticle conjugates. This method offered 500 zeptomolar (~ 10 copies in a 30 µl sample) sensitivity. The bio-bar-code assay approach has led to the multiplexed detection of oligonucleotides related to hepatitis B, variola virus, Ebola virus and HIV. [198]

A similar approach, in which a "real" biological target was detected, was performed by Storhoff *et al.* for the detection of unamplified genomic methicillin-resistant *Staphylococcus aureus* (MRSA). [199] In this approach, Storhoff *et al.* employed multiple oligonucleotide-gold nanoparticle conjugate probes with varying nanoparticle sizes, 40 and 50 nm diameters, in order to boost sensitivity of the detection method. In order to hybridise the conjugates to the sample, the dsDNA of the MRSA had to be denatured and the conjugates added upon cooling. In order to facilitate hybridisation kinetics, dextran sulphate was added to the buffer in order to form aggregates quickly. However, instead of spotting the samples to a silica plate, Storhoff *et al.* added the samples to a glass microscope slide to measure the scattered light from the nanoparticles upon hybridisation with the target. The detection of complementary target DNA resulted in a colour change from green to orange. Using multiple 50 nm oligonucleotide-gold nanoparticle conjugates allowed detection of unamplified genomic MRSA clinical samples down to 33 zmol of target, equivalent to 20,000 copies, in a 1 µl spotted aliquot.

In addition to the targets mentioned above, oligonucleotide-gold nanoparticle conjugates have been employed in the detection of the breast cancer-associated

BRCA-1 gene using multifunctional cross-linking gold nanoaggregates. [200] The ability of oligonucleotide-gold nanoparticles to resist aggregation from elevated salt levels after hybridisation of the target has been used in the detection of *mycobacterium tuberculosis*, [201] eukaryotic gene expression, [202] *E. coli* bacteria, [203] as well as the detection of cancer RNA sequences related to chronic myeloid leukemia (CML). [204] Recently, Mirkin and co-workers have expanded their scanometric detection methodology by employing spherical nucleic acid-gold nanoparticle conjugates for microRNA profiling related to prostate cancer markers. [205] Oligonucleotides functionalised to gold nanoparticles have also been used as primers to amplify DNA targets using polymerase chain reaction. [206] [207] Methods to overcome the necessity for DNA denaturation steps before the addition of nanoparticle conjugate probes have been developed with the employment of triplex forming oligonucleotides. McKenzie *et al.* showed that gold nanoparticles could be functionalised with LNA oligonucleotides that were subsequently hybridised to a double-stranded DNA target, inducing aggregation of the nanoparticles *via* Hoogsteen base-pairing. [208]

Silver nanoparticles have also been used in analogous methods to oligonucleotide-gold nanoparticle conjugates in the detection of DNA. The advantage of employing silver over gold nanoparticles is x100 greater molar extinction coefficient of silver nanoparticles compared to gold. A study by Thompson *et al.* demonstrated that oligonucleotide-silver nanoparticle conjugates can be used in conjunction with oligonucleotide-gold nanoparticle conjugates in a mixed-metal assay for the assembly of "halo-like" nanostructures since the smaller gold conjugates surround the silver conjugates upon hybridisation. [209] In addition, Thompson *et al.* reported that oligonucleotide-silver nanoparticle conjugates are just as robust as the gold nanoparticle analogues and can detect lower concentrations DNA due to the higher extinction coefficient inherent in silver nanoparticles. [210] However, the utilization of oligonucleotide-silver nanoparticle conjugates for PCR-like sensitivity of DNA detection has still to be demonstrated.

1.3.3.3 *Oligonucleotide-Nanoparticle Conjugates: Stability*

As discussed previously, the employment of oligonucleotide-gold nanoparticle conjugates for the detection of DNA is becoming increasingly more popular. However, in order to reach their full potential as biosensors, oligonucleotide-functionalised nanoparticles must be stable in increasingly challenging biological environments where buffers containing biological additives or increased salt concentrations, elevated or cycled temperatures and enzymes are commonly employed. Research has shown that oligonucleotide-gold nanoparticles conjugates are stable at moderate temperatures (~ 45 °C) but irreversibly aggregate at temperatures above 90 °C. [211] In addition, it was found that larger (> 30 nm) oligonucleotide-gold nanoparticle conjugates slowly decompose in elevated salt concentrations (0.3 M – 1 M NaCl) as well as increased temperatures. [212] The instability of thiol-modified oligonucleotide-gold nanoparticle conjugates in the presence of biological buffer additives, such as mercaptoethanol and dithiothreitol (DTT), led Mirkin *et al.* to develop a method whereby the surface coverage of oligonucleotides on the surface of gold nanoparticles can be determined. The biological additives are very effective at stripping the oligonucleotides from the particle surface, which leads to irreversible aggregation of the nanoparticles since the oligonucleotides are no longer providing stability to the surface. [213]

Strategies to improve the stability of oligonucleotide-nanoparticle conjugate have relied on the synthesis of different surface attachment groups that are included in the oligonucleotide. Letsinger *et al.* reported a method whereby monothiol surface linking group was replaced with a cyclic steroid disulfide anchoring group which was shown to improve stability of oligonucleotide-gold nanoparticle conjugates, showing resistance to elevated temperatures up to 100 °C and to DTT showing resistance to aggregation up to 100 minutes after DTT addition. [214] Li *et al.* investigated the use of multiple thiol anchors modified to oligonucleotide and immobilized onto gold nanoparticles and found that these conjugates were stable up to 10 hours after addition of 10 mM DTT. [212] Lee *et al.* reported the use of triple cyclic disulfide moieties to improve stability of oligonucleotide-silver nanoparticle conjugates showing resistance to elevated NaCl concentrations up to 1 M. [215]

Research performed by Dougan *et al.* showed that thioctic acid could be used in place of the more common monothiol moiety to immobilize oligonucleotides on to the surface of gold and silver nanoparticles, which led to improved stability after a displacement study using DTT. [216] Thioctic acid-modified oligonucleotide gold nanoparticle conjugates were stable up to 300 minutes and the silver conjugates were stable up to 30 minutes after addition of DTT. These results showed significant improvements in terms of stability compared to the monothiol oligonucleotide-nanoparticle conjugate analogues. Sharma *et al.* conjugated dithiocarbamate ligands to amino-modified oligonucleotides and subsequently functionalised gold nanoparticles, which showed resistance to aggregation by DTT for up to 2 hours, fully aggregating after 4 hours. [217]

In addition to modifying oligonucleotides with different surface-seeking linkers to improve conjugate stability, some researchers have opted to attach other molecules directly to the nanoparticle surface in an effort to improve stability. For example, low molecular weight PEGs have been used to stabilize the nanoparticle surface before addition of oligonucleotides, [218] [219] mononucleotides of dATP have been incubated with gold nanoparticles prior to oligonucleotide addition to improve stability, [220] [221] and non-ionic fluorosurfactants (zonyl FSN) have been added to stabilize gold nanoparticles, enabling the functionalisation of oligonucleotide to the nanoparticles without a salt-aging step. [222]

Nanoparticles have proven to be a robust surface for functionalisation of biomolecules. The unique optical properties afforded by gold and silver nanoparticles upon biomolecular recognition have promising implications in the field of molecular diagnostics. Most biological assays for the detection of DNA rely on spectroscopic output, usually in the form of fluorescence spectroscopy; however, other techniques have arisen in recent years, such as surface enhanced Raman spectroscopy, which utilizes the unique properties of nanoparticles to offer greater sensitivity for bioanalysis.

1.4 Surface Enhanced Resonance Raman Scattering (SERRS) Spectroscopy

The current platform of choice for spectroscopic output from molecular diagnostic assays is usually fluorescence spectroscopy. [123] Fluorescent labelling of DNA, for example, can occur during PCR amplification of the target using dye-labelled primers and a wide range of labels can be employed for multiple analyte detection. However, the major disadvantages in using fluorescence spectroscopy lie with the broad, overlapping emission spectra obtained from fluorophores, as well as photobleaching of the fluorophores and the need for multiple excitation wavelengths. As discussed in section 1.3, significant progress towards utilizing oligonucleotide-nanoparticle conjugates in diagnostic assays is an area of on-going research. The plasmonic coupling between aggregated nanoparticles has led to the detection of various biological targets and the sensitivity of detection using nanoparticles is constantly being improved. While colorimetric detection of targets using nanoparticles is attractive the single colour change invoked upon biomolecular recognition does not facilitate multiplexed analysis. A technique that has shown considerable promise for multiplexed bioanalysis is Surface Enhanced Resonance Raman Scattering (SERRS). [223]

1.4.1 Raman Scattering

The interaction of light with a molecule is the fundamental optical process that underpins spectroscopies such as absorption, fluorescence and Raman spectroscopy. In absorption spectroscopy, a photon of light interacts with the molecule of interest and is absorbed if the energy of the incident photon matches the energy difference between occupied and vacant energy levels within the molecule. Infra-red (IR) spectroscopy and ultra-violet-visible (UV-Vis) spectroscopy are commonly employed absorption spectroscopies in analytical chemistry. Fluorescence spectroscopy arises from absorption of the incident light followed by emission of a photon at longer wavelengths, which results in the emitted light having lower energy than the absorbed light.

When a source of light interacts with a molecule, the photons are known to distort the cloud of electrons surrounding the nucleus of the molecule, releasing energy in the form of scattered light. In most cases, the energy of the scattered photons equals the energy of the incident light. This is said to be an elastic process and is known as Rayleigh scattering. However, during the scattering of light, approximately one in 10^6 - 10^8 of the scattered photons will have energy different from that of the incident light which is described as an inelastic process and is known as Raman scattering. Raman scattering was first observed by C. V. Raman and K. S. Krishnan in 1928 who received the Noble Prize for physics in 1930 for their discovery. [224] There are two types of Raman scattering. The first is Stokes scattering, in which the molecule absorbs energy and is promoted to a higher energy state and is the most abundant form of scattering. The second is anti-Stokes scattering, in which the molecule loses energy, decreasing from a higher to a lower energy state (figure 1.32).
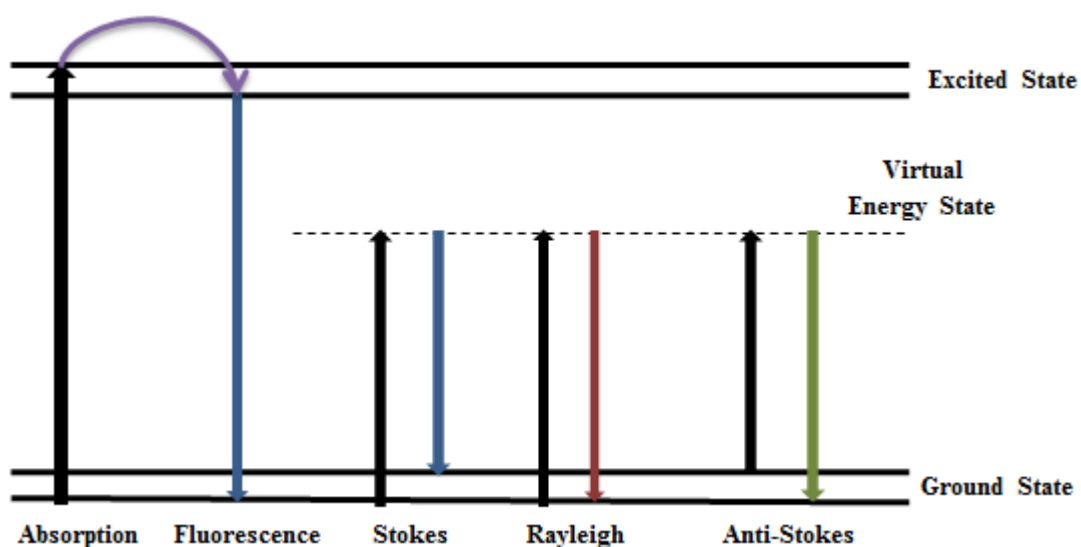
Figure 1.32. Jablonski diagram depicting the various optical processes: absorption, fluorescence and the different forms of Raman scattering.

1.4.2 Resonance Raman Scattering

The sensitivity of the Raman signal can be improved by tuning the frequency of the wavelength of interrogating light to the absorption maximum of the analyte molecule. This can lead to enhancements of up to 10^4 orders over the conventional Raman scattering technique. [225] However, interference in the Raman signal arising

from the competing fluorescence process is a known disadvantage of resonance Raman scattering.

1.4.3 Surface Enhanced Raman Scattering

In 1974, Fleischmann *et al.* reported considerable enhancement of the Raman signal from pyridine immobilized onto a roughened silver-metal surface. [226] The enhancement was attributed to the increase in the electrode surface area caused by the roughening process, allowing more pyridine molecules to be adsorbed on to the surface. This process is called Surface Enhanced Raman Scattering (SERS) and is known to increase the intensity of the Raman signal up to 10^6 orders over the conventional Raman technique. There are many suitable surfaces for use in SERS, however, the coinage metals, i.e. silver, gold and copper, have attracted the most attention in the literature. [227]

1.4.4 Surface Enhanced Resonance Raman Scattering

Surface Enhanced Resonance Raman Scattering (SERRS) combines both of the aforementioned techniques by introducing a resonant chromophore adsorbed on to a suitably roughened metal surface. SERRS was first reported by Stacy and Van Duyne in 1983. They adsorbed a chromophore onto a roughened metal surface and adjusted the excitation wavelength to be coincident with the excitation frequency of the interrogated molecule. This provided enhancement of the Raman signal up to 10^{10} orders over the conventional Raman technique. [228] In fact, using SERRS, single molecule detection has been reported. [229] [230] SERRS offers the advantage that fluorescence is effectively quenched by the metal surface meaning organic fluorophores can be employed for their resonance contribution. [231]

1.4.4.1 Nanoparticles as SERRS substrates

The surface enhancement of the Raman signal arises due to the inclusion of a roughened metal surface. Commonly, the metal surface employed for SERRS is gold and silver nanoparticles. Gold nanoparticles have been extensively studied for their SERRS properties; however, it is known that silver nanoparticles give rise to greater enhancement due to their larger scattering-to-absorbance ratio and more polarizable surface electrons. [232] Colloidal suspensions of gold and silver

nanoparticles are most commonly used as SERRS substrates due to their ease of preparation, relative stability and reproducibility. [233] Aggregation of colloidal suspensions of nanoparticles has been known to give rise to increased SERRS intensities. This is usually by the addition of salts that disrupt the citrate-protecting layer surrounding the nanoparticle leading to the formation of large clusters of nanoparticles, or by the addition of a dye molecule that can partially aggregate the nanoparticles. [234] [235] A study by Taylor *et al.* showed the SERRS enhancement obtained from gold nanoparticles aggregated by addition of different concentrations of cucurbit[*n*]urils. [236]

1.4.4.2   SERRS Detection of DNA

The use of SERRS in the sensitive detection of oligonucleotides has been extensively studied in the literature. [232] [237] [238] The unique "fingerprint"-like spectra afforded by SERRS has also allowed multiplexed analysis of six-labelled oligonucleotides. [239] In addition, SERRS has been used to detect and identify a single adenine molecule using colloidal silver clusters and near-IR wavelength excitation. [240] To achieve maximum SERRS from oligonucleotides, both the dye label and the chosen surface must have similar absorbance maxima that coincide with the wavelength of the excitation source. [232]
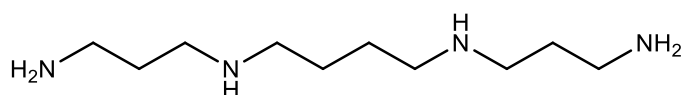
Figure 1.33.   Structure of spermine - a polyamine molecule used to aggregate nanoparticles.

SERRS has been used extensively in conjugation with PCR for the sensitive detection of DNA. For example, Graham *et al.* used HEX-labelled primers for extension of DNA during PCR. After PCR, the product was added to silver nanoparticles that were subsequently aggregated by the addition of the polyamine, spermine (figure 1.33), resulting in increased SERRS intensities and a detection limit of 8×10^{13} M. [241] A similar primer labelling approach was employed by Isola *et al.,* demonstrating the ability for SERRS to detect PCR product related to HIV by using a labelled primer to amplify the target followed by subsequent immobilization on to a

silver-deposited solid substrate. [242] Dou *et al.* amplified target DNA by PCR and used a DNA intercalator, DAPI, which only binds to dsDNA, as the SERRS label. In the absence of dsDNA a high SERRS signal is observed since it is adsorbed onto the nanoparticle surface. However, upon intercalation to dsDNA the signal disappears. [243] Graham *et al.* demonstrated a simple multiplexed genotyping assay employing SERRS-active allele-specific primers for the detection of different genes in cystic fibrosis samples after PCR amplification. [244] Recently, Harper *et al.* combined SERRS with a TaqMan assay, in which the liberated TAMRA-labelled region of the TaqMan probe was captured onto spermine-aggregated silver nanoparticles for the sensitive detection of MRSA from genomic samples. [245]

SERRS assays for DNA detection often rely on the adsorption of dye-labelled oligonucleotides to the nanoparticle surface. In order for effective adsorption and therefore improved detection of the oligonucleotides, the negative charge on the polyanionic backbone of the DNA must be neutralized. This is usually achieved by the addition of a polyamine species, such as spermine hydrochloride or poly-L-lsine, to interact with the DNA backbone. [246] The addition of polyamines also has the added benefit of aggregating the nanoparticles through electrostatic interaction of the negatively charged nanoparticles and the positively charged amines to generate sufficient "hotspots" needed for enhancement of the SERRS signals (figure 1.34). This methodology has been widely employed for SERRS-based detection of labelled oligonucleotides. [247] [248] [249] "Hotspots" are regions of high electromagnetic intensity generated from the coupling of the surface plasmon resonances of nanoparticles when the nanoparticles come into close proximately to one another during aggregation. [250]
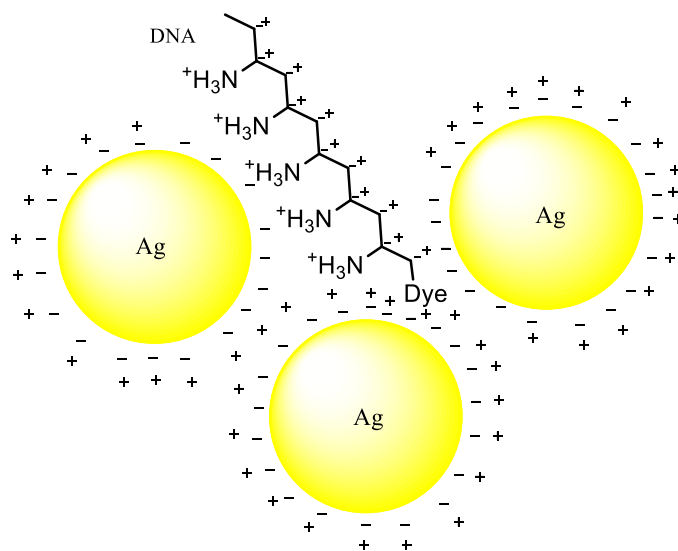
Figure 1.34. Spermine-induced aggregation of silver (Ag) nanoparticles for the detection of dye-labelled propargylamino-modified oligonucleotides. Spermine neutralises the negative DNA backbone, allowing interaction of the bases with the negative Ag surface. This places the dye label in close proximity to the nanoparticle surface to facilitate surface enhancement of the Raman signal. The + symbols represent spermine. [(241)]
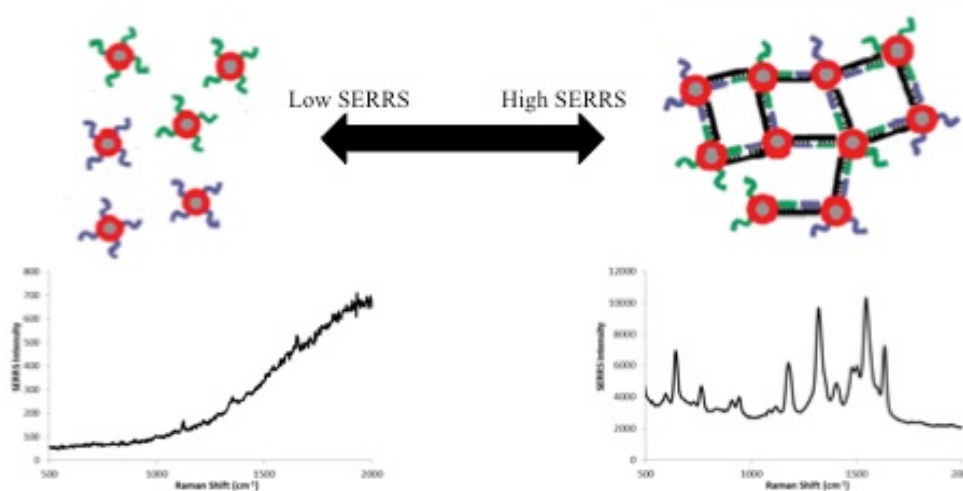
Figure 1.35. Representation of the assembly of SERRS-active oligonucleotide-nanoparticle conjugates via DNA hybridisation-induced aggregation.

Nanoparticles are often used as a substrate for providing signal enhancement in conjugation with an amplification technique for detection of DNA. Other SERRS-based DNA detection methodologies have been investigated that utilize the

"bottom-up" assembly of nanoparticles *via* biomolecular recognition, *i.e.* DNA hybridisation, more akin to the detection systems established by Mirkin and Alivisatos. [183] [184] These methods exploit the electromagnetic enhancement generated from nanoparticles after nanoparticle-bound oligonucleotides are hybridised to a complementary target in a sandwich assay format to bring the nanoparticles in close proximity in order to generate the "hotspots" need for SERRS enhancement (figure 1.35). Graham *et al.* reported the use of silver nanoparticles functionalised with a SERRS-active dye that, rather than conjugated to the oligonucleotide, is immobilized directly to the nanoparticle surface through a benzotriazole moiety followed by the addition of oligonucleotide probes. Addition of a DNA target complementary to two different oligonucleotide-nanoparticle conjugates causes hybridisation-induced aggregation. This allows the nanoparticles to come in to close proximity to one another to facilitate "hotspot" generation and thereby increasing the SERRS intensities. [251] This methodology was extended by Thompson *et al.* for the detection of single nucleotide polymorphisms (SNPs) using SERRS. [252] A similar approach was adopted by Qian *et al.*, who used gold nanocrystals functionalised with malachite green isothiocyanate. This binds directly to the nanoparticle surface through the isothiocyanate moiety. Qian *et al.* also used low molecular weight PEGs to increase conjugate stability and oligonucleotide probes to provide intense SERRS from DNA-mediated assembly of the oligonucleotide-nanoparticle conjugates. [253] More recent approaches, by McKenzie *et al.*, have shown the SERRS-based assembly of oligonucleotide-nanoparticle conjugates that were functionalised with isothiocyanate-containing dyes after oligonucleotide functionalisation. This was in an effort to allow a freedom of choice of dye since the conjugates are already afforded steric and electrostatic protection from the oligonucleotides. [254] [255] It has also been demonstrated that triplex-forming oligonucleotides can be used to induce aggregation of oligonucleotide-nanoparticle conjugates to generate intense SERRS signals. [256] In the same study, different lengths of dsDNA were used to assemble the nanoparticles demonstrating the dependence of interparticle distance on the SERRS intensities. Recently, the multiplexed detection of several different dyes functionalised to oligonucleotide-nanoparticle conjugates have been assembled through DNA hybridisation and

detected using SERRS. [257] The optimization of SERRS "hotspots" by reduction of the fluorescent background was demonstrated by Fabris, in which a bifunctional linker, hexamethylene diamine (HMD), was used to precisely control interparticle separation of SAMSA fluorescein-labelled oligonucleotide-nanoparticle conjugates. [258]

1.5   Conclusions

The merging of bio- and nanotechnologies is allowing advances in the development of new methodologies that benefit the field of molecular diagnostics. Nanoparticles provide a robust surface for functionalisation of biomolecules and their unique optical properties have allowed their application in a number of detection strategies including the detection of DNA, RNA, proteins and cells. However, while showing promise as biosensors, oligonucleotide-nanoparticle conjugates suffer from a lack of stability in demanding biological environments – PCR, assays and cells. This provides an avenue for development of stable oligonucleotide-nanoparticle conjugates that can be combined with the increasingly demanding biological environments in order to be fully implemented as biosensors.

1.6   References

1.   R. Dahm, *Am. Sci.*, 2008, **96**, 320-327.

2.   P. A. Levene, *Bioch. Z.*, 1909, **17**, 120-131.

3.   P. A. Levene, *J. Biol. Chem.*, 1919, **40**, 415-424.

4.   W. T. Astbury, *Sym. Soc. Exp. Biol.*, 1947, **1**, 66.

5.   J. D. Watson, *The Double Helix – A Personal Account of the Discovery of the Structure of DNA (1968)*. New York: Simon and Schuster, 2001.

6.   R. E. Franklin and R. G. Gosling, *Nature*, 1953, **172**, 156-157.

7.   R. E. Franklin and R. G. Gosling, *Nature*, 1953, **171**, 740-741.

8.   M. H. F. Wilkins, A. R. Stokes and H. R. Wilson, *Nature*, 1953, **171**, 738-740.

9.   J. D. Watson and F. H. C. Crick, *Nature*, 1953, **171**, 964-967.

10.   J. D. Watson and F. H. C. Crick, *Nature*, 1953, **171**, 737-738.

11.   F. H. C. Crick and J. D. Watson, *P. Roy. Soc. Lond. A. Mat.*, 1954, **223**, 80-

96.

12. F. H. C. Crick, *Brit. Med. Bull.*, 1965, **21**, 183-186.

13. F. S. Collins, E. D. Green, A. E. Guttmacher, M. S. Guyer, *Nature*, 2003, **422**, 835 - 847.

14. E. Chargaff, *Experientia*, 1950, **6**, 201-209.

15. Hanner. Image: DNA ladder. *Culturing Science*. [Online] [Cited: 17 05 2012.]http://culturingscience.files.wordpress.com/2009/12/dna-ladder.gif?w=700.

16. R. Wing, H. Drew, T. Takano, C. Broka, S. Tanaka, K. Itakura and R. E. Dickerson, *Nature*, 1980, **287**, 755-758.

17. C. O. Pabo and R. T. Sauer, *Annu. Rev. Biochem.*, 1984, **53**, 293-321.

18. F. H. C. Crick, *Symp. Soc. Exp. Biol. XII*, 1958, 139-163.

19. F. H. C. Crick, *Nature*, 1970, **227**, 561-563.

20. Y. Singh, P. Murat and E. Defrancq, *Chem. Soc. Rev.*, 2010, **39**, 2054-2070.

21. L. M. Smith, J. Z. Sanders, R. J. Kaiser, P. Hughes, C. Dodd, C. R. Connell, C. Heiner, S. B. H. Kent and L. E. Hood, *Nature*, 1986, **321**, 674-679.

22. R. K. Saiki, T. L. Bugawan, G. T. Horn, K. B. Mullis and H. A. Erlich, *Nature*, 1986, **324**, 163-166.

23. B. M. Paterson, B. E. Roberts and E. L. Kuff, *Proc. Natl. Acad. Sci. USA*, 1977, **74**, 4370-4374.

24. M. L. Stephenson and P. C. Zamecnik, *Proc. Natl. Acad. Sci. USA*, 1978, **75**, 285-288.

25. U. Maskos and E. M. Southern, *Nucleic Acids Res.*, 1992, **20**, 1679-1684.

26. M. Michelson and A. R. Todd, *J. Chem. Soc.*, 1955, 2632-2638.

27. H. G. Khorana, G. M. Tener, J. G. Moffatt and E. H. Pol, *Chem. Ind.*, 1956, 1523-1523.

28. H. G. Khorana, W. E. Razzell, P. T. Gilham, G. M. Tener and E. H. Pol, *J. Am. Chem. Soc.*, 1957, **79**, 1002-1003.

29. M. Smith, D. H. Rammler, I. H. Goldberg, H. G. Khorana, *J. Am. Chem. Soc.*, 1961, **84**, 430-440.

30. G. Weimann and H. G. Khorana, *J. Am. Chem. Soc.*, 1962, **84**, 419-430.

31. H. Schaller, G. Weimann, H. G. Khorana and B. Lerch, *J. Am. Chem. Soc.*,

1963, **85**, 3821-3827.

32.   K. L. Agarwal, H. Buchi, Caruther.Mh, N. Gupta, H. G. Khorana, K. Kleppe, A. Kumar, E. Ohtsuka, U. L. Rajbhand, J. H. Vandesan, V. Sgaramel, H. Weber and T. Yamada, *Nature*, 1970, **227**, 27-34.

33.   R. L. Letsinger, K. K. Ogilvie and P. S. Miller, *J. Am. Chem. Soc.*, 1969, **91**, 3360-3365.

34.   R. L. Letsinger and W. B. Lunsford, *J. Am. Chem. Soc.*, 1976, **98**, 3655-3661.

35.   S. L. Beaucage and M. H. Caruthers, *Tetrahedron Lett.*, 1981, **22**, 1859-1862.

36.   L. J. McBride and M. H. Caruthers, *Tetrahedron Lett.*, 1983, **24**, 245-248.

37.   R. L. Letsinger and V. Mahadevan, *J. Am. Chem. Soc.*, 1965, **87**, 3526-3527.

38.   R. L. Letsinger and V. Mahadevan, *J. Am. Chem. Soc.*, 1966, **88**, 5319-5324.

39.   R. L. Letsinger, M.H. Caruthers and D. M. Jerina, *Biochemistry*, 1967, **6**, 1379-1388.

40.   M. D. Matteucci and M. H. Caruthers, *J. Am. Chem. Soc.*, 1981, **103**, 3185-3191.

41.   G. R. Gough, M. J. Brunden and P. T. Gilham, *Tetrahedron Lett.*, 1981, **22**, 4177-4180.

42.   J. Nielsen, M. Taagaard, J. E. Marugg, J. H. Vanboom and O. Dahl, *Nucleic Acids Res.*, 1986, **14**, 7391-7403.

43.   J. S. Eadie and D. S. Davidson, *Nucleic Acids Res.*, 1987, **15**, 8333-8349.

44.   J. C. Schulhof, D. Molko and R. Teoule, *Nucleic Acids Res.*, 1987, **15**, 397-416.

45.   H. Vu, C. McCollum, K. Jacobson, P. Theisen, R. Vinayak, E. Spiess and A. Andrus, *Tetrahedron Lett.*, 1990, **31**, 7269-7272.

46.   L. C. J. Gillet, J. Alzeer and O. D. Scharer, *Nucleic Acids Res.*, 2005, **33**, 1961-1969.

47.   M. P. Reddy, N. B. Hanna and F. Farooqui, *Tetrahedron Lett.*, 1994, **35**, 4311-4314.

48.   S. A. Surzhikov, E. N. Timofeev, B. K. Chernov, J. B. Golova and A. D. Mirzabekov, *Nucleic Acids Res.*, 2000, **28**, E29-E29.

49.   T. Maniatis, A. Jeffrey and H. Vandesande, *Biochemistry*, 1975, **14**, 3787-3794.

50.   R. Frank, D. Muller and C. Wolff, *Nucleic Acids Res.*, 1981, **9**, 4967-4979.

51.   U. Birsner, U. Gilles, P. Nielsen and G. K. McMaster, *J. Chromatogr.*, 1987, **402**, 381-386.

52.   J. Liautard, C. Ferraz, J. S. Widada, J. P. Capony and J. P. Liautard, *J. Chromatogr.*, 1989, **476**, 439-443.

53.   J. M. Schmitter, Y. Mechulam, G. Fayat and M. Anselme, *J. Chromatogr.*, 1986, **378**, 462-466.

54.   B. S. Sproat, B. Beijer, P. Rider and P. Neuner, *Nucleic Acids Res.*, 1987, **15**, 4837-4848.

55.   B. S. Sproat, B. Beijer and P. Rider, *Nucleic Acids Res.*, 1987, **15**, 6181-6196.

56.   S. Mielewczyk, D. Wieckowska, E. Krzymanskaolejnik, Z. Gdaniec and R. W. Adamiak, *Acta. Biochim. Pol.*, 1989, **36**, 225-233.

57.   C. R. Petrie, M. W. Reed, A. D. Adams and R. B. Meyer, *Bioconjugate Chem.*, 1992, **3**, 85-87.

58.   D. A. Stetsenko and M. J. Gait, *Bioconjugate Chem.*, 2001, **12**, 576-586.

59.   S. K. Singh, P. Nielsen, A. A. Koshkin and J. Wengel, *Chem. Commun.*, 1998, 455-456.

60.   M. Matsukura, G. Zon, K. Shinozuka, C. A. Stein, H. Mitsuya, J. S. Cohen and S. Broder, *Gene*, 1988, **72**, 343-347.

61.   P. E. Nielsen, M. Egholm, R. H. Berg and O. Buchardt, *Science*, 1991, **254**, 1497-1500.

62.   M. Egholm, O. Buchardt, L. Christensen, C. Behrens, S. M. Freier, D. A. Driver, R. H. Berg, S. K. Kim, B. Norden and P. E. Nielsen, *Nature*, 1993, **365**, 566-568.

63.   J. C. Hanvey, N. J. Peffer, J. E. Bisi, S. A. Thomson, R. Cadilla, J. A. Josey, D. J. Ricca, C. F. Hassman, M. A. Bonham, K. G. Au, S. G. Carter, D. A. Bruckenstein, A. L. Boyd, S. A. Noble and L. E. Babiss, *Science*, 1992, **258**, 1481-1485.

64.   J. G. Wetmur, *Annu. Rev. Biophys. Bio.*, 1976, **5**, 337-361.

65.   M. Maxam and W. Gilbert, *Proc. Natl. Acad. Sci. USA*, 1977, **74**, 560-564.

66.   F. Sanger, G. M. Air, B. G. Barrell, N. L. Brown, A. R. Coulson, J. C. Fiddes, C. A. Hutchison, P. M. Slocombe and M. Smith, *Nature*, 1977, **265**, 687-695.

67. F. Sanger, S. Nicklen and A. R. Coulson, *Proc. Natl. Acad. Sci. USA*, 1977, **74**, 5463-5467.

68. L. M. Smith, S. Fung, M. W. Hunkapiller, T. J. Hunkapiller and L. E. Hood, *Nucleic Acids Res.*, 1985, **13**, 2399-2412.

69. R. G. Blazej, P. Kumaresan and R. A. Mathies, *Proc. Natl. Acad. Sci. USA,* 2006, **103**, 7240-7245.

70. D. Gresham, M. J. Dunham and D. Botstein, *Nat. Rev. Genet.*, 2008, **9**, 291-302.

71. G. V. Soni and A. Meller, *Clin. Chem.*, 2007, **53**, 1996-2001.

72. K. Healy, B. Schiedt and A. P. Morrison, *Nanomed.*, 2007, **2**, 875-897.

73. J. Clarke, H.-C. Wu, L. Jayasinghe, A. Patel, S. Reid and H. Bayley, *Nat. Nanotechnol.*, 2009, **4**, 265-270.

74. J. Shendure, G. J. Porreca, N. B. Reppas, X. X. Lin, J. P. McCutcheon, A. M. Rosenbaum, M. D. Wang, K. Zhang, R. D. Mitra and G. M. Church, *Science*, 2005, **309**, 1728-1732.

75. S. E. Calvo, A. G. Compton, S. G. Hershman, S. C. Lim, D. S. Lieber, E. J. Tucker, A. Laskowski, C. Garone, S. Liu, D. B. Jaffe, J. Christodoulou, J. M. Fletcher, D. L. Bruno, J. Goldblatt, S. DiMauro, D. R. Thorburn and V. K. Mootha, *Sci. Transl. Med.*, 2012, **4**.

76. J. Shendure and H. Ji, *Nat. Biotechnol.*, 2008, **26**, 1135-1145.

77. P. D. Wentzell and T. K. Karakach, *Analyst*, 2005, **130**, 1331-1336.

78. E. M. Southern, *J. Mol. Biol.*, 1975, **98**, 503-517.

79. F. C. Kafatos, C. W. Jones and A. Efstratiadis, *Nucleic Acids Res.*, 1979, **7**, 1541-1552.

80. L. H. Augenlicht and D. Kobrin, *Cancer Res.*, 1982, **42**, 1088-1093.

81. M. Schena, D. Shalon, R. W. Davis and P. O. Brown, *Science*, 1995, **270**, 467-470.

82. D. Shalon, S. J. Smith and P. O. Brown, *Genome Res.*, 1996, **6**, 639-645.

83. D. D. Dalma-Weiszhausz, J. Warrington, E. Y. Tanimoto and G. Miyada, *Methods Enzymol.*, 2006, **410**, 3-28.

84. S. P. A. Fodor, J. L. Read, M. C. Pirrung, L. Stryer, A. T. Lu and D. Solas, *Science*, 1991, **251**, 767-773.

85. A. C. Pease, D. Solas, E. J. Sullivan, M. T. Cronin, C. P. Holmes and S. P. A. Fodor, *Proc. Natl. Acad. Sci. USA*, 1994, **91**, 5022-5026.

86. T. Goldmann and J. S. Gonzalez, *J. Biochem. Bioph. Meth.*, 2000, **42**, 105-110.

87. J.-B. Fan, K. L. Gunderson, M. Bibikova, J. M. Yeakley, J. Chen, E. Wickham Garcia, L. L. Lebruska, M. Laurent, R. Shen and D. Barker, *Methods Enzymol.*, 2006, **410**, 57-73.

88. A. Oliphant, D. L. Barker, J. R. Stuelpnagel and M. S. Chee, *Biotechniques*, 2002, (Suppl.)**:**56–58, 60-61.

89. R. G. Sosnowski, E. Tu, W. F. Butler, J. P. O'Connell and M. J. Heller, *Proc. Natl. Acad. Sci. USA*, 1997, **94**, 1119-1123.

90. D. A. Lashkari, J. L. DeRisi, J. H. McCusker, A. F. Namath, C. Gentile, S. Y. Hwang, P. O. Brown and R. W. Davis, *Proc. Natl. Acad. Sci. USA*, 1997, **94**, 13057-13062.

91. R. M. Anthony, T. J. Brown and G. L. French, *J. Clin. Microbiol.*, 2000, **38**, 781-788.

92. J. Korimbocus, N. Scaramozzino, B. Lacroix, J. M. Crance, D. Garin and G. Vernet, *J. Clin. Microbiol.*, 2005, **43**, 3779-3787.

93. Z. Wang, P. A. Orlandi and D. A. Stenger, *J. Clin. Microbiol.*, 2005, **43**, 4121-4128.

94. Lin, B., K. M. Blaney, A. P. Malanoski, A. G. Ligler, J. M. Schnur, D. Metzgar, K. L. Russell, and D. A. Stenger.**,** *J. Clin. Microbiol.*, 2007, **45,** 443–452.

95. Lin, B., A. P. Malanoski, Z. Wang, K. M. Blaney, N. C. Long, C. E. Meador, D. Metzgar, C. A. Myers, S. L. Yingst, M. R. Monteville, M. D. Saad, J. M. Schnur, C. Tibbetts, and D. A. Stenger., *J. Clin. Microbiol.*, 2009, **47**, 988–993.

96. V. Albrecht, A. Chevallier, V. Magnone, P. Barbry, F. Vandenbos, A. Bongain, J.-C. Lefebvre and V. Giordanengo, *J. Virol. Methods*, 2006, **137**, 236-244.

97. T. Koessler, P. Francois, Y. Charbonnier, A. Huyghe, M. Bento, S. Dharan, G. Renzi, D. Lew, S. Harbarth, D. Pittet and J. Schrenzel, *J. Clin. Microbiol.*,

2006, **44**, 1040-1048.

98. J. Yue, W. Shi, J. P. Xie, Y. Li, E. L. Zeng, L. Liang and H. H. Wang, *Diagn. Microbiol. Infect. Dis.*, 2004, **48**, 47-54.

99. W. Sougakoff, M. Rodrigue, C. Truffot-Pernot, M. Renard, N. Durin, M. Szpytma, R. Vachon, A. Troesch and V. Jarlier, *Clin. Microbiol. Infect.*, 2004, **10**, 289-294.

100. K. B. Mullis and F. A. Faloona, *Method Enzymol.*, 1987, **155**, 335-350.

101. K. B. Mullis, *Sci. Am.*, 1990, **262**, 56-&.

102. K. B. Mullis, *Angew. Chem. Int. Ed.*, 1994, **33**, 1209-1213.

103. R. K. Saiki, S. Scharf, F. Faloona, K. B. Mullis, G. T. Horn, H. A. Erlich and N. Arnheim, *Science*, 1985, **230**, 1350-1354.

104. R. K. Saiki, D. H. Gelfand, S. Stoffel, S. J. Scharf, R. Higuchi, G. T. Horn, K. B. Mullis and H. A. Erlich, *Science*, 1988, **239**, 487-491.

105. A. Chien, D. B. Edgar and J. M. Trela, *J. Bacteriol.*, 1976, **127**, 1550-1557.

106. Q. Chou, M. Russell, D. E. Birch, J. Raymond and W. Bloch, *Nucleic Acids Res.*, 1992, **20**, 1717-1723.

107. M. A. Innis, K. B. Myambo, D. H. Gelfand and M. A. D. Brow, *Proc. Natl. Acad. Sci. USA*, 1988, **85**, 9436-9440.

108. M. J. Hayden, T. M. Nguyen, A. Waterman and K. J. Chalmers, *Bmc Genomics*, 2008, **9**, 80-92.

109. J. Albert and E. M. Fenyo, *J. Clin. Microbiol.*, 1990, **28**, 1560-1564.

110. U. E. M. Gibson, C. A. Heid and P. M. Williams, *Genome Res.*, 1996, **6**, 995-1001.

111. J. Compton, *Nature*, 1991, **350**, 91-92.

112. R. Johne, H. Mueller, A. Rector, M. van Ranst and H. Stevens, *Trends Microbiol.*, 2009, **17**, 205-211.

113. T. D. McHugh, C. F. Pope, C. L. Ling, S. Patel, O. J. Billington, R. D. Gosling, M. C. Lipman and S. H. Gillespie, *J. Med. Microbiol.*, 2004, **53**, 1215-1219.

114. Y. Mori and T. Notomi, *J. Infect. Chemother.*, 2009, **15**, 62-69.

115. S. Lutz, P. Weber, M. Focke, B. Faltin, J. Hoffmann, C. Mueller, D. Mark, G. Roth, P. Munday, N. Armes, O. Piepenburg, R. Zengerle and F. von Stetten,

Lab Chip, 2010, **10**, 887-893.

116. O. Piepenburg, C. H. Williams, D. L. Stemple and N. A. Armes, *Plos Biol.*, 2006, **4**, 1115-1121.

117. M. Vincent, Y. Xu and H. M. Kong, *Embo Rep.*, 2004, **5**, 795-800.

118. C. T. Wittwer, M. G. Herrmann, A. A. Moss and R. P. Rasmussen, *Biotechniques*, 1997, **22**, 130.

119. C. T. Wittwer, K. M. Ririe, R. V. Andrew, D. A. David, R. A. Gundry and U. J. Balis, *Biotechniques*, 1997, **22**, 176-181.

120. K. M. Ririe, R. P. Rasmussen and C. T. Wittwer, *Anal. Biochem.*, 1997, **245**, 154-160.

121. J. Skeidsvoll and P. M. Ueland, *Anal. Biochem.*, 1995, **231**, 359-365.

122. T. B. Morrison, J. J. Weis and C. T. Wittwer, *Biotechniques*, 1998, **24**, 954.

123. J. R. Epstein, I. Biran and D. R. Walt, *Anal. Chim. Acta*, 2002, **469**, 3-36.

124. S. Tyagi and F. R. Kramer, *Nat. Biotechnol.*, 1996, **14**, 303-308.

125. Tapp, L. Malmberg, E. Rennel, M. Wik and A. C. Syvanen, *Biotechniques*, 2000, **28**, 732.

126. F. J. Steemers, J. A. Ferguson and D. R. Walt, *Nat. Biotechnol.*, 2000, **18**, 91-94.

127. X. J. Liu and W. H. Tan, *Anal. Chem.*, 1999, **71**, 5054-5059.

128. J. A. M. Vet, A. R. Majithia, S. A. E. Marras, S. Tyagi, S. Dube, B. J. Poiesz and F. R. Kramer, *Proc. Natl. Acad. Sci. USA*, 1999, **96**, 6394-6399.

129. P. M. Holland, R. D. Abramson, R. Watson and D. H. Gelfand, *Proc. Natl. Acad. Sci. USA*, 1991, **88**, 7276-7280.

130. P. M. Holland, R. Watson, R. D. Abramson and D. H. Gelfand, *Faseb Journal*, 1991, **5**, A621-A621.

131. K. J. Livak, S. J. A. Flood, J. Marmaro, W. Giusti and K. Deetz, *PCR Methods Appl.*, 1995, **4**, 357-362.

132. C. A. Heid, J. Stevens, K. J. Livak and P. M. Williams, *Genome Res.*, 1996, **6**, 986-994.

133. L. G. Lee, C. R. Connell and W. Bloch, *Nucleic Acids Res.*, 1993, **21**, 3761-3766.

134. M. Weidmann, K. Armbruster and F. T. Hufert, *J. Clin. Virol.*, 2008, **42**, 326-

334.

135. R. P. Feynman, *Caltech Engineering and Science*, 1960, **23**, 22-36.

136. M. M. Alvarez, J. T. Khoury, T. G. Schaaff, M. N. Shafigullin, I. Vezmar and R. L. Whetten, *J. Phys. Chem. B*, 1997, **101**, 3706-3712.

137. S. W. Chen, R. S. Ingram, M. J. Hostetler, J. J. Pietron, R. W. Murray, T. G. Schaaff, J. T. Khoury, M. M. Alvarez and R. L. Whetten, *Science*, 1998, **280**, 2098-2101.

138. D. L. LesliePelecky and R. D. Rieke, *Chem. Mater.*, 1996, **8**, 1770-1783.

139. L. N. Lewis, *Chem. Rev.*, 1993, **93**, 2693-2730.

140. N. J. Halas, S. Lal, W.-S. Chang, S. Link and P. Nordlander, *Chem. Rev.*, 2011, **111**, 3913-3961.

141. K. Grieve, P. Mulvaney and F. Grieser, *Curr. Opin. Colloid In.*, 2000, **5**, 168-172.

142. H. J. Dai, *Accounts Chem. Res.*, 2002, **35**, 1035-1044.

143. C. N. R. Rao, F. L. Deepak, G. Gundiah and A. Govindaraj, *Prog. Solid State Chem.*, 2003, **31**, 5-147.

144. L. R. Hirsch, A. M. Gobin, A. R. Lowery, F. Tam, R. A. Drezek, N. J. Halas and J. L. West, *Ann. Biomed. Eng.*, 2006, **34**, 15-22.

145. A. V. Alekseeva, V. A. Bogatyrev, B. N. Khlebtsov, A. G. Mel'nikov, L. A. Dykman and N. G. Khlebtsov, *Colloid J.*, 2006, **68**, 661-678.

146. J. Liu, J. Liu, L. Yang, X. Chen, M. Zhang, F. Meng, T. Luo and M. Li, *Sensors*, 2009, **9**, 7343-7364.

147. P. Galvin, D. Thompson, K. B. Ryan, A. McCarthy, A. C. Moore, C. S. Burke, M. Dyson, B. D. MacCraith, Y. K. Gun'ko, M. T. Byrne, Y. Volkov, C. Keely, E. Keehan, M. Howe, C. Duffy and R. MacLoughlin, *Cell. Mol. Life Sci.*, 2012, **69**, 389-404.

148. J. Kneipp, H. Kneipp, B. Wittig and K. Kneipp, *Nanomed.-Nanotechnol.*, 2010, **6**, 214-226.

149. M. V. Yigit, A. Moore and Z. Medarova, *Pharm. Res.*, 2012, **29**, 1180-1188.

150. Capek, *Adv. Colloid Interfac.*, 2011, **163**, 123-143.

151. M. E. Aubin-Tam and K. Hamad-Schifferli, *Biomed. Mater.*, 2008, **3**.

152. R.-M. Kong, X.-B. Zhang, Z. Chen and W. Tan, *Small*, 2011, **7**, 2428-2436.

153. M. Arruebo, M. Valladares and A. Gonzalez-Fernandez, *J. Nanomater.*, 2009.

154. M.-C. Daniel and D. L. Astruc *Chem. Rev.*, 2004, **104**, 293-346.

155. M. Rycenga, C. M. Cobley, J. Zeng, W. Li, C. H. Moran, Q. Zhang, D. Qin and Y. Xia, *Chem. Rev.*, 2011, **111**, 3669-3712.

156. N. A. Dhas, C. P. Raj and A. Gedanken, *Chem. Mater.*, 1998, **10**, 1446-1452.

157. Z. Peng and H. Yang, *Nano Today*, 2009, **4**, 143-164.

158. U. Leonhardt, *Nat. Photonics*, 2007, **1**, 207-208.

159. British Museum - The Lycurgus Cup. [Online] [Cited: 13 06 2012.] http://www.britishmuseum.org/explore/highlights/highlight_image.aspx?imag i=k737.jpg&retpage=20945

160. M. Faraday, *Philos. Trans. R. Soc. Lond.*, 1857, **147**, 145-181.

161. J. Turkevitch, P. C. Stevenson and J. Hillier, *Discuss. Faraday Soc.*, 1951, **11**, 55-75.

162. G. Frens, *Nature Phys. Sci.*, 1973, **241**, 20-22.

163. C. D. Bain, J. Evall and G. M. Whitesides, *J. Am. Chem. Soc.*, 1989, **111**, 7155-7164.

164. C. D. Bain and G. M. Whitesides, *J. Am. Chem. Soc.*, 1989, **111**, 7164-7175.

165. P. E. Laibinis, J. J. Hickman, M. S. Wrighton and G. M. Whitesides, *Science*, 1989, **245**, 845-847.

166. M. Giersig and P. Mulvaney, *Langmuir*, 1993, **9**, 3408-3413.

167. M. Brust, M. Walker, D. Bethell, D. J. Schiffrin and R. Whyman, *J. Chem. Soc. Chem. Comm.*, 1994, 801-802.

168. M. Brust, J. Fink, D. Bethell, D. J. Schiffrin and C. Kiely, *J. Chem. Soc. Chem. Comm.*, 1995, 1655-1656.

169. P. C. Lee and D. Meisel, *J. Phys. Chem.*, 1982, **86**, 3391-3395.

170. A. Henglein and M. Giersig, *J. Phys. Chem. B*, 1999, **103**, 9533-9539.

171. Z. S. Pillai and P. V. Kamat, *J. Phys. Chem. B*, 2004, **108**, 945-951.

172. D. L. Van Hyning and C. F. Zukoski, *Langmuir*, 1998, **14**, 7034-7046.

173. S. M. Heard, F. Grieser, C. G. Barraclough and J. V. Sanders, *J. Colloid Interf. Sci.*, 1983, **93**, 545-555.

174. N. Leopold and B. Lendl, *J. Phys. Chem. B*, 2003, **107**, 5723-5727.

175. M. V. Canamares, J. V. Garcia-Ramos, J. D. Gomez-Varga, C. Domingo and S. Sanchez-Cortes, *Langmuir*, 2005, **21**, 8546-8553.

176. M. V. Canamares, J. V. Garcia-Ramos, S. Sanchez-Cortes, M. Castillejo and M. Oujja, *J. Colloid Interf. Sci.*, 2008, **326**, 103-109.

177. N. R. Yaffe and E. W. Blanch, *Vib. Spectrosc.*, 2008, **48**, 196-201.

178. I. A. Larmour, K. Faulds and D. Graham, *J. Raman Spectrosc.*, 2012, **43**, 202-206.

179. G. Mie, *Annalen Der Physik*, 1908, **25**, 377-445.

180. S. K. Ghosh and T. Pal, *Chem. Rev.*, 2007, **107**, 4797-4862.

181. P. K. Jain, X. Huang, I. H. El-Sayed and M. A. El-Sayad, *Plasmonics*, 2007, **2**, 107-118.

182. W. Rechberger, A. Hohenau, A. Leitner, J. R. Krenn, B. Lamprecht and F. R. Aussenegg, *Opt. Commun.*, 2003, **220**, 137-141.

183. C. A. Mirkin, R. L. Letsinger, R. C. Mucic and J. J. Storhoff, *Nature*, 1996, **382**, 607-609.

184. A. P. Alivisatos, K. P. Johnsson, X. G. Peng, T. E. Wilson, C. J. Loweth, M. P. Bruchez and P. G. Schultz, *Nature*, 1996, **382**, 609-611.

185. B. J. Loweth, W. B. Caldwell, X. G. Peng, A. P. Alivisatos and P. G. Schultz, *Angew. Chem. Int. Ed.*, 1999, **38**, 1808-1812.

186. W. J. Parak, D. Gerion, D. Zanchet, A. S. Woerz, T. Pellegrino, C. Micheel, S. C. Williams, M. Seitz, R. E. Bruehl, Z. Bryant, C. Bustamante, C. R. Bertozzi and A. P. Alivisatos, *Chem. Mater.*, 2002, **14**, 2113-2119.

187. S. A. Claridge, S. L. Goh, J. M. J. Frechet, S. C. Williams, C. M. Micheel and A. P. Alivisatos, *Chem. Mater.*, 2005, **17**, 1628-1635.

188. D. Zanchet, C. M. Micheel, W. J. Parak, D. Gerion and A. P. Alivisatos, *Nano Lett.*, 2001, **1**, 32-35.

189. C. Sonnichsen, B. M. Reinhard, J. Liphardt and A. P. Alivisatos, *Nature Biotechnology*, 2005, **23**, 741-745.

190. J. J. Storhoff and C. A. Mirkin, *Chem. Rev.*, 1999, **99**, 1849-1862.

191. R. Elghanian, J. J. Storhoff, R. C. Mucic, R. L. Letsinger and C. A. Mirkin, *Science*, 1997, **277**, 1078-1081.

192. J. J. Storhoff, R. Elghanian, R. C. Mucic, C. A. Mirkin and R. L. Letsinger, *J.*

Am. Chem. Soc., 1998, **120**, 1959-1964.

193. J. J. Storhoff, A. A. Lazarides, R. C. Mucic, C. A. Mirkin, R. L. Letsinger and G. C. Schatz, *J. Am. Chem. Soc.*, 2000, **122**, 4640-4650.

194. R. C. Jin, G. S. Wu, Z. Li, C. A. Mirkin and G. C. Schatz, *J. Am. Chem. Soc.*, 2003, **125**, 1643-1654.

195. R. A. Reynolds, C. A. Mirkin and R. L. Letsinger, *J. Am. Chem. Soc.*, 2000, **122**, 3795-3796.

196. C. A. Mirkin, *Inorg. Chem.*, 2000, **39**, 2258-2272.

197. J. M. Nam, S. I. Stoeva and C. A. Mirkin, *J. Am. Chem. Soc.*, 2004, **126**, 5932-5933.

198. S. I. Stoeva, J. S. Lee, C. S. Thaxton and C. A. Mirkin, *Angew. Chem. Int. Ed.*, 2006, **45**, 3303-3306.

199. J. J. Storhoff, A. D. Lucas, V. Garimella, Y. B. Bao and U. R. Müller, *Nat. Biotechnol.*, 2004, **22**, 883–887.

200. J. Li, S. Song, D. Lib, Y. Suc, Q. Huang, Y. Zhao and C. Fan, *Biosens. Bioelectron.*, 2009, **24**, 3311–3315.

201. P. V. Baptista, M. Koziol-Montewka, J. Paluch-Oles, G. Doria and R. Franco, *Clin. Chem.*, 2006, **52**, 1433-1434.

202. P. Baptista, G. Doria, D. Henriques, E. Pereira and R. Franco, *J. Biotechnol.*, 2005, **119**, 111-117.

203. P. Bakthavathsalam, V. K. Rajendran and J. A. B. Mohammed, *J. Nanobiotechnol.*, 2012, **10**, 1-10.

204. J. Conde, J. M. de la Fuente and P. V. Baptista, *J. Nanobiotechnol.*, 2010, **8**, 1-8.

205. A. H. Alhasan, D. Y. Kim, W. L. Daniel, E. Watson, J. J. Meeks, C. S. Thaxton and C. A. Mirkin, *Anal. Chem.*, 2012, **84**, 4153-4160.

206. H. B. Shen, M. Hu, Y. B. Wang and H. Q. Zhou, *Biophys. Chem.*, 2005, **115**, 63-66.

207. H. B. Shen, M. Hu, Z. N. Yang, C. Wang and L. Z. Zhu, *Chin. Sci. Bull.*, 2005, **50**, 2016-2020.

208. F. McKenzie, K. Faulds and D. Graham, *Chem. Commun.*, 2008, **20**, 2367-2369.

209. D. G. Thompson, R. J. Stokes, R. W. Martin, R. J. Lundahl, K. Faulds and D. Graham, *Small*, 2008, **4**, 1054-1057.

210. D. G. Thompson, A. Enright, K. Faulds, W. E. Smith and D. Graham, *Anal. Chem.*, 2008, **80**, 2805-2810.

211. A. R. Herdt, S. M. Drawz, Y. Kang and T. A. Taton, *Colloid. Surface. B*, 2006, **51**, 130-139.

212. Z. Li, R. C. Jin, C. A. Mirkin and R. L. Letsinger, *Nucleic Acids Res.*, 2002, **30**, 1558-1562.

213. L. M. Demers, C. A. Mirkin, R. C. Mucic, R. A. Reynolds, R. L. Letsinger, R. Elghanian and G. Viswanadham, *Anal. Chem.*, 2000, **72**, 5535-5541.

214. R. L. Letsinger, R. Elghanian, G. Viswanadham and C. A. Mirkin, *Bioconjugate Chem.*, 2000, **11**, 289-291.

215. J. S. Lee, A. K. R. Lytton-Jean, S. J. Hurst and C. A. Mirkin, *Nano Lett.*, 2007, **7**, 2112-2115.

216. J. A. Dougan, C. Karlsson, W. E. Smith and D. Graham, *Nucleic Acids Res.*, 2007, **35**, 3668-3675.

217. J. Sharma, R. Chhabra, H. Yan and Y. Liu, *Chem. Commun.*, 2008, **18**, 2140-2142.

218. X. M. Qian, X. Zhou and S. M. Nie, *J. Am. Chem. Soc.*, 2008, **130**, 14934-14935.

219. S. A. Claridge, H. Y. W. Liang, S. R. Basu, J. M. J. Frechet and A. P. Alivisatos, *Nano Lett.*, 2008, **8**, 1202-1206.

220. W. T. Zhao, L. Lin and I. M. Hsing, *Bioconjugate Chem.*, 2009, **20**, 1218-1222.

221. W. Y. Zhao, L. Lin and I. M. Hsing, *Langmuir*, 2010, **26**, 7405-7409.

222. Y. B. Zu and Z. Q. Gao, *Anal. Chem.*, 2009, **81**, 8523-8528.

223. J. A. Dougan and K. Faulds, *Analyst*, 2012, **137**, 545-554.

224. C. V. Raman and K. S. Krishnan, *Nature*, 1928, **121**, 501-502.

225. W. E. Smith, *Modern Raman Spectroscopy*, John Wiley and Sons Ltd., United kingdom, 2005.

226. M. Fleischmann, P. J. Hendra and McQuilla.Aj, *Chem. Phys. Lett.*, 1974, **26**, 163-166.

227.   W. E. Smith, *Chem. Soc. Rev.*, 2008, **37**, 955-964.

228.   A. M. Stacy and R. P.Van Duyne, *Chem. Phys. Lett.*, 1983, **102**, 365-370.

229.   S. M. Nie and S. R. Emery, *Science*, 1997, **275**, 1102-1106.

230.   K. Kneipp, Y. Wang, H. Kneipp, L. T. Perelman, I. Itzkan, R. Dasari and M. S. Feld, *Phys. Rev. Lett.*, 1997, **78**, 1667-1670.

231.   A. C. Pineda and D. Ronis, *Journal of Chemical Physics*, 1985, **83**, 5330-5337.

232.   R. J. Stokes, A. Macaskill, P. J. Lundahl, W. E. Smith, K. Faulds and D. Graham, *Small*, 2007, **3**, 1593-1601.

233.   C. H. Munro, W. E. Smith, M. Garner, J. Clarkson and P. C. White, *Langmuir*, 1995, **11**, 3712-3720.

234.   K. Faulds, R. E. Littleford, D. Graham, G. Dent and W. E. Smith, *Anal. Chem.*, 2004, **76**, 592-598.

235.   A. W. Wark, R. J. Stokes, S. B. Darby, W. E. Smith and D. Graham, *J. Phys. Chem. C*, 2010, **114**, 18115-18120.

236.   R. W. Taylor, T.-C. Lee, O. A. Scherman, R. Esteban, J. Aizpurua, F. M. Huang, J. J. Baumberg and S. Mahajan, *ACS Nano*, 2011, **5**, 3878-3887.

237.   K. Faulds, R. P. Barbagallo, J. T. Keer, W. E. Smith and D. Graham, *Analyst*, 2004, **129**, 567-568.

238.   K. Faulds, W. E. Smith and D. Graham, *Anal. Chem.*, 2004, **76**, 412-417.

239.   K. Faulds, R. Jarvis, W. E. Smith, D. Graham and R. Goodacre, *Analyst*, 2008, **133**, 1505-1512.

240.   K. Kneipp, H. Kneipp, V. B. Kartha, R. Manoharan, G. Deinum, I. Itzkan, R. R. Dasari and M. S. Feld, *Phys. Rev. E*, 1998, **57**, 6281-6284.

241.   D. Graham, W. E. Smith, A. M. T. Linacre, C. H. Munro, N. D. Watson and P. C. White, *Anal. Chem.*, 1997, **69**, 4703-4707.

242.   N. R. Isola, D. L. Stokes and T. Vo-Dinh, *Anal. Chem.*, 1998, **70**, 1352-1356.

243.   X. Dou, T. Takama, Y. Yamaguchi, K. Hirai, H. Yamamoto, S. Doi and Y. Ozaki, *Appl. Optics*, 1998, **37**, 759-763.

244.   D. Graham, B. J. Mallinder, D. Whitcombe, N. D. Watson and W. E. Smith, *Anal. Chem.*, 2002, **74**, 1069–1074.

245.   M. M. Harper, B. Robertson, A. Ricketts and K. Faulds, *Chem. Commun.*,

2012, **48**, 9412-9414.

246. A. MacAskill, D. Crawford, D. Graham and K. Faulds, *Anal. Chem.*, 2009, **81**, 8134-8140.

247. J. A. Dougan, D. MacRae, D. Graham and K. Faulds, *Chem. Commun.*, 2011, **47**, 4649-4651.

248. D. van Lierop, K. Faulds and D. Graham, *Anal. Chem.*, 2011, **83**, 5817-5821.

249. M. M. Harper, J. A. Dougan, N. C. Shand, D. Graham and K. Faulds, *Analyst*, 2012, **137**, 2063-2068.

250. E. Hao and G. C. Schatz, *J. Chem. Phys.*, 2004, **120**, 357-366.

251. D. Graham, D. G. Thompson, W. E. Smith and K. Faulds, *Nat. Nanotechnol.*, 2008, **3**, 548-551.

252. D. G. Thompson, K. Faulds, W. E. Smith and D. Graham, *J. Phys. Chem. C*, 2010, **114**, 7384-7389.

253. X. M. Qian, X. Zhou and S. M. Nie, *J. Am. Chem. Soc.*, 2008, **130**, 14934-14935.

254. F. McKenzie and D. Graham, *Chem. Commun.*, 2009, 5757-5759.

255. F. McKenzie, K. Faulds and D. Graham, *Nanoscale*, 2010, **2**, 78-80.

256. L. Guerrini, F. McKenzie, A. W. Wark, K. Faulds and D. Graham, *Chem. Sci.*, 2012, **3**, 2262-2269.

257. Z. Zhang, Y. Wen, Y. Ma, J. Luo, L. Jiang and Y. Song, *Chem. Commun.*, 2011, **47**, 7407-7409.

258. L. Fadris, *Chem. Commun.,* 2012, **48**, 9346-9348.

2 Aims

The aim of this thesis was to investigate oligonucleotide functionalised nanoparticles as viable sensors for the detection of DNA related to disease by monitoring aggregation of the nanoparticles via extinction and surface enhanced resonance Raman (SERRS) spectroscopy. The objectives were:

- To synthesise modified oligonucleotide probes for conjugation to metal nanoparticles.
    - o Synthesis of oligonucleotide probes with thioctic acid and thiol moieties.
    - o Oligonucleotide sequences chosen with biological relevance, i.e. MRSA genome.
    - o Prepare gold and silver nanoparticle conjugates with thioctic acid and/ or thiol modified MRSA detection probes.
- To investigate the stability of oligonucleotide-nanoparticle conjugates.
    - o Compare the stability of oligonucleotide-nanoparticle conjugates with different modifications, spacer moieties and dyes conjugated to the nanoparticle surface.
    - o Expose conjugates to biological environments associated with certain DNA detection assays to assess their stability, i.e. presence of biological additives, elevated temperatures and increased ionic buffer concentrations.
- To use the stable oligonucleotide-nanoparticle conjugates to detect specific, biologically relevant, DNA sequences.
    - o To confirm the biological activity of the oligonucleotide-nanoparticle conjugates through hybridisation-induced aggregation of the conjugates using synthetic target oligonucleotides.
    - o Evaluate sensitivity of the assay using SE(R)RS.
    - o Extend the conjugate hybridisation assay methodology to detect genomic and/ or PCR product related to MRSA.

3 Oligonucleotide-Nanoparticle Conjugates

There has been significant interest in using metallic nanoparticles functionalised with oligonucleotides as biodiagnostic tools. Combining the unique sequence-specific base-pairing capabilities of oligonucleotides with the distinct optical properties of metallic nanoparticles was first reported, independently, by both Mirkin *et al.* and Alivisatos *et al.* in the same issue of *Nature* in 1996. [1] [2] Both groups reported the self-assembly of aggregates induced by DNA hybridisation using gold nanoparticles functionalised with thiol-modified oligonucleotide sequences. Using oligonucleotide-nanoparticle conjugates for biodiagnostic applications offers several advantages over unmodified oligonucleotides; formation of aggregates induced by DNA hybridisation results in a colour change that can be monitored colorimetrically and the melting profile of oligonucleotide-nanoparticle conjugates is extraordinarily sharp compared to "molecular" duplex melting, allowing discrimination of single nucleotide polymorphisms (SNPs). [3] In this chapter, both gold and silver nanoparticles were functionalised with oligonucleotides modified with thiol and thioctic acid in order to evaluate their stability for use as bionanosensors for DNA detection.
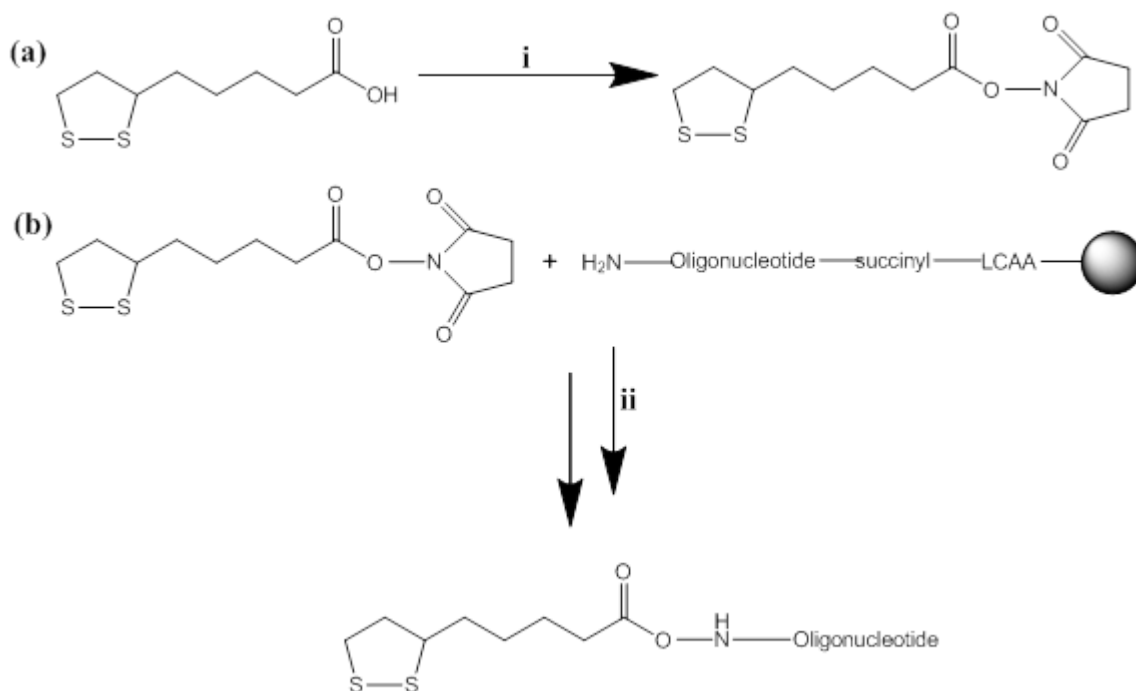
3.1 Modified Oligonucleotide Synthesis

In order to incorporate surface seeking functionality, modification of DNA is required. Surface seeking moieties can be incorporated into an oligonucleotide during automated synthesis at various positions, such as at the 5'-terminus using a modified phosphoramidite that couples to the free 5'-hydroxyl group of the final base in the sequence or at the 3'-terminus by a modified solid support with the moiety attached or mid-sequence *via* a modified base. [4] [5] [6] [7] The backbone of DNA can also be modified to incorporate a surface seeking moiety by replacing one of the oxygen atoms in the phosphodiester with a sulphur atom *via* a sulfurizing agent, producing a phosphorothioate oligonucleotide. [8] In this work, oligonucleotides

modified at either 5'- or 3'-terminus with thiol-containing moieties were utilized in nanoparticle functionalisation for subsequent stability and hybridisation experiments.

3.1.1 Synthesis of 5' Thioctic Acid-Modified Oligonucleotides

The most common and widely used method of functionalising oligonucleotides to the surface of gold nanoparticles is by using a monothiol-modified oligonucleotide that tethers to the nanoparticle surface *via* the thiol moiety. In addition to the monothiol modification, steroid cyclic disulfide groups, [9] multiple thiol-anchors, [10] triple cyclic disulfide moieties [11] and dithiocarbamate ligands [12] have been investigated to potentially increase the stability of oligonucleotide-nanoparticle conjugates. Of interest, however, is the research published by Dougan *et al.* where thioctic acid-modified oligonucleotides were shown to dramatically increase the stability of both gold and silver nanoparticles. [13] As well as offering increased stability to the resulting conjugates, thioctic acid is commercially available and stable to both the conditions used for routine synthesis and deprotection of oligonucleotides, which is why thioctic acid-modified oligonucleotides are utilized in this work. Thioctic acid can be readily introduced to an amino-modified oligonucleotide using post-synthetic solid phase modification with the active *N*-hydroxysuccinimidyl (NHS) ester of thioctic acid. Although commercially available, the thioctic acid-NHS ester was synthesised according to the literature procedure. [13] The NHS ester of thioctic acid was prepared by esterification of the carboxylic acid with hydroxysuccinimide in the presence of *N*-(3-dimethylaminopropyl)-*N'*-ethylcarbodiimide (EDC) (scheme 3.1a). The thioctic acid-NHS ester can react with a primary amine – itself readily introduced into an oligonucleotide sequence at the 5'-terminus *via* a modified phosphoramidite or at the 3' terminus *via* a modified solid support.   The oligonucleotide synthesis was carried out using standard phosphoramidite chemistry on the solid support. The final monomer added to the oligonucleotide chain was a 5'-monomethoxytrityl (MMT) protected amino group.   When synthesis of the oligonucleotide was complete, an extended deblock step (1 hour) was manually performed by addition of the standard deblock solution (3 % trichloroacetic acid in DCM) across the solid support. A longer deblock step is required because the MMTr protecting group is more stable compared to standard DNA synthesis with

dimethoxytrityl (DMT) protected 5'-alcohols. A solution of thioctic acid-NHS ester in acetonitrile and triethlyamine was added to the solid support through syringes to react with the deprotected primary amine of the oligonucleotide (scheme 3.1b).

Scheme 3.1. (a) Synthesis of thioctic acid-NHS ester via esterification of the carboxylic acid using NHS and EDC. (b) 5' modification of amino-modified oligonucleotide immobilised on the CPG column with thioctic acid-NHS ester. (i) EDC, NHS, 0 °C, DCM. (ii) TCA, DCM, Et₃N, MeCN, NH₄OH.

The thioctic acid-NHS ester was allowed to react on the column overnight. The column was washed with acetonitrile and then treated with concentrated ammonium hydroxide to remove the protecting groups and cleave the oligonucleotide from the solid support. The final mixture, after deprotection, contains failure sequences from oligonucleotide synthesis, protecting groups and unreacted thioctic acid-NHS ester which must be removed from the full thioctic acid-modified oligonucleotide sequence before it can be used for nanoparticle functionalisation. The deprotected oligonucleotide mixture was subjected to purification by reversed-phase high performance liquid chromatography (RP-HPLC) after removing the ammonium hydroxide by rotary evaporation and resuspending the oligonucleotide mixture in water. RP-HPLC separates components in a mixture based on their hydrophobicity –

the more hydrophobic species are retained longer on the column. Figure 3.1 shows a typical RP-HPLC chromatogram of a thiocotic acid-modified oligonucleotide. The peak with a retention time of 15-17 min was collected and analysed by matrix-assisted laser desorption ionisation – time of flight (MALDI-TOF) mass spectrometry to confirm the synthesis of the desired 5'-thioctic acid modified oligonucleotide.
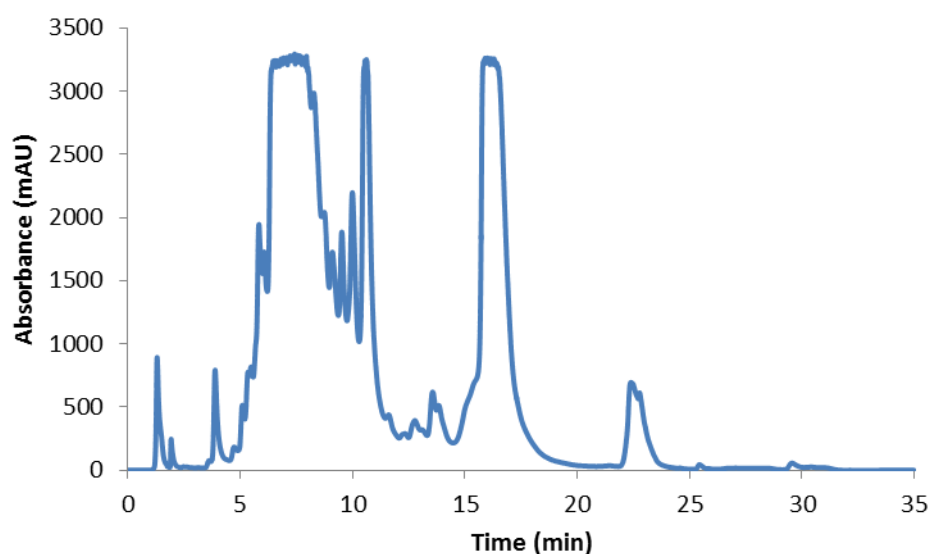

Figure 3.1. RP-HPLC of a 5'-thioctic acid modified oligonucleotide after solid-phase synthesis with thioctic acid-NHS ester monitored at 260 nm. Oligonucleotide contains 3 hexaethylene glycol (HEG) spacer units. MALDI MS required: 8234.16, MALDI MS found: 8234.89.

3.1.2 Synthesis of 5'-Thiol Modified Oligonucleotides

For 5'-thiol modification, oligonucleotide synthesis was performed using standard phosphoramidite chemistry. The final monomer added to the sequence was a DMT protected thiol group. The final deblock step was omitted from the synthesis cycle in order to retain the DMT protecting group on the 5'-thiol. Once the synthesis was complete, the base-sensitive protecting groups were removed and the oligonucleotide cleaved from the solid support by treatment with ammonium hydroxide resulting in an oligonucleotide mixture containing the desired sequence plus failure sequences and protecting groups. The oligonucleotide mixture was subjected to purification by reverse phase HPLC. The omission of the final deblock step during synthesis aids purification since the final DMT protecting group on the thiol moiety is a

hydrophobic species which is retained longer on the column thereby ensuring complete separation of the desired oligonucleotide from the failure sequences. A typical RP-HPLC chromatogram of a thiol-modified oligonucleotide sequence is shown in figure 3.2. As can be seen, the desired oligonucleotide sequence has a retention time of ~ 24 minutes which is completely separated from the failure peaks at ~ 8 minutes. After purification of the oligonucleotide, MALDI-TOF was performed to confirm the synthesis of the correct sequence. Before the oligonucleotides can be used to functionalise nanoparticles, the final DMTr protecting group must be removed. This was accomplished by treatment with silver nitrate (AgNO$_3$) and dithiothreitol (DTT). [14] The silver removes the trityl group and forms a silver salt of the thiol which is subsequently removed by reaction with the DTT to form an insoluble silver-DTT complex. After several steps of centrifugation to remove the silver-DTT complex, the supernatant containing the deprotected oligonucleotide was removed and subjected to size-exclusion chromatography to remove any excess DTT.
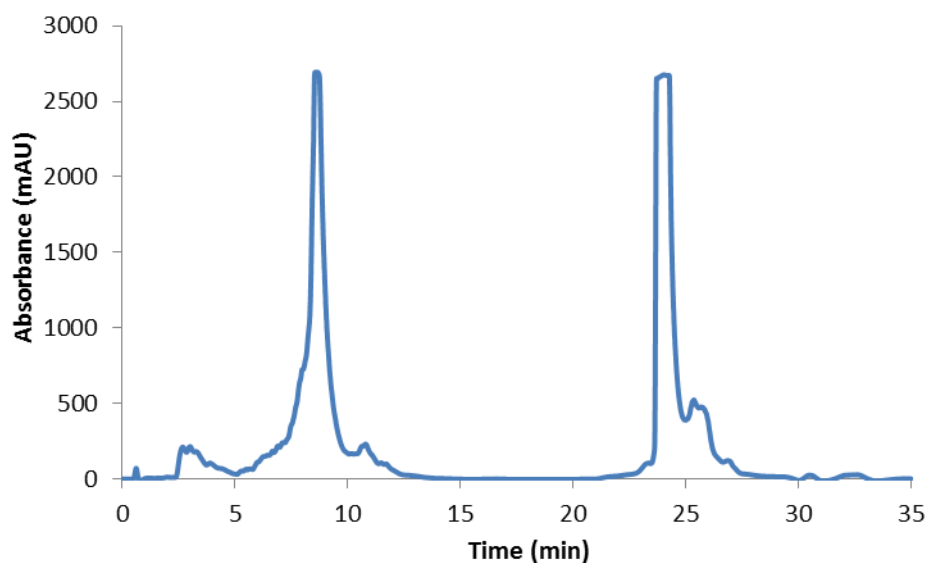

Figure 3.2. RP-HPLC of 'trityl on' oligonucleotide sequence with 5'-thiol modification and a 10 adenine nucleobase spacer monitored at 260 nm. MALDI MS required: 10161, MALDI MS found: 10166.

3.1.3 Modified Oligonucleotides and Spacer Groups

In addition to the thioctic acid and thiol modifications, the oligonucleotides in this study contain spacer groups adjacent to the terminal 5'-modification. Spacer groups are incorporated into the oligonucleotide probe design in order to distance the recognition sequence from the nanoparticle surface, thereby minimising steric crowding when hybridisation of the complementary target occurs. The spacer groups chosen were a 10 adenine nucleobase spacer, a hexaethylene glycol (HEG) spacer, and 3 hexaethylene glycol spacers. The HEG spacers were incorporated into the oligonucleotide sequence by addition of the Spacer-CE phosphoramidite 18 (17-*O*-(4,4'-dimethoxytrityl)-hexaethyleneglycol, 1-[(2-cyanoethyl)-(N, N-diisopropyl)]) monomer (structure shown in figure 3.3). Spacers composed of HEG groups have been shown to improve oligonucleotide loading onto nanoparticles surfaces, compared to spacers composed of nucleobases. [15] This is due to a reduction of electrostatic repulsion between neighbouring ethylene glycol moieties and decreased surface interactions between the ethylene glycol and the nanoparticle surface. [15]
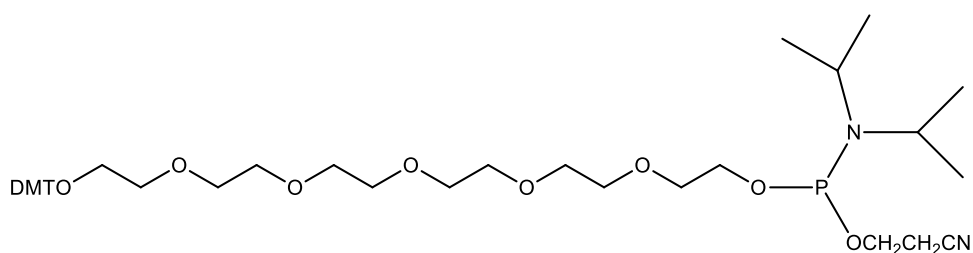

Figure 3.3. Structure of the Spacer-CE phosphoramidite 18 used to incorporate hexaethylene glycol (HEG) functionality in to oligonucleotides.

The modified oligonucleotides were conjugated to the surface of gold and silver nanoparticles so that their stability in biological buffers and biological integrity (*i.e.* hybridisation with complementary DNA) could be evaluated. The oligonucleotide-nanoparticle conjugates were investigated for their use as probes in an assay to detect specific DNA sequences related to disease by surface enhanced resonance Raman scattering (SERRS).

3.2 Oligonucleotide Functionalised Nanoparticles

Colloidal solutions of gold and silver nanoparticles can be easily and reproducibly synthesised by the reduction of the corresponding metal salt in the presence of sodium citrate. [16] [17] For gold nanoparticles, an aqueous solution of sodium tetrachoroaurate was heated until boiling at which point an aqueous solution of trisodium citrate was added and boiling maintained for approximately 15 minutes. For silver nanoparticles, distilled water was heated to 40 °C and a solution of silver nitrate was added. Heating continued to 98 °C where a solution of trisodium citrate was added. Heating was maintained at 98 °C for 90 minutes. Both methods produce stable colloids that can be readily functionalised with oligonucleotides (figures 3.4 and 3.5). To confirm that the desired particle size was obtained the nanoparticles were subjected to analysis by dynamic light scattering (DLS), which relates the Brownian motion of the particles to particle size. The analysis revealed that the silver nanoparticles were 67.5 nm ± 1.3 nm. To functionalise nanoparticles with oligonucleotides the required number of moles of oligonucleotide are added directly to a solution of gold or silver nanoparticles, followed by several incremental steps of sodium chloride addition. The addition of sodium chloride is necessary to maximise oligonucleotide loading on to the nanoparticles. Sodium ions effectively minimise inter-strand repulsion between neighbouring oligonucleotides by interacting with the DNA backbone. In addition to increasing oligonucleotide loading, sodium chloride is necessary for the subsequent hybridisation of complementary oligonucleotide sequences. It is important that the salt 'ageing' step be carried out slowly, *i.e.* increments of 0.05 M to a final concentration of 0.1 M over 48 hours, because raising the salt concentration too rapidly can result in irreversible aggregation of the nanoparticle solution. Irreversible aggregation or precipitation of the nanoparticles occurs due to disruption of the citrate layer surrounding the nanoparticle surface, thereby eliminating electrostatic repulsion that results in the formation of large nanoparticle aggregates that sediment out of solution. After the salt addition step, oligonucleotide-nanoparticle conjugates were subjected to several rounds of centrifugation to remove any excess oligonucleotides from solution. The conjugates were then analysed by UV-Vis spectroscopy to determine their concentration and to determine if any aggregation of the conjugates occurred during the salt 'ageing' or

centrifugation steps. Typical UV-Vis spectra are displayed in figure 3.4 and figure 3.5 for oligonucleotide-gold nanoparticle conjugates and oligonucleotide-silver nanoparticle conjugates, respectively. The conjugates were also analysed by DLS to determine the size of the conjugates and to confirm that DNA was functionalized to the surface. Analysis of the silver nanoparticle conjugates revealed that the particle size after oligonucleotide functionalisation was found to be 91.3 nm ± 1.5 nm.
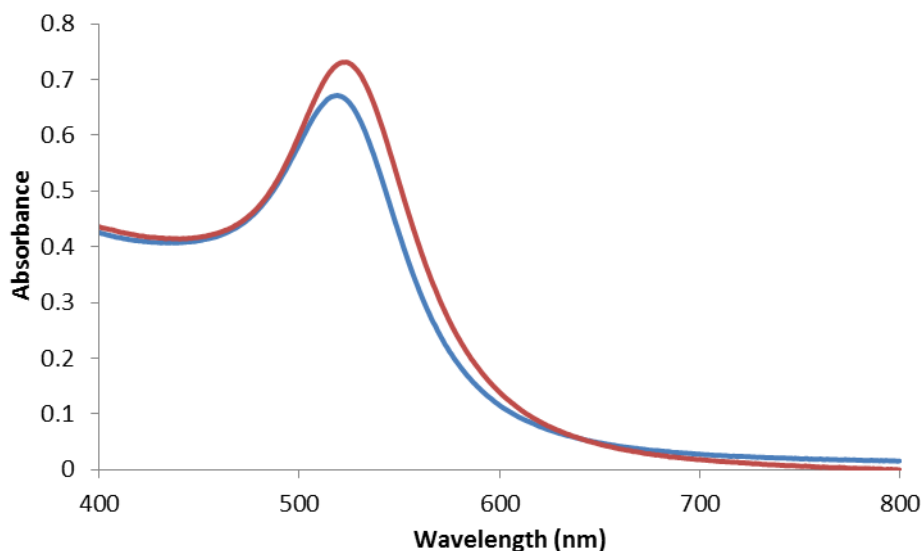

Figure 3.4. Extinction spectra of gold nanoparticles (blue, λ_{max} = 519 nm) and oligonucleotide functionalised gold nanoparticles (red, λ_{max} = 523 nm).
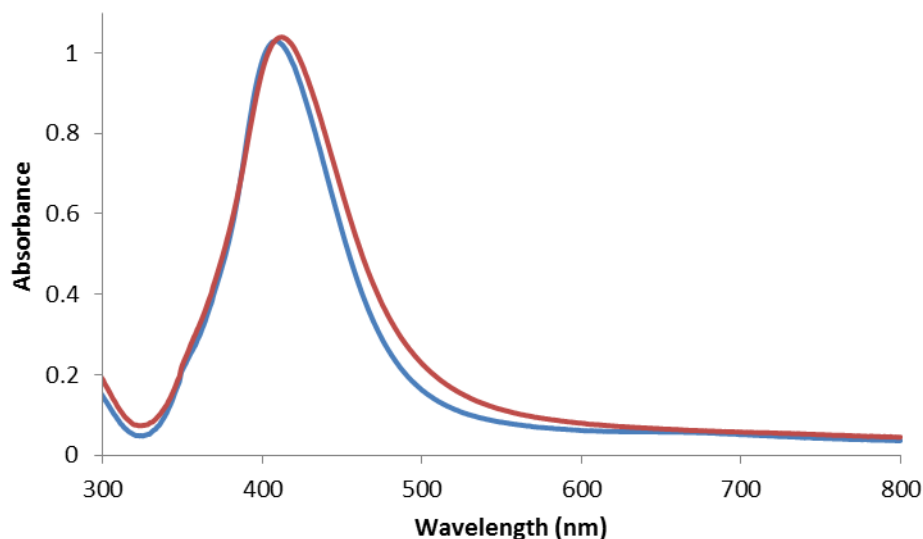
Figure 3.5.   Extinction spectra of silver nanoparticles (blue, λ_{max} = 410 nm) and oligonucleotide functionalised silver nanoparticles (red, λ_{max} = 412 nm).

For unfunctionalised gold nanoparticles, a strong surface plasmon absorbance was obtained at ~ 520 nm which is typical of small, ~ 15 nm, gold nanoparticles.   In comparison, oligonucleotide functionalised gold nanoparticles were observed to exhibit a strong plasmon absorbance ~ 5 nm red-shifted from the 'bare' gold nanoparticles.   This is a typical spectrum observed for stable oligonucleotide-gold nanoparticle conjugates.   If aggregation had occurred, there would be a larger red-shift plus broadening and dampening of the absorbance at ~ 520 nm and absorbance at longer wavelengths (~ 650 nm).   Silver nanoparticles produce similar properties when functionalised with oligonucleotides, with conjugates exhibiting a red-shift in the plasmon absorption peak (from ~410 nm to ~412 nm).

3.3   Dye-Labelled   Oligonucleotide-Nanoparticle Conjugates

In order to be SERRS active, a visible chromophore must be attached to the analyte (since the analyte does not contain a visible chromophore) to act as a label for subsequent detection of the analyte.   Typically, chromphores, in the form of a fluorescent dye, can be incorporated into an oligonucleotide during routine synthesis *via* a dye-labelled solid support (for 3'-modification) or dye phosphoramidite (for 5'-

or in-sequence modification). However, a method for labelling the nanoparticles with a SERRS-active dye, rather than the oligonucleotide, was chosen for this study since the nanoparticle are already afforded stability from the oligonucleotides, which allows a greater freedom of choice in dye. As reported by Graham *et al.*, nanoparticles can be labelled pre-oligonucleotide functionalisation where the dye is added to a solution of nanoparticles first and the remaining surface sites are functionalised with oligonucleotides. [18] This method requires a dye whose structure will not infer any non-specific aggregation to the nanoparticles, as any small clusters that are formed will be highly SERRS-active. To overcome this, a SERRS-active dye was synthesised that comprised of an azo group (chromophore), a benzotriazole group (surface complexing group), and a phenol group (negatively charged to prevent non-specific aggregation). A similar method, reported by Qian *et al.,* involved functionalising the nanoparticle surface with low molecular weight polyethylene glycol (PEG) molecules to stabilise the nanoparticles after the addition of the SERRS-active dye and oligonucleotides. [19] An alternative method, devised by MacKenzie *et al.*, used a post-oligonucleotide functionalisation step, where the nanoparticles are stabilized by the addition of the oligonucleotides first and the remaining surface sites are functionalised with the SERRS-active dye. [20] This method has the advantage that a large number of dye labels can be used that would normally cause irreversible aggregation of the nanoparticle conjugates because the nanoparticles are already afforded enhanced stability from surface-immobilised oligonucleotides. In this work, dye labels incorporating an isothiocyanate (-N=C=S) group were used for adsorption of the SERRS-active dye to the nanoparticle surface (structures shown in Figure 3.6). An aqueous solution of isothiocyanate dye was added in excess to the oligonucleotide-nanoparticle conjugate. The conjugate was then left to incubate overnight and then centrifuged to remove any excess dye molecules that did not adsorb onto the surface.
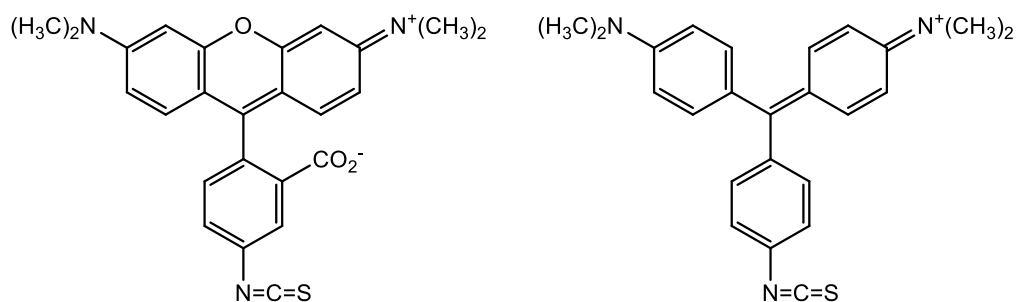
Figure 3.6. Chemical structures of dyes containing the isothiocyanate (-N=C=S) moiety. Left: Carboxytetramethylrhodamine (TAMRA), Right: Malachite Green.

With the successful preparation of conjugates using gold and silver nanoparticles, it was decided to investigate the conjugates for their stability before utilizing them as hybridisation probes for DNA detection.

3.4 Stability of Dye-Labelled Oligonucleotide-Nanoparticle Conjugates

In order to be utilized as biosensors in diagnostic assays, oligonucleotide-nanoparticle conjugates must exhibit enhanced stability in a number of increasingly challenging biological environments. It is established that conditions such as high salt concentrations (0.3 − 1.0 M NaCl), prolonged or cycled temperatures like those used in PCR, and treatment with particular biological buffer additives, *e.g.* dithiothreitol (DTT) or mercaptoethanol are known to cause irreversible aggregation of nanoparticles by desorption of the Au-S bond at the nanoparticle surface. [21]

The surface of the nanoparticles is densely packed with oligonucleotides, which inhibit aggregation of the conjugates through electrostatic repulsion and steric protection between neighbouring oligonucleotides. Oligonucleotides can be displaced from the nanoparticle surface *via* ligand exchange by treatment with a dithiothreitol (DTT, structure shown in figure 3.7), in the presence of salts. This causes irreversible aggregation of the nanoparticle solution because the electrostatic and steric protection normally afforded by the oligonucleotides is disrupted leading to the formation of large nanoparticle clusters that precipitate out of solution. Aggregation results in a red-shift of the surface plasmon to the visible region of the electromagnetic spectrum which can be easily monitored by UV-Vis spectroscopy.
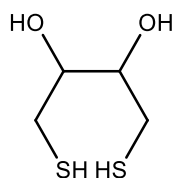
Figure 3.7. Structure of dithiothreitol (DTT), which is used for displacing the oligonucleotides from the surface of the nanoparticles.

Table 3.1 shows the different oligonucleotide linkers and spacer groups that were used for the nanoparticle stability assessment. To minimise any sequence specificity of the stability of the conjugates the same oligonucleotide sequence was used throughout the stability studies: 5'-ATGGCATGAGTAACGAAGAATA. Six sequences were used for the stability assessment, 3 sequences with a 5'-thioctic acid modification and 3 sequences with a 5'-thiol modification. In addition, a spacer group was incorporated into each oligonucleotide to assess the effect of different spacer compositions on the stability of the nanoparticle conjugates. The incorporated spacers included a 10 adenine (10A) spacer, hexaethylene glycol (HEG) spacer and 3 HEG spacers. The relative stability of the different conjugates of gold and silver nanoparticles was assessed by comparing the rates of aggregation of the nanoparticle conjugates after treatment with DTT according to protocols outlined by Mirkin *et al.* and Dougan *et al.* [13] [21]

Linker	Probe	Spacer
	P1	AAAAAAAAAA
	P2	HEG
	P3	HEG-HEG-HEG
HS——Oligo	P4	AAAAAAAAAA
	P5	HEG
	P6	HEG-HEG-HEG

Table 3.1. Linker and spacer groups used for stability studies. The oligonucleotide sequence for all linkers and spacers was 5' ATGGCATGAGTAACGAAGAATA.

3.4.1 Stability of Oligonucleotide-Gold Nanoparticle Conjugates

In order to assess their stability, oligonucleotide-modified gold nanoparticle conjugates were diluted to a concentration of 0.5 nM to which 4 µl of DTT was added (10 mM final concentration) at 37 °C. Aggregation of the nanoparticles resulted in a characteristic gradual disappearance of the surface plasmon peak at ~ 520 nm indicative of monodispersed gold nanoparticles and a gradual appearance of a new surface plasmon peak at longer wavelengths between 600 – 700 nm. Absorption spectra were taken at periodic intervals. For thioctic acid-modified oligonucleotides, spectra were recorded at 10 min intervals. In contrast, spectra for thiol-modified oligonucleotides were obtained at 1 min intervals, due to aggregation occurring much more rapidly. Figure 3.8 shows a typical UV-Vis spectrum obtained from thioctic acid-modified gold nanoparticle conjugates treated with DTT at 10 min intervals. Figure 3.9 shows a typical UV-Vis spectrum obtained from thiol-modified gold nanoparticle conjugates treated with DTT at 1 min intervals. By simply glancing at the spectra it is clear there is an obvious difference in the stability of each system. It can be clearly seen that the thiol-modified conjugates reach a state of complete aggregation within a minute compared to the thioctic-acid conjugates which do not reach a state of aggregation for several scans, each representing 10 min. However, these spectra do not provide an easy method for establishing the aggregation rates for comparison of the stabilities of each linker system. Plotting the absorbance at a specific wavelength against time provides a simpler method to establish the stability for each linker system.
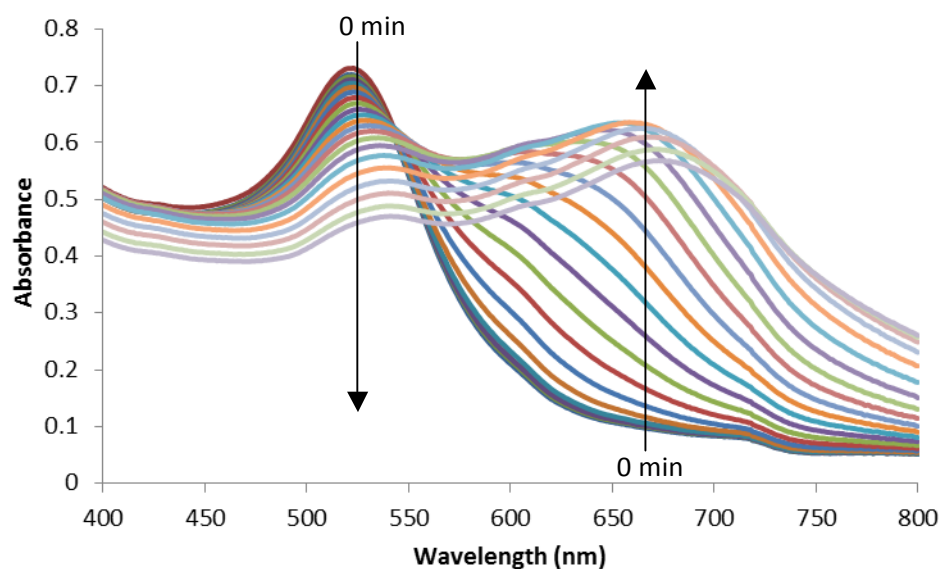
Figure 3.8. Extinction spectra showing thioctic acid-modified gold nanoparticle conjugates treated with 10 mM DTT at 10 min intervals. Arrows are included to indicate progression of aggregation with time.
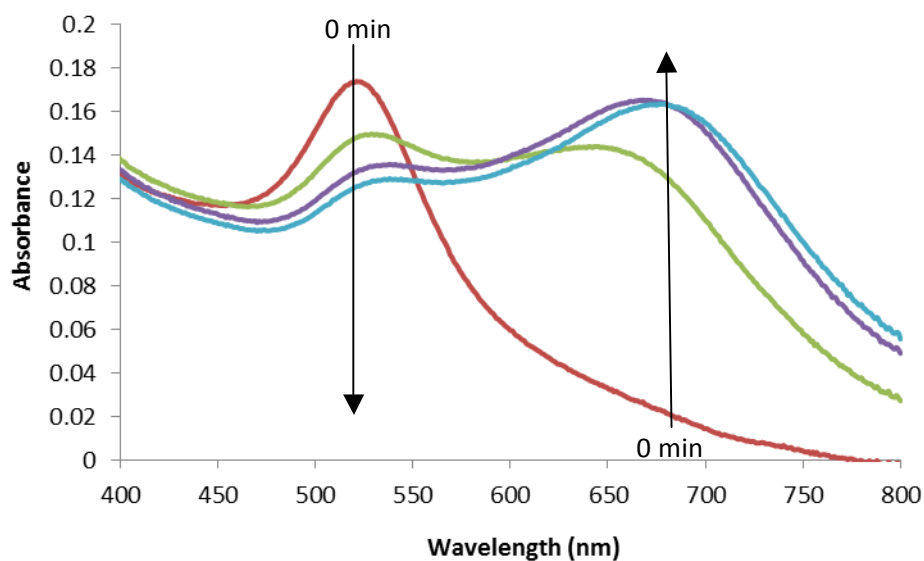

Figure 3.9. Extinction spectra showing thiol-modified gold nanoparticle conjugates treated with 10 mM DTT at 1 min intervals. Arrows are included to indicate progression of aggregation with time.

Figure 3.10 and figure 3.11 show graphs detailing the stability of thioctic acid-modified and thiol-modified conjugates, respectively. P1, P2 and P3 represent thioctic acid-modified gold nanoparticle conjugates with 10A, HEG and (HEG)$_3$ spacer groups, respectively and P4, P5 and P6 represent thiol-modified gold nanoparticle conjugates with 10A, HEG and (HEG)$_3$ spacer groups, respectively. The graphs show the absorbance at 675 nm *versus* time (min). The values at 675 nm were selected due to the increase in absorbance observed at that wavelength indicating aggregation has occurred. The half-lives, *i.e.* time taken for absorbance at 675 nm to reach half maximum of complete aggregation, for each conjugate was calculated in a similar fashion to Dougan *et al*. This allows easier comparison of the different stabilities for each linker and spacer groups.
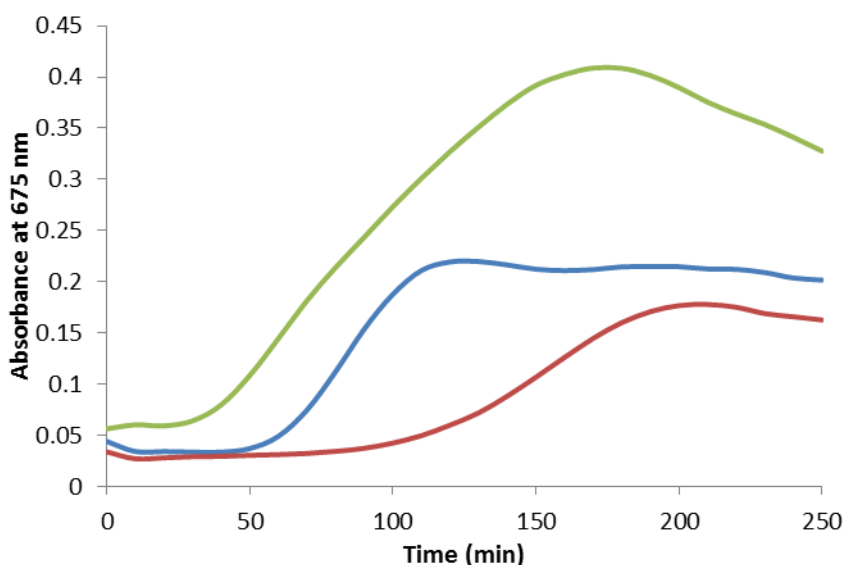

Figure 3.10. Absorbance at 675 nm versus time (min) for thioctic acid-modified oligonucleotide gold nanoparticle conjugates after treatment with DTT. Blue: 10A (P1), Red: HEG (P2), Green: (HEG)3 (P3)
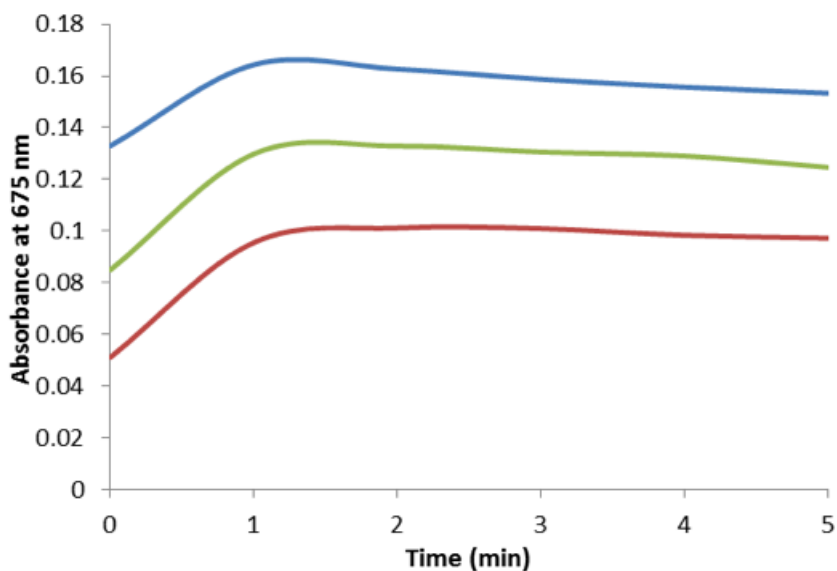
Figure 3.11. *Absorbance at 675 nm versus time (min) for thiol-modified oligonucleotide gold nanoparticle conjugates after treatment with DTT. Blue: 10A (P4), Red: HEG (P5), Green: (HEG)3 (P6)*

Table 3.2 displays the half-lives for the thioctic acid-modified gold nanoparticle conjugates and thiol-modified oligonucleotide gold nanoparticle conjugates. Examination of the half-lives for each conjugates reveals the major differences in stability of the thioctic acid-modified conjugates compared to the thiol-modified conjugates. In about 30 seconds all of the thiol-modified conjugates (10A, HEG, (HEG)$_3$) have reached a half-way point of aggregation and are completely aggregated by 1 min. In comparison, the half-lives for the thioctic acid-modified gold nanoparticle conjugates are 80, 150 and 100 min for the 10A, HEG and (HEG)$_3$ spacers, respectively. These results highlight the enhanced stability achieved by using thioctic acid as a linker for making oligonucleotide-nanoparticle conjugates.
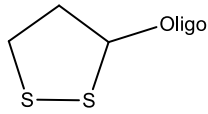
Linker	Probe	$T_{1/2}$ (min)
	P1	80
	P2	150
	P3	100
	P4	0.5
	P5	0.5
	P6	0.5

Table 3.2. Half-lives of thioctic acid-modified and thiol-modified oligonucleotide gold nanoparticle conjugates.

Examination of figure 3.10 shows that the thioctic acid-modified conjugates have an initial period of sustained stability that varies according to the spacer group. As reported by Dougan *et al.*, this is attributed to the higher loading of thioctic-acid modified oligonucleotides on the nanoparticle surface. The higher surface coverage means that in the early stages of DTT incubation, where a small number of oligonucleotides are lost, there is still sufficient coverage from neighbouring oligonucleotides to confer stability to the nanoparticles. However, there reaches a point where the surface coverage of the oligonucleotides reaches a critical point and aggregation occurs. The initial period of sustained stability is dependent on the spacer group employed: 10A (*P1*) = 30 min, HEG (*P2*) = 90 min, and (HEG)$_3$ (*P3*) = 50 min (Figure 3.8). Full aggregation of the thioctic acid-modified conjugates is reached by ~ 3 hours, after this time there is a gradual decrease in the absorbance of the plasmon band at 675 nm due to the formation of large aggregates that precipitate from solution, eventually resulting in a colourless supernatant. It should be noted that previous research has indicated that incorporation of ethylene glycol spacer units results in an increase in surface coverage of oligonucleotides, however, as reported here the increased surface coverage does not necessarily translate to an increase in stability of the nanoparticle conjugates. [15] Similarly, research reported by Mirkin *et al.*, [9] showed that a steroidal disulfide group, which

was incorporated into an oligonucleotide, increased the stability of gold nanoparticles. This observation was confirmed by spectroscopic characterisation in research performed by Garcia *et al.*, [22] who used sulfur K-edge XANES spectroscopy to confirm that dihydrolipoic acid (a reduced form of thioctic acid) anchors to gold nanoparticles *via* both sulphur atoms. Mirkin suggested that this increase in stability of the nanoparticles may have been due to the presence of the steroidal group, however, as similar results are reported here using a disulfide species in the absence of a steroidal group, it appears that the binding of both sulphur atoms to the nanoparticle surface is the driving force in providing enhanced stability.

3.4.2 Stability of Dye-labelled Oligonucleotide-Gold Nanoparticle Conjugates

In order to make the oligonucleotide-nanoparticle conjugates SERRS-active, a chromophore, in the form of an isothiocyanate dye was added to the nanoparticle conjugates post-oligonucleotide functionalisation. The dyes chosen for this study were TAMRA (TRITC) and malachite green (MGITC) (figure 3.6). Once prepared, as described in section 3.3, the dye labelled oligonucleotide-nanoparticle conjugates were subjected to the same DTT treatment as reported for the non-dye labelled conjugates.

Figure 3.12 shows the absorbance at 675 nm *versus* time for the TAMRA-labelled gold nanoparticle conjugates functionalised with thioctic acid-modified oligonucleotides. The addition of TRITC has improved the stability of the conjugates: for P1, P2 and P6 the half-lives are now 290, 200 and 180 min, respectively *c.f.* 80, 150 and 100 min for the non-dye-labelled analogues. Similarly, the addition of TRITC has improved the stability of the thiol-modified oligonucleotide-nanoparticle conjugates (Figure 3.13). The half-lives of P4, P5 and P6 are now 15, 15 and 20 min, respectively *c.f.* 0.5 min for the non-dye-labelled analogues. The addition of TRITC has introduced an initial period of sustained stability similar to the thioctic-acid analogues to the thiol-linked conjugates. For P4, P5 and P6 the initial period of sustained stability is approximately 10 min. This is an improvement over the non-dye labelled thiol-modified conjugates, which have reached the point of full aggregation in less than one minute.

Figure 3.12. Absorbance at 675 nm versus time (min) for TAMRA-labelled thioctic acid-modified oligonucleotide gold nanoparticle conjugates after treatment with DTT. Blue: 10A (P1), Red: HEG (P2), Green: (HEG)₃ (P3)

Figure 3.13. Absorbance at 675 nm versus time (min) for TAMRA-labelled thiol-modified oligonucleotide gold nanoparticle conjugates after treatment with DTT. Blue: 10A (P4), Red: HEG (P5), Green: (HEG)₃ (P6)

With the observation that increased stability could be achieved by incorporation of an isothiocyanate dye label, it was decided to test the reproducibility of the stability with a different dye – malachite green isothiocyanate. Figure 3.14 shows the results

obtained by performing the same DTT treatment experiments using MGITC-labelled thioctic-acid modified oligonucleotide-nanoparticle conjugates. With MGITC, the half-lives for thioctic acid-modified conjugates are 60, 220 and 220 min for P1, P2 and P3, respectively. Figure 3.15 shows the absorbance at 675 nm *versus* time graph for the MGITC-labelled thiol-modified oligonucleotide nanoparticle conjugates. The half-lives obtained for the MGITC-labelled thiol-modified conjugates show similar results to the TRITC-labelled thiol conjugates. The half-lives obtained for P4, P5 and P6 were 35, 25 and 25 min, respectively. In addition, as with the TRITC-thiol conjugates, an initial period of sustained stability is observed. For each of the conjugates, the period of sustained stability is 10 min, equivalent to that of the TRITC-labelled thiol-modified conjugates. A summary of the half-lives obtained for each system are shown in table 3.3.
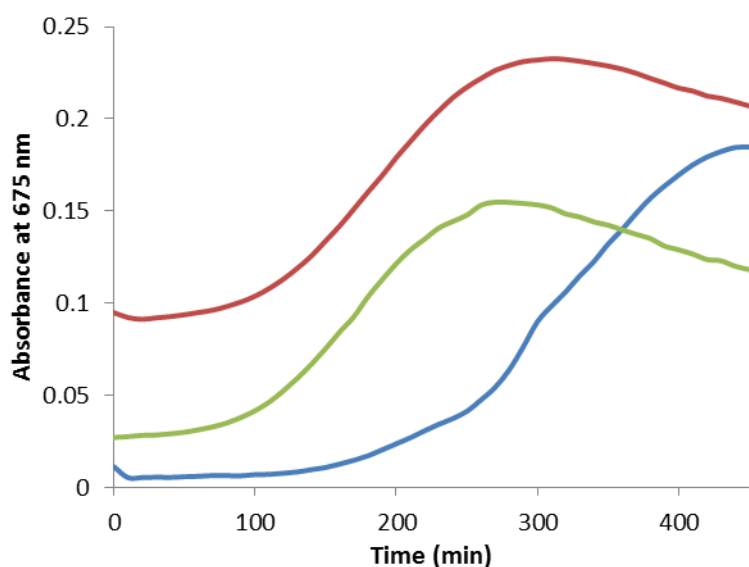

Figure 3.14. Absorbance at 675 nm versus time (min) for malachite green-labelled thioctic acid-modified oligonucleotide gold nanoparticle conjugates after treatment with DTT. Blue: 10A (P1), Red: HEG (P2), Green: (HEG)₃ (P3)
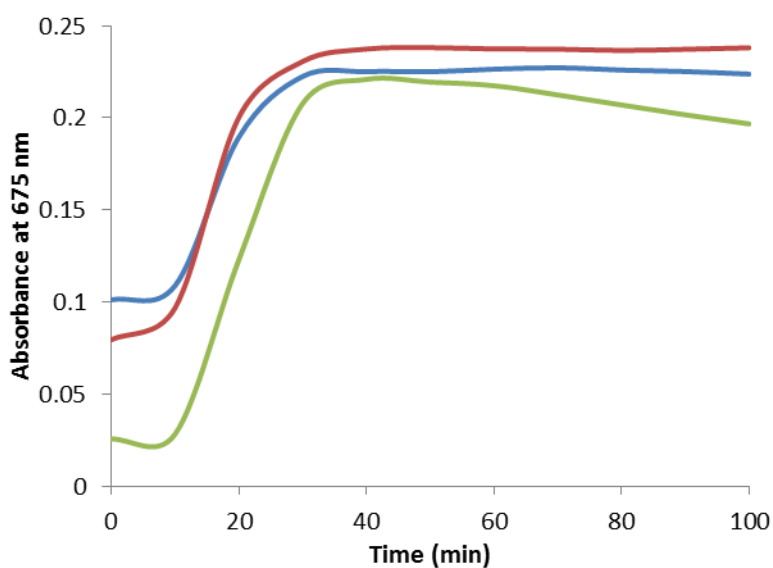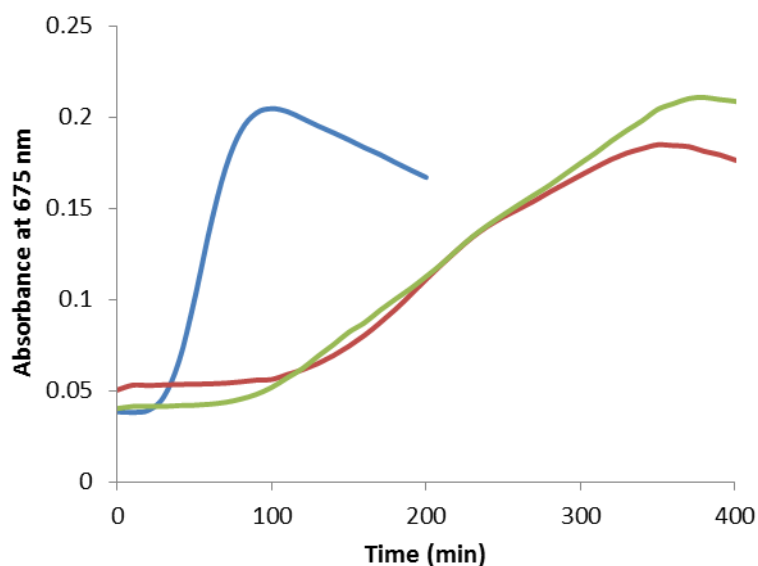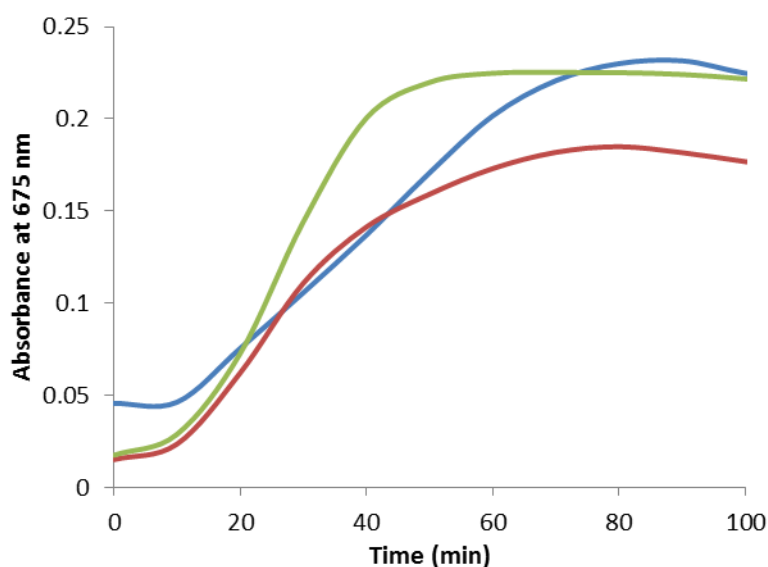
Figure 3.15. Absorbance at 675 nm versus time (min) for malachite green-labelled thiol-modified oligonucleotide gold nanoparticle conjugates after treatment with DTT. Blue: 10A (P4), Red: HEG (P5), Green: (HEG)₃ (P6)
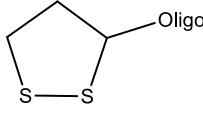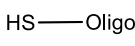
Linker	Probe	Non-dye labelled Conjugates $T_{1/2}$ (min)	TAMRA-labelled Conjugates $T_{1/2}$ (min)	Malachite green-labelled Conjugates $T_{1/2}$ (min)
Oligo (S—S)	P1	80	290	60
	P2	150	200	220
	P3	100	180	220
HS—Oligo	P4	0.5	15	35
	P5	0.5	15	25
	P6	0.5	20	25

Table 3.3. Half-lives of TAMRA-ITC and Malachite green-ITC labelled thioctic acid-modified and thiol-modified oligonucleotide gold nanoparticle conjugates.

These results show that enhanced stability can be achieved by the simple addition of an isothiocyanante dye to both thiol and thioctic acid-modified oligonucleotide-gold nanoparticle conjugates. This is significant as thiol modified oligonucleotides are more readily obtained and can now be coupled with a single post-conjugation step

for enhanced stability. In addition, this allows the potential for the SERRS-active conjugates to be used in more challenging environments due to the enhanced stability afforded by the dye label.

3.4.3 Stability of Oligonucleotide-Silver Nanoparticle Conjugates

Silver nanoparticles are less stable than gold nanoparticles; however, the molar extinction coefficient of silver nanoparticles is 100 × greater than for gold nanoparticles which benefits detection when using optical spectroscopies by increasing sensitivity. Unlike gold nanoparticles, silver nanoparticles are more difficult to reproducibly synthesize, with batches often showing differences in size, shape and optical characteristics. Despite this hurdle, a number of studies have reported the use of silver nanoparticles as optical sensors for the detection of DNA: hybridisation in a sandwich assay format, [23] mixed-metal hybridisations, [24] conjugate-to-conjugate hybridisation [11] [25] and hybridisation on a functionalised surface. [26] Functionalising silver nanoparticles with thioctic acid- and thiol-modified oligonucleotides is achieved *via* methods analogous to oligonucleotide-gold nanoparticle conjugate production, *i.e.* a solution of oligonucleotides is added directly onto a solution of silver nanoparticles, followed by slow NaCl addition over 48 hours to a final concentration of 0.1 M NaCl and, finally, centrifugation to produce the oligonucleotide-silver nanoparticle conjugate. It is important to note that for this study, to prevent irreversible aggregation of the silver nanoparticle conjugates at the centrifugation step; a two-step centrifugation method was employed where the conjugates were centrifuged at 4000 rpm for 15 minutes and the supernatant was collected and centrifuged at 6500 rpm for 15 minutes. Both pellets at the bottom of the eppindorfs were combined for the final oligonucleotide-silver nanoparticle conjugate. Figures 3.16 and figure 3.17 show spectra obtained from the DTT displacement of thioctic acid- and thiol-modified oligonucleotide silver nanoparticle conjugates, respectively. There are three visible changes that occur during progressive aggregation of oligonucleotide-silver nanoparticle conjugates: a dampening in the plasmon band at ~ 410 nm, followed by a red-shift and a clear broadening in the plasmon as the aggregation proceeds. Observation of the spectra

shows that there is a difference in stability between the two modifications. The thioctic acid-modified conjugates' spectra were recorded every 5 minutes and are more stable than the thiol-modified conjugates - spectra recorded at 1 min intervals. With the stability study of oligonucleotide-gold nanoparticle conjugates, it was easier to establish the stability of the conjugate system by plotting the absorbance at a particular wavelength *versus* time, however, where gold nanoparticles have a secondary plasmon peak emerging at longer wavelengths during aggregation, silver nanoparticles display a broadening and dampening of the plasmon and, as such, it is more informative to plot the absorbance at 410 nm *versus* time for oligonucleotide-silver nanoparticle conjugates.
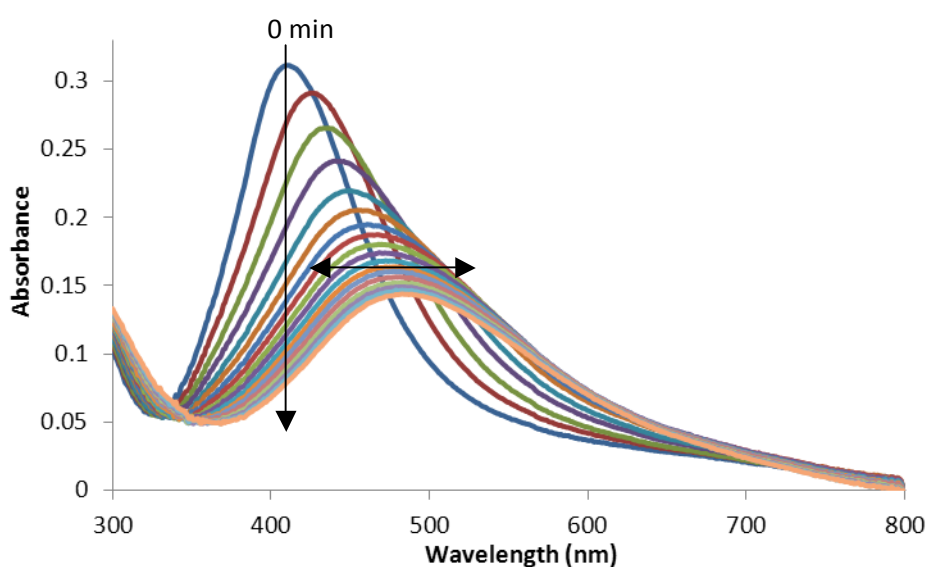

Figure 3.16. Extinction spectra showing thioctic acid-modified silver nanoparticle conjugates treated with 10 mM DTT at 5 min intervals. Arrows are included to indicate progression of aggregation with time.
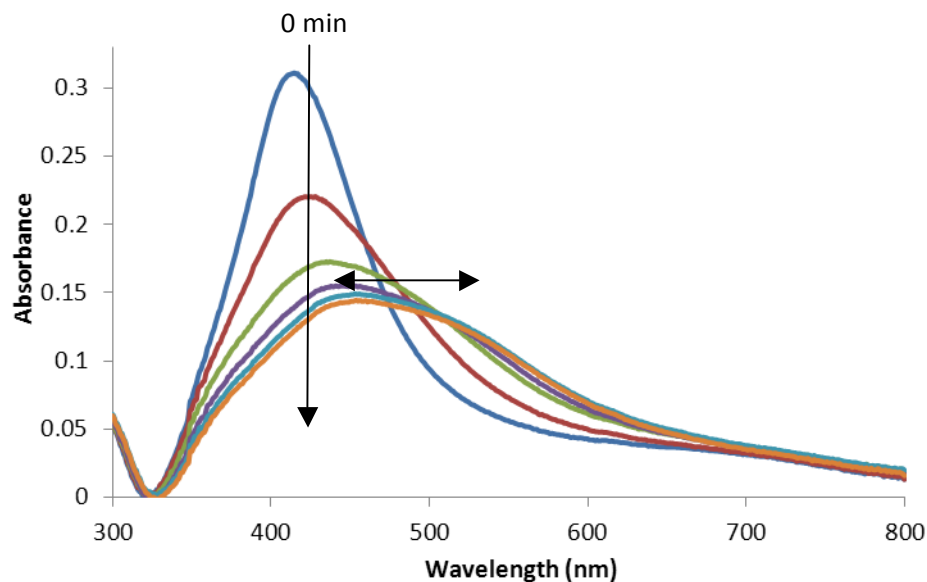
Figure 3.17.   Extinction spectra showing thiol-modified silver nanoparticle conjugates treated with 10 mM DTT at 1 min intervals.   Arrows are included to indicate progression of aggregation with time.

The oligonucleotides chosen for functionalisation of silver nanoparticles were identical in sequence and spacer groups to those used for gold-nanoparticle functionalisation.   However, attempts to functionalise silver-nanoparticles with P1 (thioctic acid-10A) were unsuccessful.   The P1-silver nanoparticle conjugates irreversibly aggregated during the salt aging process rendering them useless for further investigation.   To attempt to overcome this, a slower salt aging process was employed, *i.e.* adding smaller aliquots of NaCl over a longer time period, which resulted in the conjugates surviving the salt aging process.   However, during centrifugation the conjugates were still prone to irreversibly aggregate, as a result, the stability of P1-Ag is not reported here.   Figure 3.18 and figure 3.19 show the absorbance at 410 nm *versus* time for thioctic acid- and thiol-modified oligonucleotide-silver nanoparticle conjugates, respectively.   Examination of figure 3.18 shows that silver nanoparticles functionalised with thioctic acid-modified oligonucleotides begin to aggregate immediately upon addition of DTT, unlike on gold nanoparticles, where the same sequence shows an initial period of sustained stability.   Although irreversible aggregation occurs immediately, the rate of aggregation is slower for thioctic acid-modified conjugates than thiol-modified conjugates (figure 3.19).
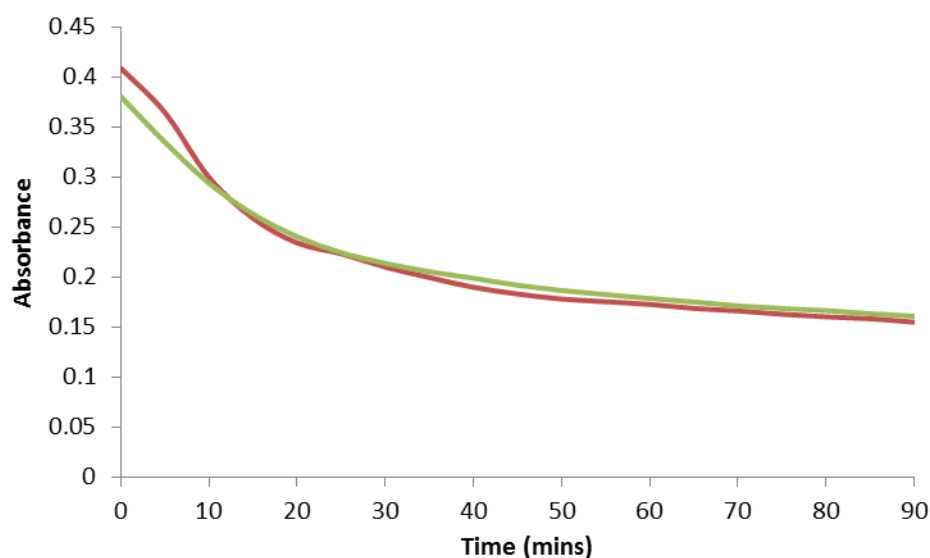
Figure 3.18. Absorbance at 410 nm versus time for thioctic acid-modified oligonucleotide-silver nanoparticle conjugates after treatment with DTT. **Red**: *HEG (P2) and* **Green**: *(HEG)₃ (P3).*
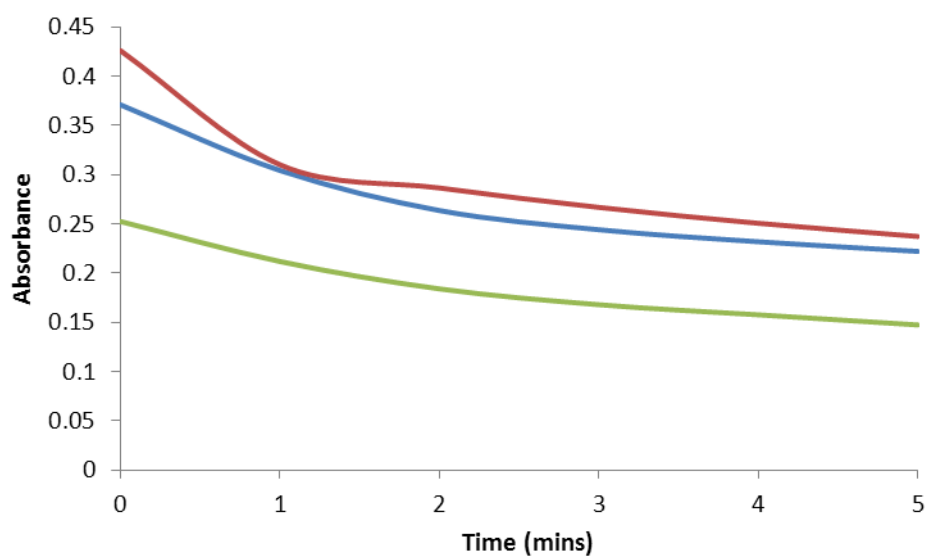
Figure 3.19. Absorbance at 410 nm versus time for thiol-modified oligonucleotide-silver nanoparticle conjugates after treatment with DTT. **Blue**: *10A (P4)* **Red**: *HEG (P5) and* **Green**: *(HEG)₃ (P6).*

The half-lives of the oligonucleotide-silver nanoparticle conjugates are shown in table 3.4 for ease of comparison. It can be concluded that there is an obvious difference between the rates of aggregation of the thioctic acid- and thiol-modified

nanoparticle conjugates. The thioctic acid modified conjugates (P2 and P3) both have half-lives of 10 minutes, which is in stark contrast to the thiol-modified conjugates, which have half-lives of 1 minute or less. These results show that thioctic acid-modified oligonucleotide-silver nanoparticle conjugates are less stable than their gold analogues and the half-lives for the thioctic acid-modified silver conjugates are within the stability region of the dye-labelled thiol-modified oligonucleotide gold nanoparticle conjugates (Table 3.2).
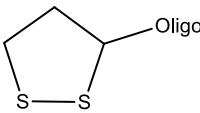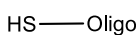
Linker	Probe	$T_{1/2}$ (min)
	P1	N/A
	P2	10
	P3	10
	P4	0.75
	P5	0.75
	P6	1

Table 3.4. Half-lives of thioctic acid-modified (P1, P2 and P3) and thiol-modified oligonucleotide silver nanoparticle conjugates (P4, P5 and P6). A half-life for P1 was not obtained due to irreversible aggregation of the conjugate during centrifugation.

3.4.4 Stability of Dye-Labelled Oligonucleotide-Silver Nanoparticle Conjugates

Oligonucleotide-silver nanoparticle conjugates were incubated with an isothiocyanate dye label in order to investigate if, like the oligonucleotide-gold nanoparticle conjugates, the incorporation of the dye label would confer extra stability to the conjugates. TRITC was added to thioctic acid- and thiol-modified oligonucleotide-silver nanoparticle conjugates using the same method derived for oligonucleotide-gold nanoparticle conjugates. The dye-labelled conjugates were then subjected to treatment with DTT and monitored using UV-Vis spectroscopy. Figure

3.20 and figure 3.21 show absorbance at 410 nm *versus* time for TRITC-labelled thioctic acid- and thiol-modified oligonucleotide-silver nanoparticle conjugates, respectively. Examination of figure 3.20 reveals that, in comparison to gold nanoparticles, incorporating the isothiocyanate dye label onto silver nanoparticles does not affect the stability of the conjugate. The half-lives of the TRITC-labelled P2- and P3-silver nanoparticle conjugates were 10 minutes for both conjugates. However, examination of figure 3.21 reveals that the isothiocyanate dye label does increase the stability of the thiol system, albeit only by a small margin. The half-lives of the TRITC-labelled thiol-modified oligonucleotide-silver nanoparticle conjugates are 2.5, 2 and 2.5 minutes for P4, P5 and P6, respectively. This is analogous to the results obtained for the dye-labelled thiol-modified oligonucleotide-gold nanoparticles. Although the stability contribution of the dye label on silver nanoparticles is not as significant as the gold nanoparticle conjugates, this result confirms that addition of an isothiocyanate dye label can enhance the stability of oligonucleotide-nanoparticle conjugates. Table 3.5 summarises the half-lives obtained for the dye-labelled oligonucleotide-silver nanoparticle conjugates.
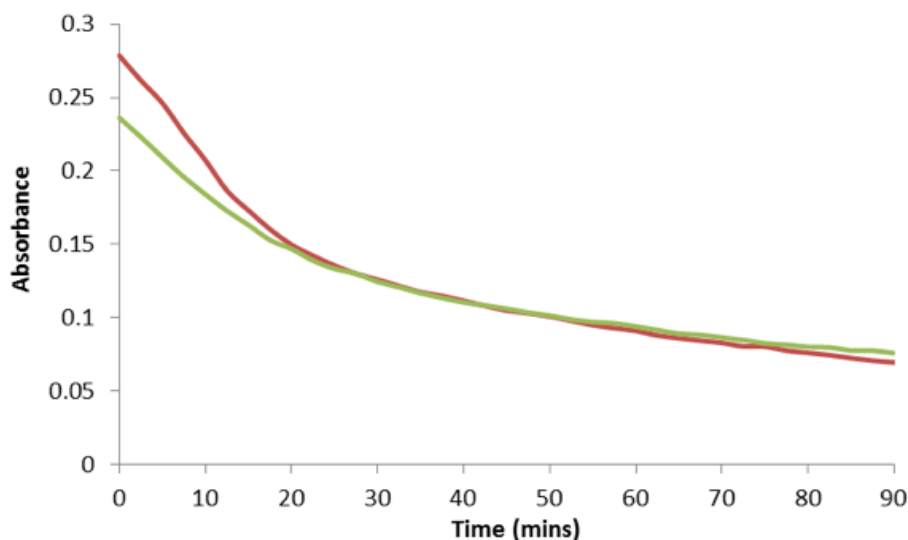
Figure 3.20. Absorbance at 410 nm versus time for TRITC-labelled thioctic acid-modified oligonucleotide-silver nanoparticle conjugates after treatment with DTT. Red: HEG (P2) and Green: (HEG)₃ (P3).
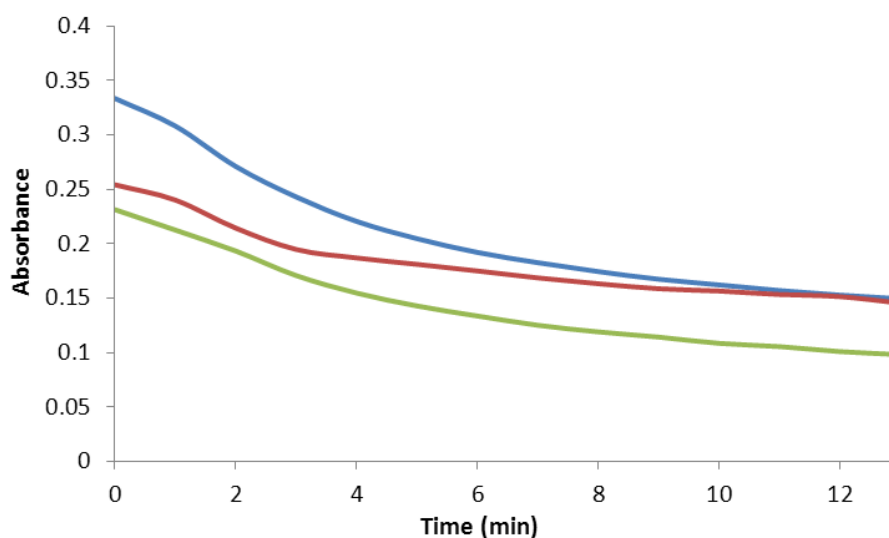
*Figure 3.21. Absorbance at 410 nm versus time for TRITC-labelled thiol-modified oligonucleotide-silver nanoparticle conjugates after treatment with DTT. **Blue**: 10A (P4), **Red**: HEG (P5) and **Green**: (HEG)₃ (P6).*
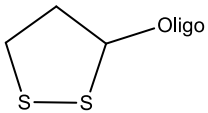
Linker	Probe	Non-dye Labelled Conjugates $T_{1/2}$ (min)	TAMRA-labelled conjugates $T_{1/2}$ (min)
	P1	N/A	N/A
	P2	10	10
	P3	10	10
	P4	0.75	2.5
	P5	0.75	2
	P6	1	2.5

Table 3.5. Half-lives of TAMRA-labelled thioctic acid-modified (P1, P2 and P3) and thiol-modified oligonucleotide silver nanoparticle conjugates (P4, P5 and P6). A half-life for P1 was not obtained due to irreversible aggregation of the conjugate during centrifugation.

3.5 Conclusions

Conjugation of oligonucleotides with thioctic acid has been successfully achieved *via* production of the active ester of thioctic acid. This conjugation was achieved by synthesising a 5'-amino-modified oligonucleotide, which was subsequently treated with the thioctic acid-NHS ester. The thioctic acid-modified oligonucleotides, plus 5'-thiol-modified oligonucleotides, were used to prepare conjugates of gold and silver nanoparticles. Successful conjugation of oligonucleotides to the nanoparticles was assessed by UV-Vis spectroscopy with conjugation resulting in a small red-shift of the absorbance spectrum compared to the unconjugated nanoparticles. In addition, the oligonucleotide-nanoparticle conjugates were prepared for subsequent SERSS experiments by the addition of an isothiocyanate-containing dye – TAMRA and malachite green.

In order to assess the viability of the oligonucleotide-nanoparticle conjugates as sensors for DNA detection assays, the stability of each conjugate system was studied. The thiol- and thioctic acid-modified oligonucleotide-nanoparticle conjugates contained differing spacer groups adjacent to the surface-seeking moiety – a 10 adenine nucleotide spacer, a hexaethylene glycol (HEG) spacer and a spacer consisting of 3 HEG units. The nanoparticle conjugates were subjected to a displacement study using dithiothreitol (DTT). The thioctic acid-modified oligonucleotide-gold nanoparticle conjugates showed greater stability than the thiol-modified conjugates. TA-Au conjugates showed half-lives of 150 minutes compared to just 0.5 minutes for the thiol-Au conjugates. Similarly, the thioctic acid-modified oligonucleotide-silver nanoparticle conjugates showed a similar trend in stability showing half-lives of 10 minutes compared to 1 minute for the thiol-Ag conjugates. While this was not as considerable as the stabilities observed for gold nanoparticle conjugates, the thioctic acid-Ag conjugates are still more stable that either the gold or silver nanoparticle thiol systems.

The dye-labelled oligonucleotide-nanoparticle conjugates were subjected to the same DTT displacement study as the non-dye labelled conjugates. Interestingly, a further increase in stability was observed for both the thioctic acid- and thiol-modified oligonucleotide-gold nanoparticle conjugates with TA-Au half-lives for the TAMRA

and malachite green-labels being up to 290 minutes and 220 minutes, respectively. For thiol-Au conjugates, the half-lives were up to 20 minutes and 35 minutes for TAMRA and malachite green labels, respectively. The thiol-Au conjugates display an initial period of sustained stability, similar to TA-Au, when subjected to displacement by DTT. In contrast, the silver nanoparticle analogues for thioctic acid-modified oligonucleotides showed no enhanced stability upon addition of the TAMRA dye label. However, while not as pronounced as that observed for the gold analogues, the thiol-Ag TAMRA labelled conjugates now have half-lives of up to 2.5 minutes. While not as considerable as the gold analogues, this shows that for the thiol system stability can be improved by the incorporation of an isothiocyanate dye label.

In conclusion, thioctic acid-modified oligonucleotide-nanoparticle conjugates have been successfully prepared for both gold and silver nanoparticles and the ability for the thioctic acid-modified nanoparticle conjugates to boost stability compared to the thiol-modified conjugates has been demonstrated. In addition, it has been demonstrated that addition of an isothiocyanate dye-label can enhance the stability of conjugates containing both thioctic acid and thiol-modified oligonucleotides.

3.6 References

1. C. A. Mirkin, R. L. Letsinger, R. C. Mucic and J. J. Storhoff, *Nature*, 1996, **382**, 607-609.

2. A. P. Alivisatos, K. P. Johnsson, X. G. Peng, T. E. Wilson, C. J. Loweth, M. P. Bruchez and P. G. Schultz, *Nature*, 1996, **382**, 609-611.

3. J. J. Storhoff, R. Elghanian, R. C. Mucic, C. A. Mirkin and R. L. Letsinger, *J. Am. Chem. Soc.*, 1998, **120**, 1959-1964.

4. B. S. Sproat, B. Beijer, P. Rider and P. Neuner, *Nucleic Acids Res.*, 1987, **15**, 4837-4848.

5. B. S. Sproat, B. Beijer and P. Rider, *Nucleic Acids Res.*, 1987, **15**, 6181-6196.

6. C. R. Petrie, M. W. Reed, A. D. Adams and R. B. Meyer, *Bioconjugate Chem.*, 1992, **3**, 85-87.

7. D. A. Stetsenko and M. J. Gait, *Bioconjugate Chem.*, 2001, **12**, 576-586.

8. M. Matsukura, G. Zon, K. Shinozuka, C. A. Stein, H. Mitsuya, J. S. Cohen

and S. Broder, *Gene*, 1988, **72**, 343-347.

9. R. L. Letsinger, R. Elghanian, G. Viswanadham and C. A. Mirkin, *Bioconjugate Chem.*, 2000, **11**, 289-291.

10. Z. Li, R. C. Jin, C. A. Mirkin and R. L. Letsinger, *Nucleic Acids Res.*, 2002, **30**, 1558-1562.

11. J. S. Lee, A. K. R. Lytton-Jean, S. J. Hurst and C. A. Mirkin, *Nano Lett.*, 2007, **7**, 2112-2115.

12. J. Sharma, R. Chhabra, H. Yan and Y. Liu, *Chem. Commun.*, 2008, **18**, 2140-2142.

13. J. A. Dougan, C. Karlsson, W. E. Smith and D. Graham, *Nucleic Acids Res.*, 2007, **35**, 3668-3675.

14. B. A. Connolly and P. Rider, *Nucleic Acids Res.*, 1985, **13**, 4485-4502.

15. S. J. Hurst, A. K. R. Lytton-Jean and C. A. Mirkin, *Anal. Chem.*, 2006, **78**, 8313-8318.

16. G. Frens, *Nature-Phys. Sci.*, 1973, **241**, 20-22.

17. P. C. Lee and D. Meisel, *J. Phys. Chem.*, 1982, **86**, 3391-3395.

18. D. Graham, D. G. Thompson, W. E. Smith and K. Faulds, *Nat. Nanotechnol.*, 2008, **3**, 548-551.

19. X. M. Qian, X. Zhou and S. M. Nie, *J. Am. Chem. Soc.*, 2008, **130**, 14934-14935.

20. F. McKenzie and D. Graham, *Chem. Commun.*, 2009, **38**, 5757-5759.

21. L. M. Demers, C. A. Mirkin, R. C. Mucic, R. A. Reynolds, R. L. Letsinger, R. Elghanian and G. Viswanadham, *Anal. Chem.*, 2000, **72**, 5535-5541.

22. B. Garcia, M. Salome, L. Lemelle, J. L. Bridot, P. Gillet, P. Perriat, S. Roux and O. Tillement, *Chem. Commun.*, 2005, **3**, 369-371.

23. D. G. Thompson, A. Enright, K. Faulds, W. E. Smith and D. Graham, *Anal. Chem.*, 2008, **80**, 2805-2810.

24. D. G. Thompson, R. J. Stokes, R. W. Martin, R. J. Lundahl, K. Faulds and D. Graham, *Small*, 2008, **4**, 1054-1057.

25. B. C. Vidal, T. C. Deivaraj, J. Yang, H. P. Too, G. M. Chow, L. M. Gan and J. Y. Lee, *New J. Chem.*, 2005, **29**, 812-816.

26. I. Tokareva and E. Hutter, *J. Am. Chem. Soc.*, 2004, **126**, 15784-15789.

4 Assembly of Oligonucleotide-Nanoparticle Conjugates via DNA Hybridisation

The controlled assembly of nanoparticles *via* biomolecular recognition has significantly impacted the field of biodiagnostics. Oligonucleotide nanoparticle conjugates have been utilized in a number of DNA detection methods, including, for example - detection of the *BRCA-1* gene using multifunctional cross-linking gold nano-aggregates, [1] unamplified detection of genomic methicillin-resistant *staphylococcus aureus (MRSA)* based on the scattering properties of gold nanoparticle probes, [2] bio-bar-code detection of anthrax using DNA-functionalised gold nanoparticles, [3] colorimetric detection of gold nanoparticle probes by parallel triplex formation [4] and PCR of gold nanoparticle-bound primers. [5] [6] In light of results indicating the enhanced stability afforded by thioctic acid-modified oligonucleotides, it was important to investigate the biological integrity of the nanoparticle conjugates through DNA hybridisation in order to establish their viability as functional bionanosensors. DNA hybridisation-facilitated assembly of nanoparticles results in a distinctive colour change due to distance-dependent coupling of the surface plasmon resonances. Thus hybridisation-induced aggregation of nanoparticles can be easily monitored by UV-Vis spectroscopy. In studies performed by Mirkin *et al.*, [7] [8] it was revealed that oligonucleotide-nanoparticle conjugate hybridisation is directed by a number of factors, namely:

> ➢   The density of the oligonucleotides on the nanoparticle surface,
> ➢   Nanoparticle size,
> ➢   Concentration of salt present, and
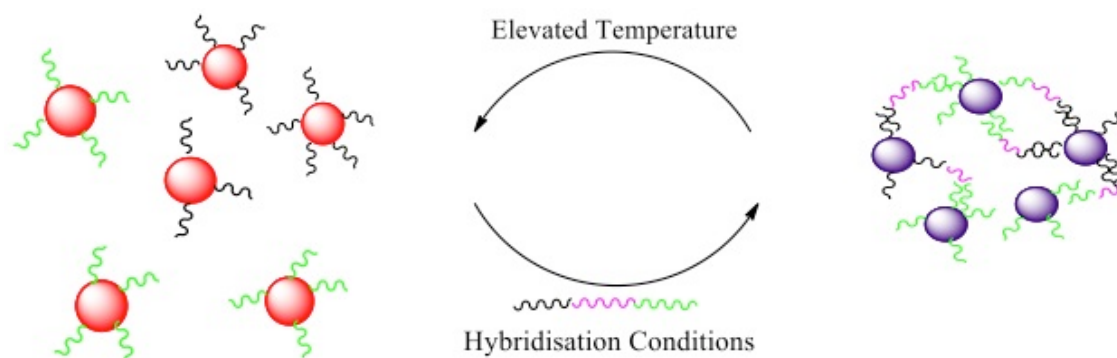> ➢   Interparticle distance.

Figure 4.2. Illustration of the hybridisation-induced aggregation of oligonucleotide-nanoparticle conjugates. Aggregation, and a colour change, is only observed when a complementary target is introduced under hybridisation conditions. In the case of gold nanoparticle conjugates, a red colour indicates monodisperse nanoparticles in the absence of target and a blue-purple colour indicates aggregation after addition of target DNA. The colour change is reversible by heating the DNA duplex above the T_m, re-dispersing the nanoparticles and a colour change from blue-purple to red.

Figure 4.1 illustrates DNA hybridisation-induced aggregation of nanoparticles. The method for hybridising oligonucleotide-nanoparticle conjugates takes the form of a split-probe assay, where two solutions of nanoparticles are functionalised with different, non-complementary oligonucleotides. The two solutions of oligonucleotide-nanoparticle conjugates are mixed together and remain monodispersed. Addition of a DNA target sequence complementary to both oligonucleotides triggers hybridisation, resulting in aggregation of the nanoparticles and a distinctive colour change observable by eye. The type of nanoparticle used to make the conjugate dictates the colour change – red to blue-purple for gold nanoparticles and yellow to orange-brown for silver nanoparticles.

Similar to duplex DNA free in solution, the hybridisation-induced aggregation of the nanoparticles can be reversed by heating above the melting temperature (T_m) of the DNA duplex, returning the nanoparticles to their monodispersed state. This chapter discusses the properties of oligonucleotide-nanoparticle conjugates under hybridisation conditions using DNA. The properties were primarily investigated using UV-Vis spectroscopy with the overall aim of using the oligonucleotide-

nanoparticle conjugates as bionanosensors to detect specific DNA targets related to disease by surface enhanced resonance Raman scattering (SERRS).

4.1   Oligonucleotide Selection and Properties

Probe Name	*Sequence (5' – 3')*
P1	<mark style="background:red">TTC CAG ATT ACA ACT TCA CCA</mark>
P2	<mark style="background:cyan">AAA GAA CCT CTG CTC AAC AAG</mark>
P1P2 comp	<mark style="background:red">TGGTGAAGTTGTAATCTGGAA</mark><mark style="background:cyan">CTTGTTGAGCAGAGGTT CTTT</mark>
P1P2 non	TTCCAGATTACAACTTCACCAAAAGAACCTCTGCTCAAC AAG

Table 4.1.   Oligonucleotide sequences used for hybridisation studies.   The colours indicate the position of each oligonucleotide in the hybridised duplex.

The focus of this research was the development of an assay to detect specific DNA sequences related to disease. To this end, the oligonucleotide probes selected are complementary to the *MecA* gene located in the genome of methicillin-resistant *staphylococcus aureus* (MRSA). The *MecA* gene is known to code for β-lactam antibiotic resistance in MRSA. [9] A list of oligonucleotide sequences, including probes and targets are displayed in table 4.1.   In order to establish their complementarity, the oligonucleotide probe sequences were hybridised in a 1:1:1 ratio at 1 µM final concentration with 100 × SYBR green I using 0.3 M phosphate buffered saline (PBS, pH 7). SYBR green produces minimal fluorescence in ssDNA and produces a significant fluorescent signal in the presence of dsDNA. Figure 4.3 shows the characteristic fluorescence melting profile of P1 and P2 hybridised to a fully complementary DNA target in the presence of SYBR green I. The graph is plotted as the negative derivative of fluorescence *versus* temperature. The software removes the background and the effect on fluorescence due to temperature to reach the 1st order derivative and it is often preferential to report melting profiles in this way to allow easier identification of the T_m. [10] Hybridisation of P1 and P2 to a fully complementary DNA target results in a T_m of 70 °C. This correlates to values obtained using online DNA melting simulators. [11] Sequence specificity of the two

probes is confirmed by the absence of a melting transition in the non-complementary DNA target.
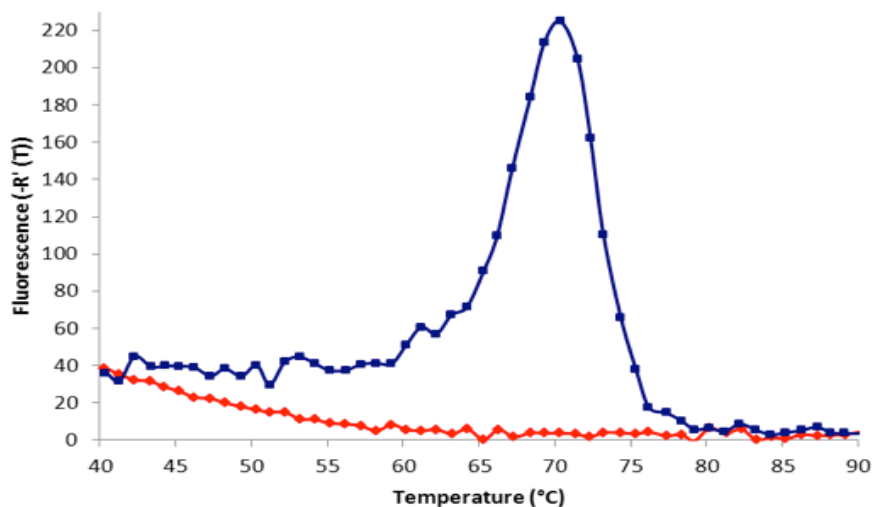
*Figure 4.3. SYBR green I melting profile of P1 and P2 hybridised to a fully complementary DNA sequence (**Blue**) and non-complementary DNA sequence (**Red**).*

4.2 Oligonucleotide-Nanoparticle Conjugates: Design Principles
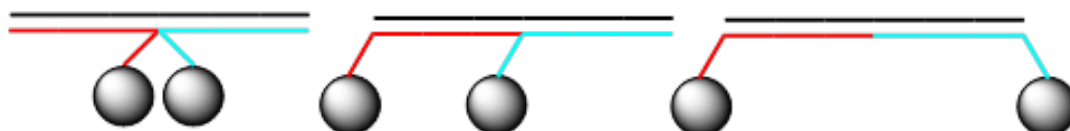
*Figure 4.4. Possible orientations of oligonucleotide-nanoparticle conjugate during hybridisation-induced aggregation (**Red** = P1 and **Yellow** = P2). From left to right - "head-to-head" (**P1** = 5'-modified, **P2** = 3'-modified), "head-to-tail" (**P1** = 5'-modified, **P2** = 5'-modified) and "tail-to-tail" (**P1** = 3'-modified, **P2** = 5'-modified).*

The position of the thioctic acid modification on the oligonucleotide affects the arrangement of the oligonucleotide-nanoparticle conjugates during hybridisation to the complementary target. There are three possible orientations: "head-to-head", "head-to-tail" and "tail-to-tail". The possible orientations of the oligonucleotide-nanoparticle conjugates are summarised in figure 4.3. The orientation has an impact

108

on the interparticle distance between the nanoparticles in the hybridised duplex, with research showing a decline in T_m with decreasing inter-particle distance. [8] Modifying the oligonucleotide at the 3'- or 5'-terminus dictates the orientation of the oligonucleotide-nanoparticle conjugates during hybridisation. In order to achieve the various oligonucleotide-nanoparticle orientations, P1 was synthesized with a 5'-thioctic acid modification and two P2 oligonucleotides were synthesized, one with a 5'-thioctic acid modification and one with a 3'-thioctic acid modification. In addition, a separate complementary target was synthesized in order to achieve a "tail-to-tail" arrangement during hybridisation. Table 4.2 shows the various oligonucleotide probes used to functionalise nanoparticles for subsequent hybridisation experiments. It was decided to incorporate the (HEG)$_3$ spacer group, rather than the HEG group, to ensure that the oligonucleotide was sufficiently distanced from the nanoparticle surface during hybridisation.

Probe Name	5' to 3' Sequence
P1	**X**-(HEG)$_3$-TTC CAG ATT ACA ACT TCA CCA
P2	**X**-(HEG)$_3$-AAA GAA CCT CTG CTC AAC AAG
P3	AAA GAA CCT CTG CTC AAC AAG-(HEG)$_3$-**X**
P1P2 comp	TGGTGAAGTTGTAATCTGGAACTTGTTGAGCAGAGGTTCTTT
P1P3 comp	CTTGTTGAGCAGAGGTTCTTTTGGTGAAGTTGTAATCTGGAA

Table 4.2. Oligonucleotide-nanoparticle conjugate sequences to achieve different arrangements during hybridisation. "X" indicates the position of the thioctic acid modification. P1P2 comp target can be used to achieve "head-to-tail" and "head-to-head" orientations and P1P3 comp can be used to achieve "tail-to-tail" orientations.

4.3 Oligonucleotide-Gold Nanoparticle Conjugates: Assembly Using DNA

The most convenient method for determining nanoparticle aggregation is colorimetrically by eye. The high extinction coefficients afforded by gold nanoparticles results in a visible colour change upon aggregation, from red to blue-purple. Figure 4.4 shows the colorimetric detection of DNA hybridisation-induced aggregation of gold nanoparticles. Both oligonucleotide-nanoparticle conjugates (Au-P1 and Au-P2) were mixed at a 0.5 nM final concentration with complementary DNA at 50 nM final concentration in 0.3 M PBS (pH 7). By visually comparing the cuvettes an obvious colour change is evident. The left cuvette shows gold nanoparticle conjugates hybridised to a non-complementary target DNA and the right cuvette shows gold nanoparticle conjugates hybridised to a fully complementary DNA target after 3 hours. The solution of the hybridised oligonucleotide-nanoparticle conjugates appears colourless because the aggregates have grown in size and precipitated from solution due continuous DNA hybridisation.
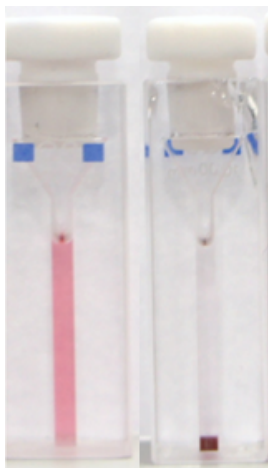

*Figure 4.5. Colorimetric detection of DNA hybridisation-induced aggregation of Au-P1 and Au-P2 in the presence of a non-complementary (**LEFT**) and fully complementary (**RIGHT**) DNA sequence. [Conjugate]= 0.5 nM, [DNA target] = 50 nM in 0.3 M PBS.*

4.3.1 Oligonucleotide-Gold Nanoparticle Conjugate Hybridisations

While visual detection of hybridisation-induced nanoparticle aggregation is a convenient method of detection it does not provide any information on the aggregation process. The most common method for monitoring the aggregation progress is UV-Vis spectroscopy. Using UV-Vis spectroscopy allows scans to be taken at allocated times during the aggregation process to monitor the effect of DNA hybridisation on the surface plasmon of the gold nanoparticles. Figure 4.5 shows hybridisation-induced aggregation of gold nanoparticles monitored by UV-Vis spectroscopy. Each spectrum represents a scan taken at 10 minute intervals. To achieve hybridisation, conjugates of P1 and P2 were mixed at 0.5 nM final concentrations with 50 nM P1P2 comp in PBS (0.3 M, pH 7). The blue spectrum in figure 4.5 has a surface plasmon band centred at 520 nm, which is indicative of monodispersed gold nanoparticles, *i.e.* no aggregation has occurred. Over time, however, the plasmon at 520 nm decreases and red-shifts as DNA hybridisation occurs. The changes in the surface plasmon indicated the formation of dimers, trimers and eventually larger aggregates as evidenced by the emergence of a secondary plasmon peak at ~ 650 nm. [7]

Figure 4.6. Extinction spectra of DNA hybridisation-induced aggregation of oligonucleotide-gold nanoparticle conjugates in a "head-to-tail" orientation. Each spectrum represents a scan taken at 10 minute intervals during the aggregation process. The arrows indicate the change in spectra over time (180 min). [Conjugates] = 0.5 nM, [DNA target] = 50 nM in PBS (0.3 M, pH 7).

In order to be employed in DNA detection assays, it was important to establish that the plasmon shifting in figure 4.5 occurred due to specific Watson-Crick base-pairing of the complementary oligonucleotides. To investigate this, P1P2 non was used in place of P1P2 comp under the same experimental conditions as those employed to obtain the spectra in figure 4.5. Figure 4.6 shows the spectra obtained using a non-complementary DNA sequence. Immediate target addition is indicated by the blue spectrum while the red spectrum indicates the progress of aggregation after 180 min (the same time period as figure 4.5). The spectra in figure 4.6 reveal that 180 min after DNA target addition the oligonucleotide-gold nanoparticle conjugates remain monodispersed and red in colour (as evidenced in figure 4.4). This result confirms that the aggregation process is sequence-specific since the nanoparticles remain monodispersed in the presence of a non-complementary DNA sequence.
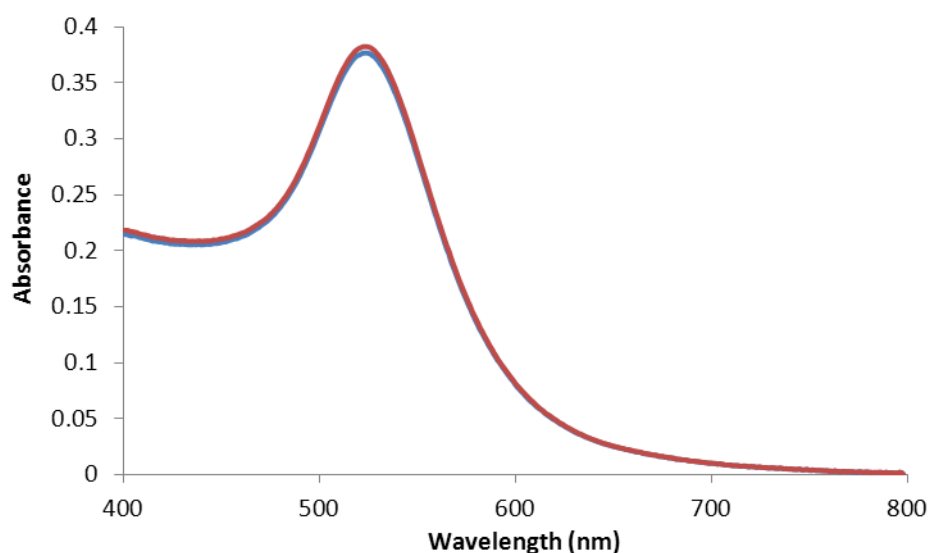
Figure 4.7.   Extinction spectra of oligonucleotide-gold nanoparticle conjugates mixed with a non-complementary DNA sequence. The blue spectrum shows target addition at 0 min and the red spectrum shows target addition at 180 min. [Conjugates] = 0.5 nM, [DNA target] = 50 nM in PBS (0.3 M, pH 7).

The effect of temperature on the hybridisation kinetics was investigated. Research conducted by Storhoff *et al.* revealed that little to no aggregation occurred at room temperature with oligonucleotide-nanoparticle conjugates with larger intertparticle distances; however by annealing the oligonucleotide-nanoparticle conjugates at a temperature just below the melting temperature resulted in greater hybridisation-induced aggregation. [7] It was hypothesized that adding the oligonucleotide-gold nanoparticle conjugate probes to the target DNA at an elevated temperature would result in aggregation occurring more rapidly. Figure 4.7 shows hybridisation-induced aggregation of oligonucleotide-nanoparticle conjugates while held at 50 °C (~ 20 °C below the melting temperature). Each spectrum represents a scan taken at 10 min intervals over a 180 min period. Comparison of figures 4.5 and 4.7 reveal that annealing the oligonucleotide-gold nanoparticles at elevated temperature does affect the rate of aggregation.
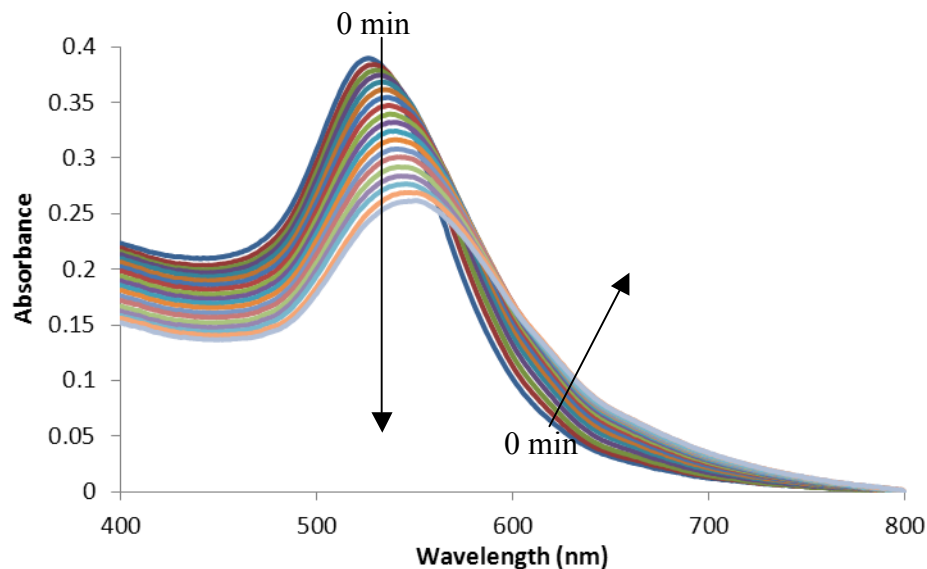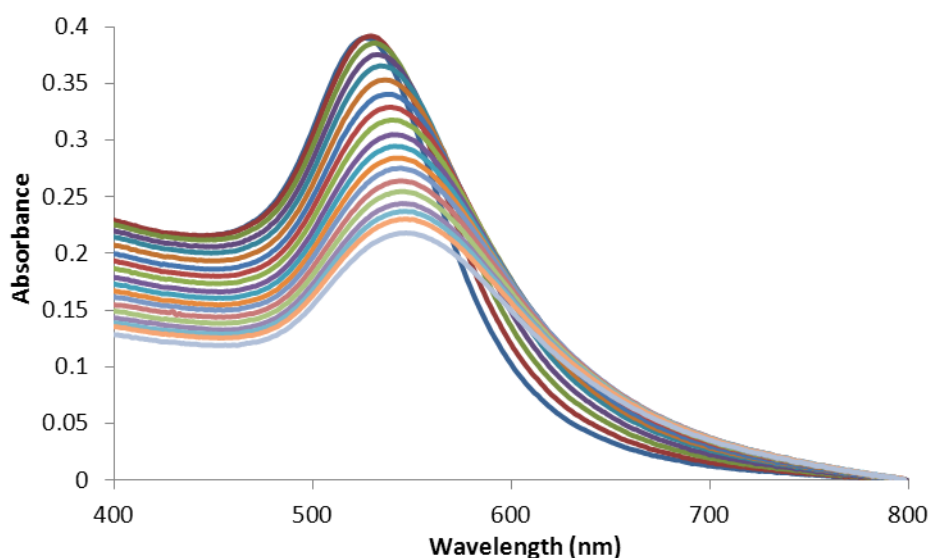
Figure 4.7. Extinction spectra of DNA hybridisation-induced aggregation of oligonucleotide-gold nanoparticle conjugates in a "head-to-tail" orientation held at 50 °C. Each spectrum represents a scan taken at 10 minute intervals over 180 minutes of the aggregation process. [Conjugates] = 0.5 nM, [DNA target] = 50 nM in PBS (0.3 M, pH 7).

Figure 4.8 shows the absorbance at 650 nm *versus* time. An increase in absorbance at 650 nm is indicative of aggregation occurring. As can be seen from figure 4.8, there is a more rapid increase in absorbance at 650 nm for oligonucleotide-gold nanoparticle conjugates hybridising at 50 °C than those hybridising at room temperature. In addition, it can be deduced from figure 4.8 that there appears to be three stages in the aggregation process – a steady increase in absorbance at 650 nm, followed by a plateau and finally a decrease in absorbance. For each variable, these stages occur at different times. The initial increase in absorbance ranges from 0 to ~ 90 min for hybridisations occurring at 50 °C and from 0 min to ~130 min for room temperature hybridisations. The plateau region for 50 °C hybridisations ranges from 90 min to ~ 120 min and from 130 min to (presumably) over 180 min for room temperature hybridisations. The final decrease in absorbance is only observed for hybridisations at 50 °C and ranges from 120 min to over 180 min. This decrease in absorbance is due to larger aggregates forming during hybridisation that eventually precipitate from solution.
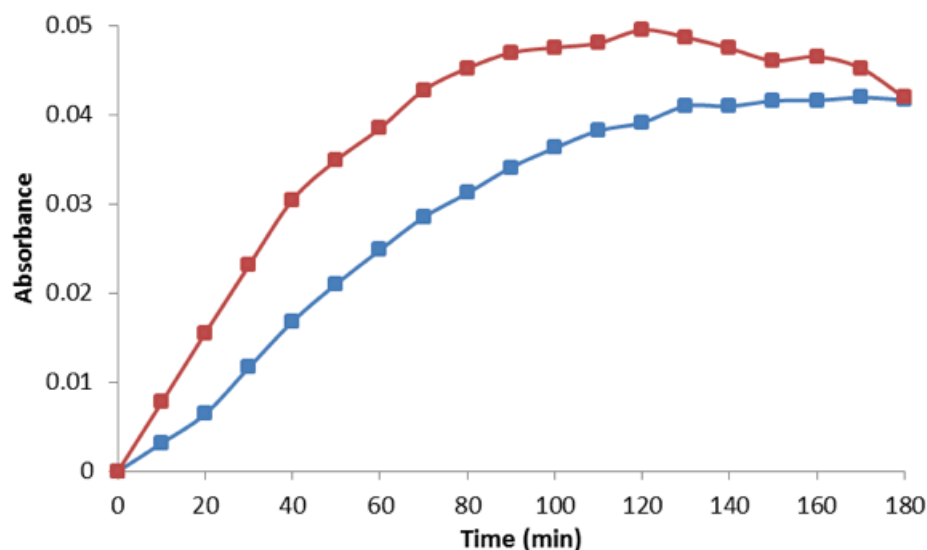
*Figure 4.8. Absorbance at 650 nm versus time plotted for oligonucleotide-gold nanoparticle hybridisation-induced aggregation at room temperature (**blue**) and 50 °C (**red**).*

The concentration dependence of the aggregation process was investigated by altering the amount of target DNA added to the nanoparticle conjugate mixture. The absorbance at 650 nm *versus* time for the different target DNA concentrations is shown in figure 4.9. The concentration of the oligonucleotide-gold nanoparticle conjugates was 0.5 nM for each hybridisation and the target concentrations investigated were 50, 100 and 250 nM, which are assigned to the blue, red, and green lines in figure 4.9, respectively. Varying the target DNA concentration results in aggregation modes similar to that previously mentioned – a steady increase in absorbance followed by a plateau and eventually a rapid decrease in absorbance as the aggregates grow in size and precipitate from solution. However, the initial increase in absorbance appears to be concentration dependent with the 50 and 100 nM concentration exhibiting similar rates for the initial increases in absorbance and the 250 nM concentration exhibiting a much slower increase in absorbance by comparison. In addition, the 100 nM concentration reaches the absorbance plateau faster than either the 50 or 250 nM concentrations.
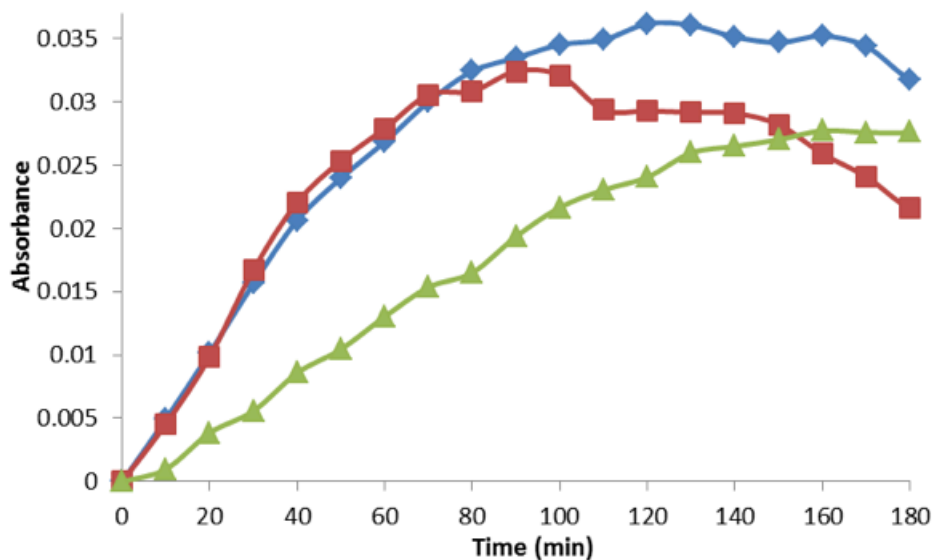
*Figure 4.9. Absorbance at 650 nm versus time for 50 nM (**blue**), 100 nM (**red**) and 250 nM (**green**) concentrations of DNA target.*

Elevated salt concentrations have been proven to improve hybridisation kinetics of oligonucleotide-gold nanoparticle conjugates. Studies have shown that increased salt concentrations results in more stable duplexes between oligonucleotide-nanoparticle conjugates. [8] Figure 4.10 shows the absorbance at 650 nm *versus* time for oligonucleotide-gold nanoparticles hybridised using different concentrations of PBS. Only the NaCl concentration (0.3 M, 0.7 M and 1.0 M) was changed for each experiment, other variables, such as the phosphate buffer (10 mM, pH 7), oligonucleotide-nanoparticle conjugate concentration (0.5 nM) and target concentration (50 nM) were kept constant. The graph reveals that the NaCl concentration in the PBS has a direct effect on the rate of hybridisation. As the concentration of NaCl increases from 0.3 M to 1 M there is a greater initial increase in absorbance at 650 nm. For each concentration of NaCl employed, there is an initial increase in absorbance at 650 nm followed by a plateau and, although the graph only extends to 180 min, there follows a sharp decrease in absorbance like that observed in figures 4.8 and 4.9 as the aggregates grow in size and eventually precipitate from solution (data not shown). The difference in absorbance between each concentration can be attributed to a screening effect of the NaCl which reduces electrostatic repulsion between oligonucleotide-nanoparticle conjugates, resulting in

an increase in hybridisation events, leading to more nanoparticles linked by DNA, thereby allowing larger aggregates to form.
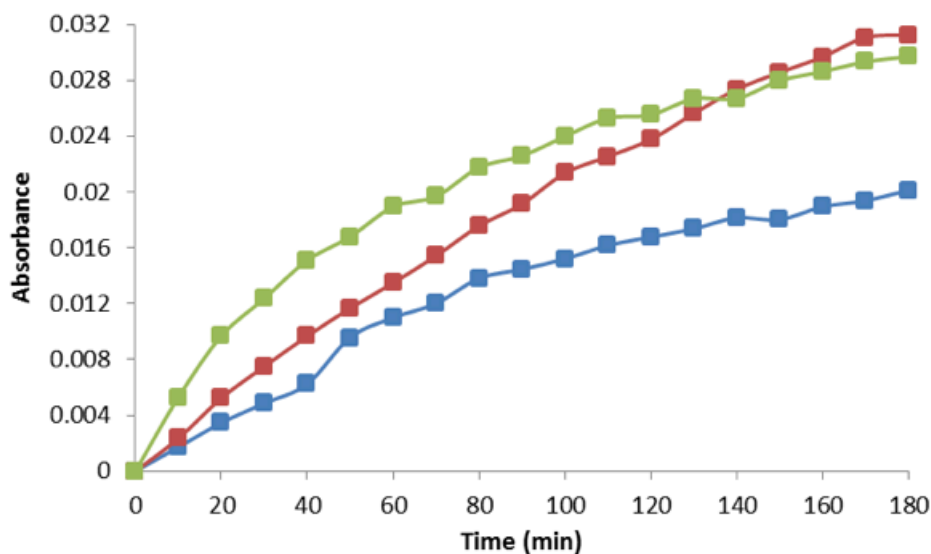
Figure 4.10. *Absorbance at 650 nm versus time for oligonucleotide-gold nanoparticle conjugates hybridised to a complementary target DNA sequence at increasing salt concentrations.* ***Blue*** *= 0.3 M PBS,* ***Red*** *= 0.7 M PBS and* ***Green*** *= 1.0 M PBS.*

The oligonucleotide-gold nanoparticle conjugates hybridise to a complementary DNA target sequence that is exactly the length of the two probe conjugates combined, *i.e.* 42 base pairs (bp). However, oligonucleotide-nanoparticle conjugates must be able to efficiently hybridise to longer DNA sequences for use in assays for direct genomic DNA detection or for detection of PCR products. An 86 bp target oligonucleotide was synthesized to test the ability of the probes to hybridise to a longer strand. Both oligonucleotide-nanoparticle conjugates (0.5 nM) were added to target DNA (50 nM) in 0.3 M PBS and allowed to hybridise at room temperature. Figure 4.11 shows the absorbance at 650 nm *versus* time for both the 42 bp target sequence and 86 bp target sequence. The graph reveals a difference in the hybridisation kinetics of the different lengths of target DNA, with the 42 bp (blue) target aggregating more rapidly than 86 bp (red) target. This trend is indicated by the more rapid increase in absorbance at 650 nm of the 42 bp target compared to the 86 bp target. By ~ 120 minutes the 42 bp hybridised gold nanoparticle conjugates have

approached a plateau and have slightly decreased in absorbance, while the 86 bp hybridised nanoparticle conjugates have yet to reach a plateau at 120 minutes.
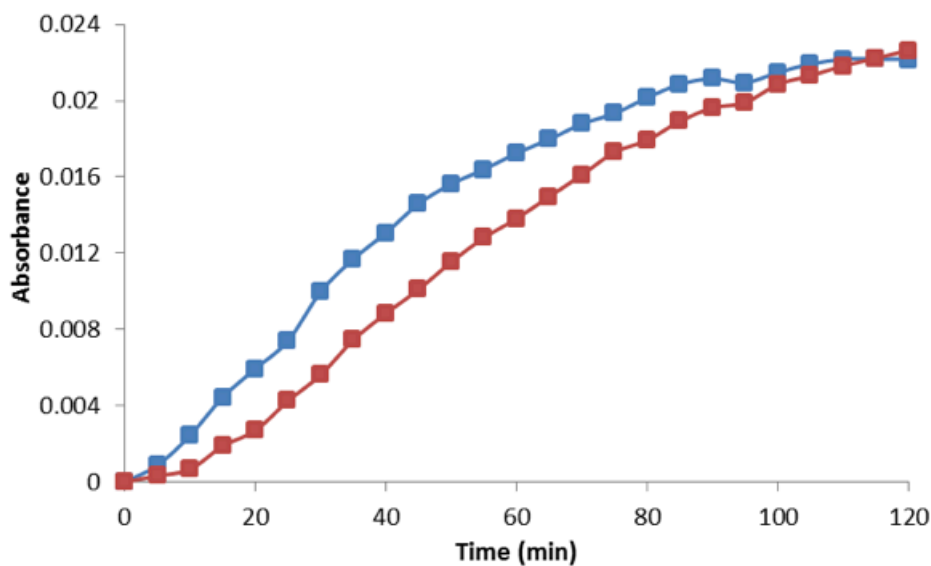
*Figure 4.11.   Absorbance at 650 nm versus time of oligonucleotide-gold-nanoparticle conjugates hybridised to a 42 bp (**blue**) and 86 bp (**red**) target DNA. The 86 bp target DNA sequence is 5'-TGG TGA AGT TGT AAT CTG GAA CTT GTT GAG CAG AGG TTC TTT TTT ATC TTG GGT TAA TTT ATT ATA TTC TTC GTT ACT CAT GCC AT.*

4.3.2 Melting Properties of Hybridised Oligonucleotide-Gold Nanoparticle Conjugates

Duplex formation between oligonucleotide-gold nanoparticle conjugates is a reversible process. Like hybridised, unmodified DNA in solution, heating the oligonucleotide-gold nanoparticle DNA duplex to high temperature (~ 95 °C) disrupts the hydrogen bonding between complementary base-pairs to form ssDNA. The point at which half of the DNA is in the duplex state and half is in the ssDNA state is known as the melting temperature or T_m and this process can be monitored by UV-Vis spectroscopy.   Conjugates of P1 and P2 were mixed at 0.5 nM final concentrations with 50 nM P1P2 comp in PBS (0.3 M, pH 7). The sample was cycled between 10 °C and 95 °C with an increment of 1 °C/min. The absorbance at 520 nm was collected at each increment. Absorbance was monitored at the λ_{max} for the surface plasmon resonance band for monodispersed gold nanoparticles – 520 nm.

While hypochromicity accounts for differences in the duplex and single-stranded absorbance of DNA free in solution, oligonucleotide gold nanoparticle conjugates have a reduced absorbance at 520 nm in the hybridised state due to aggregation of the nanoparticles. Heating the conjugates past the melting temperature of the DNA results in an increase in absorbance because the complementary base-pairing is disrupted and the gold nanoparticles return to the monodispersed state. Figure 4.12 shows a typical melting curve obtained for hybridised oligonucleotide-gold nanoparticle conjugates in the "head-to-tail" orientation. The characteristically "sharp" melting curve shown in figure 4.12 arises from a cooperative melting effect of the oligonucleotide-gold nanoparticle conjugates. Research performed by Jin *et al.* showed that it is multiple DNA duplexes between the gold nanoparticles together with an increase in local salt concentration that results in such sharp melting curves. [8] The melting curve exhibits a T_m of ~ 66 °C which is about 4 °C less than the unmodified DNA duplex as seen in figure 4.2. This can be attributed to electrostatic repulsion caused by the nanoparticles coming into close proximity with one another during hybridisation. [8] The "dip" in absorbance observed before melting of the hybridised oligonucleotide-gold nanoparticle conjugates has been investigated by Storhoff *et al.* and can be attributed to a temperature-dependent process whereby larger nanoparticle aggregates are formed at the expense of smaller aggregates. [7] [12] In his research, Storhoff notes that the melting curve of pre-hybridised oligonucleotide-nanoparticle conjugates, *i.e.* the conjugates have been added to the target and allowed to anneal before they are melted, exhibit linear absorbance in the same region before melting occurs.
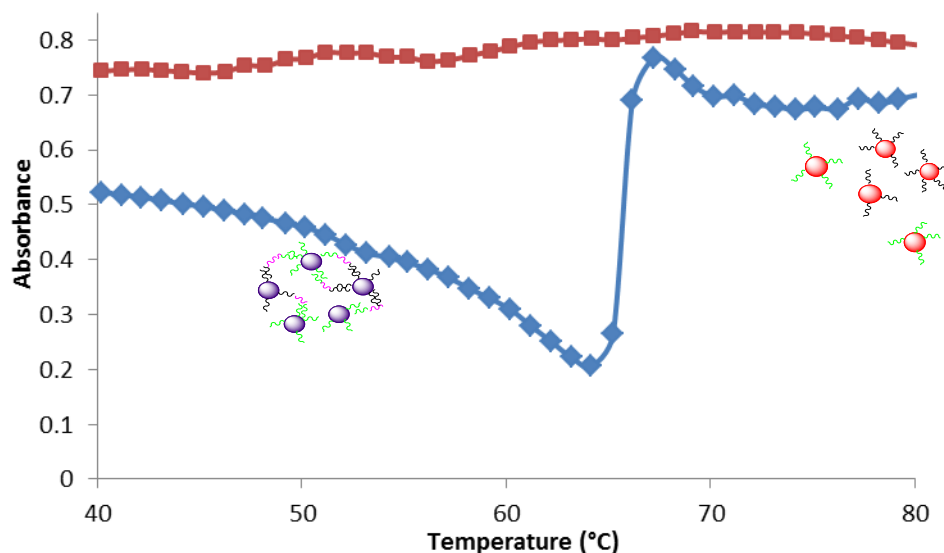
*Figure 4.12. Melting curve of hybridised oligonucleotide-gold nanoparticle conjugates obtained by UV-Vis spectroscopy: complementary target (**blue**) and non-complementary target (**red**). Absorbance monitored at 520 nm. Cartoons indicate aggregation states as temperature increases. [Conjugates] = 0.5 nM, [DNA target] = 50 nM in PBS (0.3 M, pH 7).*

In order to confirm that the observed melting transition is a result of sequence specific DNA hybridisation, the oligonucleotide-gold nanoparticle conjugates were added to a non-complementary DNA target sequence. The spectrum obtained from using a non-complementary target is shown in figure 4.12 (red line). As can be seen from the spectrum, a linear plot exhibiting absorbance at ~ 0.75 is observed which is consistent with absorbance obtained after the melting transition indicating the presence of monodispersed nanoparticles. This result confirms that melting curve analysis of oligonucleotide-gold nanoparticle conjugates is sequence specific as a linear absorbance plot was obtained using a non-complementary DNA target indicating no hybridisation event had taken place.

Since the oligonucleotide-nanoparticle conjugates undergo repeated cycles of heating and cooling to obtain a melting curve, this can be a good indication of the stability of the conjugates. Figure 4.13 shows various melting curves of oligonucleotide-gold nanoparticle conjugates obtained after several cycles of denaturation. As can be seen from figure 4.13, a T_m of ~ 66 °C can be reproducibly obtained with little loss in

absorbance. There is a small decrease in absorbance after each heating cycle that can be attributed to loss of a small number of oligonucleotides from the gold nanoparticle surface; however, this is not significant as to affect the overall stability of the hybridised conjugates. This result proves the thioctic acid-modified oligonucleotide-gold nanoparticle conjugates can be used to detect DNA in conditions where repeated heating cycles are employed, *i.e.* PCR.
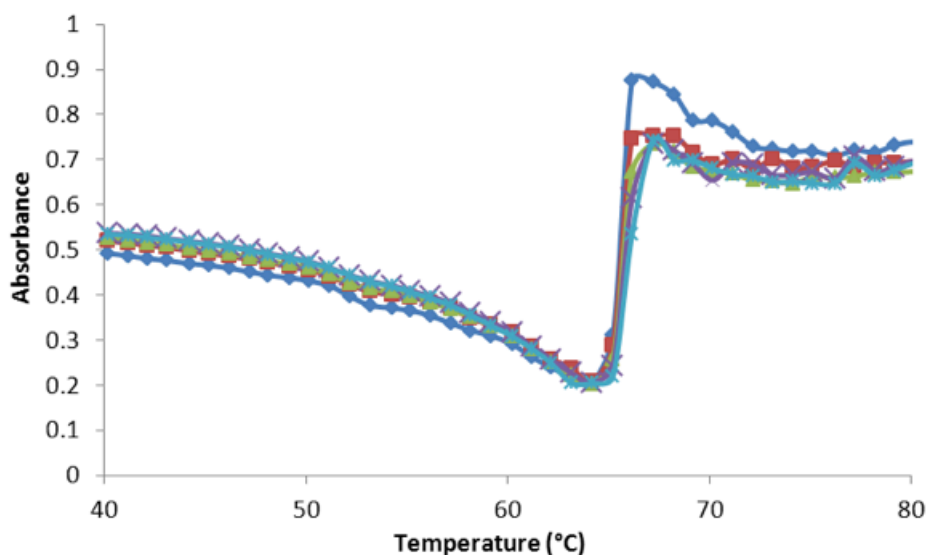
Figure 4.13. Melting curves of hybridised oligonucleotide-gold nanoparticle conjugates obtained after repeated heating and cooling cycles by UV-Vis spectroscopy. Absorbance monitored at 520 nm. [Conjugates] = 0.5 nM, [DNA target] = 50 nM in PBS (0.3 M, pH 7).

The aim of this research was to induce hybridisation-driven aggregation of the stable oligonucleotide-nanoparticle conjugates investigated in Chapter 3 to switch 'on' the SE(R)RS for detection of DNA sequences. It was therefore important to establish that the biological integrity of the oligonucleotide-gold nanoparticle conjugate was not compromised after addition of the isothiocyanate dye labels since the dye-labelled conjugates would be utilized in an assay to detect DNA by SE(R)RS. Oligonucleotide-gold nanoparticle conjugates were functionalised with ROX-ITC and MG-ITC. The dye-labelled conjugates were then subjected to hybridisation with a complementary DNA sequence to obtain a melting curve. As can be seen from figure 4.14 and 4.15, the addition of the dye-label does not affect the conjugates'

ability to hybridise to the target. The T_m obtained for both ROX- and MG-ITC was ~ 67 °C which is consistent with the T_m obtained for non-dye functionalised conjugates as seen in figure 4.12. This confirms the suitability of the dye-labelled oligonucleotide-gold nanoparticles to be used as SE(R)RS nanosensors in a DNA detection assay.
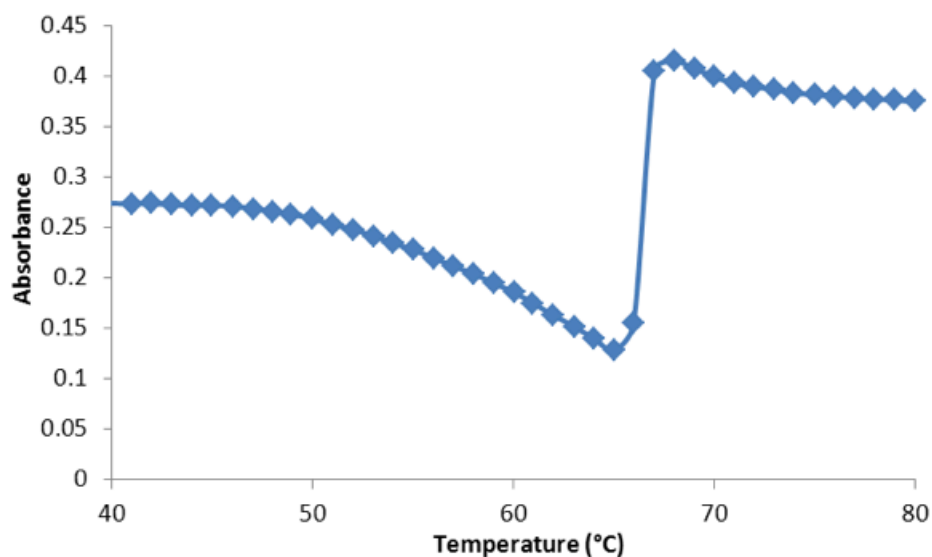
Figure 4.14. Melting curve of ROX-ITC labelled oligonucleotide-gold nanoparticle conjugates hybridised to a complementary DNA target sequence. Absorbance was monitored at 520 nm. [Conjugates] = 0.5 nM, [DNA target] = 50 nM in PBS (0.3 M, pH 7).
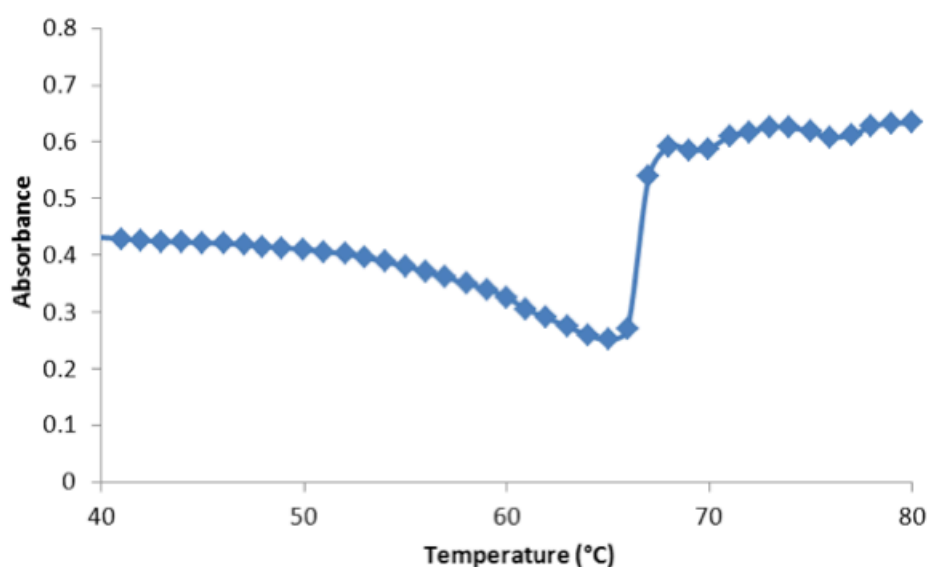
Figure 4.15. Melting curve of MG-ITC labelled oligonucleotide-gold nanoparticle conjugates hybridised to a complementary DNA target sequence. Absorbance was monitored at 520 nm. [Conjugates] = 0.5 nM, [DNA target] = 50 nM in PBS (0.3 M, pH 7).

4.4 Oligonucleotide-Silver Nanoparticle Conjugates: Assembly Using DNA

Silver nanoparticles are an attractive, alternative substrate to gold nanoparticles for biosensing applications due to increased sensitivity afforded by the higher extinction coefficient inherent in silver nanoparticles (2.8×10^{10} and 2.7×10^{8} for silver and gold nanoparticles, respectively). For this reason, it was important to establish the viability of silver nanoparticles for sensing of DNA. In a similar fashion to gold nanoparticles, the high extinction coefficient results in a visible colour change from yellow to orange-brown upon addition of a complementary DNA sequence. Figure 4.16 shows the colorimetric detection of DNA using oligonucleotide-silver nanoparticle conjugates. Hybridisation was induced by mixing Ag-P1 and Ag-P2 (20 pM each) with 2 nM P1P2 comp in 0.3 M PBS (pH 7). In order to establish that the colour change was the result of sequence specific hybridisation, Ag-P1 and Ag-P2 were hybridised with P1P2 non (Figure 4.16, left cuvette) resulting in no visible colour change confirming the sequence specificity of the hybridisation event.
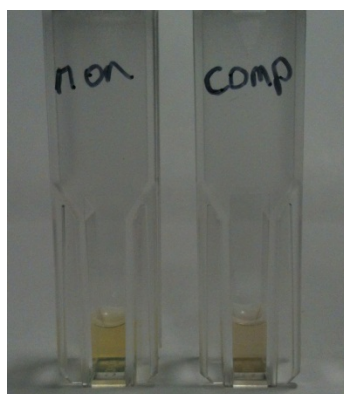
*Figure 4.16. Colorimetric detection of DNA hybridisation-induced aggregation of Ag-P1 and Ag-P2 in the presence of to a non-complementary (**LEFT**) and fully complementary (**RIGHT**) DNA sequence. [Conjugates] = 20 pM, [DNA target] = 10 nM in 0.3 M PBS, pH 7.*

4.4.1 Oligonucleotide-Silver Nanoparticle Conjugate Hybridisations

As with oligonucleotide-gold nanoparticle conjugates, the assembly process was monitored using UV-Vis spectroscopy. Early attempts to induce DNA mediated assembly in oligonucleotide-silver nanoparticle conjugates resulted in absorbance spectra that exhibited an incomplete aggregation profile. This was an unexpected result since the amount of target added indicated that complete aggregation of the system was expected. However, it was discovered that this discrepancy was possibly due to the centrifugation step. As mentioned in the previous chapter, section 3.4.3, oligonucleotide-silver nanoparticle conjugates were subjected to a two-step centrifugation process where the conjugate was centrifuged for 15 minutes at 4000 rpm, followed by a second round of centrifugation where the supernatant was removed and centrifuged for 15 minutes at 6500 rpm. Centrifugation of the nanoparticle conjugates is necessary to remove any unbound oligonucleotides in solution. It was thought that this gentler centrifugation process was inefficient at removing all unbound oligonucleotides and, as such, that unbound oligonucleotides were hybridising to the target DNA sequence in the nanoparticle conjugate solution therefore slowing the assembly process. To overcome this, two rounds of the two-step centrifugation process was employed to ensure all unbound oligonucleotides

were removed from the solution. Figure 4.17 shows the absorbance spectrum of Ag-P1 and Ag-P2 hybridised to a fully complementary DNA sequence under the same experimental conditions as depicted in figure 4.16. Monodispersed silver nanoparticles have a surface plasmon centred at around 410 nm, upon addition of a complementary DNA sequence, the surface plasmon dampens and broadens, accompanied by a red-shift to longer wavelengths due to coupling of the surface plasmon resonances when the nanoparticles come into close proximity during hybridisation. Figure 4.18 shows Ag-P1 and Ag-P2 in the presence of to a non-complementary DNA sequence indicating the sequence specificity of the assembly process. In order to visualize the aggregates formed during hybridisation, aliquots of the assembled oligonucleotide-silver nanoparticle conjugates were imaged using scanning electron microscopy (SEM). To obtain the images, silicon wafers were modified by surface adsorption of 35 % w/w poly(diallyldimethylammonium chloride) (PDDA)/ 1 mM NaCl solution in Milli-Q water for 1 hour. The wafers were then rinsed with Milli-Q water and dried by N_2 flow. At this point, 30 µl of the conjugate sample were deposited onto the modified silicon wafer in a humidity chamber for 5 min before rinsing the substrate with water in order to reduce drying-induced aggregation that would hinder the image capture. Figure 4.19 shows two representative images of the aggregates formed during DNA-mediated assembly of the oligonucleotide-silver nanoparticle conjugates.
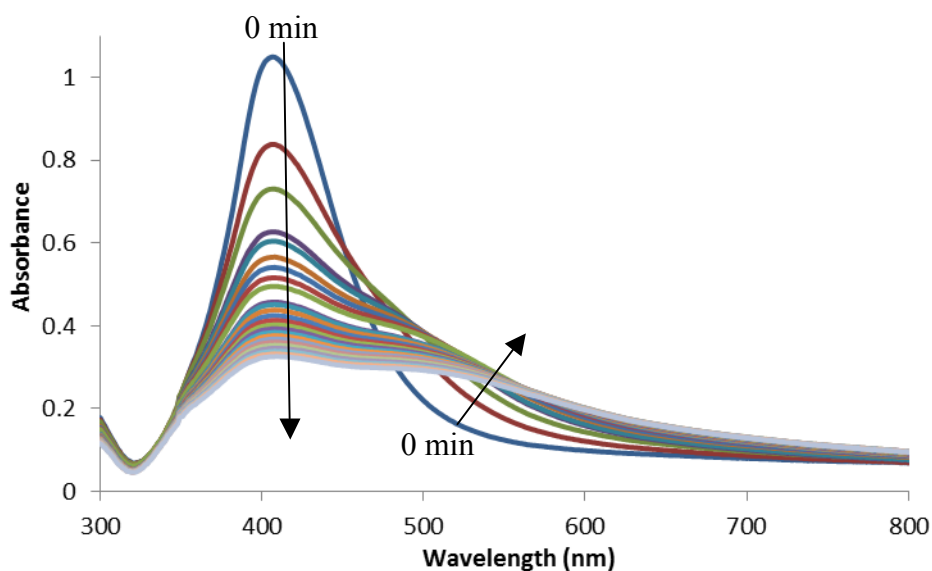
Figure 4.17. Extinction spectra of DNA hybridisation-induced aggregation of oligonucleotide-silver nanoparticle conjugates in a "head-to-tail" orientation. Each spectrum represents a scan taken at 5 minute intervals over 120 minutes of the aggregation process. [Conjugates] = 20 pM, [DNA target] = 10 nM in PBS (0.3 M, pH 7).
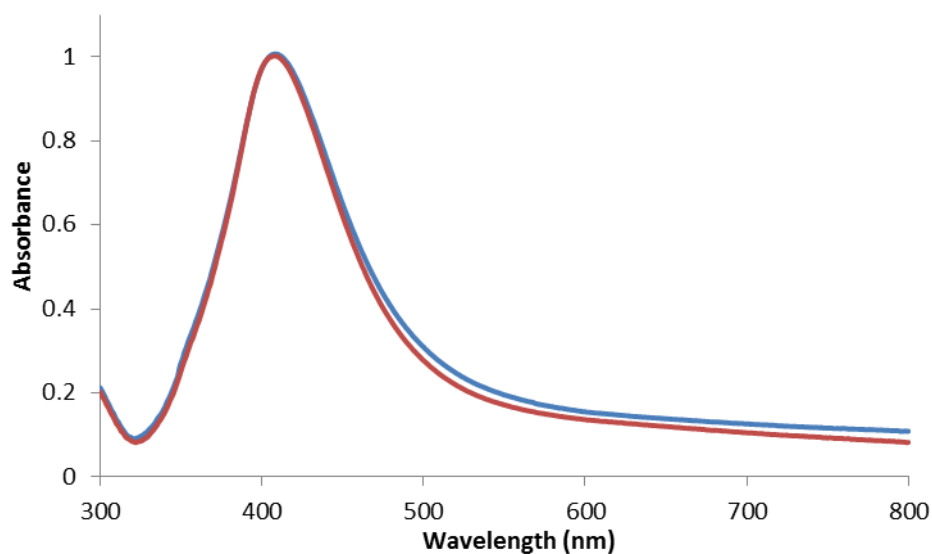
Figure 4.18. Extinction spectra of Ag-P1 and Ag-P2 mixed with a non-complementary DNA sequence. The blue spectrum represents a scan taken at complement addition and the red spectrum represents a scan obtained at 120 minutes. [Conjugates] = 20 pM, [DNA target] = 10 nM in PBS (0.3 M, pH 7).
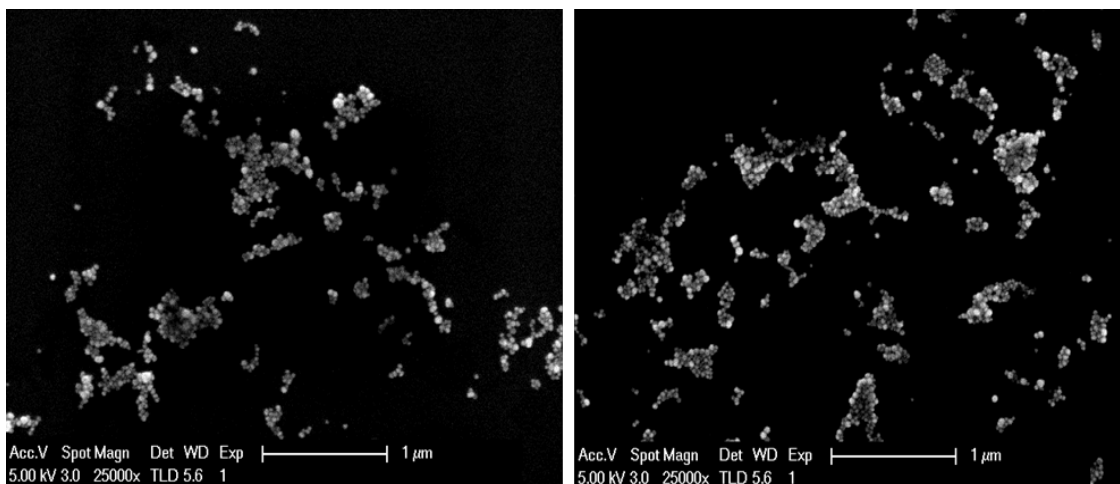
Figure 4.19. Scanning electron micrographs (SEM) of oligonucleotide-silver nanoparticle conjugates hybridised to a complementary DNA target sequence. Images were captured 60 minutes after target addition from two random spots on the SEM substrates. Images courtesy of Dr Iain Larmour.

4.4.2 Effect of DNA Target Concentration on Oligonucleotide-Silver Nanoparticle Conjugate Hybridisations

The nanoparticle assembly process can be readily influenced by the amount of complementary DNA target available for hybridisation. Typically, the target DNA is added in excess to the conjugate probes, for example, in figure 4.16-4.19, the target concentration was 10 nM, which is 500 times the concentration of conjugate probes (20 pM). It was decided to investigate if changing the target: probe ratio would result in a difference to the rate of the assembly process. The target concentrations that were investigated were 20 nM, 15 nM, 5 nM, 2 nM, 1 nM, 0.5 nM and 0.2 nM corresponding to 1000, 750, 250, 100, 50, 25 and 10 times the probe conjugate concentration (20 pM). Figure 4.20 shows the ratios of the absorbance at 410 nm (λ_{max} for monodispersed oligonucleotide-silver nanoparticle conjugates) and 550 nm (emergence of red-shifted secondary plasmon band) *versus* time for the different DNA target concentrations. The Abs_{410}/ Abs_{550} ratios reveal a concentration dependence on the aggregation rate of oligonucleotide-silver

nanoparticle conjugates – the lower the target DNA concentration, the slower the assembly process. This trend remains true for concentrations from 0.2 to 10 nM of target DNA. However, an interesting trend is observed for 15 and 20 nM concentrations. The aggregation profile for 15 and 20 nM target DNA was slower than that observed for 10 nM target DNA and more akin to the aggregation profile observed for 2 nM target DNA. This trend was also observed using the oligonucleotide-gold nanoparticle conjugates where the higher concentration of target DNA resulted in slower nanoparticle assembly (see figure 4.9). This observation could be attributed to the fact that at higher target DNA concentrations, there is an abundance of steric hindrance and interstrand repulsion due to the higher number of DNA strands present, which is preventing a larger number of nanoparticle coupling events from occurring.
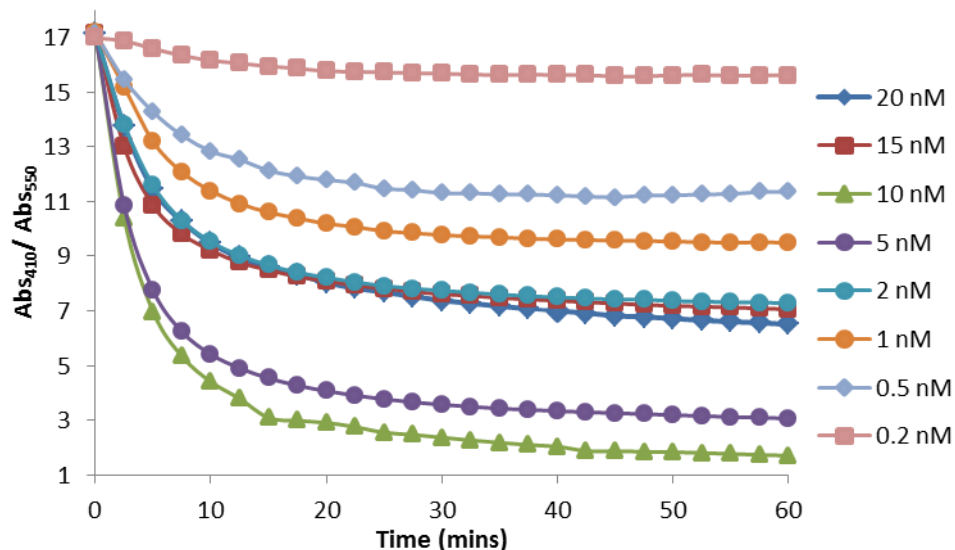
Figure 4.20. Ratios between absorbance values at 410 nm (λ_{max} for monodispersed oligonucleotide-silver nanoparticle conjugates) and 550 nm (emergence of red-shifted secondary plasmon band) versus time (minutes) for different target DNA concentrations.

The absorbance spectra depicted in figure 4.17 was the result of extended dampening and broadening of the surface plasmon resonance at 410 nm. The dampening and broadening *i.e.* red-shifting of the surface plasmon band during aggregation is a direct result of the coupling of individual nanoparticles which are brought into close

proximity with one another during DNA hybridisation. The nanoparticle conjugates form nanoparticle clusters of random orientations and the extent of this clustering is directly related to the concentration of target DNA added. In an effort to understand more clearly the red-shifted plasmon resonances arising from the coupling of nanoparticles during the DNA hybridisation process it was decided to adopt an approach whereby the initial absorption spectrum, prior to addition of target DNA, is subtracted from the other time-dependent spectra of the DNA assembly process. The resulting difference spectra have the contribution of individual nanoparticles at 410 nm removed leaving spectra resulting from the red-shifted, plasmonic contributions of interacting nanoparticles during the assembly process. This process was adopted by Taylor *et al.* to look at the dependence on cucurbit[n]uril concentration on the aggregation rate of gold nanoparticles and Guerrini *et al.* who examined the difference spectra of interacting silver nanoparticles through DNA triplex formation using DNA targets of defined lengths to control the interparticle distance. [13] [14] The difference absorbance spectra for the 10 nM target DNA concentration is shown in figure 4.21. The subtraction process reveals two distinct peaks: a strong, red-shifted contribution beginning at approximately 470 nm, attributed to "dipole-like" plasmon resonances showing differences in peak position and intensity depending on the target DNA concentration and a weaker contribution at approximately 370 nm which are attributed to "quadrupole-like" plasmon resonances and show an increase in intensity but little change in terms of peak position over the aggregation process. As the "dipole-like" plasmon resonance band shows sensitivity to changes during the aggregation process, it can be described as a collection of the plasmonic contributions arising from the coupling between the surface plasmon resonances of individual nanoparticles during DNA hybridisation. These resonances are similar to that observed for silver dimers of varying interparticle distance – the smaller the distance between the two particles, the larger the red-shift in the "dipole-like" plasmon resonance for incident polarization parallel to the dimer axis. [15] [16] [17]
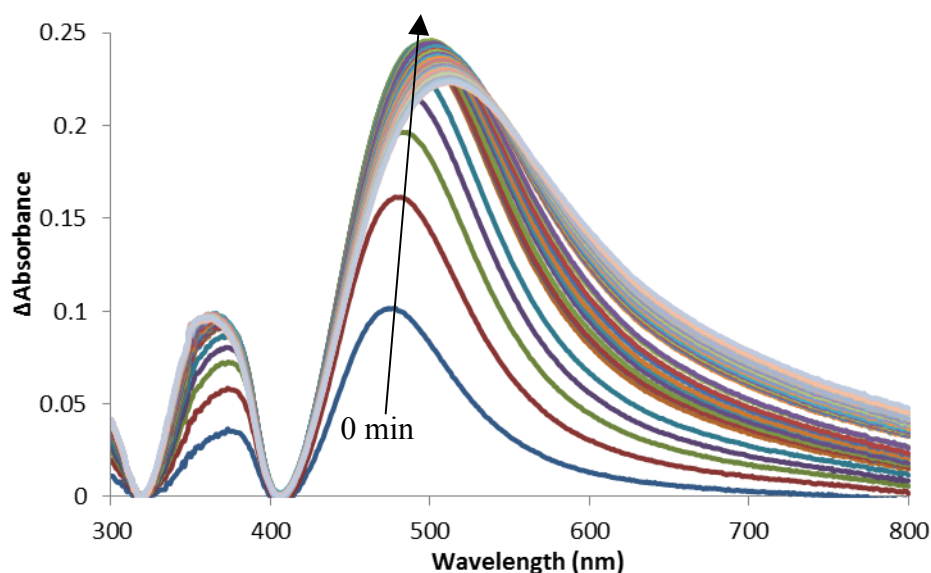
Figure 4.21. Difference absorbance spectra for the 10 nM DNA target concentration obtained by subtracting the contributions from individual silver nanoparticles at 410 nm from the other time-dependent absorbance spectra during the assembly process.

Inspection of the difference spectra (figure 4.21) reveals three clear modes of aggregation that occur over the course of the hybridisation process: (1) a rapid increase in intensity for the "dipole-like" plasmon resonance, (2) a plateau where there is no increase in intensity but still a red-shifting of the plasmon band, and, finally, (3) a decrease in intensity followed by a broadening of the plasmon band. Although not shown explicitly, each of the target DNA concentrations displays the same three modes of aggregation. Nevertheless there are differences in terms of the maximum intensity achieved for each concentration. Figure 4.22 displays the maximum intensity of the "dipole-like" plasmon resonance band for each target DNA concentration *versus* time. As can be seen, the maximum intensity of the "dipole-like" plasmon resonance band is directly correlated to the target DNA concentration. The trend is similar to that observed for the data collected in figure 4.20, the 10 nM target concentration results in the highest "dipole-like" plasmon band intensity and there is a decrease in maximum intensity as the target DNA concentration decreases. The 20 nM target concentration shows a slower increase in intensity, taking a greater amount of time to reach a maximum intensity compared to the other concentrations investigated. However, the "dipole-like" plasmon resonance

band for the 20 and 15 nM target concentrations is affected similarly in a way that is similar to the data obtained in figure 4.20, *i.e.* these concentrations hinder the assembly progress, resulting in slower aggregation dynamics, smaller difference in the degree of red-shifting and lower maximum intensities of the plasmon band.
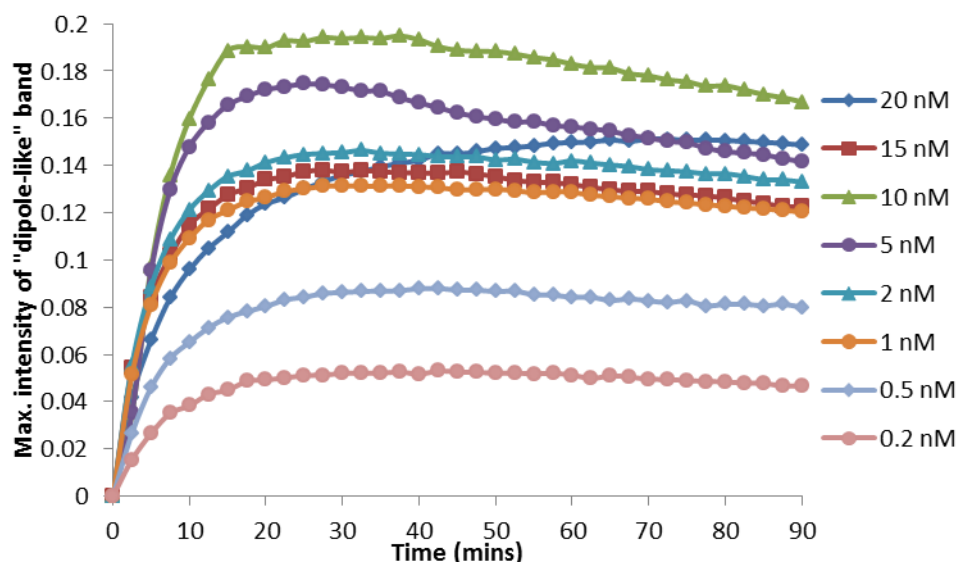
Figure 4.22. Maximum intensities of "dipole-like" plasmon resonance band versus time for different target DNA concentrations (normalized values).

While the red-shifted plasmon resonances have been shown to be sensitive to interparticle distance, [14] in this work the dependence of target DNA concentration on the degree of the red-shift in the "dipole-like" plasmon resonances was investigated. Figure 4.23 displays the "dipole-like" plasmon resonance band position *versus* time for each target DNA concentration. This shows that for each target DNA concentration there is an initial large red-shift upon target addition followed by a progressive increase in the red-shift up to a plateau value. The data correlates with that observed in figure 4.20 and figure 4.21 – the 10 nM target concentration results in the largest red-shift as this concentration promotes the greatest aggregation of the nanoparticles. Lower concentration of target results in smaller red-shifts of the absorption maxima; the addition of less target results in incomplete aggregation. In addition, the 15 nM target concentration promotes a slightly larger red-shift than the 20 nM target which correlates to that observed in figure 4.22 – the 15 nM target

concentration promotes slightly faster aggregation dynamics compared to the 20 nM target concentration.
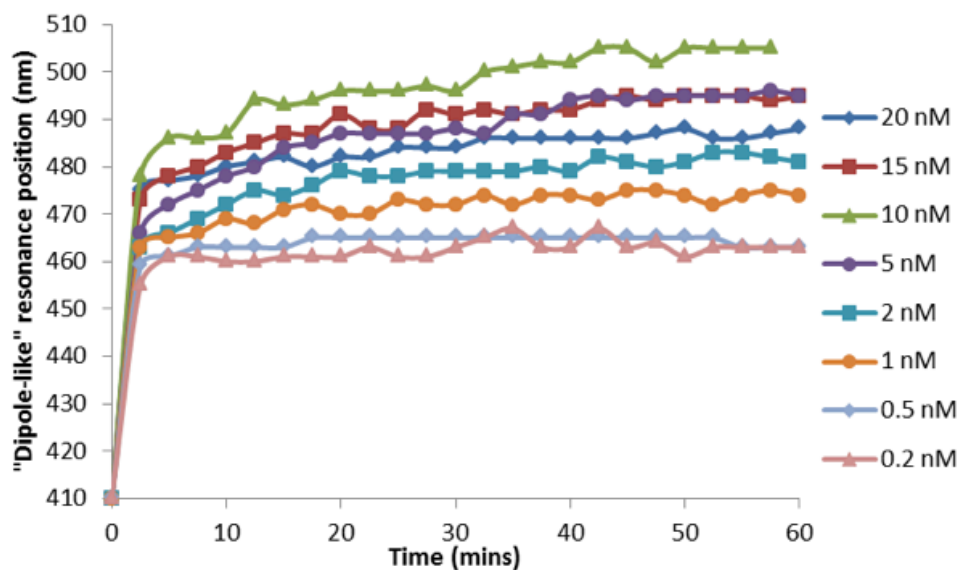
Figure 4.23. Peak position of the "dipole-like" plasmon resonance band versus time for different target DNA concentrations.

4.4.3 Effect of DNA Target Concentration on Oligonucleotide-Silver Nanoparticle Conjugate Hybridisations: Melting Properties

The effect of varying the target DNA concentration on the melting behaviour of oligonucleotide-silver nanoparticle conjugates has been reported previously. [18] Thompson *et al.* revealed that decreasing the concentration of target DNA resulted in lower melting temperatures and smaller melting transitions. [18] In this work, it was decided to compare the melting behaviour of the 10, 15 and 20 nM target concentrations. The results of the melting analysis for the different target DNA concentrations are shown in figure 4.24 and are summarised in table 4.3. The spectra displayed in figure 4.24 represent target DNA concentrations of 2 nM (purple), 10 nM (blue), 15 nM (red) and 20 nM (green). To produce the melting curves, the samples were first left to hybridise to the complementary target sequence for two hours to ensure nanoparticle assembly had fully progressed before being transferred to the UV-Vis spectrometer. The samples were cycled between 10 and 95 °C with

1 °C/ min increments monitored at 410 nm. Comparing the melting curves of the 2 nM and the 10 nM target concentrations reveals a similar trend to that observed by Thompson *et al.*, [18] with the 2 nM target concentration resulting in a lower melting temperature (68 °C) compared to 10 nM target concentration which results in melting temperature of 69 °C. In addition, the melting transition is considerably smaller for the 2 nM target concentration compared to the melting transition for the 10 nM target concentration. This difference likely arises from differences in aggregate size formed during hybridisation. Jin *et al.* reported that increasing the salt concentration, in the range 0.05 to 1 M NaCl, for hybridisation (while keeping a constant probe: target ratio) resulted in larger melting transitions due to the formation of larger aggregates. [8] In a similar fashion, increasing the target concentration means that more oligonucleotide-silver nanoparticle conjugates come into contact during hybridisation resulting in larger aggregates forming, whereas lower concentrations of target result in fewer hybridisations events and therefore smaller aggregate formation leading to smaller melting transitions.   The 15 and 20 nM target DNA concentrations exhibit lower melting temperatures (64 and 67 °C, respectively) and smaller melting transitions compared to those obtained for the 10 nM target DNA concentration. This result mimics the trend observed in figure 4.20 – assembly using the 15 and 20 nM target concentrations result in fewer hybridisation events occurring resulting in smaller aggregates forming and smaller melting transitions.
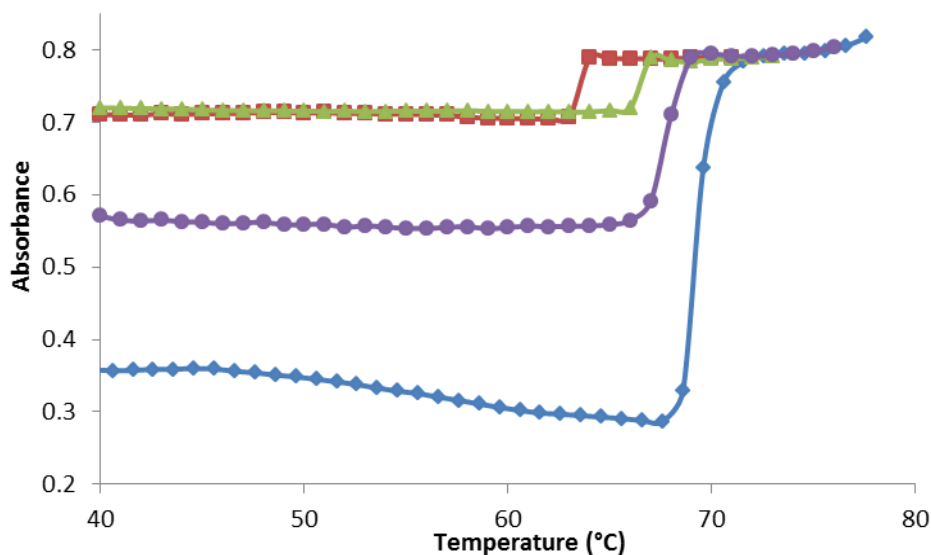
Figure 4.24. Melting curves of hybridised oligonucleotide-silver nanoparticle conjugates obtained by UV-Vis spectroscopy. Absorbance monitored at 410 nm. [Conjugates] = 20 pM, [DNA target] = 2 nM (purple), 10 nM (blue), 15 nM (red), 20 nM (green).

Target DNA Concentration (nM)	Melting Temperature (°C)
2	68
10	69
15	64
20	67

Table 4.3. Melting temperatures obtained from melting curve analysis of figure 4.24.

4.4.4 Effect of Interparticle Distance on Oligonucleotide-Silver Nanoparticle Conjugate Hybridisations

While the amount of available target DNA readily influences the aggregation kinetics of the oligonucleotide-silver nanoparticle conjugates, other factors, such as interparticle distance, can play an important role in the assembly process. The distance dependent aggregation kinetics of oligonucleotide-nanoparticle conjugates has been previously reported for gold and silver-thiol based systems, however, very little research is reported on the effect of thioctic acid-modified oligonucleotide-

silver nanoparticle conjugates on aggregation kinetics. [7] [14] Storhoff *et al.* and Guerrini *et al.* reported the effect of varying the length of the target DNA sequence on aggregation kinetics concluding that larger interparticle distances resulted in slower aggregation profiles as observed by UV-Vis spectroscopy. Another method for varying the interparticle distance, in addition to increasing the target DNA length, is to position the thioctic acid modification at an alternative site on the oligonucleotide to produce "tail-to-tail", "head-to-tail" or "head-to-head" probe orientations during hybridisations (see figure 4.3 for position of thioctic acid modification to produce the different orientations). The DNA-induced assembly of oligonucleotide-silver nanoparticle conjugates as depicted in figure 4.16 was performed in the "head-to-tail" orientation meaning the distance between the nanoparticles was approximately 7 nm. Figure 4.25 shows the DNA-induced assembly of oligonucleotide-silver nanoparticle conjugates hybridised in a "tail-to-tail" orientation, separated by a distance of approximately 14 nm. To achieve this, Ag-P1 and Ag-P3 were mixed with P1P3 comp under the same experimental conditions as that of figure 4.18 for the sake of comparison. By comparing the spectrum in figure 4.25 to the spectrum in figure 4.18, there is an observable difference in the aggregation profiles – "head-to-tail" results in considerable aggregation while "tail-to-tail" results in very little aggregation of the nanoparticles. Figure 4.26 shows a plot of the ratios between the absorbance at 410 nm and 550 nm *versus* time to further highlight the difference in aggregation rates between the two orientations. Hybridisation of the oligonucleotide-silver nanoparticle conjugates in the "tail-to-tail" orientation results in a considerably slower aggregation profile compared to the "head-to-tail" orientation due to the surface plasmon resonances of the nanoparticles coupling over a longer distance.
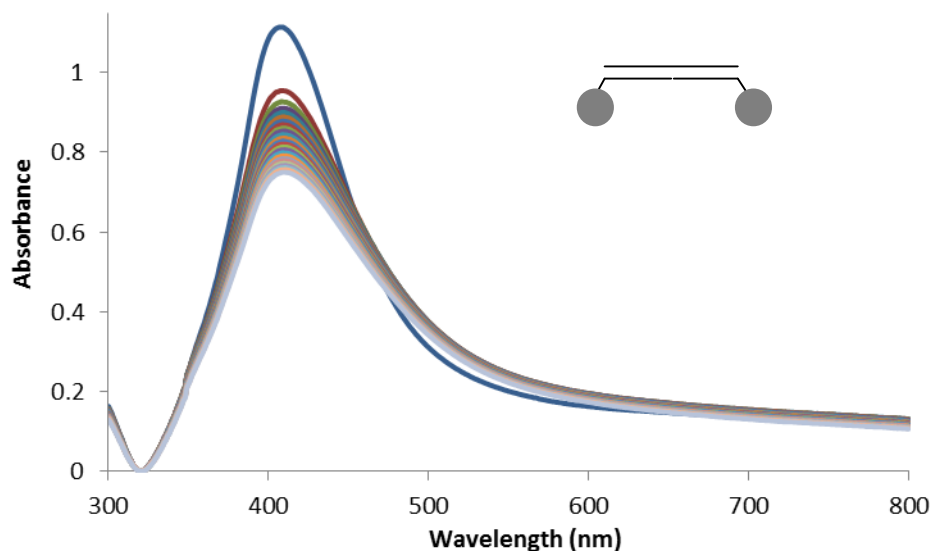
Figure 4.25. Extinction spectra of DNA hybridisation-induced aggregation of oligonucleotide-silver nanoparticle conjugates in a "tail-to-tail" orientation. Each spectrum represents a scan taken at 5 minute intervals over 120 minutes of the aggregation process. [Conjugates] = 20 pM, [DNA target] = 10 nM in PBS (0.3 M, pH 7).
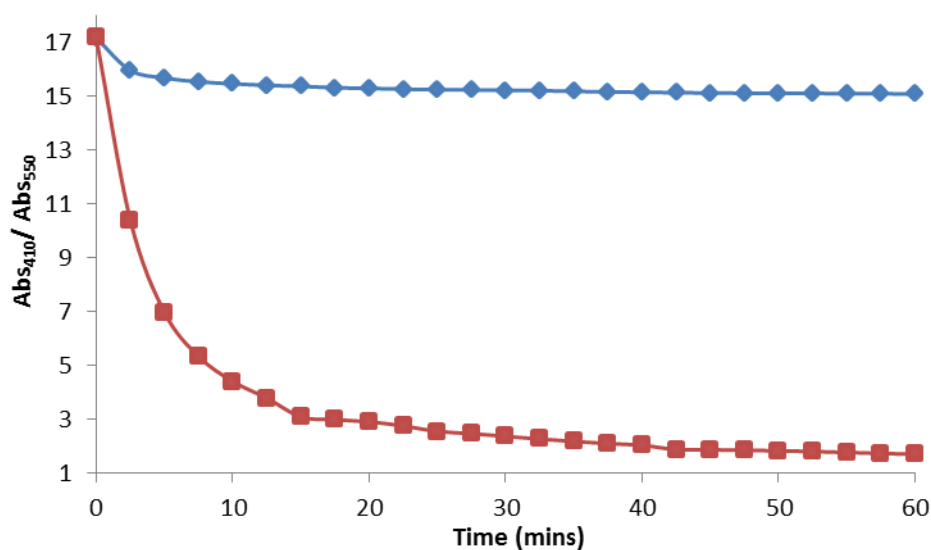
*Figure 4.26. Ratios between absorbance values at 410 nm and 550 nm versus time (minutes) for the "tail-to-tail" (**blue**) and "head-to-tail" (**red**) orientations during hybridisation. Conjugate concentration and target DNA concentration were the same for each sample.*

As the aim of this research was to use the oligonucleotide-silver nanoparticle conjugates for SERRS detection of DNA sequences, the hybridisation profiles of another orientation of nanoparticles was investigated for comparison to the other orientations. The "head-to-head" orientation of oligonucleotide-silver nanoparticle conjugates eliminates the interparticle distance between conjugates during hybridisation. This offers two distinct advantages: (1) the close proximity of the nanoparticles during hybridisation results in faster aggregation rates [7] and (2) closing the interparticle gap results in higher SERRS intensities. [14] Initially, performing "head-to-head" hybridisations using the thioctic acid-modified oligonucleotide-silver nanoparticle conjugates was met with some difficulty. Figure 4.27 shows an example of an early attempt to hybridise Ag-P1 and Ag-P3 to P1P2 comp. The spectra included in figure 4.27 are a scan taken prior to addition of the complementary DNA target sequence (0 min) and a scan taken after 60 minutes of the hybridisation process. As can be seen, no hybridisation has occurred in the hour allowed for hybridisation. It was proposed that no assembly was occurring due to the nanoparticle surface being heavily functionalised with oligonucleotide probes that were repulsed during hybridisation by the strong electrostatic barrier caused by the conjugates coming into close proximity with one another in a "head-to-head" orientation.
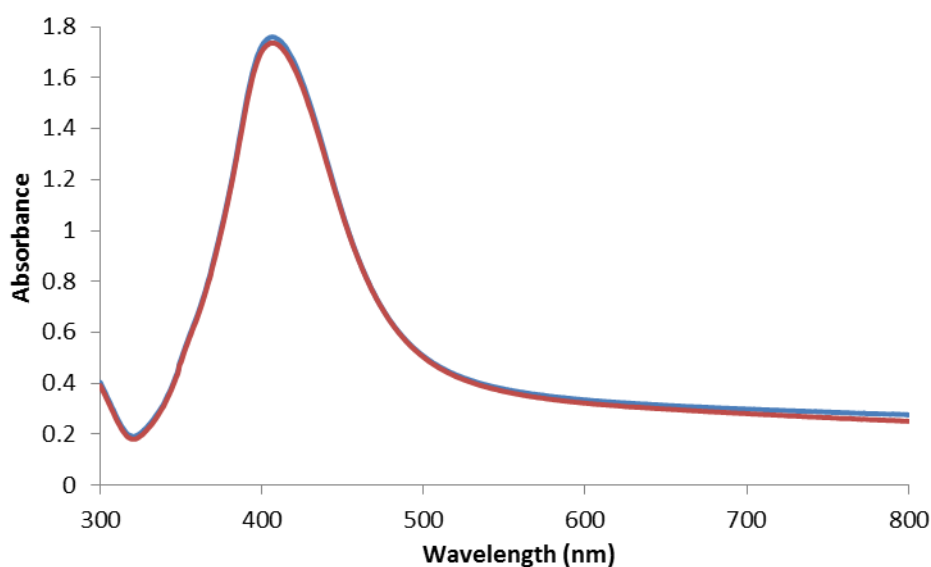
*Figure 4.27. Initial attempt at hybridising oligonucleotide-silver nanoparticle conjugates in a "head-to-head" orientation using P1P2 comp: 0 min (**blue**) and 60 min (**red**). [Conjugates] = 20 pM, [DNA Target] = 10 nM in PBS (0.3 M, pH 7).*

In light of this result, it was decided to investigate if the density of the oligonucleotides on the nanoparticles could be controlled in order to allow for hybridisation in a "head-to-head" orientation. However, the number of oligonucleotides per nanoparticle cannot easily be controlled and, in addition, there needs to be sufficient oligonucleotides coverage on the surface to confer stability to the nanoparticles. In this regard, a method whereby the nanoparticles are co-functionalised with the recognition sequence, P1 or P2, and non-hybridising sequences consisting of a 5'-thioctic acid modification and 10 thymine bases was utilized. [19] The recognition sequence was mixed with the T_{10} sequence in different molar ratios and added to a solution of silver nanoparticles according to the methods previously reported in this work (figure 4.28). The recognition: T_{10} ratios investigated were 0.8, 0.6, 0.4, 0.2, 0.1 and 0.01. Once the conjugates were successfully produced, assembly of the nanoparticles was induced by addition of 2 nM P1P2 comp in 0.3 M PBS. Figure 4.29 shows the spectrum obtained from DNA-based assembly of the 0.8 recognition: T_{10} molar ratio oligonucleotide-silver nanoparticle conjugates. As can be seen, reducing the density of oligonucleotides on the surface of the nanoparticles has successfully allowed hybridisation to occur

resulting in the characteristic dampening and broadening of the surface plasmon resonance band in the "head-to-head" orientation.
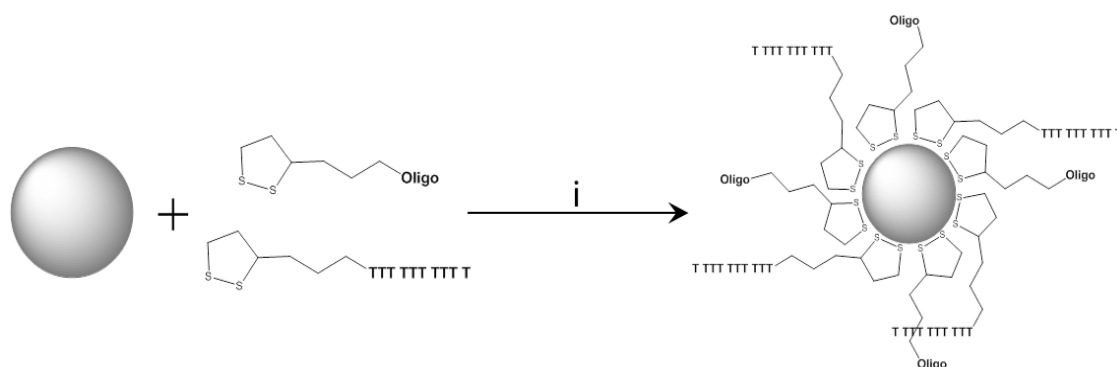
Figure 4.28. Schematic representation of the co-adsorption of the recognition oligonucleotide (P1 and P3) and the 10 thymine non-recognition sequence on to silver nanoparticles. (i) 60 mM phosphate buffer pH 7, 0.1 M NaCl.
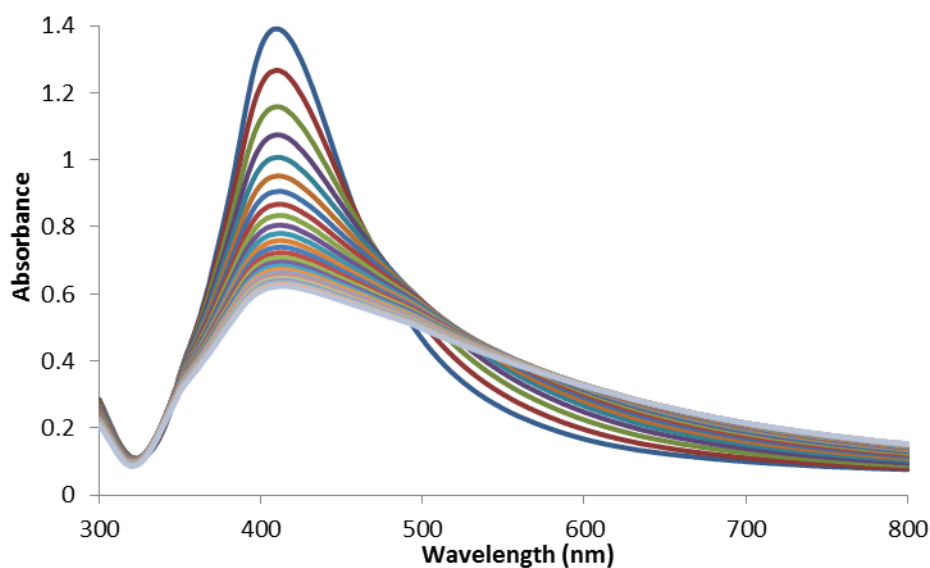
Figure 4.29. Extinction spectra of oligonucleotide-silver nanoparticle conjugates hybridising in a "head-to-head" orientation with a recognition sequence: T_{10} sequence molar ratio of 0.8. [Conjugates] = 20 pM, [DNA Target] = 2 nM in PBS (0.3 M, pH 7).

The other recognition sequence: T_{10} sequence molar ratios are displayed in figure 4.30 and are shown as the ratios between absorbance at 410 nm and 550 nm *versus*

time. As with the 0.8 molar ratio shown in figure 4.29, adjusting the molar ratio so there are less recognition oligonucleotide sequences on the surface of the nanoparticles allows for successful hybridisation in the "head-to-head" orientation. In addition, there appears to be a trend in the rate of aggregation of the different molar ratios. There appears to be an optimal rate of aggregation at a molar ratio of 0.4, which resulted in the fastest assembly profile compared to the other molar ratios. Below this the rate of aggregation decreases as the number of available recognition oligonucleotide probes decreases. However, for molar ratios of 0.8 and 0.6, the rates of aggregation are lower than that obtained for 0.4, suggesting the oligonucleotide density on the nanoparticles was still too great to afford faster aggregation dynamics. These results opened up the possibility of using the oligonucleotide-silver nanoparticle conjugates in a "head-to-head" orientation which could lead to increased SERRS intensities – a useful prospect for their use in DNA detection assays.
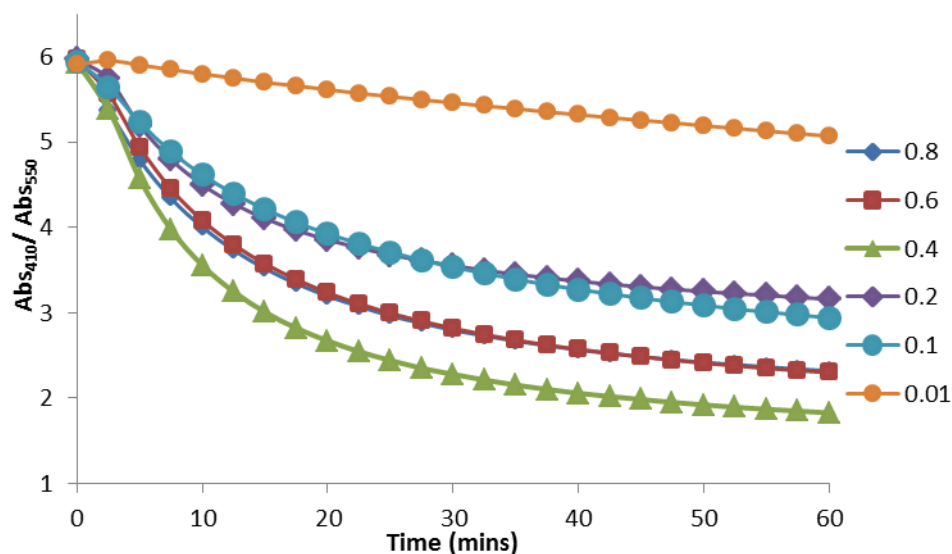
Figure 4.30. Ratios between absorbance values at 410 nm (λ_{max} for monodispersed oligonucleotide-silver nanoparticle conjugates) and 550 nm (emergence of red-shifted secondary plasmon band) versus time (minutes) for different recognition sequence: T_{10} sequence molar ratios in the "head-to-head" orientation.

4.4.5 Effect of Interparticle Distance on Oligonucleotide-Silver Nanoparticle Conjugate Hybridisations: Melting Properties

The interparticle distance can also influence the melting behaviour of oligonucleotide-silver nanoparticle conjugates. Research has shown that for smaller interparticle distances there is a decrease in the melting temperature obtained, *i.e.* T_m for "tail-to-tail" > "head-to-tail" > "head-to-head". [18] [20] Figure 4.31 shows the melting curve obtained from hybridisation of Ag-P1 and Ag-P3 mixed with P1P3 comp to achieve a "tail-to-tail" orientation. The T_m obtained is 71.5 °C ± 0.7 °C which is higher than the T_m obtained for the "head-to-tail" orientation (69 °C ± 1 °C, figure 4.24). In the literature, electrostatic interactions, *i.e.* particle-particle repulsion, have been suggested to be the dominant factor affecting the melting temperature in relation to interparticle distance. The "tail-to-tail" orientation allows for easier hybridisation between conjugates, due to the larger distance between nanoparticles, compared to "head-to-head" orientations, which have a higher repulsion rate due to the proximity of the nanoparticles during hybridisation. [8]
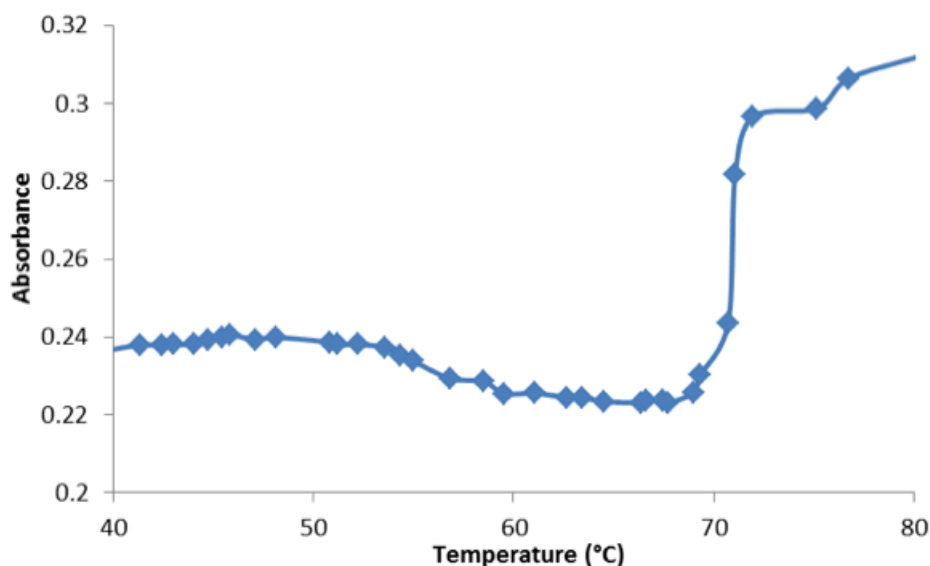
Figure 4.31. Melting curve of hybridised oligonucleotide-silver nanoparticle conjugates in the "tail-to-tail" orientation. Absorbance monitored at 410 nm. [Conjugates] = 20 pM, [DNA target] = 10 nM.

Hybridisation of oligonucleotide-silver nanoparticle conjugates in a "head-to-head" orientation typically leads to melting temperatures that are lower than either the "tail-to-tail" or "head-to-tail" orientations. [8] [18] [20] Figure 4.32 shows the melting curves obtained before the co-adsorption of T_{10} sequences and after the co-adsorption of T_{10} sequences, with a molar ratio of 0.4 (recognition sequence: T_{10} sequence). The melting temperature for the 0.4 molar ratio is 66 °C which is lower than the melting temperatures obtained for the "tail-to-tail" and "head-to-tail" orientations reported earlier in this work. Although not shown, the melting analyses for the other molar ratios (except for 0.01 which did not provide a melting curve) resulted in the same melting temperature, showing that the interparticle distance is a critical factor in determining the melting temperature even as the number of possible hybridisation events decreases.
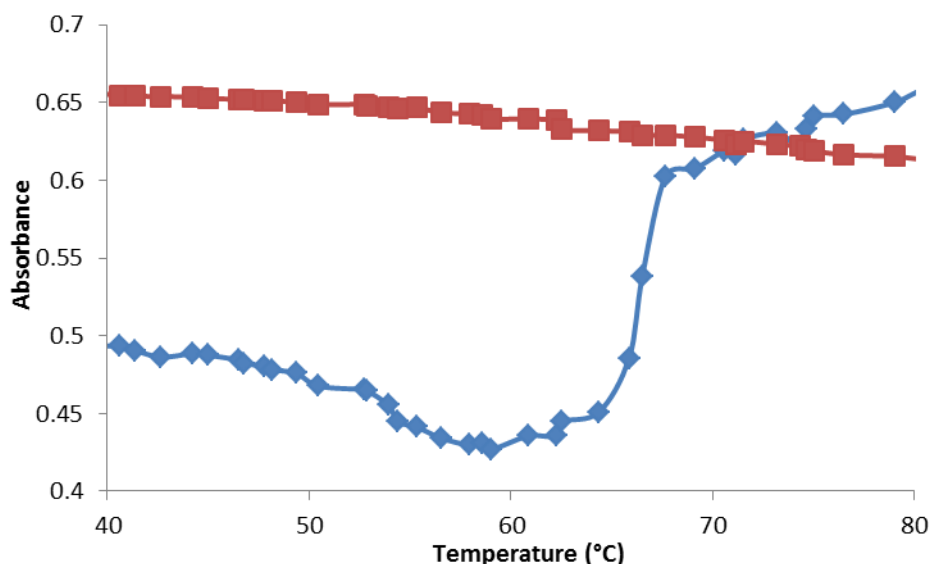
Figure 4.32. Melting curve of hybridised oligonucleotide-silver nanoparticle conjugates in the "head-to-head" orientation. Absorbance monitored at 410 nm. Red line represents an attempted melting analysis before co-adsorption of T_{10} sequences and the blue line represents a melting curve obtained from 0.4 recognition: T_{10} molar ratio. [Conjugates] = 20 pM, [DNA Target] = 2 nM.

4.5 Conclusions

Gold and silver nanoparticles functionalised with thioctic acid-modified oligonucleotide sequences were successfully investigated for their ability to hybridise

to complementary DNA target sequences in order to facilitate aggregation of the nanoparticles. These results showed that oligonucleotide-nanoparticle conjugates could be implemented as biosensors for the detection of specific DNA sequences related to disease.

The hybridisation of the oligonucleotide-nanoparticle conjugates was primarily investigated *via* UV-Vis spectroscopy. Hybridisation of the complementary target DNA sequence induces a shift of the surface plasmon resonance band of the gold and silver nanoparticles, which shifts to longer wavelengths as the hybridisation of the DNA proceeds. This event was confirmed to be sequences specific by addition of a non-complementary target sequence that resulted in no change in the optical response. The concentration dependence of the optical response of the aggregation was investigated for silver nanoparticle conjugates in the range 0.2 – 20 nM showing that high concentrations of target up to 10 nM induce the greatest degree of aggregation while lower concentrations result in the least amount of aggregation.

The reversibility of the aggregation process was investigated by performing melting analysis on the oligonucleotide-nanoparticle conjugates. These results indicated the reproducibility of the hybridisation-induced aggregation event and demonstrated the stability of the conjugates at high temperature making the conjugates viable to be included in techniques such as PCR. The melting temperature and size of the melting transition was found to be dependent on the concentration of target added, with lower concentrations demonstrating lower melting temperatures and smaller melting transitions compared to higher concentrations of target.

The dependence of the degree of aggregation on the interparticle distance was investigated. It was found that the "tail-to-tail" aggregation resulted in the least amount of aggregation because the nanoparticles were coupling over a longer distance compared to the "head-to-head" orientation that resulted in sufficient aggregation of the system. The "head-to-head" orientation was initially met with some difficulty, as strong steric and electrostatic barriers due the density of the oligonucleotides on the surface, were responsible for preventing the nanoparticles to sufficiently aggregate. This was overcome by introducing "spacer" sequences, oligonucleotides containing a thioctic acid moiety and a base-pair sequence

consisting of 10 thymine bases, which were coadsorbed on to the nanoparticle surface along with the recognition sequence. It was found that by reducing the number of recognition sequences on the surface facilitated DNA hybridisation and therefore aggregation of the nanoparticles in the "head-to-head" orientation and it was discovered that the extent of the aggregation was governed by the amount of recognition sequences on the surface, with lower concentrations of recognition sequences resulting in minimal aggregation of the nanoparticles compared to huger concentrations of recognition sequences.

In conclusion, the viability of using oligonucleotide-gold and silver nanoparticle conjugate probes for the detection of specific DNA sequences related to disease has been successfully demonstrated.

4.5 References

1.   J. Li, S. Song, D. Lib, Y. Suc, Q. Huang, Y. Zhao and C. Fan, *Biosens. Bioelectron.*, 2009, **24**, 3311–3315.

2.   J. J. Storhoff, A. D. Lucas, V. Garimella, Y. B. Bao and U. R. Müller, *Nat. Biotechnol.*, 2004, **22**, 883–887.

3.   J. M. Nam, S. I. Stoeva and C. A. Mirkin, *J. Am. Chem. Soc.*, 2004, **126**, 5932-5933.

4.   F. McKenzie, K. Faulds and D. Graham, *Chem. Commun.*, 2008, **20**, 2367-2369.

5.   H. B. Shen, M. Hu, Y. B. Wang and H. Q. Zhou, *Biophys. Chem.*, 2005, **115**, 63-66.

6.   H. B. Shen, M. Hu, Z. N. Yang, C. Wang and L. Z. Zhu, *Chin. Sci. Bull.*, 2005, **50**, 2016-2020.

7.   J. J. Storhoff, A. A. Lazarides, R. C. Mucic, C. A. Mirkin, R. L. Letsinger and G. C. Schatz, *J. Am. Chem. Soc.*, 2000, **122**, 4640-4650.

8.   R. C. Jin, G. S. Wu, Z. Li, C. A. Mirkin and G. C. Schatz, *J. Am. Chem. Soc.*, 2003, **125**, 1643-1654.

9.   P. Vannuffel, J. Gigi, H. Ezzedine, B. Vandercam, M. Delmee, G. Wauters and J. L. Gala, *J. Clin. Microbiol.*, 1995, **33**, 2864-2867.

10.   K. M. Ririe, R. P. Rasmussen and C. T. Wittwer, *Anal. Biochem.*, 1997, **245**,

154-160.

11. N. R. Markham and M. Zuker, *Nucleic Acids Res.*, 2005, **33**, W577-W581.

12. S. J. Park, A. A. Lazarides, C. A. Mirkin and R. L. Letsinger, *Angew. Chem. Int. Edit.*, 2001, **40**, 2909-2912.

13. R. W. Taylor, T.-C. Lee, O. A. Scherman, R. Esteban, J. Aizpurua, F. M. Huang, J. J. Baumberg and S. Mahajan, *ACS Nano*, 2011, **5**, 3878-3887.

14. L. Guerrini, F. McKenzie, A. W. Wark, K. Faulds and D. Graham, *Chem. Sci.*, 2012, **3**, 2262-2269.

15. E. C. Le Ru and P. G. Etchegoin, *Principles of Surface Enhanced Raman Spectroscopy*, Elsevier, Amsterdam, 2009.

16. E. Hao and G. C. Schatz, *J. Chem. Phys.*, 2004, **120**, 357-366.

17. E. C. Le Ru, C. Galloway and P. G. Etchegoin, *Phys. Chem. Chem. Phys.*, 2006, **8**, 3083-3087.

18. D. G. Thompson, A. Enright, K. Faulds, W. E. Smith and D. Graham, *Anal. Chem.*, 2008, **80**, 2805-2810.

19. L. M. Demers, C. A. Mirkin, R. C. Mucic, R. A. Reynolds, R. L. Letsinger, R. Elghanian and G. Viswanadham, *Anal. Chem.*, 2000, **72**, 5535-5541.

20. D. G. Thompson, R. J. Stokes, R. W. Martin, R. J. Lundahl, K. Faulds and D. Graham, *Small*, 2008, **4**, 1054-1057.

5 Oligonucleotide-Nanoparticle Conjugate Characterisation Using SERRS Spectroscopy

Raman scattering is an optical spectroscopic technique that provides a specific "fingerprint" spectrum of a molecule directly linked to the vibrational modes of the interrogated molecule. The Raman scattering process is inherently weak, relying on the inelastic scattering of photons, with only ~ 1 in 10^7 photons scattered inelastically. However, this weak process can be enhanced, up to 10^6 greater than Raman scattering, by the introduction of a roughened metal surface, such as metallic gold or silver nanoparticles, whose surface plasmon resonance lies close to the incoming wavelength of light. In addition, if a molecular chromophore is immobilised onto the roughened metal surface and has an absorbance maxima near the wavelength of incoming light, greater enhancement of the Raman signal is observed. This technique is called surface enhanced resonance Raman scattering (SERRS) spectroscopy (figure 5.1).

SERRS spectroscopy has shown to be a promising technique for the sensitive detection of dye-labelled oligonucleotides. [1] [2] [3] In addition, the unique molecular "fingerprint" SERRS spectrum has proven to be useful for multiplex analysis of labelled oligonucleotides. [4] DNA detection assays using SERRS spectroscopy often rely on the adsorption of dye-labelled oligonucleotides to the nanoparticle surface using a polyamine species, such as spermine hydrochloride or poly-L-lysine, to neutralise the polyanionic backbone of the oligonucleotide and to partially aggregate the nanoparticles to generate "hotspots" which facilitate increased SERRS intensity. [5] [6] [7] [8] "Hotspots" are areas of high electromagnetic intensity generated by the coupling of surface plasmon resonances in the junctions between nanoparticles [9] and have reportedly allowed detection by SERRS down to single molecule levels of sensitivity. [10] [11]
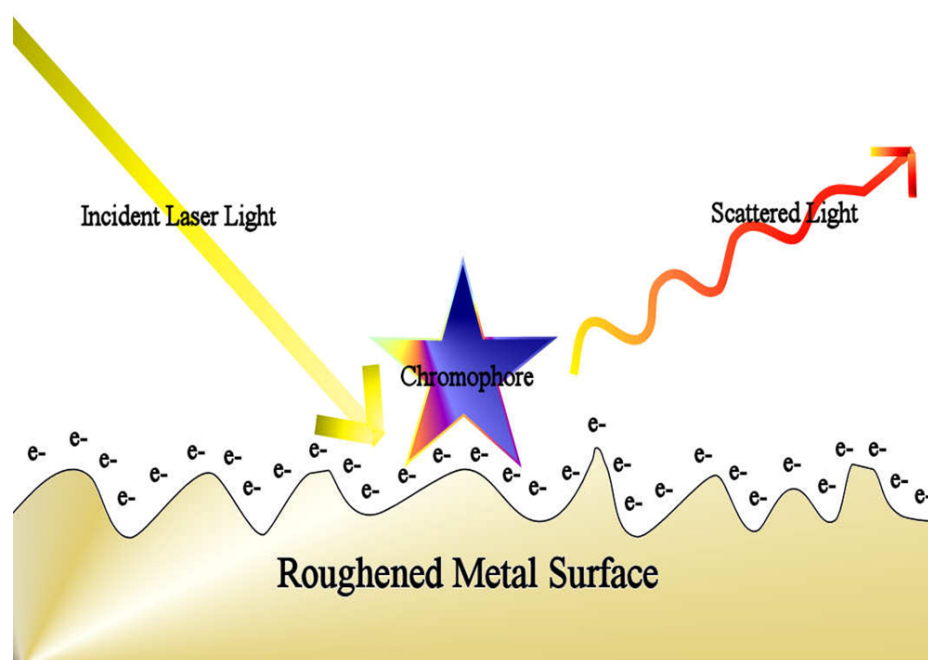
Figure 5.1. Depiction of the SERRS process. The incoming light interacts with the surface plasmon of the roughened metal surface and chromophore immobilised onto the metal surface inducing a scattering effect, which is then collected and converted into a molecularly specific "fingerprint" spectrum that is unique to the vibrational modes of the target molecule. [12]

The exploitation of electromagnetic enhancements from nanoparticle "hotspots" has led to other SERRS-based DNA detection strategies. These strategies are based upon the hybridisation-induced assembly of oligonucleotide-nanoparticle conjugates first reported by Mirkin *et al.* and Alivisatos *et al.* [13] [14] Graham *et al.* reported the functionalisation of silver nanoparticles with a SERRS-active dye and thiol-modified oligonucleotides which, upon hybridisation with a complementary target DNA sequence, result in an increase in the SERRS intensity generated by the "hotspots" formed during DNA hybridisation. [15] Thompson *et al.* used this methodology to detect SNPs by SERRS. [16] Similar research was conducted by Nie *et al.* who functionalised gold nanocrystals with a SERRS-active dye and low molecular weight polyethylene glycol molecules, to stabilize the nanoparticles, in addition to thiol-modified oligonucleotides which produced increased SERRS intensities upon hybridisation. [17] McKenzie *et al.* reported another SERRS-based nanoparticle-DNA assembly method whereby the nanoparticles were first stabilized by the addition of

oligonucleotides and subsequently functionalised with a SERRS-active dye, leading to an improved conjugate preparation method where the choice of dye could be altered since the nanoparticles were already stabilized by the oligonucleotides. [18] [19] The same approach was utilized by Guerrini *et al.* whereby oligonucleotide-silver nanoparticle conjugates were assembled *via* DNA triplex formation to examine the effect of interparticle distance in the SERRS response. [20]

In this thesis, to undertake SERRS-based analysis, the two thioctic acid-modified oligonucleotide-nanoparticle conjugate probes were assembled *via* DNA hybridisation-induced aggregation as previously reported in this work (see Chapter 4). A resonant chromophore was introduced by the functionalisation of the nanoparticle surface using an isothiocyanate (-N=C=S) modified dye. The isothiocyanate moiety adsorbs on to the surface *via* the sulfur group. [21] Recently, it was been reported that isothiocyanate dye labels that contain a dimethylamino group as part of their structure can anchor to the surface through a nitrogen atom of the dimethylamino group (in addition to the isothioscyanate sulphur) which leads to a nearly flat configuration on the nanoparticle surface. [22] The dye-label was added to the nanoparticles post-oligonucleotide functionalisation in order to widen the choice of dye label since the nanoparticles were already afforded steric and electrostatic protection from the surface-bound oligonucleotides (see Chapter 3). [18] The dye label is responsible for providing the Raman signal, rather than the DNA, and fluorescent dyes can be used since fluorescence is quenched at the nanoparticle surface, thereby minimising possible interference of the Raman signal.

The basis of the SERRS detection was to provide a spectroscopic output to discriminate between the presence or absence of specific DNA sequences in an assay format (figure 5.2). The SERRS would be effectively "switched on" by hybridising the dye-labelled oligonucleotide-nanoparticle conjugate probes to complementary DNA sequences. In the absence of target DNA or non-complementary DNA sequences, a low SERRS signal is observed and upon addition of a complementary target a high SERRS signal is observed since the coupling of the nanoparticle surface plasmon resonances produces areas of high electromagnetic intensity, or "hotspots", which result in increased SERRS intensities. This is an attractive approach since the

plasmonics approach studied in chapter 4 does not offer the capability of carrying out multiplexed analysis. That is, the simultaneous detection of multiple species in a single pot.
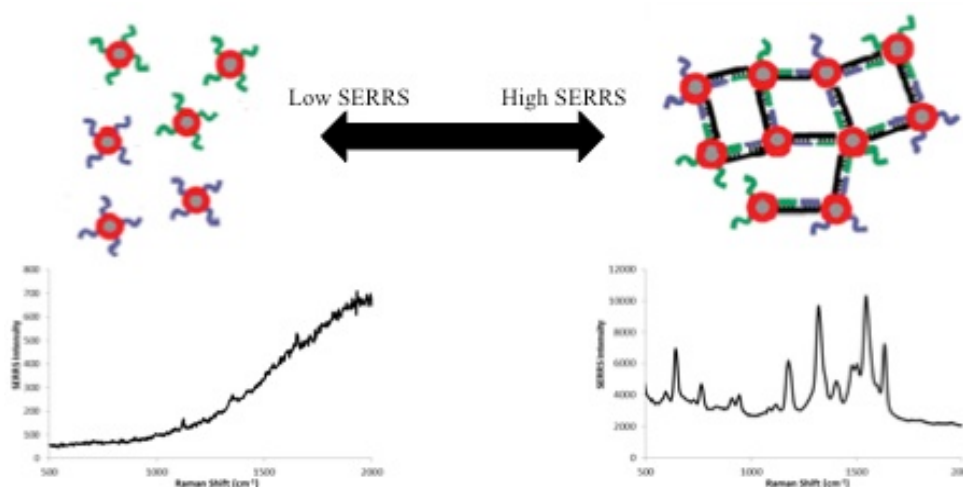
Figure 5.2. Representation of the SERRS-based analysis of the assembly of dye-labelled oligonucleotide-nanoparticle conjugates. Addition of a complementary target results in aggregation of the nanoparticles induced by DNA hybridisation, resulting in an increase in the SERRS intensity.

In this chapter, the viability of the DNA-induced assembly of thioctic acid-modified oligonucleotide-nanoparticle conjugates, whose properties were investigated in previous chapters, for biosensing of DNA related to disease for use in SERRS-based assays will be investigated.

5.1 SERRS Detection of Mixed-Metal Oligonucleotide-Nanoparticle Conjugates

Initially, it was attempted to investigate oligonucleotide gold-nanoparticle conjugates labelled with malachite green isothiocyanate (MGITC) as possible probes for the detection of DNA by SERRS. This was in light of results obtained previously (see Chapter 3) showing that MGITC enhances the stability of thioctic acid-modified oligonucleotide-gold nanoparticle conjugates. MGITC is an ideal choice of dye for functionalisation to gold nanoparticles since it has a broad absorbance profile (λ_{max} at 620 nm) allowing easier detection using an excitation wavelength of 633 nm. At

shorter excitation wavelengths, 532 or 514 nm, gold nanoparticles are known to be poor SERRS enhancers due to the absorption of energy from the laser excitation into the bulk metal energy levels at these wavelengths. [3] Figure 5.3 shows assembly of oligonucleotide-gold nanoparticle conjugates labelled with MGITC and analysed at 633 nm excitation. Assembly of the nanoparticles was induced by the addition of 50 nM complementary DNA to 0.5 nM of Au-P1 and Au-P2. As can be seen, no enhancement of the SERRS signal was obtained using gold nanoparticle conjugates. This was possibly due to the inherently poor enhancement properties related to the small size of the gold nanoparticles, ~ 15 nm, as it has been shown that surface enhancement from aggregated nanoparticles is dependent upon nanoparticle size. [23]
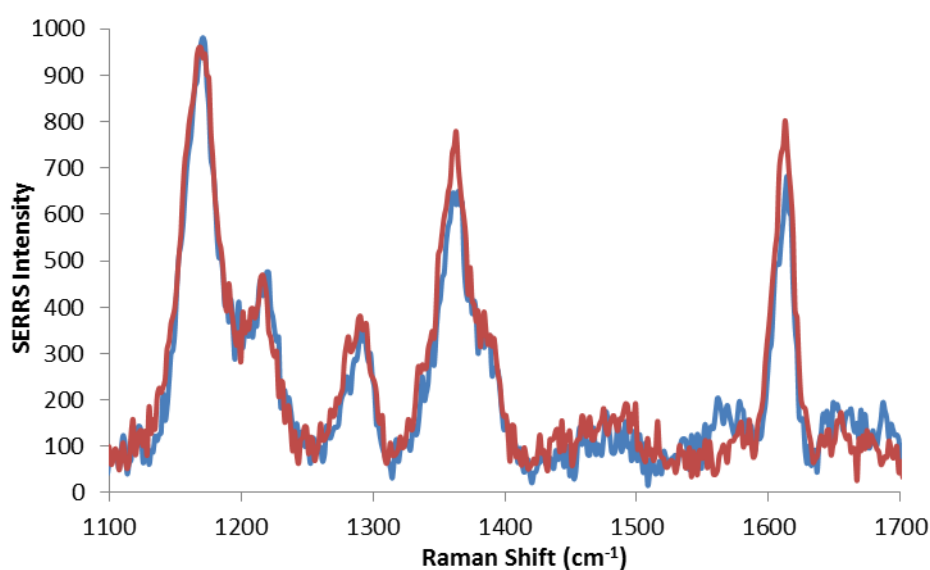
Figure 5.3. SERRS analysis of DNA assembly using oligonucleotide-gold nanoparticle conjugates in a "head-to-tail" orientation at 633 nm excitation wavelength and 10 second scan time. Blue line: non-complementary DNA sequence, Red line: complementary DNA sequence 60 minutes after target addition.

It has been reported that gold and silver oligonucleotide-nanoparticle conjugates can be mixed together and assembled *via* DNA hybridisation. [19] [23] Mckenzie *et al.* reported the use of a split-probe assay in which one probe consisted of gold nanoparticle functionalised with thiol-modified oligonucleotides and MGITC while the other probe consisted of silver nanoparticles functionalised with thiol-modified oligonucleotides only. Upon hybridisation of a complementary target, an increase in

the SERRS intensity was observed due to coupling of the surface plasmon resonances during hybridisation. [19] In this manner, the more beneficial surface chemistry of gold nanoparticles was exploited while the silver nanoparticles provided the enhancement of the Raman signal during hybridisation.
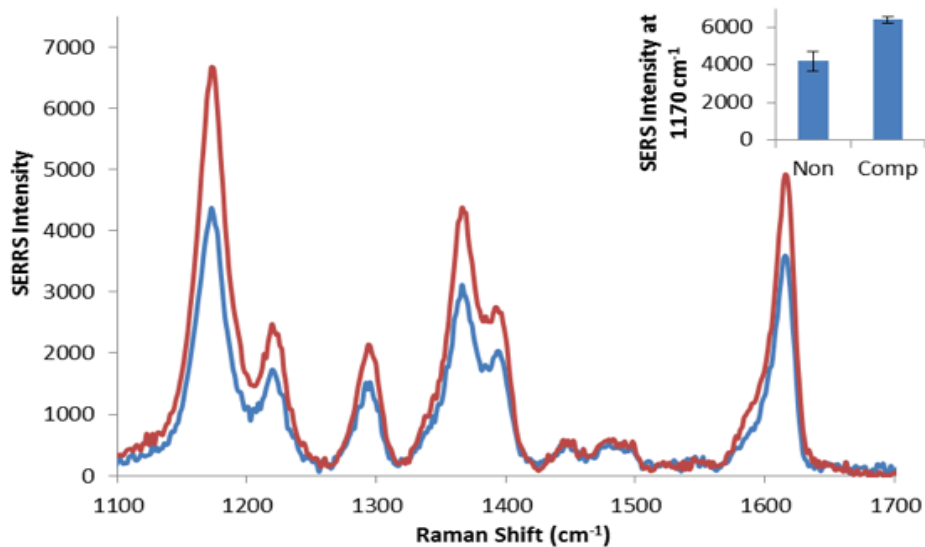
Figure 5.4. SERRS analysis of DNA assembly using MGITC-labelled mixed-metal nanoparticle conjugates in a "head-to-tail" orientation at 633 nm excitation wavelength and 10 second scan time. Blue line: non-complementary DNA sequence, Red line: complementary DNA sequence 60 minutes after target addition. Inset: SERRS intensities of the non-complementary and complementary target DNA for the 1170 cm^{-1} peak. Error bars represent the standard deviation from 3 replicate analyses.

A similar approach was therefore attempted in this work, gold nanoparticles were functionalised with P1 and silver nanoparticles were functionalised with P2. After successful conjugation of the oligonucleotides, MGITC was added to the P1 conjugate using methods previously outlined in this work (see Chapter 3). Assembly of the nanoparticles was undertaken in a "head-to-tail" orientation by the addition of 50 nM complementary DNA target to Au-P1 (0.5 nM) and Ag-P2 (50 pM) and analysis was carried out using a 633 nm excitation wavelength. Figure 5.4 displays the spectra obtained from the mixed-metal nanoparticle SERRS experiment 60 minutes after target addition (red line) and with the addition of a non-complementary

target (blue line). The inset shows the averaged SERRS intensities and standard deviations of the 1170 cm^{-1} peak for the non-complementary and complementary target DNA (3 replicate analyses).

As can be seen, the results obtained were disappointing as the discrimination between the complementary and non-complementary target was not as great as desired. However, compared to gold-gold nanoparticle conjugate hybridisations there is an improvement of the enhancement related to the inclusion of the silver nanoparticle conjugate probe. In light of these results, the samples were examined by UV-Vis spectroscopy to ensure that aggregation of the nanoparticles was occurring. The absorbance spectra for the complementary and non-complementary targets are shown in figure 5.5. As can be seen, due to the higher extinction coefficient the silver nanoparticle plasmon band at 410 nm dominates over the gold plasmon band which appears as a shoulder on the silver peak at ~ 520 nm. The spectra reveal that significant aggregation of the system has occurred as evidenced by the dampening and red-shifting of the complementary target peak compared to the non-complementary target. However, it was hypothesised that in this case the combination of the gold and silver nanoparticle conjugates was not effectively generating the "hotspots" needed to provide enough enhancement to increase the SERRS intensity. As such, it was decided to start investigating silver-silver aggregation in order to provide better SERRS enhancement.

Figure 5.5. Extinction spectra of the non-complementary and complementary DNA target SERRS samples from figure 5.4. Red line: complementary target sample, Blue line: non-complementary target sample.

5.2 SERRS Detection of Oligonucleotide-Silver Nanoparticle Conjugates

Silver nanoparticles are typically a more attractive substrate for SERRS analysis than gold nanoparticles due to the larger scattering-to-absorbance ratio of silver compared gold and silver has more polarisable surface electrons than gold nanoparticles. [3] Thiol-modified oligonucleotide-silver nanoparticle conjugates have been successfully employed for the SERRS detection of DNA-mediated assembly. [15] [18] [20] In this work, thioctic acid-modified oligonucleotide-silver nanoparticle conjugate, Ag-P1, were labelled with ROX isothiocyanate (ROXITC) in order to be SERRS active. A study by Mckenzie *et al.* showed that it was not necessary for both probes to be dye labelled as the difference in discrimination between complementary and non-complementary target for both or one labelled conjugate was unchanged. [18] Once the conjugate was prepared, assembly was induced by the addition of 10 nM complementary target to Ag-P1 and Ag-P2 (20 pM each) and analysed using a 532 nm excitation wavelength. This concentration of target was chosen since results obtained in a previous chapter in this work (Chapter 4, figure 4.22) revealed that a concentration of 10 nM target DNA caused the greatest amount of aggregation of the

nanoparticle conjugates. Figure 5.6 displays the SERRS spectra obtained from the DNA-mediated assembly of oligonucleotide-silver nanoparticle conjugate analysed using a 532 nm excitation wavelength. The inset shows the averaged SERRS intensities and standard deviations of the 1647 cm^{-1} peak for the non-complementary and complementary target DNA (3 replicate analyses). Figure 5.7 shows the time-dependence of the SERRS intensity of the complementary and non-complementary target DNA sequences. The spectra were recorded every 10 minutes for 60 minutes. The absorbance spectra for the SERRS analyses are shown in figure 5.8.
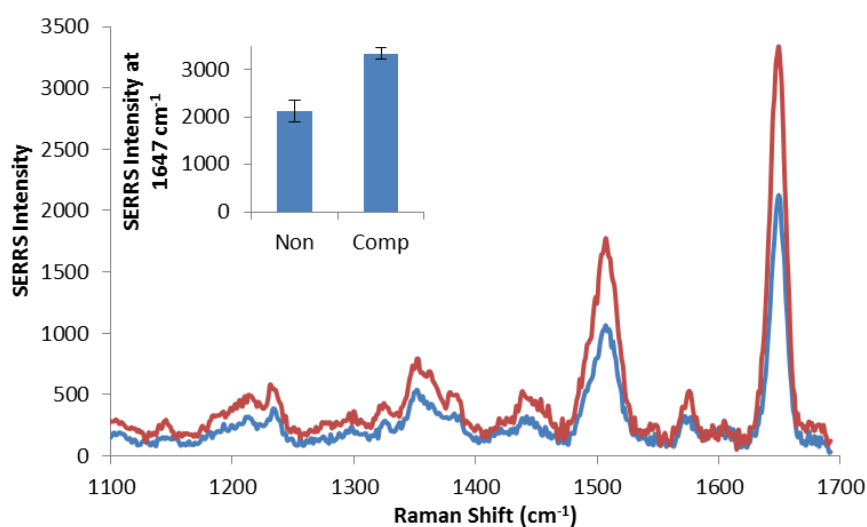
Figure 5.6. SERRS analysis of DNA assembly using ROXITC-labelled oligonucleotide-silver nanoparticle conjugates in a "head-to-tail" orientation at 532 nm excitation wavelength and 10 second scan time. Blue line: non-complementary DNA sequence, Red line: complementary DNA sequence 60 minutes after target addition. Inset: SERRS intensities of the non-complementary and complementary target DNA for the 1647 cm^{-1} peak. Error bars represent the standard deviation from 3 replicate analyses.
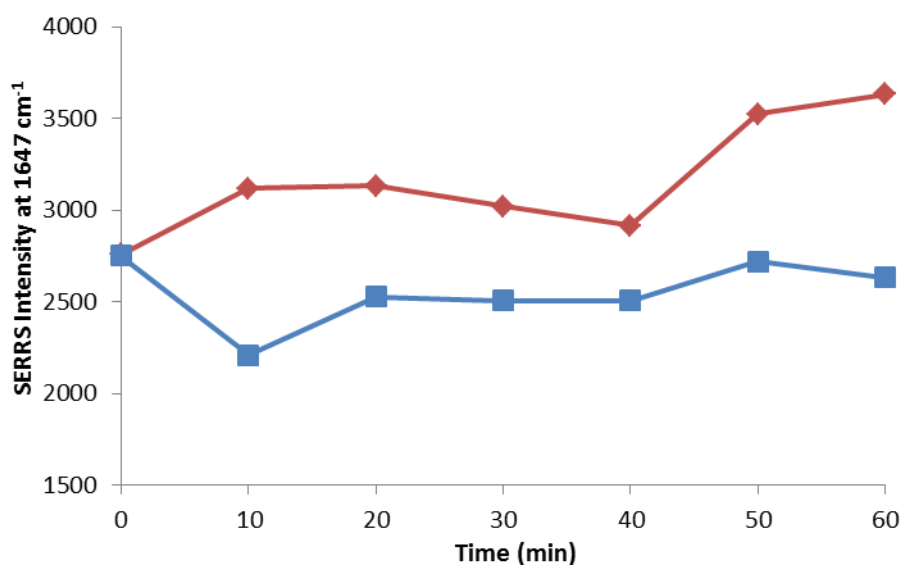
Figure 5.7. SERRS intensity at 1647 cm^{-1} versus time for the ROXITC-labelled oligonucleotide-silver nanoparticle conjugates. Blue line: non-complementary sequence, Red line: complementary sequence. Spectra recorded every 10 minutes over 1 hour.

Similar to the mixed-metal nanoparticle conjugate analysis, the assembly of the silver nanoparticles results in a disappointing enhancement of the SERRS signal. Addition of the complementary sequence results in a steady increase in SERRS intensity over the course of 1 hour while the non-complementary sequence results in a slight decrease in intensity after addition and remains at a steady level of intensity showing no increase intensity above the complementary sequence. As evidenced in figure 5.8, a considerable amount of aggregation of the system has occurred and there is a significant colour change between the complementary and non-complementary samples, however, this has not translated to a considerable increase in the SERRS intensity as was expected. This was possibly due to the interparticle distance. For the above hybridisations, assembly of the nanoparticles was induced in the "head-to-tail" orientation. For the probes used in this work, the distance between the nanoparticles is approximately 10 nm, which has been reported to produce a smaller increase in SERRS intensity compared to shorter interparticle distances. [20]
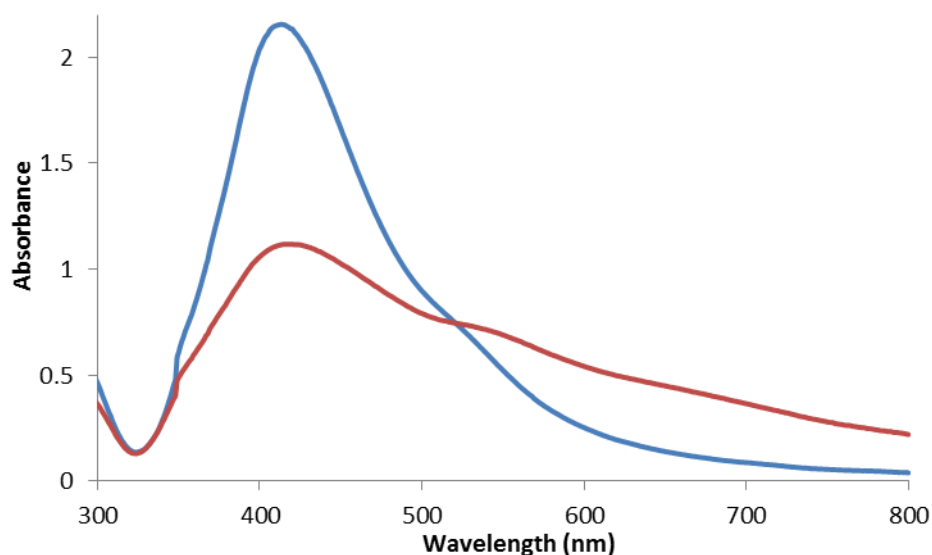
155
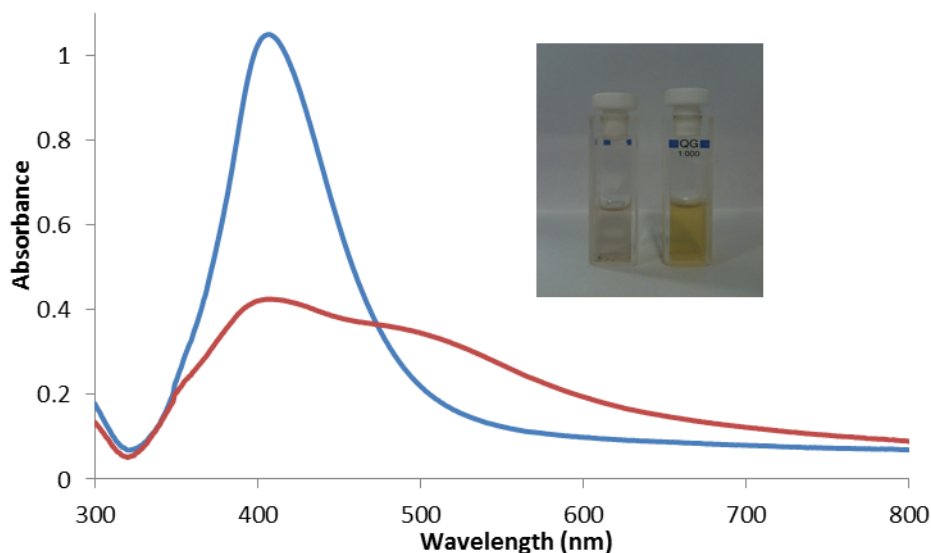
Figure 5.8. Extinction spectra of the non-complementary and complementary DNA target SERRS samples from figure 5.6. Red line: complementary target sample, Blue line: non-complementary target sample. Inset: Visual colour change of the complementary (left) and non-complementary targets (right).

It was discovered that there was a considerable batch-to-batch variability in the observed SERRS signals following assembly. Oligonucleotide-silver nanoparticle conjugates often resulted in low yields so in order to repeat the assay; production of more conjugates was regularly required. Figure 5.9 shows a representative result of an attempted SERRS assembly of the oligonucleotide-silver nanoparticle conjugates using a different batch of conjugates. As can be seen, in this instance, a negligible discrimination between the complementary and non-complementary target sequences was obtained. The same result was obtained for various other batches of oligonucleotide-silver nanoparticle conjugates that were made using the same methods described previously.
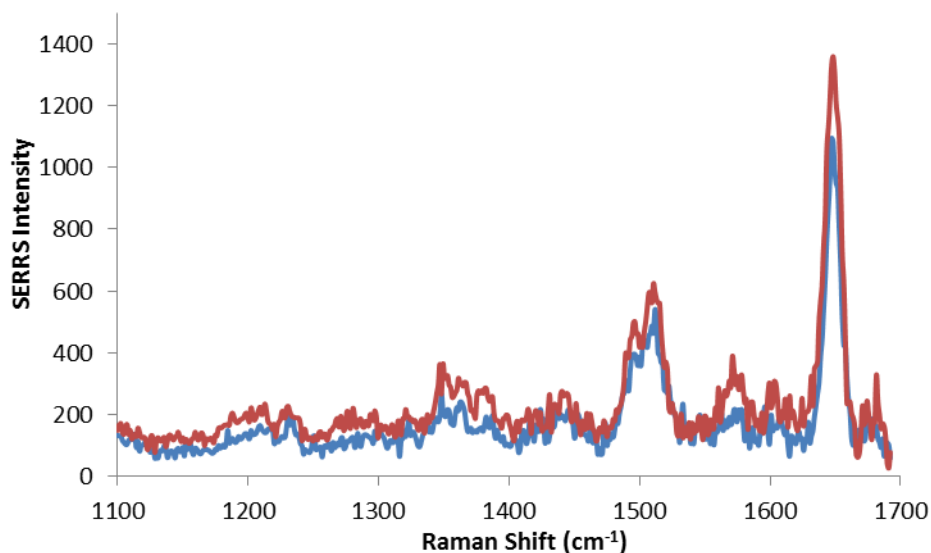
Figure 5.9. Representative example of the SERRS-based assembly of ROXITC-labelled oligonucleotide-nanoparticle conjugates using different batches of the conjugates. Blue line: non-complementary sequence, Red line: complementary sequence.

The assembly process was repeated with TAMRA isothiocyanate-labelled (TRITC) oligonucleotide nanoparticle conjugates, however, similar to the ROXITC labelled conjugates, the TRITC labelled conjugates displayed negligible discrimination between the complementary and non-complementary target sequence. As it was hypothesised that the interparticle distance was too great for effective coupling of the nanoparticles, it was decided to test if the SERRS could be effectively switched "on" by irreversible, non-specific aggregation of the nanoparticle conjugates. To do this, an aliquot of 1 M $MgSO_4$ was added to the conjugate solution to induce indiscriminate, irreversible aggregation. This resulted in a considerable increase in the SERRS intensity which is attributed to the nanoparticles coming in to close proximity to one another during aggregation to facilitate "hotspot" formation that is no long driven and therefore affected by interparticle DNA hybridisation. The SERRS spectrum for the addition of $MgSO_4$ to the oligonucleotide-nanoparticle conjugates is shown in figure 5.10. The inset shows the averaged SERRS intensities and standard deviations of the 1647 cm^{-1} peak for the non-complementary and complementary target DNA (5 replicate analyses). This result showed that by

reducing the distance between the nanoparticles during hybridisation, a stronger enhancement of the SERRS signal could be obtained.
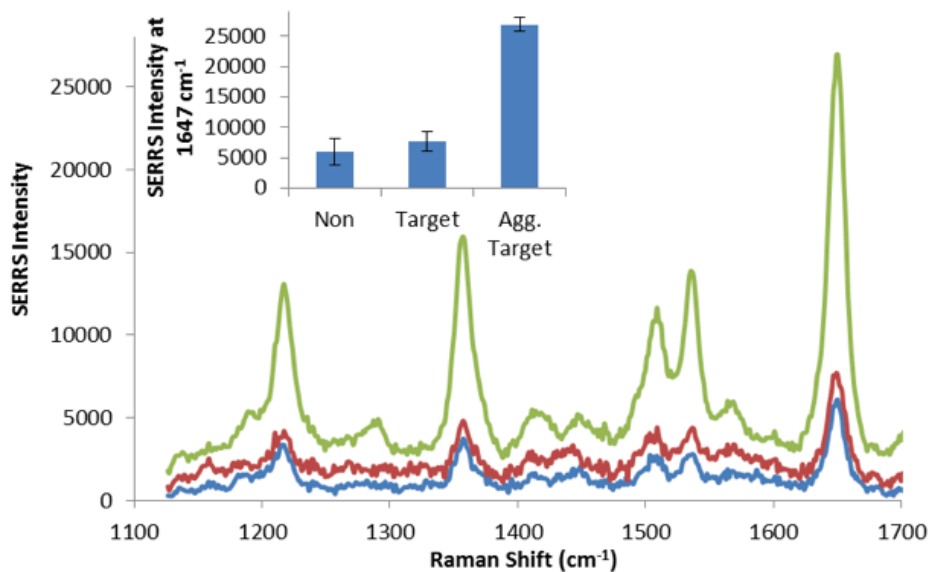
Figure 5.10. SERRS spectra of assembled TRITC-labelled oligonucleotide-silver nanoparticle conjugates using a 532 nm excitation wavelength. Blue line: non-complementary sequence, Red line: complementary sequence 60 minutes after addition and Green line: complementary sequence conjugates aggregated with 1 M MgSO₄. Inset: SERRS intensities of the non-complementary and complementary target DNA for the 1647 cm⁻¹ peak. Error bars represent the standard deviation from 5 replicate analyses.

As discussed in Chapter 4, hybridisation of the oligonucleotide-silver nanoparticle conjugates in the "head-to-head" orientation was initially met with some difficulty. The "head-to-head" orientation results in no interparticle distance during hybridisation. This has been shown to generate strong SERRS intensities compared to longer interparticle distances. [20] Figure 5.11 shows an initial attempt at the SERRS-based assembly of the silver nanoparticle conjugates in a "head-to-head" orientation. Assembly was induced by the addition of complementary DNA target (10 nM) to ROXITC-labelled Ag-P1 and Ag-P3 (20 pM each) and analysed at a 532 nm excitation wavelength. As can be seen, a negligible difference in the SERRS intensities of the complementary (red line) and non-complementary (blue line) was obtained. However, this was attributed to interparticle repulsion of the conjugates

due to the more densely packed surface of thioctic acid-modified oligonucleotides which results in a strong electrostatic barrier to hybridisation when the conjugates are trying to come into close proximity in the "head-to-head" orientation.
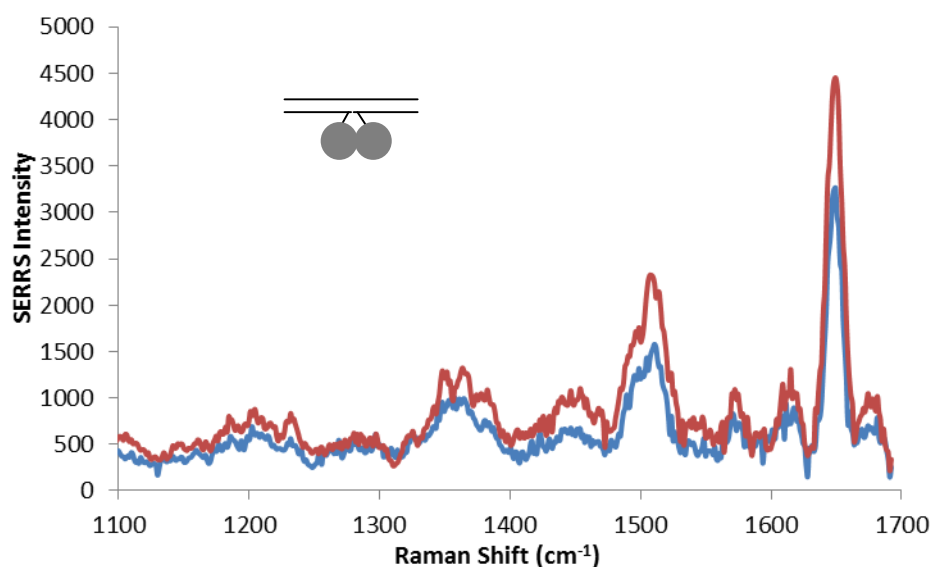
Figure 5.11. SERRS analysis of DNA assembly using ROXITC-labelled oligonucleotide-silver nanoparticle conjugates in a "head-to-head" orientation at 532 nm excitation wavelength and 10 second scan time. Blue line: non-complementary DNA sequence, Red line: complementary DNA sequence 60 minutes after target addition.

When it was concluded from Chapter 4 that co-adsorption of non-recognition sequences (T_{10}) and the recognition sequence (P1 and P2) on to the nanoparticle surface resulted in successful aggregation of the nanoparticle conjugates, in "head-to-head" format, the SERRS analysis of these conjugates was investigated. FAMITC was used in this portion of the study as it is negatively charged so it was thought that it would not irreversibly aggregate the colloid *via* electrostatic interactions (structure shown in figure 5.12).
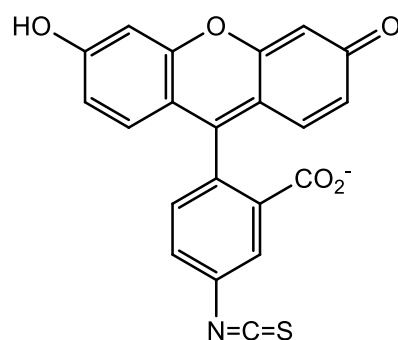
Figure 5.12. Chemical structure of FAM isothiocyanate (-N=C=S). Note negative charge on the carboxyl group.

Figure 5.13 shows the SERRS-based assembly of the 0.6 recognition sequence: T_{10} sequence molar ratio achieved by adding 2 nM complementary target to FAMITC-labelled Ag-P1 and Ag-P3 (20 pM each). The inset shows the averaged SERRS intensities and standard deviations of the 1321 cm^{-1} peak for the non-complementary and complementary target DNA (3 replicate analyses). As can be seen, the co-adsorption of T_{10} sequences with the recognition sequence on the nanoparticle surface generated an increase in the SERRS intensity once hybridisation had taken place. However, while this was a promising early result, issues of conjugate stability and batch-to-batch reproducibility made it difficult to repeat the assay. The dye-addition step proved to be capricious as irreversible aggregation was often observed after centrifugation.
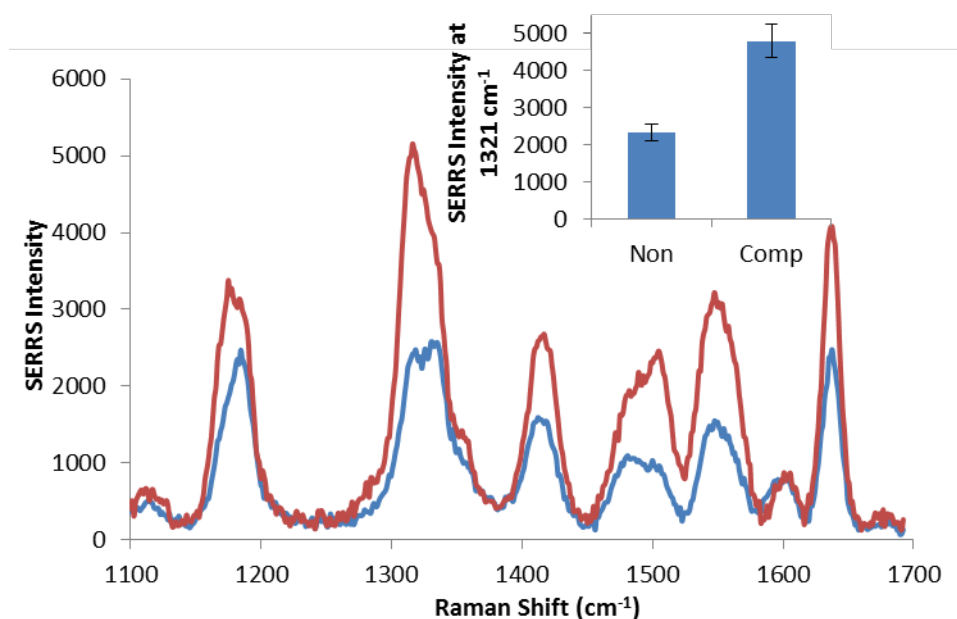
Figure 5.13. SERRS analysis of DNA assembly using FAMITC-labelled oligonucleotide-silver nanoparticle conjugates with a 0.6 recognition sequence: T_{10} sequence molar ratio at 532 nm excitation wavelength and 10 second scan time. Blue line: non-complementary DNA sequence, Red line: complementary DNA sequence 60 minutes after target addition. Inset: SERRS intensities of the non-complementary and complementary target DNA for the 1321 cm^{-1} peak. Error bars represent the standard deviation from 3 replicate analyses.

Attempts were made to analyse the 0.8 and 0.4 recognition sequence: T_{10} sequence molar ratios, however, very little SERRS signal was observed for these samples. A representative example of the attempted assembly of the 0.4 recognition sequence: T_{10} sequence molar ratio conjugates is displayed in figure 5.14. The spectra show that there is no observable difference in the SERRS intensities between the complementary and non-complementary target DNA sequences. While no enhancement of the SERRS was observed for these samples, it should be noted that a visible colour change from yellow to orange-brown in the complementary sequence was consistently observed indicating hybridisation, and therefore aggregation, had occurred.
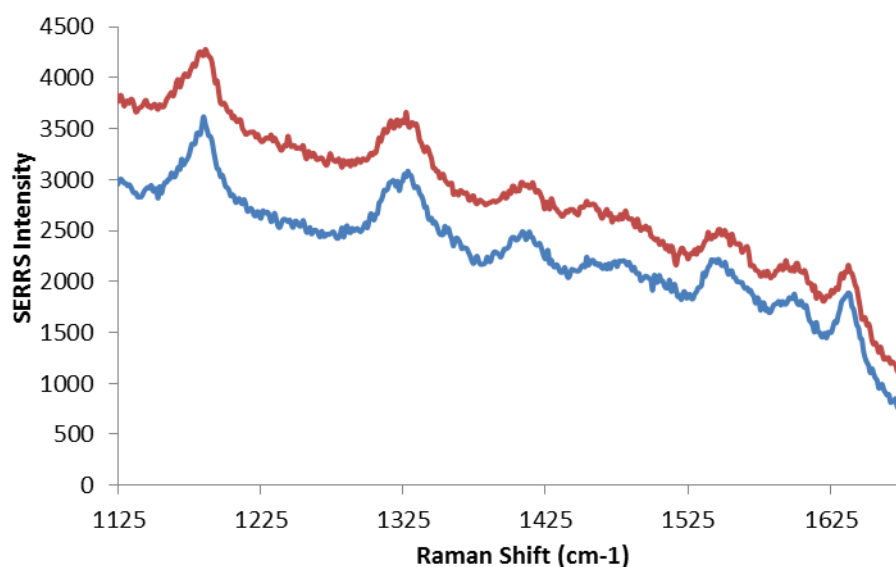
Figure 5.14. Representative SERRS analysis of the 0.4 recognition sequence: T_{10} sequence molar ratio oligonucleotide-silver nanoparticle conjugates analysed using a 532 nm excitation wavelength. Other molar ratio conjugates displayed similar results. Blue line: non-complementary DNA sequence, Red line: complementary DNA sequence 60 minutes after target addition.

The reason for the differences in SERRS activity between batches is unknown; so it was decided to investigate a different route to conjugate preparation. To investigate this hypothesis, subsequent conjugate preparations steps reverted back to the methods outlined by Graham *et al.* whereby the dye molecule was added to the nanoparticles pre-oligonucleotide functionalisation. [15] An attempt was made at preparing the silver nanoparticle conjugates by first adding 1 μM FAMITC to 1 ml of the bare nanoparticle solutions followed by the addition of the thioctic acid-modified oligonucleotides. Adopting this procedure resulted in a stable dye-labelled oligonucleotide-silver nanoparticle conjugate that was subsequently used for the SERRS-based assembly. As it was known that "head-to-head" hybridisations did not occur with conjugates functionalised with only recognition probe sequences on the nanoparticle surface, this new conjugate was used in conjugation with the Ag-P3 probe with a molar ratio of 0.6. However, it was discovered that this new method did not improve the SERRS results, with spectra obtained displaying similar results to that previously observed. A representative example of the attempted assembly using the FAM-labelled oligonucleotide-silver nanoparticle conjugates is shown in figure

5.15. As can be seen, no observable discrimination in the SERRS intensities between the complementary (red line) and non-complementary (blue line) targets was observed.
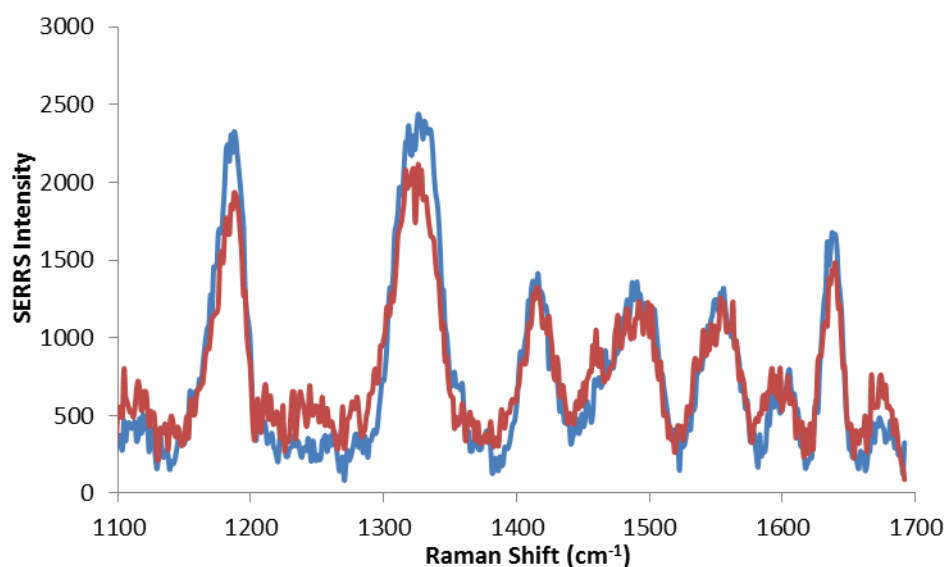
Figure 5.15. Representative SERRS analysis of the nanoparticle conjugates labelled with FAMITC pre-oligonucleotide functionalisation analysed using a 532 nm excitation wavelength. Blue line: non-complementary DNA sequence, Red line: complementary DNA sequence 60 minutes after target addition.

5.3 Conclusions

Dye-labelled oligonucleotide gold and silver nanoparticle conjugates were investigated for their use as SERRS-based sensors for DNA hybridisation. The procedure involved the "switching on" of the SERRS signal upon addition of a complementary DNA target sequence. However, the results obtained showed variable results in terms of the SERRS activity observed.

It was first attempted to assemble oligonucleotide-gold nanoparticle conjugates with MGITC, which resulted in no observable discrimination between the complementary and non-complementary target sequence, which was attributed to the small size of the gold nanoparticles. A further attempt was made, this time using a gold nanoparticle conjugate labelled with MGITC and a silver nanoparticle conjugate.

This method resulted in an observable discrimination between the complementary and non-complementary targets but the discrimination needs to be improved to be applicable to "real world" samples.

Oligonucleotide-silver nanoparticle conjugates labelled with ROXITC were assembled *via* DNA hybridisation and analysed by SERRS. Again, an observable discrimination between the complementary and non-complementary target sequences was observed but the difference between the "off" to "on" SERRS signals was not great. This was attributed to the larger interparticle distance inherent in the "head-to-tail" orientation that was too great to effectively generate the necessary "hotspots" for SERRS enhancement.

To this end, attempts were made to obtain SERRS analyses in the "head-to-head" orientation by co-adsorbing T_{10} sequences with the recognition sequence to the nanoparticle surface. This resulted in an observable discrimination in the SERRS intensities of the complementary and non-complementary targets, however, the other attempts at utilizing these probes for SERRS analysis was met with difficulty due to the poor yields of the conjugates and batch-to-batch variability in the SERRS signals.

It is unknown why the SERRS detection met with such variable results, however, for future work an investigation in reducing the background signal from the non-complementary samples could be an important step possibly leading to improved discrimination between the complementary and non-complementary DNA targets.

5.4 References

1.   K. Faulds, R. P. Barbagallo, J. T. Keer, W. E. Smith and D. Graham, *Analyst*, 2004, **129**, 567-568.
2.   K. Faulds, W. E. Smith and D. Graham, *Anal. Chem.*, 2004, **76**, 412-417.
3.   R. J. Stokes, A. Macaskill, P. J. Lundahl, W. E. Smith, K. Faulds and D. Graham, *Small*, 2007, **3**, 1593-1601.
4.   K. Faulds, R. Jarvis, W. E. Smith, D. Graham and R. Goodacre, *Analyst*, 2008, **133**, 1505-1512.
5.   MacAskill, D. Crawford, D. Graham and K. Faulds, *Anal. Chem.*, 2009, **81**, 8134-8140.

6.   J. A. Dougan, D. MacRae, D. Graham and K. Faulds, *Chem. Commun.*, 2011, **47**, 4649-4651.

7.   D. van Lierop, K. Faulds and D. Graham, *Anal. Chem.*, 2011, **83**, 5817-5821.

8.   M. M. Harper, J. A. Dougan, N. C. Shand, D. Graham and K. Faulds, *Analyst*, 2012, **137**, 2063-2068.

9.   E. Hao and G. C. Schatz, *J. Phys. Chem.*, 2004, **120**, 357-366.

10.   S. M. Nie and S. R. Emery, *Science*, 1997, **275**, 1102-1106.

11.   K. Kneipp, Y. Wang, H. Kneipp, L. T. Perelman, I. Itzkan, R. Dasari and M. S. Feld, *Phys. Rev. Lett.*, 1997, **78**, 1667-1670.

12.   J. A. Dougan, *Modified Oligonucleotides for the Functionalisation of Nanoscale Materials,* 2009, University of Strathclyde: Glasgow.

13.   C. A. Mirkin, R. L. Letsinger, R. C. Mucic and J. J. Storhoff, *Nature*, 1996, **382**, 607-609.

14.   A. P. Alivisatos, K. P. Johnsson, X. G. Peng, T. E. Wilson, C. J. Loweth, M. P. Bruchez and P. G. Schultz, *Nature*, 1996, **382**, 609-611.

15.   D. Graham, D. G. Thompson, W. E. Smith and K. Faulds, *Nat. Nanotechnol.*, 2008, **3**, 548-551.

16.   D. G. Thompson, K. Faulds, W. E. Smith and D. Graham, *J. Phys. Chem. C*, 2010, **114**, 7384-7389.

17.   X. M. Qian, X. Zhou and S. M. Nie, *J. Am. Chem. Soc.*, 2008, **130**, 14934-14935.

18.   F. McKenzie and D. Graham, *Chem. Commun.*, 2009, 5757-5759.

19.   F. McKenzie, K. Faulds and D. Graham, *Nanoscale*, 2010, **2**, 78-80.

20.   L. Guerrini, F. McKenzie, A. W. Wark, K. Faulds and D. Graham, *Chem. Sci.*, 2012, **3**, 2262-2269.

21.   W. E. Doering and S. Nie, *Anal. Chem.*, 2003, **75**, 6171-6176.

22.   X. Qian, S. R. Emory and S. Nie, *J. Am. Chem. Soc.*, 2012, **134**, 2000-2003.

23.   D. G. Thompson, R. J. Stokes, R. W. Martin, R. J. Lundahl, K. Faulds and D. Graham, *Small*, 2008, **4**, 1054-1057.

24.   Z. H. Zhu, T. Zhu and Z. F. Liu, *Nanotechnology*, 2004, **15**, 357-364.

6 Oligonucleotide-Nanoparticle Conjugate Characterisation Using Fluorescent DNA Intercalator

In order to be effective sensors for SERRS detection of DNA, oligonucleotide-nanoparticle conjugates must hybridise to the complementary sequence in order to provide enough enhancement to increase the SERRS intensity. However, difficulties were experienced when attempting to "switch on" the SERRS effect by hybridisation-induced aggregation of the nanoparticles. As an alternative, it was decided to investigate metal enhanced fluorescence and whether this would be more successful. Furthermore, it was recognised that the investigations could also reveal information about the hybridisation efficiency of the oligonucleotide-nanoparticle conjugates that could be applied to develop their use as SERRS biosensors. It was thought that a method that incorporates a fluorescent DNA intercalator into the oligonucleotide-nanoparticle conjugates could provide such insight into the characteristics of DNA hybridisation on the surface of the oligonucleotide-nanoparticle conjugates.

Fluorescent DNA intercalators, such as SYBR green I, [1] ethidium bromide [2] or YO-PRO-1, [3] are commonly employed in molecular biology to detect and quantify double-stranded DNA (dsDNA) in techniques such as gel electrophoresis and real-time PCR. DNA intercalators exhibit minimal fluorescence in the presence of single-stranded DNA (ssDNA) and produce significant fluorescence when intercalated to dsDNA. In PCR, intercalators are used to monitor reaction progress in real-time – a fluorescence measurement is taken after each PCR cycle with successful amplification indicated by an increase in fluorescence above a threshold value since amplification results in the production of dsDNA. [1]
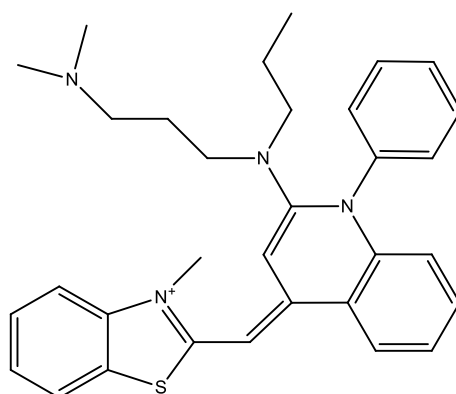
Figure 6.8. Structure of SYBR green I – a DNA intercalator.

SYBR green I belongs to the cyanine family of dyes (structure shown in figure 6.1). In a study performed by Zipper *et al.* SYBR green I was shown to preferentially intercalate to dsDNA *via* the stacked base-pairs at the centre of the double helix. [4] It was reported that SYBR green I has a secondary binding mode at high dye-base-pair ratios (dbprs) showing interactions with the minor groove of the dsDNA. In addition, at high dbprs SYBR green I was shown to have a significant preference for A-T base-pair rich sequences. Figure 6.2 shows a typical PCR amplification plot using SYBR green I to assess reaction progress.
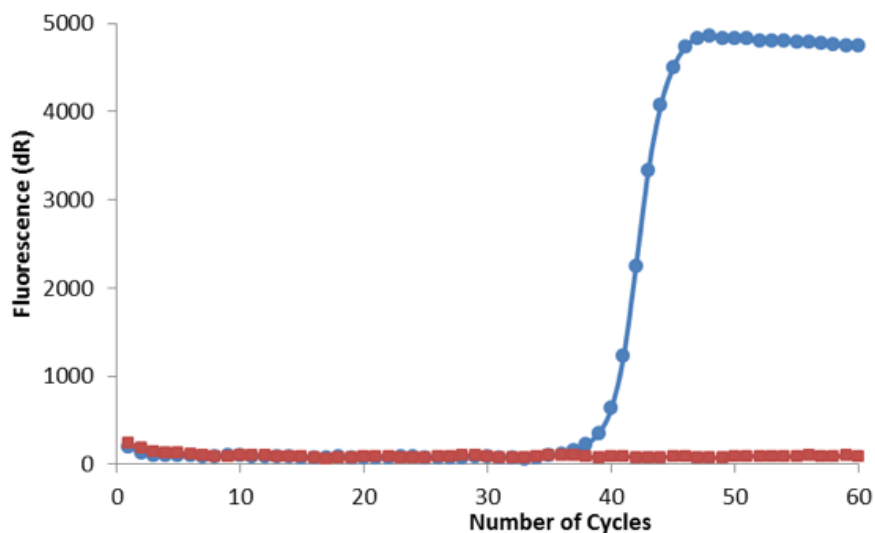
Figure 6.9. Amplification plot from PCR of MRSA using SYBR green I to monitor reaction progress. Blue line represents PCR using positive MRSA sample indicating successful amplification and red line represents PCR using a negative sample of MRSA indicating no amplification of the product.

167

In recent years, to improve the sensitivity of fluorescence-based detection and quantification of DNA hybridisation, metal enhanced fluorescence (MEF) has been employed. MEF arises from near-field interactions of the excited-state fluorophore with the surface plasmon resonance on the metal nanoparticle surface generated by incident light. [5] [6] The MEF effect has been known to increase the fluorescence quantum yield at the cost of fluorescence lifetime but increases brightness and photostability. [7] The resulting enhancement is controlled by a number of factors, including, the nanoparticle shape, size and composition, [8] emission wavelength [9] and distance between the fluorophore and the nanoparticle surface. [10]

MEF has been employed in various biomedical applications, including protein, [11] cell, [12] RNA [13] and DNA detection. [14] Dragan *et al.* have reported the use of silver nanoparticles immobilized on a glass slide (silver island films, SiFs) to enhance fluorescence detection of DNA sequences intercalated with Pico Green, a fluorescent probe, [15] [16] and ethidium bromide, a common dsDNA stain. [17] A similar study, reported by Zhang *et al.*, showed the fluorescence enhancement achieved from a DNA-bound YOYO intercalator between sliver nanoparticles. [18] These studies have demonstrated the ability of MEF to be coupled with fluorescent DNA intercalators for the detection of DNA using silver nanoparticles.

In this chapter, thioctic acid-modified oligonucleotide gold and silver nanoparticle conjugates were assembled *via* DNA hybridisation in a similar fashion to that previously reported (see Chapter 4). Once the nanoparticle conjugates were assembled, SYBR green I was added to bind to the dsDNA between the nanoparticle conjugates and the fluorescence characteristics were investigated (figure 6.3).
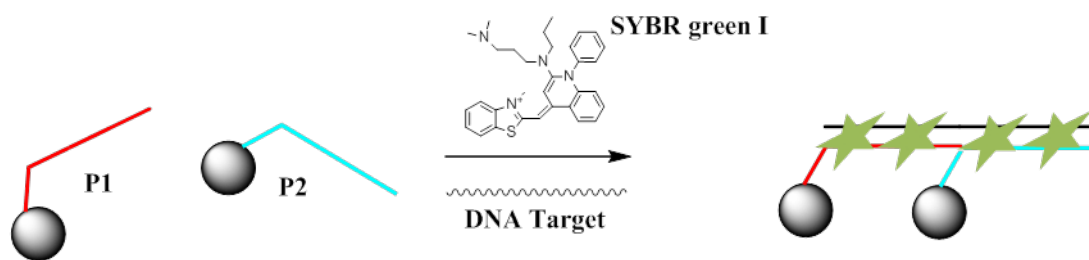
Figure 6.3. Representation of hybridisation-induced aggregation of oligonucleotide-nanoparticle conjugates. Once hybridisation has occurred, SYBR green I was added to bind to dsDNA between nanoparticles (green stars).

Both gold and silver nanoparticles were functionalised with thioctic acid-modified oligonucleotides containing three HEG units as a spacer group (P1 and P2, see Chapter 3).   The HEG units function to distance the recognition sequence, which the SYBR green I will be intercalating, from the nanoparticle surface since it is reported in the literature that fluorescence is quenched at distances shorter than approximately 5 nm from the nanoparticle surface, while a progressive increase in enhancement of fluorescence is known to occur up to a maximum of 8-10 nm from the nanoparticle surface. [5] [19] Gold nanoparticles of ~ 45 nm were prepared *via* a seeded growth method using gold nanoparticles of ~ 15 nm diameter as the seed. [20] [21] Silver nanoparticles were prepared using the citrate-reduction method reported by Lee and Meisel. [22] Functionalisation of both gold and silver nanoparticles was achieved using methods outlined in a previous chapter (see Chapter 3).

Assembly of the gold and silver nanoparticles was achieved by addition of a complementary target (P1P2 comp) to the two oligonucleotide-nanoparticle conjugate probes (Au-P1 and Au-P2, Ag-P1 and Ag-P2). The concentration of complementary target DNA was chosen to be 3 and 5 nM for gold and silver nanoparticle conjugate probes, respectively. This was to ensure that extended aggregation of the nanoparticles would occur upon hybridisation of the DNA. The absorbance spectra for the hybridisation-induced aggregation of the oligonucleotide-nanoparticle conjugates are shown in figures 6.4 and 6.5 for gold nanoparticles and silver nanoparticles, respectively.
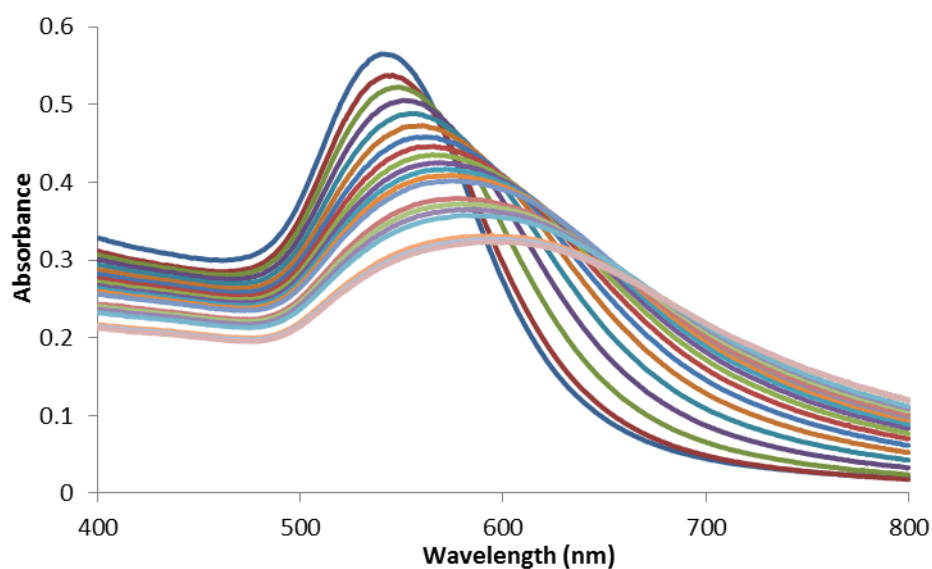
Figure 6.4. Hybridisation-induced aggregation of thioctic acid-modified oligonucleotide-gold nanoparticle conjugates (Au-P1 and Au-P2) using P1P2 comp. [Conjugates] = 30 pM, [Target] = 5 nM.
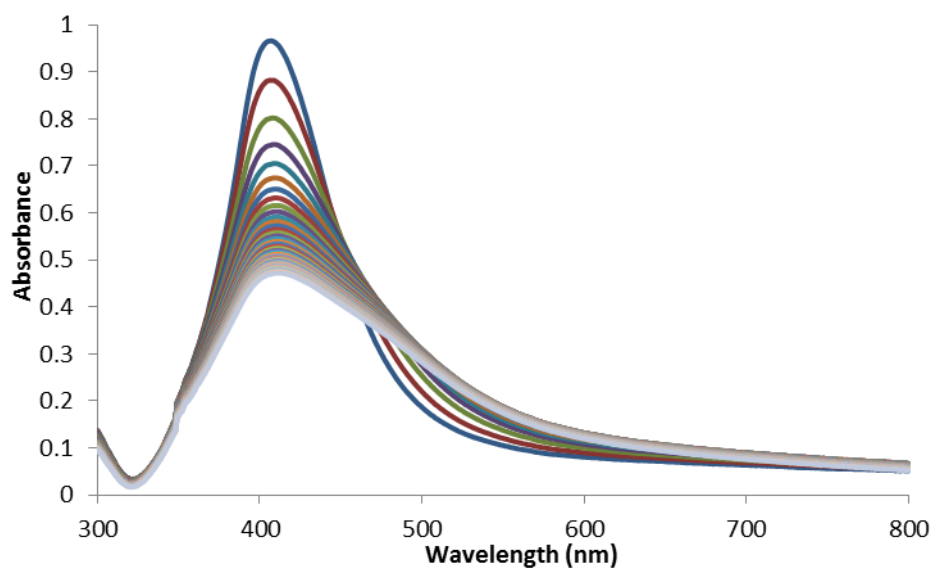
Figure 6.5. Hybridisation-induced aggregation of thioctic acid-modified oligonucleotide-silver nanoparticle conjugates (Ag-P1 and Ag-P2) using P1P2 comp. [Conjugates] = 30 pM, [Target] = 5 nM.
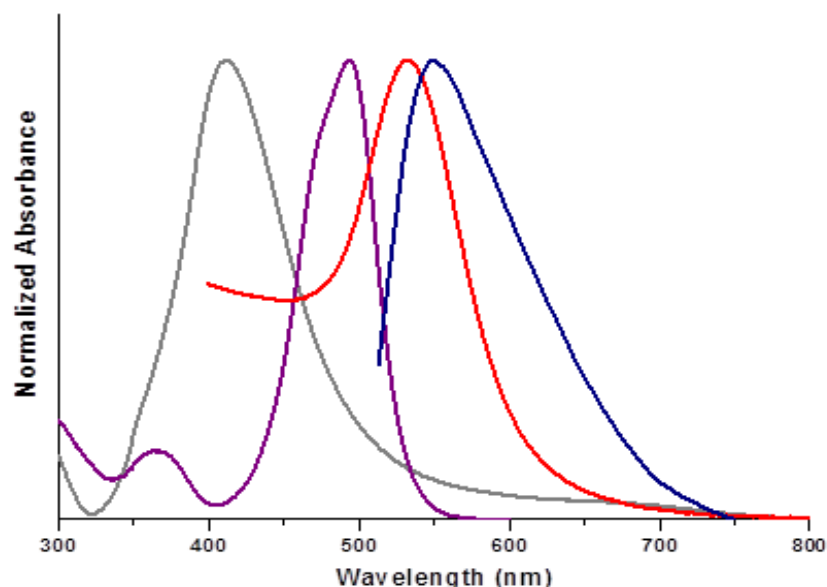
Figure 6.6. Normalized absorbance spectra of silver nanoparticle conjugates (410 nm, grey line)), gold nanoparticle conjugates (530 nm, red line), SYBR green I absorbance (495 nm, purple line) and SYBR green I emission (560 nm, blue line) measured in aqueous solutions.

Figure 6.6 shows the absorbance spectra of the gold and silver nanoparticle conjugates (λ_{max} 530 nm and 410 nm, respectively) together with the absorption and emission spectra of SYBR green I. SYBR green I has an absorbance maximum at ~ 495 nm and emits light at longer wavelengths, with a maximum at ~ 560 nm.

6.1 Quenching and Enhancement of SYBR green I Fluorescence Using Oligonucleotide-Nanoparticle Conjugates

Once aggregation was completed, SYBR green I was added to the solution (dbpr = 1) in order to bind to the dsDNA between nanoparticles. The dye will then be localised at the nanoparticle "hotspots" – areas of high electromagnetic intensity arising from the coupling of the surface plasmon resonances of adjacent nanoparticles during hybridisation. As a consequence, near-field interactions of the excited-state fluorophore with the surface plasmon resonances of the nanoparticles alter the fluorescence response, resulting in enhancement or quenching of the fluorescence

response. Figure 6.7 shows the fluorescence intensities of the oligonucleotide gold and silver nanoparticle probes and the oligonucleotides in the absence of gold and silver nanoparticles. As can be seen, the resulting enhancement or quenching of the fluorescence signal was dependent on the composition of the nanoparticle used and whether the nanoparticles were aggregated *via* DNA hybridisation. For all fluorescence intensities obtained, they were compared to the signal observed for single-stranded target DNA in the presence of SYBR green I (SG + ssDNA, purple bar).
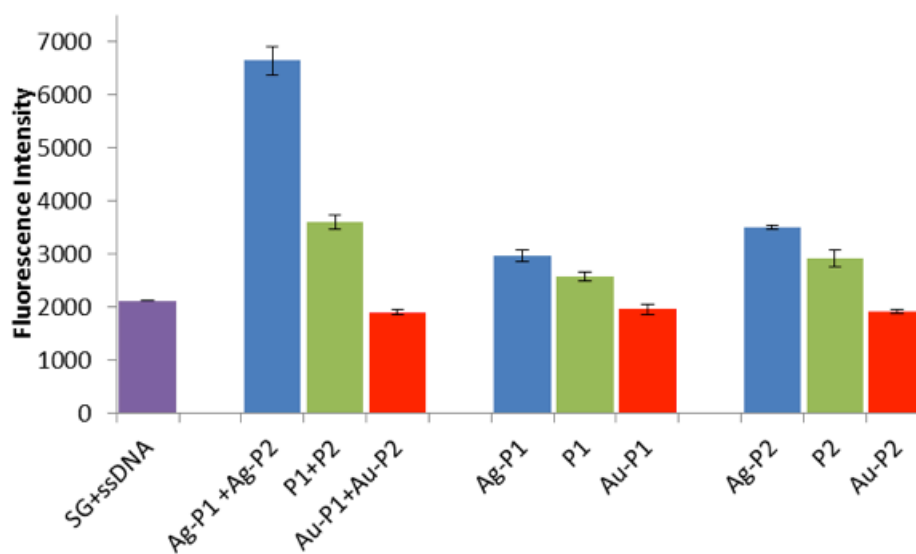
Figure 6.7. Fluorescence intensities obtained after the addition of complementary target DNA and SYBR green I. Blue bars represent intensities obtained for silver nanoparticle conjugate, red bars represent intensities obtained for gold nanoparticle conjugates, green bars represent intensities obtained for unbound oligonucleotides and the purple bar represents fluorescence intensity obtained from target ssDNA in the presence of SYBR green I. For all hybridisation experiments the dbpr was 1. Error bars represent the standard deviation from 2 replicate analyses.

The fluorescence response from SYBR green I and ssDNA arises from partial stacking with adjacent bases and hydrophobic interactions. [23] Fluorescence intensities obtained from unbound oligonucleotides in solution were performed in equimolar concentrations of probes and complementary target DNA (5 nM). Examination of figure 6.7 reveals that, for oligonucleotide-silver nanoparticle

conjugates, addition of the complementary target DNA to the monodispersed nanoparticles results in an enhancement of the fluorescence response when compared to the same unbound oligonucleotides (Ag-P1 *versus* P1 and Ag-P2 *versus* P2), however, when the nanoparticle conjugates are aggregated *via* DNA hybridisation-induced assembly, the enhancement of the fluorescence signal is significantly increased compared to the hybridised, unbound oligonucleotide probes (Ag-P1 + Ag-P2 *versus* P1 + P2). This signal enhancement is a result of high electric field intensity at the junctions between nanoparticles due to plasmon coupling. [24]

There also appears to be sequence specificity for SYBR green I fluorescence. Examination of the fluorescence intensities of Ag-P1 and P1 *versus* Ag-P2 and P2 reveal that there is slight sequence specificity in favour of P2, with the fluorescence intensities being consistently higher for P2 compared to P1, both functionalised to the nanoparticles surface and unbound. This sequence-specificity has been observed for SYBR green I and is attributed to the existence of minor groove binding when the dbpr is greater than 0.2.

In contrast, oligonucleotide-gold nanoparticle conjugates exhibit quenching of the fluorescence intensities, with the signals obtained being approximately equal to or slightly less than that observed for target DNA in the presence of SYBR green I (Au-P1 + Au-P2, Au-P1 and Au-P2 *versus* SG + ssDNA). As reported in the literature, gold nanoparticles are known to be effective quenchers of fluorescence unless longer wavelength fluorophores are employed. [25] In this instance, however, the emission of SYBR green I overlaps significantly with the surface plasmon band of gold nanoparticles (see figure 6.6) hence the requirement for longer wavelength fluorophores when employing gold nanoparticles.

6.2 Fluorescence Melting Profiles of SYBR Green I Using Oligonucleotide-Nanoparticle Conjugates

Melting curves of oligonucleotide-nanoparticle conjugates are typically monitored at the λ_{max} of the surface plasmon resonance peak of the nanoparticles investigated, *i.e.* ~ 410 nm for silver nanoparticle conjugates and ~520 nm for gold nanoparticle conjugates. When the conjugates are hybridised to complementary target DNA, the

surface plasmon resonance peak absorbance is dampened due to aggregation of the nanoparticles, however, by heating the conjugates past the melting temperature of the duplex DNA, thereby disrupting the base-pairing between complementary DNA strands, the duplex denatures and the nanoparticles return to a monodispersed state and the surface plasmon resonance peak absorbance increases. Figures 6.8 and 6.9 show melting curves obtained for gold and silver oligonucleotide-nanoparticle conjugates. The melting curves were obtained using the same experimental conditions as in figures 6.4 and 6.5 for gold and silver nanoparticles, respectively.
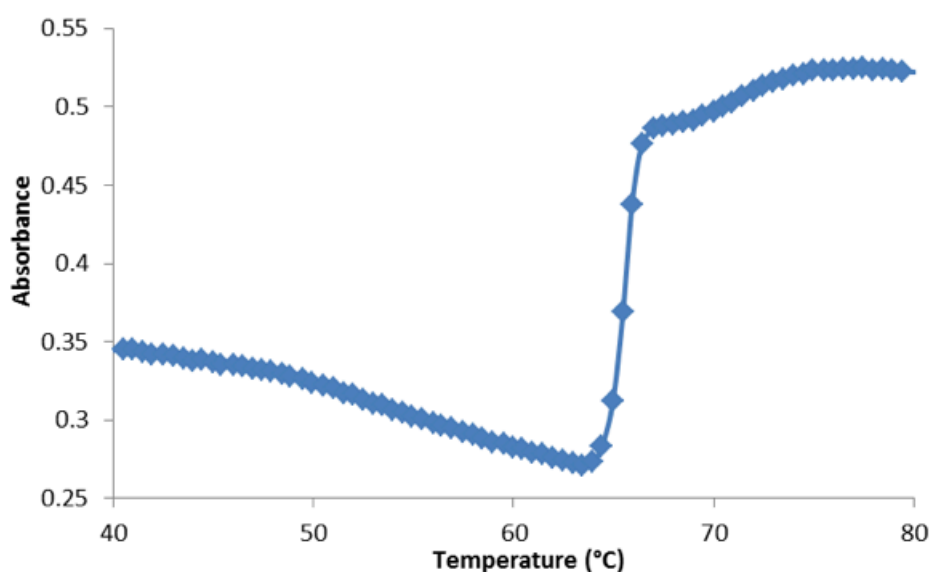
Figure 6.8.   Melting curve obtained from hybridisation of oligonucleotide-gold nanoparticle conjugates monitored at 530 nm. Melting temperature obtained was 65 °C. [Conjugates] = 30 pM, [Target] = 3 nM with a heat/ cool rate of °C/ minute.

174
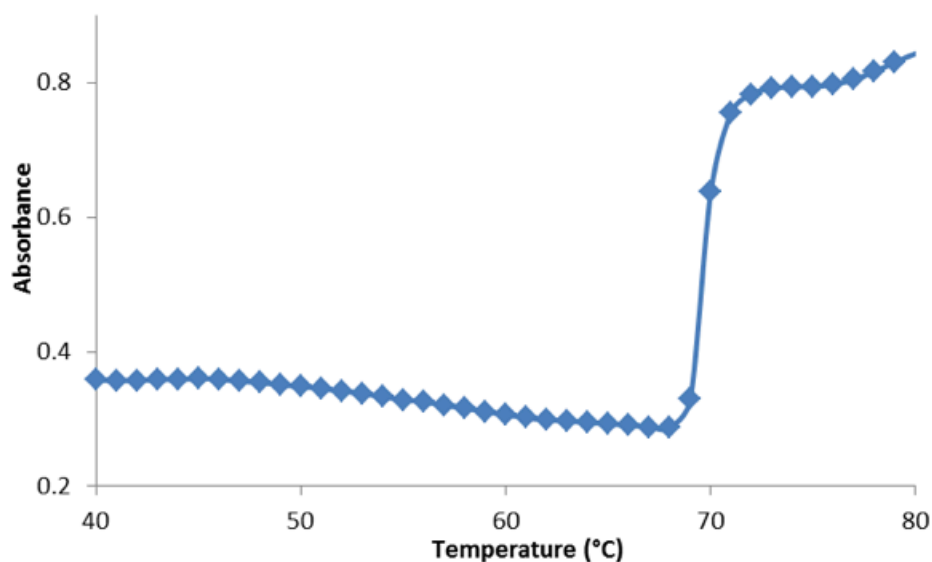
Figure 6.9. Melting curve obtained from hybridisation of oligonucleotide-silver nanoparticle conjugates monitored at 410 nm. Melting temperature obtained was 70 °C. [Conjugates] = 30 pM, [Target] =5 nM with a heat/ cool rate of 0.5 °C/ minute.

In order to investigate the fluorescence melting profiles, SYBR green I was added to hybridised solutions of gold and silver oligonucleotide-nanoparticle conjugates and the conjugates transferred to a PCR thermocycler to perform the temperature ramping. In addition to the nanoparticle/ SYBR green I conjugates, unbound oligonucleotides hybridised to form duplex DNA with SYBR green I were also added to the thermocycler. Figure 6.10 shows the SYBR green I fluorescence melting profiles of Ag-P1 + Ag-P2, Ag-P1 and Ag-P2. The conjugates were mixed at a concentration of 30 pM with a target DNA concentration of 5 nM and dbpr of 1. The melting curves are displayed as the negative derivative of the fluorescence *versus* temperature for ease of identifying the melting temperature for each conjugate. The melting temperatures of Ag-P1, Ag-P2 and Ag-P1 + Ag-P2 were 60, 65 and 70 °C, respectively. The corresponding SYBR green I melting curves for the unbound oligonucleotides were also obtained. The first derivative melting curves for P1, P2 and P1 + P2 are displayed in figure 6.11. Each probe was used in equimolar ([P1] = [P2] = [P1 + P2]) concentrations at 5 nM with a dbpr of 1. The melting temperatures obtained for P1, P2 and P1 + P2 were 63, 66 and 66 °C, respectively.
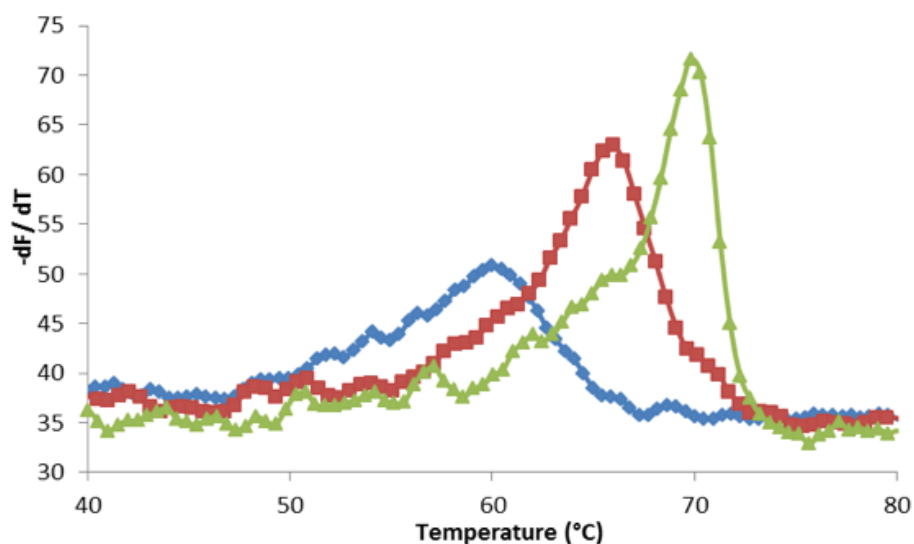
Figure 6.10. SYBR green I melting curves obtained from oligonucleotide-silver nanoparticle conjugates in the presence of complementary target DNA. Curves are displayed as the negative derivative of fluorescence for ease of identifying the melting temperature of the conjugates. Dbpr = 1. Blue line: Ag-P1, 60 °C; Red line: Ag-P2, 65 °C; Green line: Ag-P1 + Ag-P2, 70 °C. [Conjugtes = 30 pM], [Target = 5 nM].
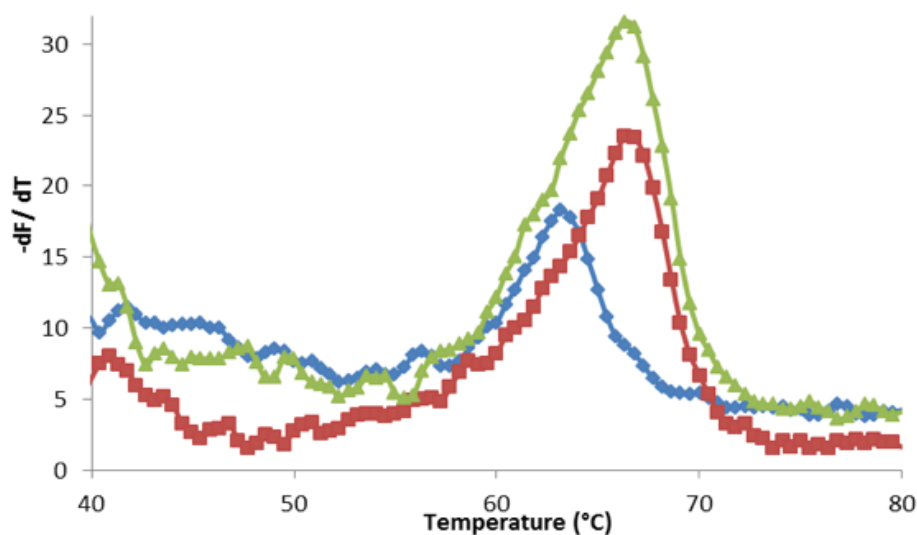
Figure 6.11. SYBR green I melting curves obtained from unbound oligonucleotides. Curves are displayed as the negative derivative of fluorescence for ease of identifying the melting temperatures. Dbpr = 1. Blue line: P1, 63 °C; Red line: P2, 66 °C; Green line: P1 + P2, 66 °C. [P1] = [P2] = [P1 + P2] = 5 nM.

The melting curve analysis reveals that for the individual silver conjugates, Ag-P1 and Ag-P2, when hybridised to complementary target, the melting temperatures are less than that observed for unbound oligonucleotides (60 and 65 °C for Ag-P1 and Ag-P2, respectively compared to 63 and 66 °C for P1 and P2, respectively). The higher melting temperature associated with the P2 probe is attributed to the higher G-C content (P1 G-C = 38 % and P2 G-C = 43 %) which is known to facilitate a more stable duplex. In contrast, when both oligonucleotide-nanoparticle conjugates are assembled *via* DNA hybridisation the melting temperature is greater than that observed for both unbound oligonucleotides hybridised to the complementary target (70 °C for Ag-P1 + Ag-P2 compared to 66 °C for P1 + P2). The melting curve of Ag-P1 + Ag-P2 is also characteristically sharp compared to the other melting curve which is due to the well-known cooperative melting mechanism of multiple DNA duplexes linked between nanoparticles. [26] The addition of SYBR green I to obtain a melting curve for the individual Ag-P1 and Ag-P2 conjugates is an attractive method for characterisation of DNA hybridisation as a melting curve cannot be obtained from the individual conjugates using the more traditional UV-Vis spectroscopy since this method relies on the plasmonic coupling between nanoparticles to obtain a melting curve.

The melting curves obtained so far in this study have been obtained using a target DNA concentration of 5 nM. Interestingly, when a further excess of target was added to the already extensively aggregated conjugates, other melting curves are obtained in addition to the curve observed at 70 °C. The SYBR green I fluorescence melting profile obtained from adding a further excess (10 nM) of target DNA is shown in figure 6.12 along with the melting curve obtained from the addition of a non-complementary DNA target sequence. The melting curve reveals three distinct peaks appearing at 60, 66 and 70 °C. The appearance of the additional two peaks has been attributed to the release of target DNA from the surface of each individual nanoparticle conjugates (Ag-P1 and Ag-P2), *i.e.* denaturation of duplexes that are not directly involved in linking the conjugates together to induce aggregation. This result suggests the denaturation of the duplexes at the nanoparticle surface occurs in three steps: (1) at 61 °C, the target DNA hybridised uniquely to Ag-P1 separates from the nanoparticle bound oligonucleotide, followed by, (2) at 66 °C, the target

DNA hybridised only to Ag-P2 separates from the surface-bound oligonucleotide, and, finally, (3) at 70 °C, separation of linked duplexes between nanoparticle conjugates which have caused aggregation of the nanoparticles. The three-step process is outlined in figure 6.13.
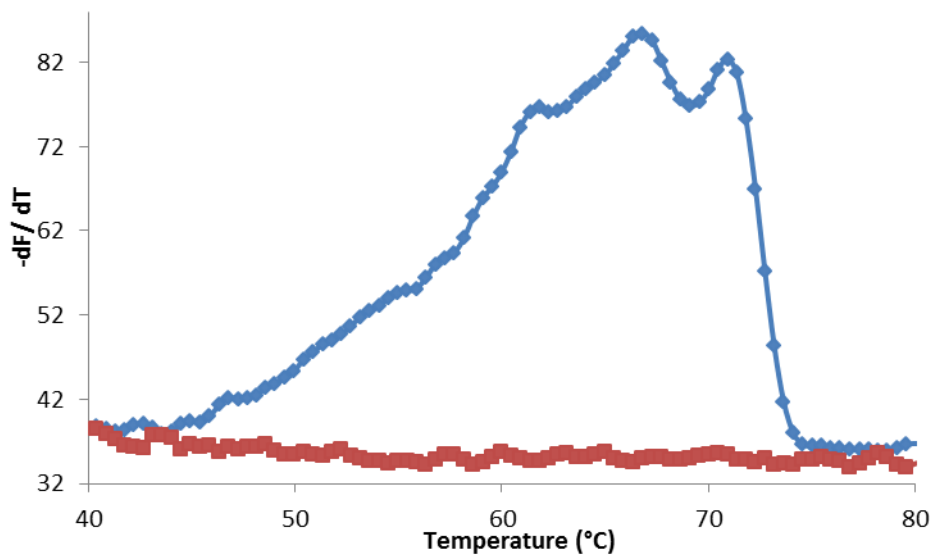
Figure 6.12. SYBR green I fluorescence melting curve obtained from an addition excess of target DNA (10 nM) to oligonucleotide-silver nanoparticle conjugates. Blue line: Peak 1: 61 °C; Peak 2: 66 °C; Peak 3: 70 °C. Red line: non-complementary target DNA sequence.
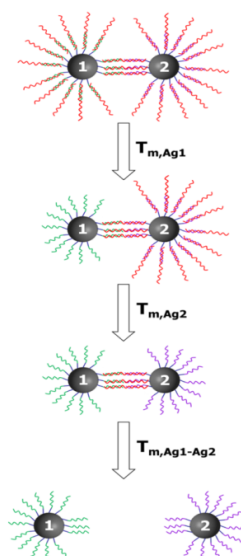
Figure 6.13. Schematic representation of the three step denaturation process observed during SYBR green I fluorescence melting of oligonucleotide-silver nanoparticle conjugates hybridised with 5 nM target DNA followed by an additional 10 nM target DNA.

When the SYBR green I fluorescence profile was examined for oligonucleotide-gold nanoparticle assemblies, the resulting melting curve obtained was a sharp negative peak indicating an appearance of weak fluorescence signal upon denaturation of the duplex DNA. The SYBR green I melting curve of oligonucleotide-gold nanoparticle conjugates, Au-P1 + Au-P2, is shown in figure 6.14. The melting temperature obtained for of Au-P1 + Au-P2 was 65 °C. The melting curve was obtained from the addition of 30 pM gold conjugates to 3 nM target DNA with a dbpr of 1. The weak fluorescence signal observed for oligonucleotide-gold nanoparticle assemblies can be attributed to the intrinsic fluorescent background of SYBR green I interaction with unbound oligonucleotides in solution. The SYBR green I melting temperatures obtained for both gold and silver oligonucleotide-nanoparticle assemblies were similar to those observed by UV-Vis spectroscopy (figures 6.8 and 6.9 for gold and silver, respectively). The differences in the two melting temperatures can be due to the larger silver nanoparticle diameter, difference in oligonucleotide density and higher target DNA concentrations. [24]
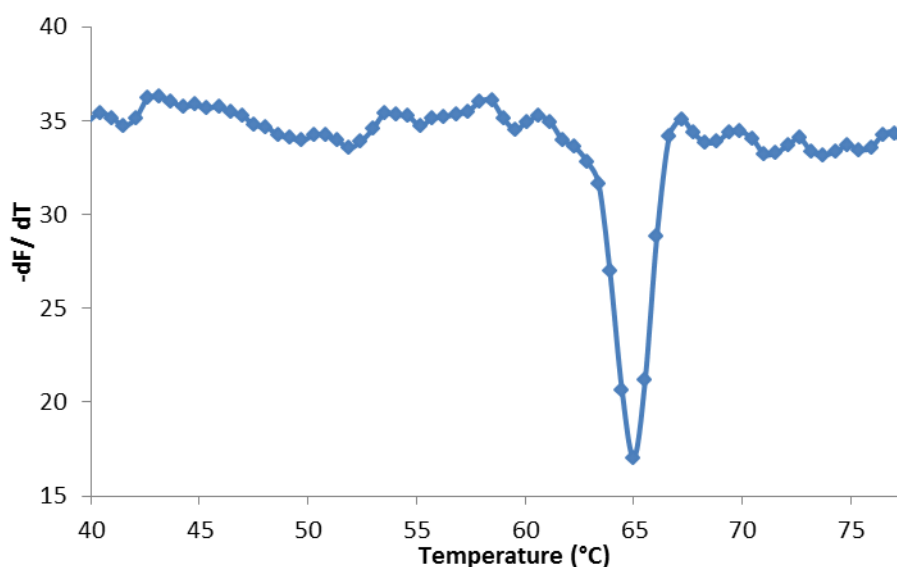
Figure 6.14.   SYBR green I melting curve of oligonucleotide-gold nanoparticle conjugate assemblies.   Melting temperature of Au-P1 + Au-P2 was 65 °C. [Conjugates] = 30 pM, [Target] = 3 nM, dbpr = 1.

6.3 *Hybridisation Efficiency of Oligonucleotide-Nanoparticle Conjugates Using SYBR Green I*

Previous studies have employed dye-labelled oligonucleotides to determine the hybridisation efficiency of nanoparticle-bound oligonucleotides. [27] However, such oligonucleotides can be expensive. SYBR green I provides a simple, flexible and cheap fluorescence-based alternative to UV-Vis spectroscopy to characterise the melting transitions of individual metallic nanoparticle conjugates and can also be used in non-plasmonic structures, such as magnetic nanoparticles and silica nanoparticles. The hybridisation efficiency of the oligonucleotide-silver nanoparticle conjugates was investigated using Ag-P1. For this study, aliquots of different target DNA/ SYBR green I solutions (dbpr = 10) were added to Ag-P1 samples (10 pM) and left overnight to ensure sufficient aggregation of the system will occur. This was followed by two rounds of centrifugation to remove any unbound SYBR green I or DNA and subsequent redispersion in Milli-Q water. A higher dbpr was used for this study to ensure full coverage of SYBR green I on to the dsDNA for each sample, *i.e.* to ensure that the increase in fluorescence intensity was directly related to the extent of the hybridisation event. The fluorescence responses of the Ag-P1 conjugate are

displayed in figure 6.15. The results indicate a gradual increase in SYBR green I fluorescence as the concentration of target DNA increases. This is expected as SYBR green I will exhibit an increase in fluorescence only in the presence of duplex DNA, therefore more DNA leads to more hybridisation events occurring meaning there is more duplex DNA on the surface of the nanoparticles. The increase in fluorescence occurs until a plateau value is reached at 40 nM target DNA concentration indicating a maximum loading of target DNA on to the Ag-P1 conjugates which corresponds to approximately 4000 hybridised oligonucleotides per nanoparticle.
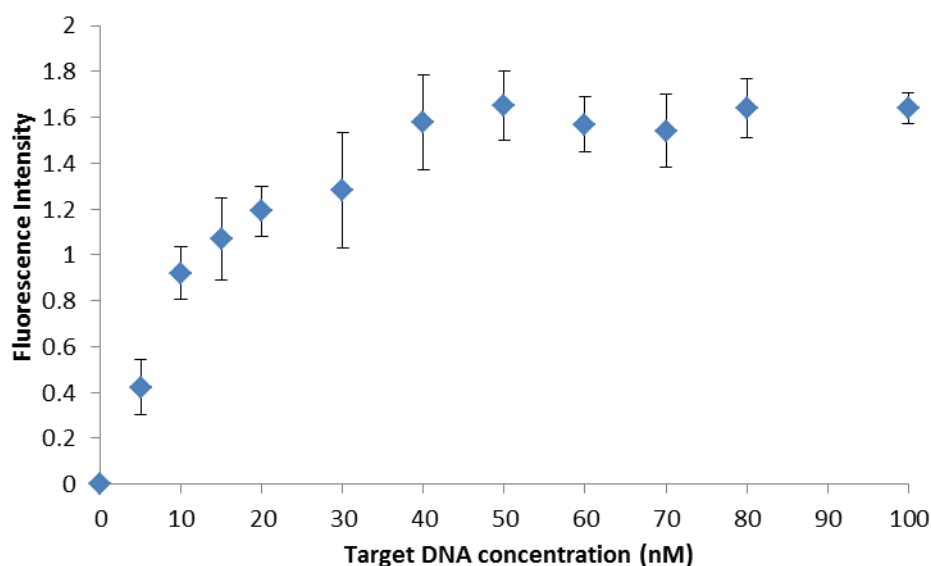
Figure 6.15. Hybridisation efficiency of Ag-P1 using different target DNA concentrations (dbpr = 10). Error bars represent the standard deviation of two repeat measurements.

6.4 Conclusions

SYBR green I, a fluorescent DNA intercalator, was successfully used to characterise the fluorescence enhancement or quenching effects during hybridisation of oligonucleotide-nanoparticle conjugates. This was accomplished by first hybridising complementary DNA target to the nanoparticle conjugates followed by the addition of SYBR green I in a specific dye-base pair ratio followed by subsequent monitoring of the fluorescence intensities. The results indicated an enhancement of fluorescence intensities in the case of oligonucleotide-silver nanoparticle conjugates, with the

greatest fluorescence intensities observed when the nanoparticles are aggregated *via* DNA-mediated assembly caused by the coupling of the surface plasmon resonances. In the case of oligonucleotide-gold nanoparticle conjugates, the fluorescence is effectively quenched at the surface due to the overlapping of the emission of SYBR green I and the surface plasmon resonance of gold nanoparticles.

The melting characteristics of the oligonucleotide-nanoparticle conjugates were also investigated by using SYBR green I fluorescence. It was determined that SYBR green I could be successfully employed to determine the melting temperatures of the individual nanoparticle conjugates in addition to the nanoparticle assemblies, with the melting temperatures obtained *via* SYBR green I fluorescence exhibiting similar melting temperatures as obtained using UV-Vis spectroscopy. It was discovered that by adding an excess of target DNA in addition to the target DNA already used to assemble the nanoparticles, a three step denaturation process was revealed where the duplexes linked to the individual conjugates melted first in order of their duplex stability followed by the duplexes linking both conjugates together. In addition, a negative fluorescence melting curve was obtained for oligonucleotide-gold nanoparticle conjugates due to a weak fluorescence signal resulting from denaturation of the duplex.

Finally, the viability of using SYBR green I as an alternative to dye-labelled oligonucleotides to determine hybridisation efficiency of surface-bound oligonucleotides was investigated. This was accomplished by hybridising varying concentrations of target DNA and SYBR green I in the range 5 – 100 nM (dbpr = 10) to the nanoparticle conjugate and measuring the fluorescence response. The results indicated a gradual increase in fluorescence due to an increase in duplex formation on the nanoparticle surface up to a plateau value of 40 nM target DNA, indicating maximum loading of target DNA on to the nanoparticle-bound oligonucleotides.

6.5 References

1.   K. M. Ririe, R. P. Rasmussen and C. T. Wittwer, *Anal. Biochem.*, 1997, **245**, 154-160.

2.   R. Higuchi, C. Fockler, G. Dollinger and R. Watson, *Bio-Technology*, 1993,

11, 1026-1030.

3. T. Ishiguro, J. Saitoh, H. Yawata, H. Yamagishi, S. Iwasaki and Y. Mitoma, *Anal. Biochem.*, 1995, **229**, 207-213.

4. H. Zipper, H. Brunner, J. Bernhagen and F. Vitzthum, *Nucleic Acids Res.*, 2004, **32**.

5. K. Aslan, I. Gryczynski, J. Malicka, E. Matveeva, J. R. Lakowicz and C. D. Geddes, *Curr. Opin. Biotechnol.*, 2005, **16**, 55-62.

6. J. R. Lakowicz, K. Ray, M. Chowdhury, H. Szmacinski, Y. Fu, J. Zhang and K. Nowaczyk, *Analyst*, 2008, **133**, 1308-1346.

7. J. R. Lakowicz, *Anal. Biochem.*, 2005, **337**, 171-194.

8. J. Zhang, Y. Fu, M. H. Chowdhury and J. R. Lakowicz, *J. Phys. Chem. C*, 2008, **112**, 18-26.

9. J. Zhang, Y. Fu, M. H. Chowdhury and J. R. Lakowicz, *J. Phys. Chem. C*, 2008, **112**, 9172-9180.

10. Gryczynski, J. Malicka, Y. B. Shen, Z. Gryczynski and J. R. Lakowicz, *J. Phys. Chem. B*, 2002, **106**, 2191-2195.

11. Y. Fu, J. Zhang and J. R. Lakowicz, *Biochem. Bioph. Res. Co.*, 2008, **376**, 712-717.

12. J. Zhang, Y. Fu, D. Liang, R. Y. Zhao and J. R. Lakowicz, *Anal. Chem.*, 2009, **81** 883-889.

13. K. Aslan, J. Huang, G. M. Wilson and C. D. Geddes, *J. Am. Chem. Soc.*, 2006, **128**, 4206-4207.

14. J. Malicka, I. Gryczynski and J. R. Lakowicz, *Biochem. Bioph. Res. Co.*, 2003, **306**, 213-218.

15. Dragan, E. S. Bishop, J. R. Casas-Finet, R. J. Strouse, M. A. Schenerman and C. D. Geddes, *J. Immunol. Methods*, 2010, **362**, 95-100.

16. Dragan, E. S. Bishop, J. R. Casas-Finet, R. J. Strouse, M. A. Schenerman and C. D. Geddes, *Anal. Biochem.*, 2010, **396**, 8-12.

17. Dragan, E. S. Bishop, R. J. Strouse, J. R. Casas-Finet, M. A. Schenerman and C. D. Geddes, *Chem. Phys. Lett.*, 2009, **480**, 296-299.

18. J. Zhang, Y. Fu and J. R. Lakowicz, *Langmuir*, 2007, **23**, 11734-11739.

19. M. Lessard-Viger, M. Rioux, L. Rainville and D. Boudreau, *Nano Lett.*, 2009,

9, 3066-3071.

20. G. Frens, *Nature-Phys. Sci.*, 1973, **241**, 20-22.

21. S. H. Liu and M. Y. Han, *Adv. Funct. Mater.*, 2005, **15**, 961-967.

22. P. C. Lee and D. Meisel, *J. Phys. Chem.*, 1982, **86**, 3391-3395.

23. B.A. Armitage, *Cyanine dye-DNA interactions: Intercalation, groove binding, and aggregation*, in *DNA Binders and Related Subjects*, M.J. Waring and J.B. Chaires, Editors. 2005, Springer-Verlag Berlin: Berlin, 55-76.

24. J. Zhang, Y. Fu, M. H. Chowdhury and J. R. Lakowicz, *Nano Lett.*, 2007, **7**, 2101-2107.

25. J. Zhang and J. R. Lakowicz, *Opt. Express*, 2007, **15**, 2598-2606.

26. R. C. Jin, G. S. Wu, Z. Li, C. A. Mirkin and G. C. Schatz, *J. Am. Chem. Soc.*, 2003, **125**, 1643-1654.

27. L. M. Demers, C. A. Mirkin, R. C. Mucic, R. A. Reynolds, R. L. Letsinger, R. Elghanian and G. Viswanadham, *Anal. Chem.*, 2000, **72**, 5535-5541.

7 *Conclusions*

Oligonucleotide-nanoparticle conjugates have been investigated for their suitability as sensors to detect DNA sequences related to disease using surface enhanced resonance Raman scattering (SERRS). To achieve this, thioctic acid and thiol modified oligonucleotides were conjugated to the surface of gold and silver nanoparticles. Functionalisation of oligonucleotides by the thioctic acid moiety was accomplished *via* solid-phase modification of a 5'-amino-modified oligonucleotide using a thioctic acid-NHS ester and preparation of the thiol moiety was accomplished by incorporating the 5'-thiol-modified phosphoramidite during routine oligonucleotide synthesis. Thioctic acid and thiol-modified oligonucleotide-nanoparticle conjugates were successfully and reproducibly synthesised. The successful conjugation of oligonucleotides to nanoparticles was confimed by UV-Vis spectroscopy and dynamic light scattering (DLS).

The stabilities of the thioctic acid- and thiol-modified oligonucleotide gold and silver nanoparticle conjugates were assessed and it was found that thioctic acid-modified oligonucleotides conferred the greatest stability compared to the standard "monothiol" analogue for both gold and silver nanoparticles. Three different linking strategies were also assessed for stability – 10A, HEG and (HEG)$_3$ of which HEG was the most stable.

As the overall aim of this work was to utilize the nanoparticle conjugates for SERRS detection of DNA, the conjugates were made SERRS-active by the incorporation of an isothiocyanate dye molecule. This was achieved post-oligonucleotide functionalisation, which was found to allow a freedom in the choice of dye. TAMRA-ITC and malachite green-ITC were functionalized to thioctic acid- and thiol-modified gold and silver nanoparticle conjugates and their stability was assessed. It was found the incorporation of the isothiocyanate dye conferred enhanced stability for both thioctic acid- and thiol-modified oligonucleotide gold nanoparticle conjugates. On silver nanoparticles, the isothiocyanate dye conferred enhanced stability with respect to the thiol-modified oligonucleotide nanoparticle

conjugates. Although this was not as great as for gold nanoparticle conjugates, these promising results showed that stability could be improved by the addition of an isothiocyanate dye molecule, opening up the possibility of using the conjugates in more challenging (bio)chemical environments. It would be advantageous to assess the stability of the conjugates under PCR conditions in order to assess the possibility of using the conjugates for real-time PCR-based SERRS detection of DNA.

The biological integrity of the oligonucleotide-nanoparticle conjugates was investigated using UV-Vis spectroscopy. This was achieved by the addition of a complementary DNA target sequence that caused aggregation of the nanoparticles *via* DNA hybridisation. Several factors, such as the concentration of target DNA, interparticle distance and density of oligonucleotide probes on the nanoparticle surface, were discovered to influence the hybridisation profiles of the oligonucleotide-nanoparticle conjugates. In addition, the hybridisation event was confirmed to be reversible by performing melting experiments in which the conjugates were heated in order to denature the hybridised DNA duplex. The denaturation of the DNA duplexes was also found to be sensitive to differences in the concentration of target DNA, interparticle distance and the density of oligonucleotide probes on the nanoparticle surface.

The ability of the hybridisation-induced aggregation of dye-labelled nanoparticle conjugates to "switch on" a SERRS signal was assessed. While an increase in the presence of target was observed for mixed-metal conjugate hybridisations, *i.e.* gold and silver nanoparticle conjugates, and silver nanoparticle conjugates, the results were disappointing. The discrimination between the signals generated by the addition of complementary and non-complementary "target" was not sufficient for the approach to be extended to real samples. It would be advantageous to investigate the ways to minimise the background signal arising with the addition of the non-complementary sequence in order to maximise the discrimination between the complementary and non-complementary DNA targets.

In light of the difficulties encountered with "switching on" the SERRS signal, metal enhanced fluorescence (MEF) was investigated as an alternative avenue for the detection of hybridisation-driven aggregation of oligonucleotide-nanoparticle

conjugates. It was discovered that intercalating SYBR green I into the hybridised oligonucleotide-nanoparticle conjugates resulted in enhancement of the fluorescence signal from silver nanoparticles and quenching of gold nanoparticle conjugates. SYBR green I could be successfully used to determine the melting characteristics of the individual silver nanoparticle conjugates, in addition to the assembled nanoparticles. This approach also provided an avenue for characterising the hybridisation efficiency of the individual nanoparticle conjugates. It would be advantageous to investigate other factors, such as interparticle distance and oligonucleotide probe density, in order for this method to be fully implemented for the detection of DNA. In addition, it would be useful to investigate this method for potential implementation into real-time PCR conditions after optimisation of the system.

Overall, oligonucleotide-nanoparticle conjugates were investigated for their stability and biological integrity for use as potential sensors for the SERRS-based detection of DNA related to disease. Methods to increase their stability have been reported and alternative avenues for detection were achieved.

8 Experimental

8.1 Chemical Reagents

- Chemical reagents were supplied by Sigma-Aldrich, U.K.

- All oligonucleotide synthesis reagents, including phosphoramidites, CPG columns and anhydrous solvents, were purchased from Link Technologies, U.K.

- Isothiocyanate dyes were supplied by Invitrogen, U.K.

- Thin-walled PCR tubes (200 μl) were supplied by Agilent Technologies, UK.

8.2 Instrumentation

- Oligonucleotide synthesis was carried out using a Mermade 6 Nucleic Acid Synthesiser using standard phosphoramidite chemistry.

- Reverse-Phase HPLC purification was performed using a Phenomenex Clarity Column coupled to a Dionex HPLC system, fitted with a UVD170U detector and a P680 pump.

- Size-exclusion NPLC purification was performed using a Hi-Trap Desalt column coupled to a Dionex HPLC system, fitted with a UVD170U detector and a P680 pump.

- UV-Vis spectroscopy was carried out using a Cary 300 Bio UV-Vis spectrophotometer fitted with a 6×6 cell changer and Peltier temperature controller.

- Fluorescence measurements were performed on a Stratagene MX3000P QPCR.

- Dynamic light scattering (DLS) measurements were performed on a High Performance Malvern Zatasizer.

- SERRS was performed on a Renishaw System 2000 Raman Spectrometer with a 633 nm Helium/Neon fitted with a Leica DMLM microscope equipped with ×20 long-working distance (LWD) objective lens and a RenCam charge

coupled device (CCD) or on a Renishaw Probe spectrometer with an Argon 532 nm laser equipped with a ×50 LWD objective, as specified in the text.

- SEM analysis was performedby Dr Iain Larmour on a Sirion 200 Schottky field-emission electron microscope (5 kW).

- MALDI-TOF mass spectrometry was performed on a Shimadzu Axima-CFR mass spectrometer in linear negative mode. Oligonucleotide standards were supplied by Brüker Daltonics.

8.3 Chemical Synthesis of 1-{[5-(1,2-dithiolan-3-yl) pentanoyl]oxy}-2,5-pyrrolidinedione, 1 [(1)]
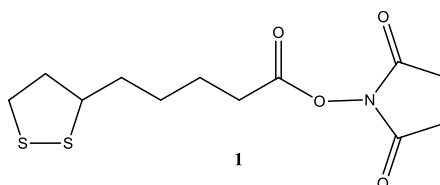
1

N-(3-Dimethylaminopropyl)-*N'*-ethylcarbodiimide hydrochloride (EDC.HCl) (0.613 g, 9.6 mmol, 1.2 eq) was dissolved in DCM (anhydrous, 7 ml), to which, 0.57 ml diisopropylethylamine (DIPEA) (anhydrous, 9.6 mmol, 1.2 eq) was added and stirred for 10 min. To the solution *N*-hydroxysuccinimide (0.43 g, 11.2 mmol, 1.4 eq) was added and the reaction mixture stirred in an ice bath. Thioctic acid (0.55 g, 8.0 mmol, 1.0 eq) was dissolved in anhydrous DCM (3 ml) and added to the reaction over 5 min and stirred overnight. The reaction mixture was washed with HCl (5% (v/v), 17 ml × 2) and water (distilled, 17 ml). The organic layer was dried over Na_2SO_4. Solvents were concentrated *in vacuo* to yield 0.15 g of ester **1**, as a yellow solid. δ_H (400 MHz; DMSO) 1.4–1.7 (6H, m, CH_2 ×3), 1.84–1.93 (1H, m, CH), 2.38–2.46 (1H, m, CH), 2.68 (2H, t, *J* 7.2, CH2), 2.81 (4H, s, succinimidyl CH_2×2), 3.12–3.21 (2H, *m*, CH_2), 3.56–3.65 (1H, *m*, CH). dC (400 MHz; DMSO) 24.415, 25.830, 28.026, 30.425, 34.217, 38.485, 56.011, 169.287, 170.612. *M/Z* 321.0937 ([M+NH4^{+}] $C_{12}H_{17}NO_4S_2$ requires, 321.0937).

8.4 Oligonucleotide Syntheses, Modification and Purification

8.4.1 Oligonucleotide Synthesis

Automated oligonucleotide synthesis was performed on a 1 μmol scale using 1000 Å CPG columns. Prior to loading on to the synthesiser, base phosphoramidite monomers were dissolved in anhydrous MeCN (0.1 M). The following base monomers were routinely used for oligonucleotide synthesis:

- Bz-CE-dA phosphoramidite
- Ac-CE-dC phosphoramidite
- Dmf-CE-dG phosphoramidite
- dT-CE-phosphoramidite

Other phosphoramidite monomers were also routinely used to incorporate modifications to the oligonucleotide sequence. Modifier bases were dissolved in anhydrous MeCN (0.1 M) prior to use on the synthesiser. Modified base monomers included:

- 5'-Thiol-modifier C6-CE phosphoramidite
- 5'-MMT-Amino-modifier C6-CE phosphoramidite
- Spacer-18 CE phosphoramidite (HEG)
- 3'-Amino-modifier C7 CPG 1000

The following commercially available solutions were used for routine oligonucleotide synthesis:

- Deblock – 3 % trichloroacetic acid/DCM
- Activator – 0.25 M 5-ethylthio-1H-tetrazole/MeCN
- Cap Mix A – THF/pyridine/acetic anhydride (8:1:1)
- Cap Mix B – 10 % methylimidazole/THF
- Oxidiser – 0.02 M iodine in THF/pyridine/water (7:2:1)

The following synthesis cycle was routinely employed for oligonucleotide synthesis:

1. Deblock   × 2   (220 µL, 36 s)
2. MeCN   × 2   (274 µL, 5 s)
3. Coupling   × 2   (90 µL Amidite, 110 µL Activator, 100 s)
4. MeCN   × 1   (274 µL, 5 s)
5. Capping   × 1   (125 µL Mix A, 125 µL Mix B, 50 s)
6. MeCN   × 1   (274 µL, 5 s)
7. Oxidise   × 1   (200 µL, 60 s)
8. MeCN   × 2   (274 µL, 5 s)

8.4.1.1 *Synthesis of 5'-Thiol-Modified Oligonucleotides*

Oligonucleotide synthesis was carried out on a standard support (1 µmol). The synthesis was carried out on a Mermade 6 Nucleic Acid Synthesiser using standard phosphoramidite chemistry. If required, the hexaethylene glycol (HEG) spacer was added to the sequence adjacent to the modification by addition of a Spacer-CE 18 (17-O-(4,4'-dimethoxytrityl)-hexaethyleneglycol,1-[(2-cyanoethyl)-(*N,N*-diisopropyl)]) phosphoramidite. The final base added to the sequence was a 5'-dimethoxytrityl protected thiol modifier phosphoramidite. The final deblock step was omitted from the synthesis steps. Once synthesis was complete, the oligonucelotide was removed from the CPG support by incubating in 1 ml of concentrated NH_4OH at 40 °C for 18 h. The ammonium hydroxide was removed *in vacuo* at room temperature. The clear residue was resuspended in 1 ml distilled H_2O and the CPG removed using a 13 mm syringe filter. The oligonucleotides were purified by reversed-phase HPLC. After HPLC purification the fractions were collated and concentrated *in vacuo* and redissolved in 1 ml distilled H_2O. To remove the dimethoxytrityl (DMT) group from the 5'-thiol-modifier, the water was evaporated *in vacuo* and the residue resuspended in TEAA (600 µl, 0.1 M, pH 7). $AgNO_3$ (90 µl, 1 M) was added and left at room temperature for 30 min. Dithiothreitol (DTT) (138 µl, 1 M) was added and the solution left at room temperature for 5 min. The solution was centrifuged at 7000 rpm for 10 min and the

supernatant was recovered and set aside. The pellet was resuspended in TEAA (500 μl, 0.1 M, pH 7) and centrifuged again at 8000 rpm for 10 min. This procedure was repeated another two times and the three supernatants were combined into a single eppendorf™ tube and stored at 4 °C.

8.4.1.2   Synthesis of 5'-Thioctic acid-Modified Oligonucleotides

Oligonucleotide synthesis was carried out on a standard support (1 μmol) using a Mermade 6 Nucleic Acid Synthesizer using standard phosphoramidite chemistry. If required, the hexaethylene glycol (HEG) spacer was added to the sequence adjacent to the modification by addition of a Spacer-CE 18 (17-O-(4, 4'-dimethoxytrityl)-hexaethyleneglycol,1-[(2-cyanoethyl)-(*N*,*N*-diisopropyl)]) phosphoramidite. The final base added to the sequence was a 5'-monomethoxytrityl protected amino modifier phosphoramidite. The final deblock step was omitted from the synthesis steps. Once synthesis was complete, 1 ml of deblock solution (3 % trichloroacetic acid in DCM) was applied across the column and left for 1 hour. The column was then washed with 1 ml of MeCN before being treated with a solution of the NHS ester, **1**, in MeCN (10 mg ml^{-1}, triethylamine 1 % (v/ v)) overnight. The column was washed again with 1 ml of MeCN before being treated with NH_4OH (30 %, 1 ml) for 36 h at room temperature. The ammonium hydroxide was removed *in vacuo* at room temperature. The clear residue was resuspended in 1 ml distilled H_2O and purified by reversed-phase HPLC. After HPLC purification the fractions were collated and concentrated *in vacuo* (room temperature) and redissolved in 1 ml distilled H_2O. All oligonucleotides were stored at 4 °C.

8.4.1.3   Synthesis of 3'-Thioctic acid-Modified Oligonucleotides

Oligonucleotide synthesis was carried out on a 3'-amino-modifier C7 CPG solid support (1 μmol) using a Mermade 6 Nucleic Acid Synthesizer using standard phosphoramidite chemistry. The Fmoc protected column was pre-treated with piperidine/MeCN (1 mL, 20 % (v/v)) for 30 min. The column was then washed with 1 ml of MeCN before being treated with a solution of the NHS ester, **1**, in MeCN (20 mg ml^{-1}, triethylamine 1 % (v/ v)) overnight. The column was then placed in the synthesiser and used as the solid support for oligonucleotide synthesis. The synthesis

cycle was altered to include two capping steps before the initial deblock.   If required, the hexaethylene glycol (HEG) spacer was added to the sequence as the first monomer adjacent to the modification by addition of a Spacer-CE 18 (17-O-(4,4'-dimethoxytrityl)-hexaethyleneglycol,1-[(2-cyanoethyl)-(*N*,*N*-diisopropyl)]) phosphoramidite. After synthesis, the column was treated with NH_4OH (30 %, 1 ml) for 36 h at room temperature. The ammonium hydroxide was removed *in vacuo* at room temperature. The clear residue was resuspended in 1 ml distilled H_2O and purified by reversed-phase HPLC. After HPLC purification the fractions were collated and concentrated *in vacuo* (room temperature) and redissolved in 1 ml distilled H_2O. All oligonucleotides were stored at 4 °C.

8.4.2 Purification of Oligonucleotides

8.4.2.1   RP-HPLC

Reversed-phase HPLC was performed on a Dionex UVD170U detector fitted with a P680 pump through a Phenomenex Clarity column. Buffer A: TEAA (0.1 M, pH 7), Buffer B: MeCN; T = 0, 95 % TEAA: 5 % MeCN, with a gradient of 1 % min^{-1} B over 15 min and held at 20 % B for 5 min at a flow rate of 1 ml/ min.

8.4.2.2   SEC-HPLC

Size exclusion HPLC was performed on a Dionex UVD170U detector fitted with a P680 pump through a HiTrap™ Desalting Column. Eluent: 100 % H_2O at 3 ml/ min for 5 min.

8.4.3 Determination of Oligonucleotide Concentrations

After purification, oligonucleotides were analysed by UV-Vis spectroscopy to determine their concentrations. Oligonucleotides absorb light in the UV region with absorption maxima, λ_{max}, in the range 260 – 280 nm. The absorbance is caused by electronic transitions in the purine and pyrimidine bases, with intensity and exact wavelength dependent upon the base sequence, base-pair interactions, salt concentration and pH. The oligonucleotides were measured to obtain an absorbance value which was applied to the Beer-Lambert law to determine the concentration:

$$A = \varepsilon Cl$$

Where,

A = Absorbance

ε = Molar extinction coefficient ($mol^{-1}\, cm^{-1}$)

C = Concentration ($mol\, l^{-1}$)

l = Path length (cm)

To obtain the molar extinction coefficient for an oligonucleotide the extinction coefficients for the individual bases in the sequence are added together. Typically, the accumulated value obtained for the molar extinction coefficient of the oligonucleotide is multiplied by 0.9 – a factor for hypochromicity. The molar extinction coefficients for the individual bases are:

A = $15,400\ mol^{-1}\, cm^{-1}$
C = $7,400\ mol^{-1}\, cm^{-1}$
G = $11,500\ mol^{-1}\, cm^{-1}$
T = $8,700\ mol^{-1}\, cm^{-1}$

8.4.4 MALDI-TOF Analysis of Oligonucleotides

ZipTip™ C_{18} pipette tips were used to purify and concentrate the oligonucleotide samples prior to addition to the metal plate. MALDI matrix was prepared by dissolving 3-hydroxypiccolinic acid in 50:50 MeCN/H_2O (Milli-Q) (50 mg ml^{-1}) and mixing in a 9:1 ratio with ammonium citrate in H_2O (Milli-Q) 50 mg ml^{-1}. Oligonucleotides for MALDI-TOF analysis were eluted from the ZipTip™ directly in 2 µl of the MALDI matrix onto a metal plate. MALDI-TOF experiments were performed using a Shimadzu Axima-CFR mass spectrometer in linear negative mode and calibration was achieved immediately prior to analysis using oligonucleotide standards (Brüker Daltronics).

8.5   Preparation of Nanoparticle Colloids

All glassware used for nanoparticle synthesis was soaked in *aqua regia* (1 HNO$_3$: 3 HCl) for 4 hours and rinsed thoroughly with distilled water prior to synthesis.

8.5.1 Gold Nanoparticle Synthesis [2] [3]

15 nm gold nanoparticles were prepared *via* citrate reduction of NaAuCl$_4$.   An aqueous solution of NaAuCl$_4$ (12.5 mM, 10ml) was added to distilled water (500 ml) and heated to boiling with continuous stirring.   Upon boiling, sodium citrate (25 mM, 10 ml) was added and the solution was left to stir for 15 minutes at boiling point. After 15 minutes, the solution was allowed to cool to room temperature. The concentration of gold nanoparticles was determined by UV-Vis spectroscopy and application of the Beer-Lambert law (see section 8.4.3) using an extinction coefficient of 2.7×10^8 mol^{-1} cm^{-1} at λ_{max} 520 nm.

45 nm Au nanoparticles were prepared *via* a second step seeded growth method. 37 μmol of NaAuCl$_4$ was added to 125 ml of Milli-Q water and heated to boiling. Subsequently, 5 ml of gold colloidal dispersion (15 nm sized nanoparticles acting as seeds) was added, followed by addition of 1 % w/w aqueous trisodium citrate (21.7 μmol, 638 μl). The mixture was refluxed for 30 minutes under vigorous stirring. To assure the stability of colloidal dispersion, 4.9 ml of 1 % w/w aqueous trisodium citrate was then added and further refluxed for 1 hour. The concentration of gold nanoparticles was determined by UV-Vis spectroscopy and application of the Beer-Lambert law (see section 8.4.3) using an extinction coefficient of 1.9×10^{10} mol^{-1} cm^{-1} at λ_{max} 530 nm.

8.5.2 Silver Nanoparticle Synthesis [4]

Silver nanoparticles were prepared *via* modification of the method first reported by Lee and Meisel. An aqueous solution of AgNO$_3$ (53 mM, 10 ml) was added to distilled water (500 ml) which was heated to 40 °C with continuous stirring. Heating continued to 97 °C at which point an aqueous solution of sodium citrate (43 mM, 10 ml) was added and stirring maintained at 97 °C for a further 90 minutes.

After 90 minutes, the solution was allowed to cool to room temperature. The concentration of silver nanoparticles was determined by UV-Vis spectroscopy and application of the Beer-Lambert law (see section 8.4.3) using an extinction coefficient of 2.8×10^{10} mol^{-1} cm^{-1} at λ_{max} 410 nm.

8.6 Functionalisation of Nanoparticles with Oligonucleotides

- The following procedures were applied for both Au (17 nM, 3 ml) and Ag (0.3 nM, 3 ml) nanoparticles and for both thiol- and thioctic acid-modified oligonucleotides.

- Thiol-modified oligonucleotides were desalted directly on to the nanoparticles using a HiTrap (5 ml) size exclusion column on a Dionex UVD170U detector fitted with a P680 pump.

8.6.1 Preparation of Oligonucleotide-Nanoparticle Conjugates

Desalted thiol- or thioctic acid-modified oligonucleotides (10 μM, 1 ml) were added to Au or Ag colloid in a 5 ml glass vial. After 18 hours, phosphate (NaH$_2$PO$_4$/ Na$_2$HPO$_4$) buffer (60 mM) was added to 10 mM final concentration. NaCl (2 M) was then added at 18 hour intervals, increasing the salt concentration by 0.05 M increments to a final concentration of 0.1 M. For Au nanoparticles, the conjugates were centrifuged at 7000 rpm for 20 minutes and the pellet resuspended in phosphate buffered saline (PBS, 1 ml, 10 mM phosphate/ 0.3 M NaCl). For Ag nanoparticles, the conjugates were initially centrifuged at 4000 rpm for 15 minutes at which point the supernatant was removed and subsequently centrifuged at 6500 rpm for 15 minutes. The two pellets were then combined in to a single eppendorf™ tube and resuspended in PBS. The centrifugation process was repeated once more for Ag nanoparticle conjugates. The concentration of gold and silver nanoparticle conjugates were determined by UV-Vis spectroscopy and application of the Beer-Lambert law (see section 8.4.3) using extinction coefficients of 2.7×10^8 mol^{-1} cm^{-1} at λ_{max} 520 nm for 15 nm Au, 1.9×10^{10} mol^{-1} cm^{-1} at λ_{max} 530 nm for 45 nm and 2.8×10^{10} mol^{-1} cm^{-1} at λ_{max} 410 nm for Ag nanoparticles. Both Au and Ag nanoparticle

conjugates were stored at 4 °C.

In Chapter 4, Section 4.4 (Oligonucleotide-Silver Nanoparticle Conjugates: Assembly Using DNA) the ratio of recognition probe (P1 or P2) to T_{10} probe was varied. The recognition sequence and T_{10} sequences were added together to a total concentration of 10 µM in 1 ml distilled water and added directly on to Ag nanoparticles as described in 8.6.1. Table 8.1 shows the concentrations required to achieve the different recognition sequence: T_{10} sequence ratios.

Recognition Sequence: T_{10} Sequence Ratio	Recognition Sequence (µM)	T_{10} Sequence (µM)
1.0	10	0
0.8	8	2
0.6	6	4
0.4	4	6
0.2	2	8
0.1	1	9
0.01	0.1	9.9

Table 8.1. Different recognition sequence: T_{10} sequence ratios added to Ag nanoparticles in Chapter 4, Section 4.4.

8.7 Dye labelling of Oligonucleotide-Nanoparticle Conjugates

The following procedure was used for both thiol- and thioctic acid-modified oligonucleotide gold and silver nanoparticle conjugates. A solution of isothiocyanate dye (malachite green, ROX or TAMRA; 500 µl, 1 µM) was added to 500 µl of the respective Au or Ag oligonucleotide-nanoparticle conjugate. The solution was stored in the dark for 18 hours and subsequently centrifuged to remove any excess dye. For Au nanoparticles, the conjugates were centrifuged at 7000 rpm for 20 minutes and the pellet resuspended in phosphate buffered saline (PBS, 1 ml, 10 mM phosphate/ 0.3 M NaCl). For Ag nanoparticles, the conjugates were initially centrifuged at 4000 rpm for 15 minutes at which point the supernatant was removed and centrifuged at

6500 rpm for 15 minutes. The two pellets were then combined in to a single eppendorf™ tube and resuspended in PBS. The centrifugation process was repeated for Au and Ag conjugates. The concentration of silver nanoparticles was determined by UV-Vis spectroscopy using an extinction coefficient of 2.7×10^8 mol^{-1} cm^{-1} at λ_{max} 520 nm for Au and 2.8×10^{10} mol^{-1} cm^{-1} at λ_{max} 410 nm for Ag. The dye-labelled conjugates were stored at 4 °C.

In Chapter 5, Section 5.2 (SERRS Detection of Oligonucleotide-Silver Nanoparticle Conjugates), FAM-ITC (1×10^{-3} M, 30 μl) was added to Ag nanoparticles (0.3 nM, 3 ml) followed by addition of thioctic acid-modified oligonucleotides (10 nmoles). After 18 hours, phosphate (NaH$_2$PO$_4$/ Na$_2$HPO$_4$) buffer (60 mM) was added to 10 mM final concentration. NaCl (2 M) was then added at 18 hour intervals, increasing the salt concentration by 0.05 M increments to a final concentration of 0.1 M. , the conjugates were initially centrifuged at 4000 rpm for 15 minutes at which point the supernatant was removed and subsequently centrifuged at 6500 rpm for 15 minutes. The two pellets were then combined in to a single eppendorf™ tube and resuspended in PBS. The centrifugation process was repeated again. The concentration of the silver nanoparticle conjugate was determined by UV-Vis spectroscopy and application of the Beer-Lambert law (see section 8.4.3) using extinction coefficients of 2.8×10^{10} mol^{-1} cm^{-1} at λ_{max} 410 nm for Ag nanoparticles. The FAM-ITC labelled Ag conjugates were stored at 4 °C.

8.8 Oligonucleotide-Nanoparticle Conjugate Stability

For Au nanoparticle conjugates (both thiol- and thioctic acid-modified), the conjugates were diluted to 0.5 nM in 400 μl 0.3 M PBS. For Ag nanoparticle conjugates, the conjugates were diluted to 10 pM in 400 μl 0.3 M PBS. To each solution, DTT (1 M) was added to the solution to a final concentration of 10 mM. Full spectrum scans were performed on a Cary 300 Bio UV-Vis spectrophotometer using the 'Scanning Kinetics' program. For thiol-modified oligonucleotide-nanoparticle conjugates, full spectrum scans (200 – 800 nm) were collected at 1 minute intervals and for thioctic acid-modified oligonucleotide-nanoparticle conjugates, scans were collected every 10 minutes.

8.9 Assembly of Oligonucleotide-Nanoparticle Conjugates

8.9.1 Oligonucleotide-Nanoparticle Conjugate Hybridisation

Each probe conjugate (P1 + P2 or P1 + P3), in the "head-to-tail", "head-to-head" or "tail-to-tail" orientation, was added to a final concentration of 0.5 nM (15 nm Au nanoparticles), 30 pM (45 nm Au nanoparticles) or 20 pM (Ag nanoparticles) in 400 µl 0.3 M PBS. Hybridisation was initiated by the addition of an appropriate concentration of complementary or non-complementary target sequence as described in Chapter 4.

8.9.2 Oligonucleotide-Nanoparticle Conjugate Hybridisations: Melting Properties

The same probe conjugate concentrations were used as in Section 7.9.1. Melting analyses were performed using a UV-Vis spectroscopy was carried out using a Cary 300 Bio UV-Vis spectrophotometer and Peltier temperature controller and the 'Thermal' program. The temperature was cycled between 10 and 95 °C 8 times with a 1 °C/ min increment. For 15 nm Au, 45 nm Au and Ag nanoparticles the absorbance was monitored at 520 nm, 530 nm and 410 nm, respectively.

8.9.3 SEM Analysis of Oligonucleotide-Nanoparticle Conjugates

Silicon wafers were cleaned with methanol before being modified by surface adsorption of 30 µl of a 35 % w/w poly(diallyldimethylammonium chloride) (PDDA) and 1 ml of 1 mM NaCl solution in Milli-Q water for 1 hour. After 1 hour, the wafers were rinsed with Milli-Q water and dried by N_2 flow. 30 µl of a hybridised conjugate solution was deposited onto a modified silicon wafer in a humidity chamber and left for 5 min. The substrate was then rinsed with Milli-Q water. The wafer was then dried by N_2 flow and imaging carried out on a Sirion 200 Schottky field-emission electron microscope operating at an accelerating voltage of 5 kW.

8.10 SERRS Analysis of Oligonucleotide-Nanoparticle Conjugates

8.10.1 Mixed Metal Nanoparticle Conjugate SERRS Analysis

For Au hybridisations, P1 (with MGITC) and P2 were mixed to a final concentration of 0.5 nM in 400 µl 0.3 M PBS. P1-Au (with MGITC) and P2-Ag were combined at a concentration of 0.5 nM and 50 pM, respectively, in 400 µl 0.3 M PBS. Hybridisation was initiated with the addition of 50 nM complementary target DNA. The analysis was performed using a Renishaw System 2000 Raman Spectrometer with a 633 nm Helium/ Neon fitted with a Leica DMLM microscope equipped with ×20 long-working distance (LWD) objective lens and a RenCam charge coupled device (CCD). The scan time was 10 seconds with 1 accumulation and 100 % power. Spectra were background corrected using Grams software.

8.10.2 Silver Nanoparticle Conjugate SERRS analysis

P1-Ag (with ROX-ITC, TAMRA-ITC or FAM-ITC) and P2-Ag were combined to a final concentration of 20 pM in 400 µl 0.3 M PBS. Hybridisation was initiated by the addition of 10 nM complementary target DNA. The analysis was performed using a Renishaw Probe spectrometer with an Argon 532 nm laser equipped with a × 50 LWD objective. The scan time was 10 seconds with 1 accumulation and 100 % power. Spectra were background corrected using Grams software.

The time study of the ROX-ITC labelled Ag nanoparticle conjugates was performed by collecting spectra every 10 minutes after addition of the complementary target DNA up to 60 minutes.

8.11 Fluorescence   Characterisation   of
Oligonucleotide-Nanoparticle Conjugates

8.11.1 Addition   of   SYBR   Green   I   to   Assembled
Oligonucleotide-Nanoparticle Conjugates

The Ag nanoparticle probe conjugates were combined to a final concentration of 30 pM each and added to thin-walled PCR tubes. Hybridisation was initiated by the addition of 5 nM complementary DNA target in 200 µl 0.3 M PBS. The conjugates were left to hybridise overnight to ensure full aggregation of the nanoparticles. SYBR green I was added to the solution at a dye-base pair ratio (dbpr) of 1, [5] *i.e.* the final SYBR green I concentration added to the solution was twice that of the individual Ag nanoparticle conjugates. After the addition of SYBR green I, the solution was left for 1 hour at which point the assembled nanoparticle conjugate solutions were monitored using a Stratagene MX3000P QPCR and a FAM filter set (Excitation = 492 nm, Emission = 516 nm) to obtain SYBR green I fluorescence (Abs = 492 nm, Emission = 520 nm). SYBR green I melting profiles were obtained by cycling between 25 and 95 °C with 1 °C/ min increments while using the FAM filter set to measure the fluorescence response.

For Au nanoparticle assembly, each conjugate probe was combined at a concentration of 30 pM with 3 nM complementary target DNA in 200 µl 0.3 M PBS in thin-walled PCR tubes. The methods for hybridisation and melting analysis of Au nanoparticle conjugates were the same as for Ag nanoparticle conjugates.

Oligonucleotides without nanoparticles were used in a 1: 1 ratio, *i.e.* [P1 = P2 = P3 = 5 nM] with a dbpr of 1. The same methods for hybridisation and melting were employed for oligonucleotide probes as with Au and Ag nanoparticle conjugates.

8.11.2 Hybridisation Efficiency Study

Ag-P1 (10 pM) was added to thin-walled PCR tubes with different concentrations of complementary target DNA (0 – 100 nM) and SYBR green I (dbpr = 10) in 200 µl

0.3M PBS. The conjugates were left overnight. The assembled nanoparticles were subjected to centrifugation to remove any unbound SYBR green I or target DNA and resuspended in 0.3 M PBS. The SYBR green I fluorescence was monitored using a Stratagene MX3000P QPCR and a FAM filter set (Excitation = 492 nm, Emission = 516 nm).

8.12 References

1.   J. A. Dougan, C. Karlsson, W. E. Smith and D. Graham, *Nucleic Acids Res.*, 2007, **35**, 3668-3675.

2.   G. Frens, *Nature-Phys. Sci.*, 1973, **241**, 20-22.

3.   S. H. Liu and M. Y. Han, *Adv. Funct. Mater.*, 2005, **15**, 961-967.

4.   P. C. Lee and D. Meisel, *J. Phys. Chem.*, 1982, **86**, 3391-3395.

5.   H. Zipper, H. Brunner, J. Bernhagen and F. Vitzthum, *Nucleic Acids Res.*, 2004, **32**.

9 Appendix: Publications

Stable dye-labelled oligonucleotide-nanoparticle conjugates for nucleic acid detection

Lee Barrett, Jennifer A. Dougan, Karen Faulds and Duncan Graham*

Metallic nanoparticles functionalized with oligonucleotides are used for a number of nucleic acid detection strategies. However, oligonucleotide-nanoparticle conjugates suffer from a lack of stability when exposed to certain conditions associated with DNA detection assays. In this study, we report the synthesis of thiol and thioctic acid-modified oligonucleotide gold nanoparticle (OGNs) conjugates functionalized with a dye label and varying spacer groups. The thioctic acid-modified conjugates exhibit increased stability when treated with dithiothreitol (DTT) compared to the more commonly used thiol modification. When the dye labelled oligonucleotide nanoparticle conjugates are exposed to the same conditions there is a pronounced increase in the stability for both thioctic acid and thiol modified sequences. These results open up the possibility of simply using a dye label to enhance the stability of oligonucleotide-nanoparticle conjugates in DNA detection assays where the enhanced stability of the conjugate system can be advantageous in more complex biological environments.

Introduction

The use of metallic nanoparticles functionalised with oligonucleotides has proven to be a promising tool in the field of molecular diagnostics in recent years. Combining the optical properties of metallic nanoparticles with the unique base-pairing capabilities of DNA was first reported on gold nanoparticles functionalized with thiol-modified oligonucleotide sequences.[1,2] Discrete clusters were shown to form upon aggregation of the nanoparticles, induced by DNA hybridization. The aggregation event of the nanoparticles causes a distinct colour change from red to blue due to the coupling of the surface plasmon resonance when the nanoparticles come in close proximity to one another. This causes a red-shift in the absorbance band that can be easily monitored by optical spectroscopy and colourimetrically by eye. Significantly, the melting profile of DNA-nanoparticle conjugates is extraordinarily sharp compared to "molecular" duplex melting, allowing discrimination of single nucleotide polymorphisms.[3] The unique optical properties of nanoparticles functionalised with oligonucleotide sequences has been utilized in a number of nucleic acid detection strategies, including the detection of the breast cancer-associated BRCA-1 gene using multifunctional cross linking gold nanoaggregates,[4] unamplified detection of genomic DNA based on the colorimetric scatter of gold nanoparticle probes,[5] colorimetric detection of gold nanoparticle probes by parallel triplex formation,[6] and polymerase chain reaction (PCR) of gold nanoparticle-bound primers for DNA detection.[7,8]

Conjugation of oligonucleotides to the nanoparticle surface is usually accomplished through a thiol modification located at the 5′ or 3′ end of the oligonucleotide. However, in order to be used in complex biological analysis, oligonucleotide nanoparticle conjugates need to exhibit enhanced stability in conditions required for DNA analysis. In conditions such as high NaCl concentrations, prolonged or cycled elevated temperatures like those used in the polymerase chain reaction, and treatment with particular biological buffer additives such as dithiothreitol (DTT) or mercaptoethanol are known to cause irreversible aggregation of nanoparticles by desorption of the Au–S bond at the nanoparticle surface.[9] A number of strategies have been employed by many different research groups to produce oligonucleotide nanoparticle conjugates with enhanced stability. These include the use of steroid cyclic disulfide groups,[10] multiple thiol-anchors,[9] and triple cyclic disulfide moieties[11] to adsorb onto the nanoparticle surface. In work by Dougan *et al.*, thioctic acid-modified oligonucleotides were shown to greatly enhance the stability of gold nanoparticle conjugates over the more commonly used thiol modification.[12] The use of low molecular weight polyethylene glycols (PEGs) have been reported to stabilize the nanoparticle surface.[13,14] A mononucleotide-mediated conjugation strategy has been reported where the nanoparticles are first incubated with dATPs in order to stabilize the nanoparticles before oligonucleotide addition.[15,16] Mirkin *et al.* reports that altering the spacer composition contributes to enhancing the stability of nanoparticle conjugates.[17] Non-ionic fluorosurfactant (Zonyl FSN) has been used to stabilize gold nanoparticle surfaces enabling the one-step functionalisation of

Centre for Molecular Nanometrology, WestCHEM, Department of Pure and Applied Chemistry, University of Strathclyde, 295 Cathedral St., Glasgow, G1 1XL. E-mail: duncan.graham@strath.ac.uk; Tel: +44 141 548 4701

203

oligonucleotides without the need for slow salt ageing.[18] In a recent study, Liu *et al.* report the use of dithiocarbamate ligands to anchor oligonucleotides onto gold nanoparticle surfaces.[19] These strategies contribute to enhancing the stability of nanoparticles, however, to date, no comparison has been made of the effect that a dye label and/or hexaethylene glycol spacer units have on the stability of the conjugate system for both thiol and thioctic acid modified oligonucleotides.

Dye labelled oligonucleotide-nanoparticle conjugates have been used as probes in the detection of specific nucleic acid sequences by surface enhanced Raman scattering (SERS).[20] Labelling of the oligonucleotide-nanoparticle conjugate with a Raman-active dye can occur pre-oligonucleotide functionalisation, where the dye is added to a solution of colloidal nanoparticles first and any remaining surface sites are functionalised with oligonucleotides.[21,22] Alternatively, the dye can be added post-oligonucleotide functionalisation, where oligonucleotides are added first to stabilize the nanoparticles and the remaining surface sites are functionalized with the Raman-active dye.[23] The latter method was used by McKenzie *et al.*[24] in a SERS assay incorporating mixed metal nanoparticle conjugates. In this split-probe assay, one probe consisted of a gold nanoparticle functionalized with thiol-modified oligonucleotides and a Raman-active dye label and the other probe consisted of a silver nanoparticle functionalized with thiol-modified oligonucleotides only. Here, the more beneficial surface chemistry of the gold nanoparticles were exploited while the silver nanoparticles provide the surface enhancement of the Raman signal producing a hybridization driven nanoparticle assembly for DNA detection.

In this work, we report the effect on stability of dye-labelled gold nanoparticles functionalized with oligonucleotides containing 5′ thioctic acid and 5′ thiol moieties and spacer groups composed of 10 adenine bases (polyA), a single hexaethylene glycol (HEG) unit and three HEG units. It is envisioned that the conjugates will be used for detection of specific nucleic acids related to disease by methods previously described in this report where the biological buffer environment and prolonged and elevated temperature cycles would normally compromise the stability of the nanoparticle conjugate.

Experimental

Materials

All chemicals, with the exception of those used in oligonucleotide synthesis, were purchased from Sigma-Aldrich, U.K. All DNA monomers, reagents and CPG columns were purchased from Link Technologies, Bellshill, U.K. The isothiocyanate dyes were purchased from Invitrogen, Paisley, U.K.

1-{[5-(1,2-Dithiolan-3-yl)pantanoyl]oxy}-2,5-pyrrolidinedione, 1

N-(3-Dimethylaminopropyl)-*N*′-ethylcarbodiimide hydrochloride (EDC.HCl) (0.613 g, 9.6 mmol, 1.2 eq) was dissolved in DCM (anhydrous, 7 ml), which, 0.57 ml diisopropylethylamine (DIPEA) (anhydrous, 9.6 mmol, 1.2 eq) was added and stirred for 10 min. To the solution *N*-hydroxysuccinimide (0.43 g, 11.2 mmol, 1.4 eq) was added and the reaction mixture stirred in an ice bath. Thioctic acid (0.55 g, 8.0 mmol, 1.0 eq) was dissolved in

anhydrous DCM (3 ml) and added to the reaction over 5 min and stirred overnight. The reaction mixture was washed with HCl (5% (v/v), 17 ml × 2) and water (distilled, 17 ml). The organic layer was dried over Na_2SO_4. Solvents were concentrated *in vacuo* to yield 0.15 g of ester 1, as a yellow solid. δ_H (400 MHz; DMSO) 1.4–1.7 (6H, m, CH_2 × 3), 1.84–1.93 (1H, m, CH), 2.38–2.46 (1H, m, CH), 2.68 (2H, t, *J* 7.2, CH2), 2.81 (4H, s, succinimidyl CH_2 × 2), 3.12–3.21 (2H, *m*, CH_2), 3.56–3.65 (1H, *m*, CH). δ_C (400 MHz; DMSO) 24.415, 25.830, 28.026, 30.425, 34.217, 38.485, 56.011, 169.287, 170.612. *m/z* 321.0937 ([M + $NH4^+$] $C_{12}H_{17}NO_4S_2$ requires, 321.0937).

Synthesis of 5′-disulfide-modified oligonucleotides

Oligonucleotide synthesis was carried out on a standard support (1 μmol) on a Mermade 6 Nucleic Acid Synthesizer using standard phosphoramidite chemistry. The hexaethylene glycol (HEG) spacer was added to the sequence adjacent to the modification by addition of a Spacer-CE 18 (17-*O*-(4, 4′-dimethoxytrityl)-hexaethyleneglycol, 1-[(2-cyanoethyl)-(*N*,*N*-diisopropyl)]) phosphoramidite. The final base added to the sequence was a 5′-monomethoxytrityl protected amino modifier phosphoramidite. The final deblock step was omitted from the synthesis steps. Once synthesis was complete, 1 ml of deblock solution (3% trichloroacetic acid in DCM) was applied across the column and left for 1 h. The column was then washed with 1 ml of MeCN before being treated with a solution of the NHS ester, 1, in MeCN (10 mg ml⁻¹, triethylamine 1% (v/v) overnight. The column was washed again with 1 ml of MeCN before being treated with NH_4OH (30%, 1 ml) for 36 h at room temperature. The ammonium hydroxide was removed *in vacuo* at room temperature. The clear residue was resuspended in 1 ml distilled H_2O and purified by reversed-phase HPLC on a Dionex UVD170U detector fitted with a P680 pump through a Phenomenex Clarity column. Buffer A: TEAA (0.1 M, pH 7), Buffer B: MeCN; T = 0, 95% TEAA: 5% MeCN, with a gradient of 1% min⁻¹ B over 15 min and held at 20% B for 5 min at a flow rate of 1 ml/min. After HPLC purification the fractions were collated and concentrated *in vacuo* (room temperature) and redissolved in 1 ml distilled H_2O. All oligonucleotides are stored at 4 °C. HPLC analysis of 5′-thioctic acid-modified oligonucleotides indicated modification had occurred.

Synthesis of 5′-thiol-modified oligonucleotides

Oligonucleotide synthesis was carried out on a standard support (1 μmol). The synthesis was carried out on a Mermade 6 Nucleic Acid Synthesiser using standard phosphoramidite chemistry. The hexaethylene glycol (HEG) spacer was added to the sequence adjacent to the modification by addition of a Spacer-CE 18 (17-*O*-(4, 4′-dimethoxytrityl)-hexaethyleneglycol, 1-[(2-cyanoethyl)-(*N*,*N*-diisopropyl)]) phosphoramidite. The final base added to the sequence was a 5′-dimethoxytrityl protected thiol modifier phosphoramidite. The final deblock step was omitted from the synthesis steps. Once synthesis was complete, the oligonucleotide was removed from the CPG support by incubating in 1 ml of concentrated NH_4OH at 40 °C for 18 h. The ammonium hydroxide was removed *in vacuo* at room temperature. The clear residue was resuspended in 1 ml distilled H_2O and

204

the CPG removed using a 13 mm syringe filter. The oligonucle-otides were purified by reversed-phase HPLC on a Dionex UVD170U detector fitted with a P680 pump through a Phe-nomenex Clarity column. Buffer A: TEAA (0.1 M, pH 7), Buffer B: MeCN; T = 0, 95% TEAA: 5% MeCN, with a gradient of 1% min^{-1} B over 15 min and held at 20% B for 5 min at a flow rate of 1 ml/min. After HPLC purification the fractions were collated and concentrated *in vacuo* and redissolved in 1 ml distilled H$_2$O. To remove the dimethoxytrityl (DMT) group from the 5′-thiol-modifier, the water was evaporated *in vacuo* and the residue resuspended in TEAA (600 μl, 0.1 M, pH 7). AgNO$_3$ (90 μl, 1 M) was added and left at room temperature for 30 min. Dithio-threitol (DTT) (138 μl, 1 M) was added and the solution left at room temperature for 5 min. The solution was centrifuged at 7000 rpm for 10 min and the supernatant was recovered and set aside. The pellet was resuspended in TEAA (500 μl, 0.1 M, pH 7) and centrifuged again at 8000 rpm for 10 min. This procedure was repeated another two times and the three supernatants were combined into a single eppendorf tube and stored at 4 °C. HPLC analysis of 5′-thiol-modified oligonucleotides indicated modifi-cation had occurred.

Functionalization of nanoparticles with oligonucleotides

Preparation of gold nanoparticles. 15 nm gold (Au) nano-particles were prepared *via* citrate reduction of HAuCl$_4$. An aqueous solution of NaAuCl$_4$ (12.5 mM, 10ml) was added to distilled water (500 ml) and heated. Upon boiling, sodium citrate (25 mM, 10 ml) was added and the solution was left to stir for 15 min at boiling temperature.

Thioctic acid-modified oligonucleotides. An aliquot of purified oligonucleotide (1 ml, 10 μM) was added to Au (3 ml, 17 nM) colloid in a 5 ml glass vial. After 18 h, phosphate (NaH$_2$PO$_4$/Na$_2$HPO$_4$) buffer (60 mM) was added to 10 mM final concen-tration. NaCl (2 M) was then added at 18 h intervals, increasing the salt concentration by 0.05 M increments to a final concen-tration of 0.1 M. The oligonucleotide conjugates were then centrifuged at 7000 rpm for 20 mins and the pellet resuspended in phosphate buffered saline (1 ml, 10 mM phosphate/0.3 M NaCl) (PBS). The oligonucleotide-gold conjugates were stored in the dark at room temperature.

Thiol-modified oligonucleotides. Desalting of oligonucleotides was performed using a HiTrap (5 ml) size exclusion column on a Dionex UVD170U detector fitted with a P680 pump. An aliquot of desalted oligonucleotide (1 ml, 10 μM) was added to Au (3 ml, 17 nM) colloid in a 5 ml glass vial. After 18 h, phos-phate (NaH$_2$PO$_4$/Na$_2$HPO$_4$) buffer (60 mM) was added to 10 mM final concentration. NaCl (2 M) was then added at 18 h intervals, increasing the salt concentration by 0.05 M increments to a final concentration of 0.1 M. The oligonucleotide conjugates were then centrifuged at 7000 rpm for 20 min and the pellet resuspended in phosphate buffered saline (1 ml, 10 mM phos-phate/0.3 M NaCl). The oligonucleotide-gold conjugates were stored in the dark at room temperature.

Dye-labelling of oligonucleotide-nanoparticle conjugates. For both thioctic acid-modified and thiol-modified oligonucleotide-nanoparticle conjugates an aliquot (500 μl, 17–53 nM) of each conjugate was combined with a solution of either TAMRA iso-thiocyanate (TRITC) or malachite green isothiocyanate (MGITC) (500 μl, 1 μM). The solution was stored in the dark for 18 h then centrifuged at 7000 rpm for 20 min and the pellet resuspended in PBS (1 ml, 0.3M). The dye-labelled oligonucle-otide-gold conjugates were stored in the dark at room temperature.

Results and discussion

SERS has been established as a powerful technique for the sensitive detection of DNA in a variety of assay formats.[20-28] In order to use SERS in more complex diagnostic assays the oligonucleotide-nanoparticle conjugates must be stable in increasingly challenging environments. For oligonucleotide-nanoparticle conjugates to be SERS active an appropriate dye label must be incorporated, typically in the form of an iso-thiocyanate fluorophore. To date, the effect on the stability of the conjugate systems by the inclusion of a simple dye has not been investigated. This study shows the improved stability of SERS active oligonucleotide-nanoparticle conjugates that will allow for their use in a wider variety of conditions.

Synthesis of thioctic acid and thiol-modified oligonucleotides

The active ester of thioctic acid, **1**, was synthesized using a previously reported method.[12] In contrast to the DNA modi-fication reported previously, where the thioctic acid NHS ester was conjugated to the 3′ terminus of the oligonucleotide *via* an amino-modified solid support, we report the 5′ terminus modi-fication of oligonucleotides with thioctic acid. The oligonucleo-tide synthesis was carried out using standard phosphoramidite chemistry where the final monomer added to the sequence was a 5′-MMTr-amino-modified phosphoramidite. After synthesis, an extended deblock step (1 h) was manually performed with standard deblock solution in order to remove the final mono-methoxytrityl group. The active ester of thioctic acid was added to the CPG in acetonitrile with triethylamine and left overnight. The CPG was then treated with ammonium hydroxide for 16 h at room temperature in order to cleave the oligonucleotide from the solid support and remove the protecting groups.

Six oligonucleotide sequences were prepared, three sequences with a 5′ thioctic acid modification and three sequences with a 5′ thiol modification (Table 1). In addition to the 5′ terminal modifications of the oligonucleotides, different spacer groups were incorporated adjacent to the modification to asses how each contributed to the stability of the resulting oligonucleotide-nanoparticle conjugates. Spacer groups are an important addi-tion to oligonucleotide probe design as they move the recognition sequence further from the nanoparticle surface to ensure there is no steric crowding of the sequence during hybridization of a complementary target. The three spacer groups chosen were a 10 adenine nucleobase spacer, a hexaethylene glycol (HEG) spacer, and a spacer containing 3 HEG units. Oligonucleotide sequences containing an A$_{10}$ spacer group are more likely to lie on the nanoparticle surface compared to other nucleotide-con-taining spacer groups,[29] while spacers containing ethylene glycol moieties have been shown to improve oligonucleotide loading

205

Table 1 List of modifications and spacer compositions for oligonucleotide sequence

Probe Name	5′ Modification	Spacer Composition	Sequence
Probe1 (P1)	Thioctic Acid	10 Adenine (10A)	ATGGCATGAGTAACGAAGAATA
Probe2 (P2)	Thioctic Acid	HEG	ATGGCATGAGTAACGAAGAATA
Probe3 (P3)	Thioctic Acid	(HEG)₃	ATGGCATGAGTAACGAAGAATA
Probe4 (P4)	Thiol	10A	ATGGCATGAGTAACGAAGAATA
Probe5 (P5)	Thiol	HEG	ATGGCATGAGTAACGAAGAATA
Probe6 (P6)	Thiol	(HEG)₃	ATGGCATGAGTAACGAAGAATA

onto the nanoparticle surface, compared to nucleotide-containing spacer groups.[17] This is due to the absence of electrostatic repulsion between neighbouring ethylene glycol moieties and decreased interactions between the ethylene glycol and the gold surface.

Oligonucleotide-nanoparticle functionalisation and stability studies

The modified oligonucleotide sequences were immobilized onto the surface of Au nanoparticles following the incremental elevation of the NaCl concentration. NaCl facilitates the adsorption of more oligonucleotides onto the nanoparticle surface by minimizing inter strand repulsion between neighbouring oligonucleotides. It is important to control the concentration of NaCl when making oligonucleotide-nanoparticle conjugates as raising the concentration too rapidly can lead to irreversible aggregation of the nanoparticles. In this respect, the salt concentration was added over 2 days with 0.05 M increments to a final concentration of 0.1 M in order to maintain nanoparticle stability.

In order to assess their stability, the nanoparticle conjugates of P1, P2, P3, P4, P5 and P6 were treated with DTT (10 mM final concentration) at a temperature of 37 °C and monitored using UV-Vis spectroscopy. For thioctic acid-modified oligonucleotide gold nanoparticle conjugates, scans were obtained at 10 min intervals, while scans for thiol-modified oligonucleotide gold nanoparticle conjugates were obtained at 1 min intervals. Spectra of the conjugates treated with DTT are shown in Fig. 1. By comparing the spectra in Fig. 1, the difference in stability of the

two oligonucleotide linker modifications can be clearly observed. Fig. 1a shows the enhanced stability of the thioctic acid modification over the thiol modification as each line in the spectrum represents a scan taken at 10 min intervals compared to scans taken at 1 min intervals in Fig. 1b. With gold nanoparticles, as aggregation occurs, there is a distinct disappearance of the plasmon band at ∼520 nm and an emergence of a new plasmon band between ∼600 and 700 nm.

In order to get a clear indication of the stability of the system, the absorbance at a particular wavelength (675 nm; indicative of nanoparticle aggregation) can be plotted against time. Fig. 2 shows the absorbance at 675 nm against time for P1-Au, P2-Au, P3-Au, P4-Au, P5-Au and P6-Au. Fig. 2a shows the thioctic acid-modified oligonucleotide gold nanoparticle conjugates plotted together so the effect of the different spacer groups can be observed. The same is shown in Fig. 2b for the thiol-modified oligonucleotide gold nanoparticle conjugates.

By comparing the half-lives of the gold nanoparticle conjugates (Table 2) the difference in the stability of the different systems is obvious. The Au-thiol systems have reached the halfway point of full aggregation in approximately half a minute and reached total aggregation in less than 2 min even with the HEG spacer units, which were incorporated in the sequence to increase the stability of oligonucleotides. For Au-thioctic acid systems the half-lives were considerably longer at 80, 150 and 100 min for P1-Au, P2-Au and P3-Au, respectively and total aggregation was not achieved until after 4 h. This result confirms the enhanced stability of the thioctic acid-modified oligonucleotide gold nanoparticle conjugates over the thiol-modified conjugate systems for both nucleotide and ethylene glycol spacers. It also
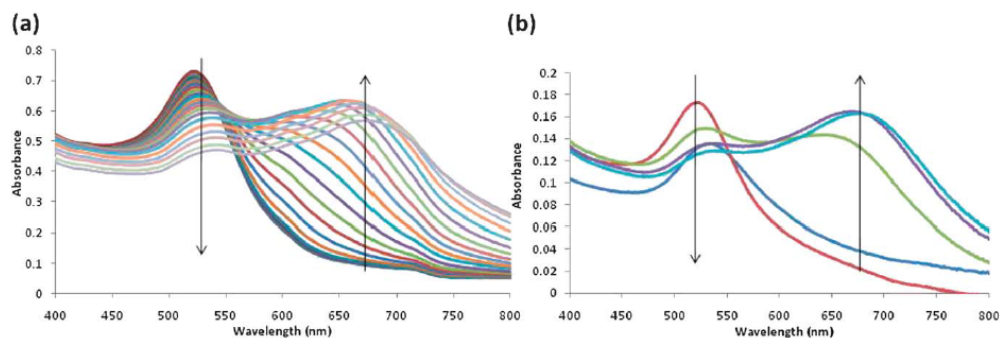

Fig. 1 UV-Vis spectra showing aggregation upon treatment with 10 mM DTT of (a) thioctic acid-modified Au conjugates at 10 min intervals and (b) thiol-modified Au conjugates at 1 min intervals. Arrows indicate the change in spectra with time.
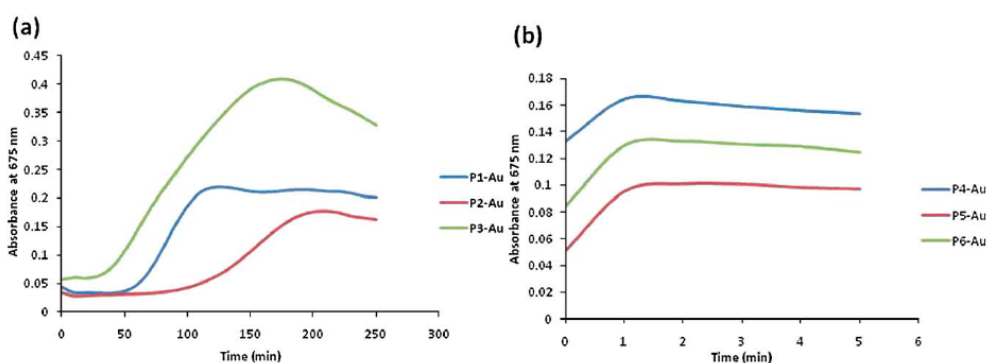
206

Fig. 2 Absorbance at 675 nm against time for (a) thioctic acid-modified oligonucleotide gold nanoparticle conjugates and (b) thiol-modified oligonucleotide gold nanoparticle conjugates.

Table 2 Half-lives of Au-oligonucleotide nanoparticle conjugates

Probe Name	Non-dye labelled Conjugate $T_{1/2}$ (min)	TAMRA labelled Conjugates $T_{1/2}$ (min)	Malachite Green Labelled Conjugates $T_{1/2}$ (min)
P1-Au	80	290	60
P2-Au	150	200	220
P3-Au	100	180	220
P4-Au	0.5	15	35
P5-Au	0.5	15	25
P6-Au	0.5	20	25

shows that although ethylene glycol units have been reported as increasing surface coverage this does not translate to an increase in stability in the thiol system.

Dye-labelled oligonucleotide-nanoparticle functionalisation and stability studies

The dye-labelling of the nanoparticle surface occurs post-oligonucleotide functionalisation. When the oligonucleotides were immobilized onto the nanoparticle surface, the conjugate solution was incubated with an aqueous solution of the SERS-active dye, in this case TAMRA isothiocyanate (TRITC) and malachite green isothiocyanate (MGITC) were used according to previously reported methods.[23,24] The dye label binds to the nanoparticle surface through the isothiocyanate moiety (–N=C=S).[30] Labelling the nanoparticle surface post-oligonucleotide functionalisation means that the nanoparticles are already stabilized by the steric and electrostatic protection from adjacent oligonucleotides and are therefore more amenable to further modification.

The TRITC-labelled and MGITC-labelled oligonucleotide gold nanoparticle conjugates were subjected to the same DTT treatment as reported for the non-labelled conjugates. By comparing the half-lives of the non-dye and dye labelled conjugates there is a clear increase in stability (Table 2). The thioctic acid-modified Au conjugates now exhibit further stability when the dye label is functionalized to the nanoparticle surface. A particularly interesting observation is the increase in stability associated with the thiol-modified Au conjugates. The half-lives for the TAMRA-labelled thiol-modified oligonucleotide Au
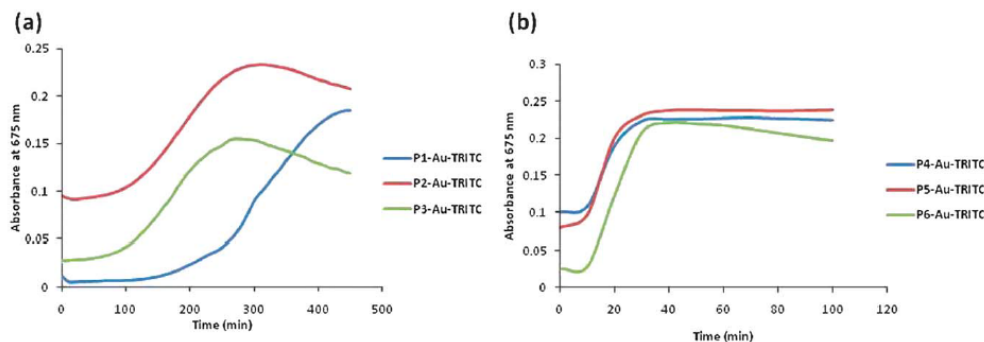

Fig. 3 Absorbance at 675 nm against time for TAMRA isothiocyanate-labelled (a) thioctic acid-modified gold nanoparticle conjugates and (b) thiol-modified oligonucleotide gold nanoparticle conjugates.

207

Fig. 4 Absorbance at 675 nm against time for Malachite Green isothiocyanate-labelled (a) thioctic acid-modified gold nanoparticle conjugates and (b) thiol-modified oligonucleotide gold nanoparticle conjugates.
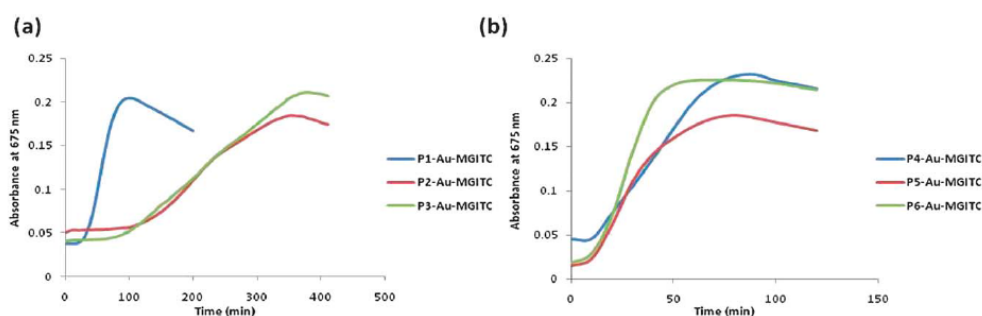
nanoparticle conjugates are now 15, 15, and 20 mins for P4, P5 and P6, respectively. Similarly, for Malachite Green-labelled thiol-modified oligonucleotide Au nanoparticle conjugates the half-lives are now 35, 25 and 25 mins for P4, P5 and P6, respectively. This is in stark contrast to the half-lives obtained in the absence of dye labelling. The absorbance *versus* time graphs of P4-Au, P5-Au and P6-Au for both TRITC and MGITC (Fig. 3b and Fig. 4b, respectively) now exhibit an initial period of sustained stability of approximately 10 min, similar to the graphs observed for thioctic acid Au conjugates (Fig. 2a). This shows that Au conjugate stability can be enhanced for both thiol and thioctic acid modified oligonucleotides simply by the addition of an isothiocyanate dye label. This is significant as thiol modified oligonucleotides are readily obtained but can now be coupled with a single post-conjugation step for enhanced stability. In addition, for SERS detection strategies increasingly challenging environments can now be investigated with the stable conjugate systems reported here.

In order to confirm that the dye-labelled oligonucleotide-nanoparticle conjugates were SERS active, an analysis of the conjugates was performed. Fig. 5 shows the SERS spectrum of MGITC labelled thioctic acid-HEG modified oligonucleotide-nanoparticle conjugates. The characteristic peaks relating to malachite green can be clearly observed with a remarkably low RSD of only 2.6% indicating their suitability for further more complex bionanosensing applications.

Storage stability of nanoparticle conjugates

It was observed that non-dye labelled nanoparticle conjugates can remain stable for up to 6 months. Conjugates containing a polyA spacer group irreversibly aggregate first, while conjugates with a HEG spacer group remain stable for weeks after the polyA-containing conjugates have aggregated. However, when the conjugate was functionalized with a dye label, the long-term stability was reduced further. The polyA conjugates aggregate after approximately a week, while the HEG conjugates can remain stable for up to 3 months. This observation further indicates the advantage of incorporating a HEG spacer group into the oligonucleotide design to aid the stability of nanoparticle conjugates.

Dye-labelled oligonucleotide-nanoparticle conjugates hybridization

It was important to confirm the retention of the biological integrity of the DNA probe sequences post-functionalisation. Fig. 6 shows the characteristically sharp T_m melting profile of MGITC functionalized thioctic acid-HEG gold nanoparticle conjugates obtained from hybridization to a fully complementary oligonucleotide sequence monitored at the absorbance maxima of gold nanoparticles (520 nm). Two batches of gold
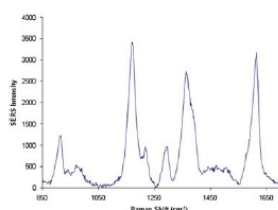

Fig. 5 Typical SERS spectrum of MGITC labelled thioctic acid-HEG modified oligonucleotide-nanoparticle conjugates (0.5 nM) recorded on a Renishaw System 2000 Raman Spectrometer, with 633 nm wavelength, ×20 obj, 10 s scan time, 1 accumulation and 100% power.
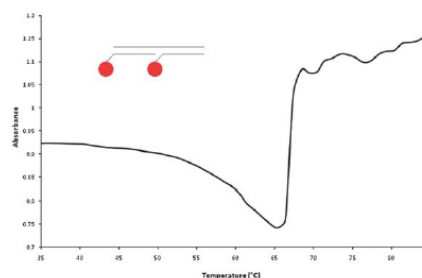

Fig. 6 Melting profile of MGITC thioctic acid–HEG oligonucleotide functionalized gold nanoparticles hybridized with a fully complementary sequence in a sandwich assay format monitored at 520 nm.

208

nanoparticles were functionalized with different, non-complementary thioctic acid-HEG modified oligonucleotide sequences and functionalized with MGITC. Both probes were hybridized to an unmodified complementary oligonucleotide sequence. This demonstrates the efficacy of the dye labelled oligonucleotide gold nanoparticle conjugates and their potential to be used in DNA detection.

Conclusions

In conclusion, the results show that oligonucleotide nanoparticle conjugates of improved stability can be easily prepared by the inclusion of a simple isothiocyanate dye compound. The results have demonstrated the versatility of the dye labelled oligonucleotide nanoparticle conjugates, with increased stability observed for both thioctic acid modified sequences and the more commonly used thiol modification. The spacer composition appears to have an effect on the stability of the conjugate system, with increases in stability observed for oligonucleotides containing a single HEG spacer group. Importantly, the spacer group and dye do not adversely affect the bio-activity of the DNA of the conjugate. The work undertaken here indicates that a suitable oligonucleotide nanoparticle conjugate system can be prepared that will show enhanced stability in environments that would not normally be considered to be ideal conditions for nanoparticle conjugates, opening more opportunities for nanoparticle conjugates to be used in DNA detection assays. The inclusion of a dye label on the metal surface also makes these systems amenable to SERS analysis.

Acknowledgements

Notes and references

1 C. A. Mirkin, R. L. Letsinger, R. C. Mucic and J. J. Storhoff, *Nature*, 1996, **382**, 607–609.
2 A. P. Alivisatos, K. P. Johnsson, X. G. Peng, T. E. Wilson, C. J. Loweth, M. P. Bruchez and P. G. Schultz, *Nature*, 1996, **382**, 609–611.
3 J. J. Storhoff, R. Elghanian, R. C. Mucic, C. A. Mirkin and R. L. Letsinger, *J. Am. Chem. Soc.*, 1998, **120**, 1959–1964.
4 J. Li, S. Song, D. Lib, Y. Suc, Q. Huang, Y. Zhao and C. Fan, *Biosens. Bioelectron.*, 2009, **24**, 3311–3315.
5 J. J. Storhoff, A. D. Lucas, V. Garimella, Y. B. Bao and U. R. Müller, *Nat. Biotechnol.*, 2004, **22**, 883–887.
6 F. McKenzie, K. Faulds and D. Graham, *Chem. Commun.*, 2008, 2367–2369.
7 H. B. Shen, M. Hu, Y. B. Wang and H. Q. Zhou, *Biophys. Chem.*, 2005, **115**, 63–66.
8 H. B. Shen, M. Hu, Z. N. Yang, C. Wang and L. Z. Zhu, *Chin. Sci. Bull.*, 2005, **50**, 2016–2020.
9 Z. Li, R. C. Jin, C. A. Mirkin and R. L. Letsinger, *Nucleic Acids Res.*, 2002, **30**, 1558–1562.
10 R. L. Letsinger, R. Elghanian, G. Viswanadham and C. A. Mirkin, *Bioconjugate Chem.*, 2000, **11**, 289–291.
11 J. S. Lee, A. K. R. Lytton-Jean, S. J. Hurst and C. A. Mirkin, *Nano Lett.*, 2007, 7, 2112–2115.
12 J. A. Dougan, C. Karlsson, W. E. Smith and D. Graham, *Nucleic Acids Res.*, 2007, 35, 3668–3675.
13 X. M. Qian, X. Zhou and S. M. Nie, *J. Am. Chem. Soc.*, 2008, **130**, 14934.
14 S. A. Claridge, H. Y. W. Liang, S. R. Basu, J. M. J. Frechet and A. P. Alivisatos, *Nano Lett.*, 2008, **8**, 1202–1206.
15 W. T. Zhao, L. Lin and I. M. Hsing, *Bioconjugate Chem.*, 2009, **20**, 1218–1222.
16 W. Y. Zhao, L. Lin and I. M. Hsing, *Langmuir*, 2010, **26**, 7405–7409.
17 S. J. Hurst, A. K. R. Lytton-Jean and C. A. Mirkin, *Anal. Chem.*, 2006, **78**, 8313–8318.
18 Y. B. Zu and Z. Q. Gao, *Anal. Chem.*, 2009, **81**, 8523–8528.
19 J. Sharma, R. Chhabra, H. Yan and Y. Liu, *Chem. Commun.*, 2008, 2140–2142.
20 D. Graham, R. Stevenson, D. G. Thompson, L. Barrett, C. Dalton and K. Faulds, *Faraday Discuss.*, 2011, **149**, 291–299.
21 D. Graham, D. G. Thompson, W. E. Smith and K. Faulds, *Nat. Nanotechnol.*, 2008, **3**, 548–551.
22 D. G. Thompson, K. Faulds, W. E. Smith and D. Graham, *J. Phys. Chem. C*, 2010, **114**, 7384–7389.
23 F. McKenzie and D. Graham, *Chem. Commun.*, 2009, 5757–5759.
24 F. McKenzie, K. Faulds and D. Graham, *Nanoscale*, 2010, **2**, 78–80.
25 K. Faulds, R. Jarvis, W. E. Smith, D. Graham and R. Goodacre, *Analyst*, 2008, **133**, 1505–1512.
26 D. Graham, B. J. Mallinder, D. Whitcombe and W. E. Smith, *ChemPhysChem*, 2001, **2**, 746.
27 A. MacAskill, D. Crawford, D. Graham and K. Faulds, *Anal. Chem.*, 2009, **81**, 8134–8140.
28 J. A. Dougan, D. MacRae, D. Graham and K. Faulds, *Chem. Commun.*, 2011, **47**, 4649.
29 L. M. Demers, M. Ostblom, H. Zhang, N. H. Jang, B. Liedberg and C. A. Mirkin, *J. Am. Chem. Soc.*, 2002, **124**, 11248–11249.
30 W. E. Doering and S. Nie, *Anal. Chem.*, 2003, 75, 6171–6176.

209

Combining functionalised nanoparticles and SERS for the detection of DNA relating to disease

Duncan Graham,* Ross Stevenson, David G. Thompson, Lee Barrett, Colette Dalton and Karen Faulds

DNA functionalised nanoparticle probes offer new opportunities in analyte detection. Ultrasensitive, molecularly specific targeting of analytes is possible through the use of metallic nanoparticles and their ability to generate a surface enhanced Raman scattering (SERS) response. This is leading to a new range of diagnostic clinical probes based on SERS detection. Our approaches have shown how such probes can detect specific DNA sequences by using a biomolecular recognition event to 'turn on' a SERS response through a controlled assembly process of the DNA functionalised nanoparticles. Further, we have prepared DNA aptamer functionalised SERS probes and demonstrated how introduction of a protein target can change the aggregation state of the nanoparticles in a dose-dependant manner. These approaches are being used as methods to detect biomolecules that indicate a specific disease being present with a view to improving disease management.

1 Introduction

The development of new techniques capable of providing useful diagnostic or clinical markers is an area of research growth. Issues of cost, both of consumables and equipment, ease of use and robustness dominate the uptake of use of any new technologies. However, the advent of new instrumentation coupled with complex optics are leading to new, more sensitive diagnostic techniques capable of providing a genuine clinical benefit. Here we report on how we use metal nanoparticles to detect specific DNA sequences when combined with SERS.

Coinage metal nanoparticles (1–100 nm) have been used as both delivery vehicles for biomolecular uptake into cells and as detection probes for a variety of targets. They are easily synthesised by a variety of methods, can be stored long-term and consequently have low associated costs. Gold[1,2] and silver[3] are the most commonly used nanoparticles and their small size (comparable to mid-large proteins) leads to unique physical characteristics not observed with bulk materials or molecular salts.[4–6] Nanoparticles are stable, have a large surface area to mass ratio, can be functionalised with a choice of ligands, and their optical brightness and massive scattering efficiency makes them ideally suited for *in vitro* and *in vivo* applications.[7,8] The characteristic colour of gold and silver nanoparticle suspensions is due to the localised surface plasmon resonance (LSPR) of the cloud of electrons associated with the surface of the nanoparticle. The absorbance maximum of the LSPR of a colloidal suspension is dependant upon a range of factors including the metal

Centre For Molecular Nanometrology, WestCHEM, Department of Pure and Applied Chemistry, University of Strathclyde, 295 Cathedral Street, Glasgow, UK G1 1XL. E-mail: duncan.graham@strath.ac.uk

210

used, size, shape, and the dielectric constant of the medium.[4] The LSPR is also dependant upon the aggregation state of the nanoparticles with larger aggregates red-shifting the LSPR band and leading to spectroscopic (Raman/SERS) and visual colour changes. SERS is an optical spectroscopic technique that provides molecularly specific fingerprints directly related to the vibrational and stretching modes of a target analyte. Developed in 1974, it offers researchers a significant advancement over conventional Raman spectroscopy with sensitivity typically 10^6 greater than the classical technique.[9] Raman spectroscopy is an inherently weak process relying on the collection of inelastically scattered photons. With an estimated 1 in every 10^8 photons scattered inelastically, the technique requires large, expensive equipment and is predominantly a fringe technique. The observation that adsorption of the analyte on a roughened metallic surface leads to significant signal enhancement led to a renaissance in Raman spectroscopy and the technique is now accepted as one of the most sensitive and specific detection methods available. Use of gold and silver nanoparticles in SERS has been extensively studied and enhancement of the Raman signal due to the interaction between the surface adsorbed analyte and the LSPR of the nanoparticle. Further enhancement can be achieved by the controlled formation of electromagnetic 'hot spots' between 2 or more aggregated nanoparticles.[10] SERS gives rise to exquisite sensitivity with single molecule detection reported.[11] Further, SERS offers excellent opportunities in the detection of multiple analytes as the narrow, sharp, fingerprint spectra lend themselves to a multicomponent detection technique.[12–14]

Gold and silver nanoparticles can be functionalised with a range of chemical moieties, commonly achieved by coupling surface atoms to a thiol group. Oligonucleotide-gold nanoparticle (OGN)[15,16] and oligonucleotide-silver nanoparticle (OSN)[17,18] conjugates provide robust and versatile detection systems. Synthesis of OGN and OSN conjugates is relatively simple. A thiol-modified oligonucleotide is introduced to a suspension of gold or silver nanoparticles and is salt aged over a short period (2–48 h). When oligonucleotide-nanoparticle conjugates are used for detection, two different methodologies can be applied: (1) using the nanoparticle as a label for an analyte of interest and (2) inducing the assembly of the nanoparticles to create a measurable visual or spectroscopic response.

Nanoparticle assembly can be controlled to such an extent that a biological interaction, such as DNA hybridisation, can be detected by the changes caused in the LSPR.[19,20] An assembly-based assay using OGN or OSN conjugates typically uses two batches of nanoparticle probes functionalised with different, non-complementary oligonucleotides. Addition of a target sequence, complementary in part to both conjugates, can cause hybridisation to occur. The nanoparticle assembly ensures individual nanoparticles are brought into close enough proximity to red-shift the LSPR band and allow DNA detection solely through colorimetry

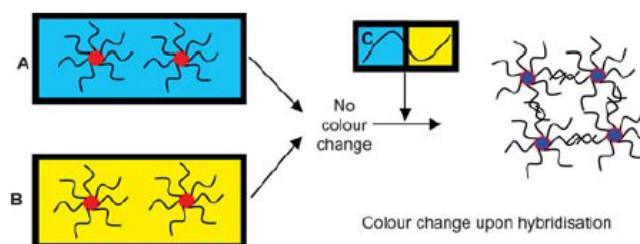**Fig. 1** Schematic representation of an OGN/OSN conjugate assay. Nanoparticle conjugates functionalised with two different, non-complementary oligonucleotides (A + B) hybridize upon addition of target oligonucleotide (C). The molecular recognition event and the formation of structured nanoparticle assemblies cause a visual colour change in the nanoparticle suspension.

This journal is © The Royal Society of Chemistry 2011

211

(Fig. 1). OGN and OSN conjugates have been used to detect a wide variety of biologically relevant targets including genomic DNA,[21] bacterial DNA,[22] and duplex and triplex binding sequences[23] and have been coupled with optical,[24] electrochemical[25] and vibrational[26] detection systems.

Protein detection is also possible using OGN conjugates in the form of an aptamer sequence adsorbed to the nanoparticle surface. Aptamers are nucleic acid ligands selected to bind a target molecule with high selectivity and specificity. Typically short sequences of both ssDNA and RNA of 20–80 nucleotides ($\sim$6–26 kDa) have been successfully selected to interact with a range of analytes including proteins, peptides and small molecules. Aptamers form unique tertiary folded structures that present grooves and clefts capable of binding targets with affinities that often rival if not surpass an antibody alternative. First developed in 1990,[27,28] most aptamers are selected using the 'systematic evolution of ligands by exponential enrichment' (SELEX) process. SELEX is a reiterative amplification technique that screens a starting library of up to 10^{15} unique sequences to a final optimized pool of 10–100 candidates. The real strengths of the technique stem from the diversity of the starting pool, which can lead to highly sensitive aptamers being selected with extremely high specificity. An example being the ability of a theophylline aptamer to molecularly discriminate between its target and caffeine.[29] These small molecules differ by a single methyl group, and the theophylline aptamer has a greater than 10 000-fold preference for its target over caffeine.[29]

The properties of aptamers are commonly compared to antibodies due to their molecular targeting abilities. Both species can be used for sensitive and specific detection though aptamers have a number of further advantages over antibody alternatives. Aptamers are selected with a relatively easy and effective selection technique. Once selected, they can be reproduced in sizeable amounts using fast, cheap synthetic approaches with little batch to batch variability and where simple, diverse modifications are possible. Further advantages include their relatively small size, their low toxicity and their slow degradation kinetics compared to any protein-based alternative. A sign of their success and potential as clinical drug candidates can be illustrated in that in less than two decades since their introduction to the scientific community, the FDA approved pegaptanib (or Macugen®, marketed by Pfizer) as an aptamer drug for use in the treatment of age-related macular degeneration (AMD).[30] More recently, researchers have looked to functionalize nanoparticles with DNA and aptamer sequences.

Aptamer functionalised nanoparticles have been reported for a diverse range of targets including prostate specific membrane antigen (PSA),[31] platelet derived growth factor (PDGF),[32] and cocaine.[33] The cocaine aptamer is specially noteworthy as it utilises a unique 'reverse molecular beacon' approach. In the absence of target, the aptamer adopts an almost linear conformation. Addition of target causes the aptamer to fold around the drug and brings the 3′ end of the oligonucleotide into close contact with the surface of the nanoparticle. When the 3′ end is functionalised with a fluorescent dye, the conformational change on binding switches on the SERS and the cocaine can be detected by the SERS signal.

Here we show the development of oligonucleotide-nanoparticle conjugates with enhanced stability for the assembly-based detection of the *mecA* gene of methicillin-resistant *Staphylococcus aureus* (MRSA) and the use of aptamer functionalised nanoparticles and SERS for the detection of thrombin.

2 Results and discussion

Development of a MRSA detection oligonucleotide-nanoparticle system

Functionalised nanoparticles offer excellent opportunities as SERS active DNA probes. SERS from both OGN and OSN conjugates has been used to detect specific oligonucleotide sequences at low concentrations (Fig. 2).[34–37]
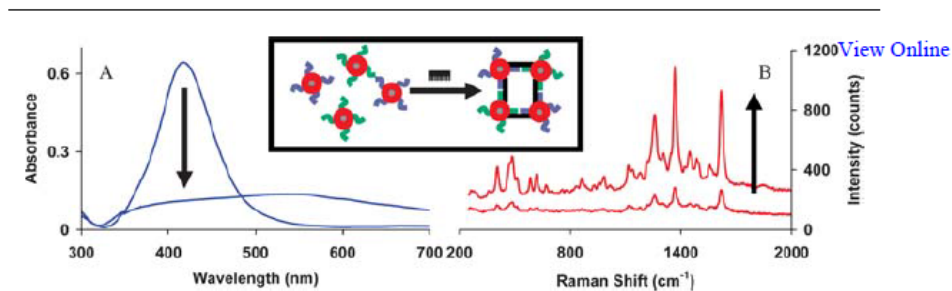
212

View Online

Fig. 2 SERS and LSPR analysis of sequence specific DNA nanoparticle probes. Combined diagram showing the simultaneous decrease in LSPR (A) and increase in SERS intensity (B) caused by the hybridisation of dye-coded DNA functionalised silver nanoparticles to an unmodified complementary target oligonucleotide (inset).

The first approach used dye-coded oligonucleotide-silver nanoparticle (DOSN) conjugates to detect an unmodified target oligonucleotide.[34] Two batches of silver nanoparticles were coated with different surface-seeking Raman reporter molecules.[38] Each batch was then functionalised with probe oligonucleotides non-complementary to each other, yet antisense to half a target sequence. When exposed to the target, the probe sequences hybridise, causing aggregation of the nanoparticles, changing the LSPR and increasing the intensity of the SERS response. Initial work discriminated between targets that were either fully complementary or non-complementary, but this was later refined to discriminate single base mismatches in the target sequence at room temperature.[39] Although performed using model sequence oligonucleotides, it was assumed that extending this system to sequences of interest would present no significant problem. However, attempts to move to biologically relevant targets found that far from being universally suited to all sequences, the stability and ability of the conjugates was found to be highly dependant on the sequence used. Short-term and long-term conjugate stability is vital for a successful assembly-based assay; short-term stability to ensure a robust control as the response from any non-complementary sequence should not change and long-term stability to ensure repeatable results over time. The reasons assumed for the
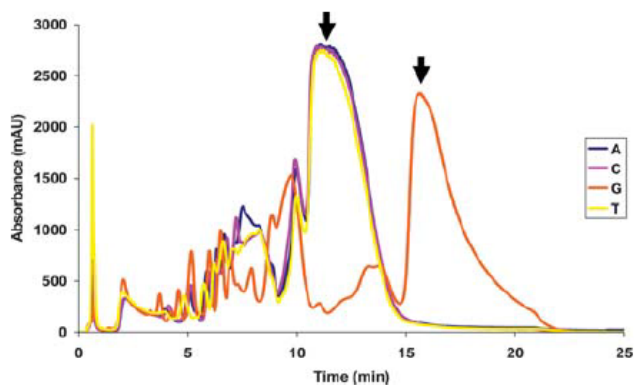
Fig. 3 HPLC analysis of four synthetic oligonucleotides that differ by a single base. The traces of the final synthesis products (designated with arrows) of four thiol-modifed oligonucleotide sequences from their failure sequences are illustrated. The sequences were (5′–3′): A, thiol-AAAAAAAAAAGGACAACCT; C, thiol-AAAAAAAAAAGGACCACCT; G, thiol-AAAAAAAAAAGGACGACCT; T, thiol-AAAAAAAAAAGGACTACCT. Note that the sequences only differed by a single base. The ten adenine bases act as a 'tether', distancing the sequence of interest from the nanoparticle surface, minimising any steric effects that could affect hybridisation efficiency.

213

sequence dependence are varied. Sequences that contain a high degree of self-complementarity are unsuitable as the conjugates self-hybridise. Sequences that take some form of secondary structure can also be unsuitable (shown in Fig. 3).

Fig. 3 contains the HPLC traces from the purification of four oligonucleotide sequences that differ only by a single base. Traces were obtained using ion-exchange chromatography, separating DNA sequences based upon the number of negatively charged phosphate residues present. The data indicates that the sequence containing guanine at the midpoint is retained longer than the others and suggests formation of a secondary structure or the possible incorporation of a second oligonucleotide. Significantly, oligonucleotide-nanoparticle conjugates could be successfully created using all except that sequence containing the mid-point guanine. This issue suggests applications that require specific sequences for disease detection may need further surface stabilisation or passivation to enable a SERS probe to work to the best of its ability. The secondary-structure dependence could also impact the creation of ap-tamer-nanoparticle conjugates which can form highly convoluted structures.

For this reason we have undertaken extensive research to define suitable sequences as well as developing a new, more stable form of oligonucleotide attachment. Although linkers containing multiple thiol groups can be used to improve the stability of oligonucleotide-nanoparticle conjugates, 5′ mono-thiol oligonucleotides are currently the easiest, cheapest and therefore most commonly used approach for the attachment of DNA to a nanoparticle. Multiple thiol attachment groups have been shown to greatly increase the stability of OGN and OSN conjugates to higher salt concentrations, displacement molecules and high temperatures.[17,40,41] Our developments have led to the commercialisation of multiple thiol anchor groups based on thioctic acid.[41] In that particular study model sequences of both OGN and OSN conjugates were used throughout. Fig. 4 shows the absorbance data from OGN conjugates created using single- or dual-thiol attachments. The approach is significant as it used a sequence complementary to part of the *mecA* gene of MRSA, a relevant biological target.

Fig. 4 also illustrates the stability of OGN conjugates when treated with DTT, a small molecule that displaces thiol moieties from the nanoparticle surface. Fig. 4A and 4B compare the increase in absorbance at 675 nm over time and
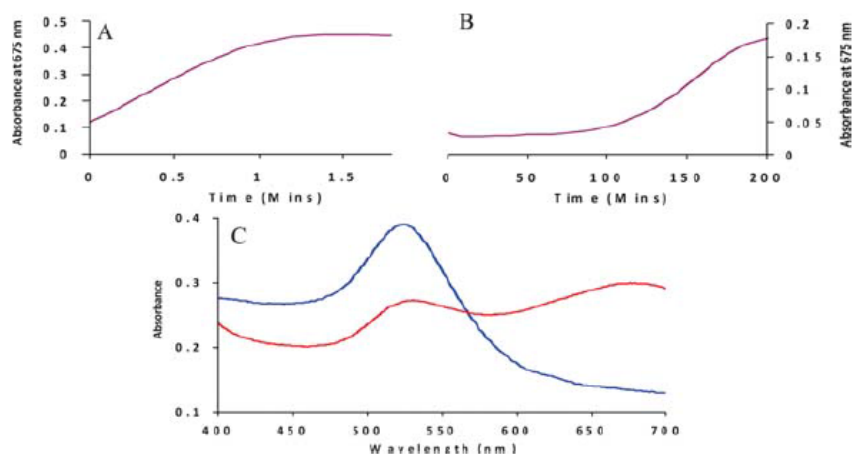
Fig. 4 Analysis of thiol-nanoparticle stability. UV/vis absorbance analysis of oligonucleotide probe conjugates before and after the addition of dithiothreitol (DTT). The absorbance of mecA-OGN conjugates monitored at 675 nm with (A) monothiol attachment and (B) multiple thiol attachment after the addition of DTT. The UV-Vis spectra of OGN conjugates (C) before (blue) and after (red) the addition of DTT. Note the formation of a second maximum at 675 nm.

214

correspond to the aggregation of the nanoparticles. The data indicates the mono-thiol attachment is displaced much quicker than the dithiol anchor thus providing a less stable linker molecule. Conjugates created with thioctic acid, containing the *mecA* complement sequence, were more stable than those created with the single thiol attachment This shows that surface attachment chemistry is crucial in producing probes suitable for use in diagnostic applications.

Development of a thrombin nanosensor

As demonstrated with the *mecA* OGNs, nanoparticles offer facile, robust and specific SERS detection platforms. DNA-DNA interactions are well studied and the sense-antisense attraction provides researchers an excellent platform to aggregate nanoparticles. Less well studied are DNA-protein interactions and specifically the use of aptamer-functionalised nanoparticles as a sensitive protein detection assay. Our approach looked at the feasibility of using aptamer-functionalised nanoparticles to detect thrombin. Thrombin protein plays a key role in homeostasis, as well as regulating many inflammation processes and aiding tissue repair.[42] In blood, thrombin is typically found at low-nanomolar levels, whereas significantly lower levels can often be indicative of a blood coagulation abnormality. The thrombin aptamer was one of the earliest published, and is one of the most studied DNA aptamers.[42] X-Ray crystallographic analysis of the DNA 15-mer interacting with the protein found that the aptamer forms a G-quartet, stabilized by Hoogstein hydrogen bonding.[43] The Bock aptamer[42] interacts at two distinct regions on the thrombin molecule, the fibrinogen exosite and the heparin binding site.[44] Here we show how the LSPR and Raman enhancement effects observed when nanoparticles are brought into close proximity can be exploited by using SERS active silver nanoparticles functionalized with thrombin DNA aptamers.

Mixed monolayer Raman nanoparticle probes were prepared using the same method as DOSN conjugates but with a 5′ thiol-modified version of the Bock aptamer (5′ - (thiol) TTT TTT TTT TTT TTT GGT TGG TGT GGT TGG). Thrombin was added to the colloidal suspension and UV spectra were recorded periodically over a 90 min period (shown in Fig. 5A). The data indicates that molecular recognition by the aptamer probes induces a change in the LSPR. This suggests that the aptamers remain functional when adsorbed to the nanoparticle surface. SERS analysis was then performed to observe the Raman signal from probes in the presence and absence of thrombin (Fig. 5B). Although both spectra look similar, the subtle change in peak intensities is indicative of nanoparticle aggregation. Further,
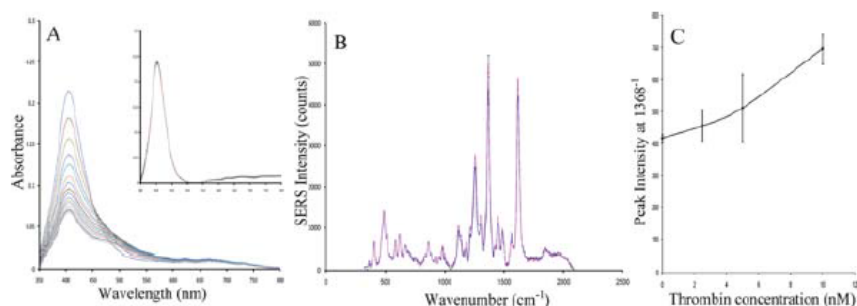
Fig. 5 Aptamer functionalised nanoparticles to detect thrombin. The UV-Vis data (A) and SERS analysis (B) of a thrombin aptamer adsorbed to a SERS nanoparticle binding to target, and SERS thrombin concentration study (C). The UV data shows the incremental decline in adsorption as nanoparticle aggregates form over a 90 min period (the inlayed figure shows the control with no thrombin added). SERS analysis shows the increase in SERS in the presence (pink) and absence of thrombin (blue). Figure C shows the effect of thrombin concentration on the change in intensity of the peak at 1368 cm^{-1}.

215

a concentration-dependant Raman response was observed (Fig. 5C) where the peak height increases with an increase in concentration of added thrombin. Comparison of DNA and thrombin detection using DOSN conjugates show that the magnitude of the response for unmodified oligonucleotide and protein are quite different, with the oligonucleotide detection yielding a much greater change in intensity (Fig. 2 and Fig. 5B). The recognition of the protein shows a modest SERS response which is probably due to the large size of the thrombin. This means that although active and bound to the target, the aptamer nanoparticles may be too far apart to allow a plasmon overlap, hindering electromagnetic SERS enhancement and leading to the modest SERS improvements over the monodisperse colloidal suspension.

The turning on of SERS through the interaction of the aptamer nanoparticles with the protein target shows that this concept can be extended from a purely nucleic acid system and offers opportunities in terms for protein detection related to disease.

3 Conclusion

DNA-functionalised SERS probes offer excellent opportunities in molecular recognition. The use of mixed monolayers on nanoparticles, containing a Raman dye and specific oligonucleotide sequences, can lead to a novel range of detection systems capable of screening both nucleotide sequences and proteins. The approaches developed show how DNA-functionalised nanoparticle probes can be used in the detection of DNA sequences related to disease and in clinically relevant protein targets. Although work is still in the preliminary stages, it is possible to envisage how such systems could offer real opportunities to sensitively detect the expression of multiple genes and/or proteins in a cellular environment. Further, the ability of SERS to detect two very different recognition events should allow for the multiplexed detection of biological interactions including protein-protein and protein-small molecule. Recent developments in *in vitro* and *in vivo* nanoparticle delivery, coupled to such a highly sensitive spectroscopic technique, may yield a highly sensitive and specific technique of use in clinical diagnosis.

4 Experimental

All reagents were purchased from Sigma Aldrich, UK, apart from those used in oligonucleotide synthesis which were purchased from Link Technologies, UK. Aptamer sequences were purchased from Europhins MWG Operon, Germany.

Oligonucleotide-nanoparticle synthesis

All conjugates were synthesised by previously published methods.[18,34] Both gold[45] and silver[46] nanoparticles were synthesised *via* citrate reduction methods. Briefly, a 10 μM solution of thiol or thioctic acid modified DNA prepared in 60 mM phosphate buffer pH 8.5 was desalted using a Sephadex superfine desalting column fitted to a Dionex HPLC using distilled water as eluent directly onto a 3 mL solution of concentrated gold nanoparticles or as prepared silver nanoparticles. For the synthesis of DOSN conjugates the silver nanoparticles were first exposed to a Raman reporter molecule for 24 h at a final concnetration of 1×10^{-5} M. The solutions were then left in the dark for 24 h before gradual salt aging. The conjugates were then centrifuged twice at 7000 rpm for 20 min with resuspension in 0.3 M PBS pH 7.

SERS

A Leica DM/LM microscope equipped with an Olympus $20\times/0.4$ long working distance objective was used to collect 180° backscattered light from a standard cuvette. The spectrometer system was a Renishaw inVia and a Spectra Physics Argon ion laser (514.5 nm) was used as the excitation source with a power output

216

measured to be 6 mW at the sample. Dielectric edge filters were used to reject Rayleigh scattered light.

DOSN assay

For SERS analysis, a 30 pM solution of DOSN conjugates was prepared. An unmodifed complementary oligonucleotide was added to this solution in a $100\times$ excess. For UV-Vis analysis the DOSN conjugate solution concentration was 10 pM. For both techniques, scans were taken immediately after target addition and 30 min later.

mecA-OGN stability

2 nM of OGN conjugates were prepared in a quartz glass cuvette. To this an aliquot of DTT was added at a final concentration of 10 mM. The change in absorbance was then monitored using a Cary Win 300 UV-Visible spectrometer.

HPLC

HPLC traces were obtained using a Dionex P680 pump fitted with a UVD 170U detector and a 1 mL ResourceQ column with sodium perchlorate used as the counter ion.

Thrombin aptamer nanoparticles

DOSN conjugates were prepared using the method previously stated apart from that a buffer containing 0.21 M NaCl, 0.01 M KCl, 9 mM Na phosphate buffer pH 7.5 was used throughout rather than 0.3 M PBS.

UV-vis analysis: Thrombin (20 nM) was added to OSN conjugates (10 pM) and the change in absorbance was recorded every 5 min over a 90 min period using a Cary Win 300 UV-Visible spectrometer. The control study repeated the work in the absence of thrombin.

SERS: Thrombin (5 nM) was added (or buffer for control) to DOSN conjugates (50 pM) and allowed to incubate for 45 min. An extended scan was performed (300–2100 cm^{-1}) using a 10 s accumulation time. Analysis was performed in triplicate. The concentration analysis used functionalised nanoparticles (10 pM) incubated with thrombin (0, 2.5, 5, 10 nM) for 45 min prior to SERS analysis.

References

1 M. Faraday, *Philos. Trans. R. Soc. London*, 1857, **147**, 145.
2 J. Turkevich, P. C. Stevenson and J. Hiller, *Discuss. Faraday Soc.*, 1951, **11**, 55.
3 P. C. Lee and D. Meisel, *J. Phys. Chem.*, 1982, **86**, 3391.
4 G. Schmid and U. Simon, *Chem. Commun.*, 2005, 697.
5 M. C. Daniel and D. Astruc, *Chem. Rev.*, 2004, **104**, 293.
6 Y. Sun and Y. Xia, *Analyst*, 2003, **128**, 686.
7 J. Yguerabide and E. E. Yguerabide, *Anal. Biochem.*, 1998, **262**, 157.
8 J. Yguerabide and E. E. Yguerabide, *Anal. Biochem.*, 1998, **262**, 137.
9 M. Fleishman, P. J. Hendra and A. J. McQuillan, *Chem. Phys. Lett.*, 1974, **26**, 163.
10 K. Faulds, R. E. Littleford, D. Graham, G. Dent and W. E. Smith, *Anal. Chem.*, 2004, **76**, 592.
11 S. Nie and S. R. Emory, *Science*, 1997, **275**, 1102.
12 K. Faulds, R. Jarvis, W. E. Smith, D. Graham and R. Goodacre, *Analyst*, 2008, **133**, 1505.
13 K. Faulds, F. McKenzie, W. E. Smith and D. Graham, *Angew. Chem., Int. Ed.*, 2007, **46**, 1829.
14 A. MacAskill, D. Crawford, D. Graham and K. Faulds, *Anal. Chem.*, 2009, **81**, 8134.
15 A. P. Alivastos, K. P. Johnsson, X. Peng, T. E. Wilson, C. J. Loweth, M. P. Bruchez and P. G. Schultz, *Nature*, 1996, **382**, 609.
16 C. A. Mirkin, R. L. Letsinger, R. C. Mucic and J. J. Storhoff, *Nature*, 1996, **382**, 607.
17 J. S. Lee, A. K. R. Lytton-Jean, S. J. Hurst and C. A. Mirkin, *Nano Lett.*, 2007, 7, 2112.

217

measured to be 6 mW at the sample. Dielectric edge filters were used to reject Rayleigh scattered light.

DOSN assay

For SERS analysis, a 30 pM solution of DOSN conjugates was prepared. An unmodifed complementary oligonucleotide was added to this solution in a 100× excess. For UV-Vis analysis the DOSN conjugate solution concentration was 10 pM. For both techniques, scans were taken immediately after target addition and 30 min later.

mecA-OGN stability

2 nM of OGN conjugates were prepared in a quartz glass cuvette. To this an aliquot of DTT was added at a final concentration of 10 mM. The change in absorbance was then monitored using a Cary Win 300 UV-Visible spectrometer.

HPLC

HPLC traces were obtained using a Dionex P680 pump fitted with a UVD 170U detector and a 1 mL ResourceQ column with sodium perchlorate used as the counter ion.

Thrombin aptamer nanoparticles

DOSN conjugates were prepared using the method previously stated apart from that a buffer containing 0.21 M NaCl, 0.01 M KCl, 9 mM Na phosphate buffer pH 7.5 was used throughout rather than 0.3 M PBS.

UV-vis analysis: Thrombin (20 nM) was added to OSN conjugates (10 pM) and the change in absorbance was recorded every 5 min over a 90 min period using a Cary Win 300 UV-Visible spectrometer. The control study repeated the work in the absence of thrombin.

SERS: Thrombin (5 nM) was added (or buffer for control) to DOSN conjugates (50 pM) and allowed to incubate for 45 min. An extended scan was performed (300–2100 cm^{-1}) using a 10 s accumulation time. Analysis was performed in triplicate. The concentration analysis used functionalised nanoparticles (10 pM) incubated with thrombin (0, 2.5, 5, 10 nM) for 45 min prior to SERS analysis.

References

1 M. Faraday, *Philos. Trans. R. Soc. London*, 1857, **147**, 145.
2 J. Turkevich, P. C. Stevenson and J. Hiller, *Discuss. Faraday Soc.*, 1951, **11**, 55.
3 P. C. Lee and D. Meisel, *J. Phys. Chem.*, 1982, **86**, 3391.
4 G. Schmid and U. Simon, *Chem. Commun.*, 2005, 697.
5 M. C. Daniel and D. Astruc, *Chem. Rev.*, 2004, **104**, 293.
6 Y. Sun and Y. Xia, *Analyst*, 2003, **128**, 686.
7 J. Yguerabide and E. E. Yguerabide, *Anal. Biochem.*, 1998, **262**, 157.
8 J. Yguerabide and E. E. Yguerabide, *Anal. Biochem.*, 1998, **262**, 137.
9 M. Fleishman, P. J. Hendra and A. J. McQuillan, *Chem. Phys. Lett.*, 1974, **26**, 163.
10 K. Faulds, R. E. Littleford, D. Graham, G. Dent and W. E. Smith, *Anal. Chem.*, 2004, **76**, 592.
11 S. Nie and S. R. Emory, *Science*, 1997, **275**, 1102.
12 K. Faulds, R. Jarvis, W. E. Smith, D. Graham and R. Goodacre, *Analyst*, 2008, **133**, 1505.
13 K. Faulds, F. McKenzie, W. E. Smith and D. Graham, *Angew. Chem., Int. Ed.*, 2007, **46**, 1829.
14 A. MacAskill, D. Crawford, D. Graham and K. Faulds, *Anal. Chem.*, 2009, **81**, 8134.
15 A. P. Alivastos, K. P. Johnsson, X. Peng, T. E. Wilson, C. J. Loweth, M. P. Bruchez and P. G. Schultz, *Nature*, 1996, **382**, 609.
16 C. A. Mirkin, R. L. Letsinger, R. C. Mucic and J. J. Storhoff, *Nature*, 1996, **382**, 607.
17 J. S. Lee, A. K. R. Lytton-Jean, S. J. Hurst and C. A. Mirkin, *Nano Lett.*, 2007, 7, 2112.

218

18 D. G. Thompson, A. Enright, K. Faulds, W. E. Smith and D. Graham, *Anal. Chem.*, 2008, **80**, 2805.
19 J. J. Storhoff, R. Elghanian, R. C. Mucic, C. A. Mirkin and R. L. Letsinger, *J. Am. Chem. Soc.*, 1998, **120**, 1959.
20 R. C. Mucic, J. J. Storhoff, C. A. Mirkin and R. L. Letsinger, *J. Am. Chem. Soc.*, 1998, **120**, 12674.
21 J. J. Storhoff, A. D. Lucas, V. Garimella, Y. P. Bao and U. R. Muller, *Nat. Biotechnol.*, 2004, **22**, 883.
22 H. D. Hill, R. A. Vega and C. A. Mirkin, *Anal. Chem.*, 2007, **79**, 9218.
23 A. K. R. Lytton-Jean, M. S. Han and C. A. Mirkin, *Anal. Chem.*, 2007, **79**, 6037.
24 T. A. Taton, C. A. Mirkin and R. L. Letsinger, *Science*, 2000, **289**, 1757.
25 S. J. Park, T. A. Taton and C. A. Mirkin, *Science*, 2002, **295**, 1503.
26 Y. C. Cao, R. Jin and C. A. Mirkin, *Science*, 2002, **297**, 1536.
27 C. Tuerk and L. Gold, *Science*, 1990, **249**, 505.
28 A. D. Ellington and J. W. Szostak, *Nature*, 1990, **346**, 818.
29 R. D. Jenison, S. C. Gill, A. Pardi and B. Polisky, *Science*, 1994, **263**, 1425.
30 S. A. Vinores, *Curr. Opin. Mol. Ther.*, 2003, **5**, 673.
31 O. C. Farokhzad, S. Jon, A. Khademhosseini, T.-N. T. Tran, D. A. LaVan and R. Langer, *Cancer Res.*, 2004, **64**, 7668.
32 C.-C. Huang, Y.-F. Huang, Z. Cao, W. Tan and H.-T. Chang, *Anal. Chem.*, 2005, **77**, 5735.
33 J. Chen, J. Jiang, X. Gao, G. Liu, G. Shen and R. Yu, *Chem.–Eur. J.*, 2008, **14**, 8374.
34 D. Graham, D. G. Thompson, W. E. Smith and K. Faulds, *Nat. Nanotechnol.*, 2008, **3**, 548.
35 F. McKenzie, K. Faulds and D. Graham, *Nanoscale*, 2010, **2**, 78.
36 X. Qian, X. Zhou and S. Nie, *J. Am. Chem. Soc.*, 2008, **130**, 14934.
37 D. Graham, K. Faulds, D. G. Thompson, F. McKenzie, R. J. Stokes, C. Dalton, R. Stevenson, J. Alexander, P. Garside and E. McFarlane, *Biochem. Soc. Trans.*, 2009, **37**, 697.
38 G. McAnally, C. McLaughlin, R. Brown, D. C. Robson, K. Faulds, D. R. Tackley, W. E. Smith and D. Graham, *Analyst*, 2002, **127**, 838.
39 D. G. Thompson, K. Faulds, W. E. Smith and D. Graham, *J. Phys. Chem. C*, 2010, **114**, 7384.
40 R. L. Letsinger, R. Elghanian, G. Viswanadham and C. A. Mirkin, *Bioconjugate Chem.*, 2000, **11**, 289.
41 J. A. Dougan, C. Karlsson, W. E. Smith and D. Graham, *Nucleic Acids Res.*, 2007, **35**, 3668.
42 L. Griffin, G. Tidmarsh, L. Bock, J. Toole and L. Leung, *Blood*, 1993, **81**, 3271.
43 K. Padmanabhan, K. P. Padmanabhan, J. D. Ferrara, J. E. Sadler and A. Tulinsky, *J. Biol. Chem.*, 1993, **268**, 17651.
44 K. Padmanabhan and A. Tulinsky, *Acta Crystallogr., Sect. D: Biol. Crystallogr.*, 1996, **52**, 272.
45 K. C. Grabar, R. G. Freeman, M. B. Hommer and M. J. Natan, *Anal. Chem.*, 1995, **67**, 735.
46 C. H. Munro, W. E. Smith, M. Garner, J. Clarkson and P. C. White, *Langmuir*, 1995, **11**, 3712.

219